CALIFORNIA INSTITUTE OF TECHNOLOGY

EARTHQUAKE ENGINEERING RESEARCH LABORATORY

DYNAMIC CHARACTERISTICS OF WOODFRAME BUILDINGS

THESIS BY

VANESSA CAMELO

REPORT NO. EERL 2003-04

PASADENA, CALIFORNIA
MAY 2003

(DEFENDED MAY 23, 2003)

Dynamic Characteristics of Woodframe Buildings

Thesis by

Vanessa Sabrina Camelo

In Partial Fulfillment of the Requirements

for the Degree of

Doctor of Philosophy

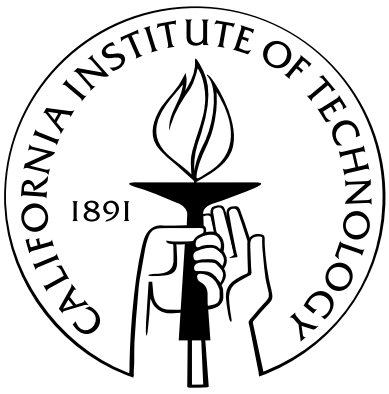

California Institute of Technology

Pasadena, California

2003

(Defended May 23, 2003)

To Dean Gray, who worked countless hours by my side.

His love supported me throughout this journey.

Acknowledgements

Funding for this research was provided by the Consortium of Universities for Research in Earthquake Engineering (CUREE) as part of the CUREE-Caltech Woodframe Project ("Earthquake Hazard Mitigation of Woodframe Construction"), under a grant administered by the California Office of Emergency Services and funded by the Federal Emergency Management Agency. Continuation of this project was made possible by the three-year fellowships received from the Pacific Earthquake Engineering Research (PEER) Center and the Harold Hellwig Fellowship received from the California Institute of Technology (Caltech).

The author would like to thank Professor Ziyad Duron for his generosity in lending the Harvey Mudd shaker and in sharing his expertise throughout this project. Also, special thanks to Professor Khalid Mosalam and the staff at the University of California at Berkeley, Richmond Field Station, for making the 3-story building on the shake-table available (the tests described in section 5.2). The author is grateful for the assistance and encouragement received from Prof. James Beck and Prof. John Hall, as well as from the many staff and graduate students who helped with this project, specially Matt Muto for his invaluable assistance during the UC Berkeley tests.

Abstract

A database of dynamic characteristics of woodframe buildings was developed through analysis of recorded earthquake response and by forced vibration and shake-table testing. Modal identification was performed on eight sets of strong-motion records obtained from five buildings, and forced vibration tests were performed on five other buildings. The periods identified were sensitive to the amplitude of shaking, due to the reduction in lateral stiffness at stronger shaking levels. The equivalent viscous damping ratios were usually more than 10% of critical during earthquake shaking. A regression analysis was performed on the earthquake and forced vibration test data to obtain a simple, but reasonably accurate, period formula for woodframe buildings at low drift levels (less than 0.1%). Data obtained from the UC San Diego and UC Berkeley full-scale shake-table tests illustrate the shift in periods due to increasing shaking amplitude. Forced vibration tests of the UC Berkeley 3-story building before and after the shake-table tests showed how the periods and modeshapes shift due to damage. A simple analytical model of masses and springs was used to model the UC Berkeley test structure. The effects of diaphragm stiffness and mass distribution assumptions were evaluated and found to have a significant effect on the model torsional response. This model was used to find the equivalent wall stiffnesses giving frequency-response curves that best-fit the experimental data. These spring values were used to quantify the stiffness loss resulting from severe shaking of the structure, and the observed damage corresponded to stiffness losses of over 75%. The correlation between stiffness loss and damage to woodframe buildings has potential structural health monitoring implications.

Contents

List of Figures

List of Tables

Chapter 1

Introduction

The 1994 Northridge earthquake exposed some significant vulnerabilities in woodframe construction and other structures as well. It is estimated that there was at least $20 billion in property loss in woodframe construction during this earthquake (Kircher et al., 1997), far outweighing the loss to any other single type of construction. There were more fatalities and injuries in woodframe construction than in all other kinds of buildings combined, although this is probably due to the fact that the earthquake occurred at 4:31 a.m. and most people were at home. In average, it is estimated that 80 to 90% of all U.S. buildings are woodframe (Malik, 1995).

The CUREE-Caltech Woodframe Project, funded by the Federal Emergency Management Agency (FEMA), had as its main objective to significantly reduce earthquake-induced losses to woodframe construction. One objective of this project was to identify the characteristics that make a woodframe building more or less vulnerable to earthquake damage, characteristics such as tuck-under parking (see Figure 1.1), cripple walls, hillside location, wall finish materials, connections, etc. Another objective was to evaluate the current relevant codes and standards, as well as engineering procedures and construction practices, and to make recommendations to improve current practices.

The research described in this dissertation was originally funded by CUREE as Task 1.3.3 of the Testing and Analysis Element of the Woodframe Project. Under this task, the dynamic properties of woodframe shearwall buildings were evaluated, mainly modal parameters such as frequencies, damping and mode shapes of the structures

Figure 1.1: Northridge Apartments (collapse of 1st floor garage)

and how these parameters change with motion amplitude. The focus was on the behavior of the entire structure in the range of small amplitude of vibrations (drifts ¡ 0.1%), and a database of fundamental-mode parameters was compiled based on the reviewed literature and on vibration tests and analysis of recorded earthquake response performed in this work. A simplified period formula for woodframe buildings at low drift levels was derived by regression analysis on this database. The scope of the Woodframe Project also included full-scale shake-table tests of a 2-story house and a 3-story apartment building with tuck-under parking, performed at UC San Diego and UC Berkeley, respectively. Selected records from the shake-table tests of the 2-story house were analyzed and included in this dissertation. After the conclusion of the Task 1.3.3 research, the author performed forced vibration tests on the 3-story apartment building at UC Berkeley before and after each phase of shake-table testing. A simple analytical model of masses and springs was then used to find the equivalent wall stiffnesses giving frequency-response curves best-fitting the experimental data.

The goal of this research was to provide further insight into the dynamics of woodframe buildings by analyzing earthquake records, by performing field tests, and by examining how period and modeshape data can be used to indicate degree and location of damage. The following chapters detail the methodology, results and conclusions from each phase of this project. Chapter 2 discusses available literature and

previous research on the dynamics of woodframe buildings, including the simplified methods prescribed in building codes for computing building periods. Chapter 3 describes the system identification methodology used and the results obtained from the analysis of the earthquake records from woodframe buildings. Chapter 4 describes the ambient and forced vibration tests performed. Chapter 5 describes the analysis of the data obtained from the full-scale shake-table tests performed at UC San Diego and at UC Berkeley, including the analytical modelling of the UC Berkeley test specimen. Chapter 6 details the period regression analysis performed on the database compiled throughout this project. Finally, Chapter 7 gives a summary of the conclusions from this dissertation and lists some of the research opportunities identified during the course of this project.

Chapter 2

Literature Review

Much research has been done on the dynamic and hysteretic characteristics of wood subsystems and connection panels (e.g., Polensek and Schimel 1991; Falk 1986), but full-scale testing of wood shearwall buildings has been sparse. Since the behavior of the entire woodframe structure can differ significantly from that of its individual components such as walls or diaphragms, this literature review will focus mainly on research of full-scale woodframe structures.

2.1 Research on Woodframe Structures

On the general behavior of wood subsystems, Polensek and Schimel (1991) evaluated the degree of nonlinearity and degradation of damping and stiffness properties in wood subsystems with and without finish materials (gypsum wallboard). They observed that energy was dissipated by slipping interfaces of connected materials, and that damping tends to increase with increasing amplitude of vibration up to some limit, after which prior damage tends to reduce interface friction and therefore reduce damping and stiffness of shear wall, bending and connection panels. They also noted that the dynamic behavior of the panels was the same regardless of the lumber grade, suggesting that panel damping and stiffness depend mostly on nailed joints and less on the grade of lumber used in framing.

Seo et al. (1981) performed static and cyclic lateral load tests on wooden frames with tenon beam-column joints. The tests showed nonlinear and inelastic behavior,

with estimated equivalent viscous damping ratios between 13% and 27% for these types of structures. The frame stiffness was significantly reduced with increased amplitude of displacement.

Hirashima (1988) tested a 2-story building with diagonal braces built in post-and-beam frames with no wall cladding, neither exterior nor interior. He used static loading tests to obtain spring constants to use in a mathematical model of the building and forced vibration tests to observe the dynamic behavior. He noted that the test building oscillated mainly in its fundamental mode of vibration in each direction, and that the corresponding periods of vibration were almost constant throughout the motion at 0.25 sec (4.0 Hz) transverse and 0.22 sec (4.5 Hz) longitudinal. The corresponding damping ratios were quite low, 2.4% transverse and 1.4% longitudinal, from a free vibration test with initial peak-to-peak displacements of about 1/2 mm. These low damping ratios compared with other buildings tested suggest that plywood and wall finish materials are major contributors to the damping in woodframe buildings. An earthquake record was also obtained in the test building with 6%g peak acceleration at the roof. A Fourier amplitude spectrum of the roof accelerations showed a fundamental period for each direction of about 0.25 sec (4 Hz).

Yokel, Hsi and Somes (1973) performed full-scale tests on a 2-story house with a partial brick-veneer front at the lower story, stucco exterior finish and gypsum-board interior. Several tests were conducted to determine the dynamic response of the house to an impulse load. The natural frequency of the structure was approximately 0.11 sec (9 Hz) and damping averaged 6% of critical, varying from 4% to 9%. The validity of these findings is questioned by those authors, since the resolution of the displacement time history records was marginal.

Foliente and Zacher (1994) report on dynamic tests of timber structural systems. Table 2.1, taken from their paper, gives a summary of periods from tests performed in several different countries. Because of the differences in construction, results from other countries may not be especially relevant, and there are only a few tests of conventional North American woodframe residential construction. These show periods in the range 0.06 to 0.33 sec (3 to 18 Hz), which are consistent with the values identified

in the tests and analysis performed in this project.

Table 2.1: Summary of Natural Periods and Frequencies of Low-Rise Wood and Wood-Based Buildings

Building Type	Natural Period Tn (sec)	Natural Frequency 1/Tn (Hz)	Reference(s)
2- and 3-story N. American residential	0.14 to 0.33	3.0 to 7.0	[36]
1-, 1.5- and 2-story N. American residential and school buildings	0.06 to 0.25	4.0 to 18.0	[35]
1- and 2-story New Zealand residential	0.1 to 0.6	1.7 to 10.0	[11]
1-story truss-frame residential	0.14 to 0.26	3.8 to 7.2	[18]
2-story residential (Greece)	0.18 to 0.22	4.5 to 5.6	[39]
1-, 2- and 3-story Japanese residential	0.11 to 0.33	3.0 to 9.0	[2]
3-story Japanese residential	0.16 to 0.20	4.7 to 6.2	[28], [42]
1- and 2-story N. American comm'l/industrial (plywood roof diaphragm and concr./masonry walls)	0.20 to 0.80	1.2 to 5.1	[9]
Range of Values for N. American residential	0.06 to 0.33	3.0 to 18.0	

Filiatrault performed full-scale shake-table tests on a 2-story single-family wood-frame house under Task 1.1.1 of the CUREE-Caltech Woodframe Project (see Fischer et al., 2001). The structure was tested during 10 phases of construction to determine the performance of the structure with fully sheathed shearwalls, symmetrical and unsymmetrical door and window openings, perforated shearwall construction, conventional construction, and with and without non-structural wall finish materials. The building had plan dimensions of 16' x 20' and height of 20' (to top of roof). They performed four types of shake-table tests: quasi-static in-plane floor diaphragm tests, frequency evaluation tests, damping evaluation tests, and seismic tests using various scalings of ground motions recorded during the 1994 Northridge earthquake. The results presented by Fischer et al. (2001) for the fully configured building (wall

finish applied, Phase 10 tests) show that the fundamental transverse frequency was 6.5 Hz (from ambient vibrations), 6.3 Hz (0.05g PGA), 5.8 Hz (0.36g PGA), and 5.5 Hz (0.50g and 0.89g PGA). The equivalent viscous damping ratios were based on the log-decrement method and increased from 3.1% at ambient levels to 12% at 0.22g PGA, then decreased to about 6% at 0.5g PGA and beyond.

Mosalam et al. (2002) performed shake-table tests on a 3-story woodframe building with tuck-under parking as part of the CUREE-Caltech Woodframe Project. The testing specimen was full-scale with respect to height, but the shaking table limited the building dimensions to 16'x32'. The specimen was tested during three main phases: Phase I - no wall finishes, no retrofit scheme; Phase II - wall finishes installed, retrofitted structure; and Phase III - wall finishes installed, no retrofit scheme. Ground motions recorded during the 1994 Northridge earthquake were used, scaled at increasing intensity levels. The dynamic test results confirmed the torsional tendency of the structure and the asymmetric damage pattern was induced by the multi-component motions in the walls perpendicular to the garage openings due to the combined effect of the three components of ground motion. Damage remained non-critical even after severe shaking, which might be a consequence of the better construction of the test building and the inability of the shake-table to produce ground velocities and displacements as high as those observed at some locations during the earthquake. It was observed that the wall finishes reduced the maximum story drifts by a factor of 2.3 while increasing story shear by a factor of 1.8.

2.2 Current Code Period Formulas

Current building codes require a design earthquake load based on the building's system characteristics, site location, occupancy, etc. The code specifies simplified formulas to approximate the building's dynamic behavior. The fundamental period is an important factor in determining how the building will behave during an earthquake. This is used, for example, to help determine the appropriate seismic base shear coefficient for the design of a structure. Recent research has shown that the 1997 Uniform

Building Code period formulas substantially underestimate the building periods for concrete and steel moment-resisting frame buildings as well as for concrete shearwall buildings (Goel and Chopra, 1997, 1998). An important objective of this work is to evaluate and to improve the current code period formulas for wood structures.

2.2.1 Uniform Building Code (1997)

The 1997 UBC, published by the International Conference of Building Officials (ICBO), prescribes the following period formulas for buildings (ICBO, 1997):

Method A

$$T = C_t h_n^{3/4} \tag{2.1}$$

where

h_n = height, in feet, above the base to the uppermost level in the main portion of the structure

$C_t = 0.035$ (steel moment resisting frames)

$C_t = 0.030$ (reinf. concrete moment resist. frames and eccentric braced frames)

$C_t = 0.020$ (all other buildings)

For concrete or masonry shear-wall buildings, the following value of C_t may be used instead:

$$C_t = \frac{0.1}{A_c^{1/2}} \tag{2.2}$$

where

$$A_c = \sum A_e[0.2 + (\frac{D_e}{h_n})^2] \tag{2.3}$$

$$\frac{D_e}{h_n} \leq 0.9 \tag{2.4}$$

and

A_e = minimum cross-sectional area, in sq. feet, of the shear walls in the first story of structure

D_e = length, in feet, of a shear wall in the first story in the direction parallel to the applied forces

Method B

$$T = 2\pi\sqrt{\frac{\sum_{i=1}^{n} w_i\delta_i^2}{g\sum_{i=1}^{n} f_i\delta_i}} \tag{2.5}$$

where

w_i = that portion of the total seismic dead load located at or assigned to level i

δ_i = horizontal displacement at level i relative to the base due to applied lateral forces, f

f_i = lateral force at level i

g = acceleration due to gravity

n = uppermost level in the main portion of the structure

The UBC-97 limits the maximum period obtained from Method B (simplified structural analysis) to 1.3 times the period obtained by Method A for Zone 4 buildings or 1.4 times period obtained by Method A period for Zones 1, 2 and 3.

2.2.2 FEMA-273

This document presents approaches for the seismic rehabilitation of buildings that will limit the expected earthquake damage due to a certain level of ground shaking. In FEMA-273 Section 3.3 - Analysis Procedures, it offers a linear static method equivalent to that of the UBC-97, and the period can be determined by one of three methods:

Method 1 Eigenvalue (dynamic) analysis of a mathematical model

Method 2 Similar to UBC-97 Method A,

$$T = C_t h_n^{3/4} \tag{2.6}$$

where the values of C_t are same as in UBC-97 except:

$$C_t = 0.060 \text{ (for wood buildings)}$$

Method 3 For a 1-story building with single span flexible diaphragm,

$$T = (0.1\Delta_w + 0.078\Delta_d)^{0.5} \tag{2.7}$$

where

Δ_w = in-plane wall displacement in inches due to lateral load equal to the weight tributary to the diaphragm

Δ_d = in-plane diaphragm displacement in inches due to lateral load equal to the weight tributary to the diaphragm

In Method 3, the period obtained from equation 2.7 for various diaphragms and walls that maximizes the design base shear (pseudo lateral load) is to be used.

2.3 Recent Developments

Goel and Chopra (1997, 1998) have presented alternative period formulas for reinforced concrete and steel moment-resisting frame buildings and for concrete shearwall buildings. They obtained information about the fundamental modes of vibration of a number of buildings by analyzing their recorded motion from various California earthquakes. These structures were shaken strongly but not so strongly as to enter

the inelastic range. They were divided into two categories depending on the strength of the earthquake shaking they experienced, i.e., whether or not the peak ground acceleration was less than 0.15 g. After determining that the current code formulas substantially underestimated the natural vibration periods for these structures, they re-evaluated the theory upon which the code formulas were based and derived new formulas by regression analysis. These period formulas led to a best fit, in the least-squares sense, to the measured period data. The final recommended period formulas were derived looking at the trend obtained from only the buildings experiencing peak ground accelerations of 0.15g or greater. At smaller acceleration levels, the periods tend to be smaller because the non-structural components contribute significantly to the lateral stiffness. This fact should also be kept in mind when interpreting the period formula derived during this project because all data on which it was based came from low-amplitude response.

Goel and Chopra concluded that Rayleigh's method was sufficient to give a good approximation of the dynamic behavior of moment resisting frame buildings. Based on this method, the period formula should be of the form $T = Ch_n^{\gamma}$, where C and γ are to be determined from regression analysis in the form $\ln T = \ln C + \gamma \ln h_n + s_e^2$. The least-squares estimates of $\ln C$ and γ then give the median estimate of the period, that is, there is a 50% probability that the actual period of the building is greater that the period estimated by the regression formula. Since for determination of design base shear the formula should provide lower values of the period (to be conservative), Goel and Chopra chose a lower bound of a standard deviation from the best fit line. Also, they provided an upper limit for periods found using rational analysis rather than the code formula. The resulting lower-bound period formulas were the following, with standard-error estimates of $s_e = 0.209$ for reinforced concrete moment resisting frame buildings and $s_e = 0.233$ for steel moment resisting frame buildings:

$$T = 0.016 h_n^{0.90} \text{ (reinforced concrete moment resisting frame)} \tag{2.8}$$

or no larger than 1.4 T if using rational analysis.

$$T = 0.028 h_n^{0.80} \text{ (steel moment resisting frame)} \tag{2.9}$$

or no larger than 1.6 T if using rational analysis.

In the above equations, h_n is the total building height from the base of the structure, in feet. Rayleigh's method was not sufficient to give a good estimate for the dynamic characteristics of shearwall buildings, so Goel and Chopra chose to use various other well-established analytical procedures, such as Dunkerley's method, which combines both flexural and shear deformations of a cantilever. Based on this particular method, the period formula should be of the following form:

$$T = C \frac{h_n}{\sqrt{\overline{A}_e}} \tag{2.10}$$

where

$$\overline{A}_e = 100 \frac{A_e}{A_B}, \qquad A_e = \frac{A}{[1 + 0.83(\frac{h_n}{D})^2]}$$

and

h_n = the total building height from base of structure, ft

C = constant to be defined by regression

A_B = plan area of building, ft^2

A = total area of shear walls, ft^2

D = building dimension parallel to direction being considered, ft

Regression analysis yielded the following formula, with an error of estimate $s_e = 0.143$ while the UBC-97 error estimate is $s_e = 0.546$.

$$T = 0.0019 h_n / \sqrt{\overline{A}_e} \text{ (reinforced concrete shear wall)} \tag{2.11}$$

or no larger than 1.4 T if using rational analysis.

Chapter 3

Analysis of Earthquake Records

Several earthquake records were obtained from woodframe buildings instrumented by the California Strong Motion Instrumentation Program (for earthquake time histories, see Appendix A). This chapter describes the method used for system identification, the characteristics of each set of records analyzed, the buildings in which these records were obtained, and the identified modal system parameters for each building. The results are summarized in Table 3.1 at the end of this chapter.

3.1 MODE-ID Method for System Identification

Modal identification is an important application of system identification in structural dynamics, where modal parameters based on a model with linear dynamics are estimated using dynamic data from a structure. Modal identification can be performed in the time domain without the need to develop a structural model involving mass, stiffness and damping matrices (Beck, 1978). The method was initially applied to the measured seismic response from tall buildings where only a single input (the recorded base acceleration) was used (Beck and Jennings, 1980). The method was then extended to handle multiple inputs in order to find the modal parameters from seismic motions recorded on a bridge (Werner et al., 1987). The computer program, called MODE-ID, that implements this approach has been extensively applied to earthquake and other dynamic data. MODE-ID is based on a nonlinear least-squares output-error method, which utilizes a class of models defined as follows.

Structural motion at the N_o observed degrees of freedom is modeled as a superposition of N_m dominant modes:

$$x_i(t) = \sum_{r=1}^{N_m} x_{ir}(t), \qquad i = 1, \ldots, N_o \tag{3.1}$$

where x_{ir} is the contribution of the rth mode to the response at the ith degree of freedom.

The response for the $(N_m - 1)$ dynamic modes of vibration is calculated numerically using a very accurate discrete-time recursive approximation (Beck and Dowling, 1988) of the well-known equation of motion:

$$\ddot{x}_{ir} + 2\zeta_r \omega_r \dot{x}_{ir} + \omega_r^2 x_{ir} = \varphi_{ir} \sum_{k=1}^{N_I} p_{rk} f_k(t) \tag{3.2}$$

with

$$x_{ir}(0) = \varphi_{ir} c_r; \qquad \dot{x}_{ir}(0) = \varphi_{ir} d_r; \qquad \sum_{i=1}^{N_o} \varphi_{ir}^2 = 1$$

where the f_k, $k = 1, ..., N_I$ are the measured accelerations at the N_I structural supports (e.g., defining the motion at the base of the structure). A pseudostatic "mode" is also necessary:

$$\ddot{x}_{ir} = \sum_{k=1}^{N_I} r_{ik} f_k(t) \tag{3.3}$$

This accounts for the quasi-static contributions to the structural motions induced by the support motions during the earthquake, ignoring inertial and damping effects since these are accounted for in the dynamic response contributions (Werner et al., 1987). The simplest pseudostatic mode is rigid-body motion such as the direct contributions from rocking and translation of the base of a building.

The model parameters $\underline{a}$ to be estimated are the modal parameters for each of the identified $(N_m - 1)$ dynamic modes, that is, the natural frequencies and damping ratios, ω_r and ζ_r, the initial modal displacement and velocity, c_r and d_r, the modeshape components at the observed degrees of freedom $(\varphi_{ir}, i = 1, ..., N_o)$, and the input

participation factors ($p_{rk}, k = 1, ..., N_I$); together with the pseudostatic influence coefficients ($r_{ik}, i = 1, ..., N_o, k = 1, ..., N_I$). The latter parameters can be fixed on a theoretical basis in some situations (e.g., for the pseudostatic response due to rocking and translation of the base of a building). Only the modeshape components at the observed degrees of freedom can be identified since the "missing" modeshape components at the unobserved degrees of freedom cannot be identified directly without introducing a structural model as a basis for the "interpolation."

The model parameters $\underline{a}$ are estimated by minimizing the mean square of the prediction errors at all the observed degrees of freedom, that is:

$$J(\underline{a}) = \frac{1}{N_o N} \sum_{i=1}^{N_o} \sum_{n=1}^{N} [\hat{y}_i(n) - x_i(n; \underline{a})]^2 \tag{3.4}$$

Typically, the discrete system output ($\hat{y}_i(n) : n = 1, ..., N; i = 1, ..., N_o$) in Equation 3.4 consists of measured acceleration time histories at the N_o observed degrees of freedom for some sampling interval Δ_t. The model output $x_i(n; \underline{a})$ in Equation 3.4 is a nonlinear function of the parameters and so the minimization of $J(\underline{a})$ must be done numerically by an iterative optimization algorithm. The algorithm used in the MODE-ID program is a robust one exploiting the linearity of the model dynamics (Beck, 1978; Werner et al., 1987). Although MODE-ID assumes time invariant modal parameters, it is possible to divide a set of records into time windows of nearly constant modal parameters. MODE-ID analysis of each window (windowing analysis) can show how these modal parameters vary throughout the entire record.

There is a post-processor for MODE-ID, called DYN-ID, which computes the time-history response of the linear model identified by MODE-ID. Appendix B (Figures B.1 through B.13) compares the earthquake time histories to the DYN-ID output time histories (computed using the time-invariant MODE-ID results) at selected channels for each building analyzed in sections 3.2.1 through 3.2.5.

3.2 Available Seismic Records

Eight sets of earthquake records were obtained from five CSMIP instrumented woodframe buildings (for earthquake time histories, see Appendix A). Sections 3.2.1 through 3.2.5 describe each set of records, the building in which they were recorded and the results from the MODE-ID analysis performed. The results are summarized in Table 3.1 at the end of this chapter.

3.2.1 San Bernardino – 3-Story Motel

Three sets of earthquake records obtained at this site were analyzed. This building is highly irregular, forming an asymmetrical T. Built in 1986, the building has plywood shearwalls in the first story along the transverse directions and gypsum board on the upper stories and along the longitudinal directions. There were nine channels in the NS direction, five in the EW direction, and onep recording vertical motion. Channels 2 and 3 were taken as the input when using MODE-ID (See Figure 3.1).

The three earthquakes recorded included two near-field earthquakes (epicentral distance less than 1 km). The horizontal maximum accelerations generated in the structure were 9.2%g (from the $M_L = 4.2$ magnitude, June 28, 1997 earthquake), 7.8%g (from the $M_L = 3.7$ magnitude, July 26, 1997 earthquake), and 7.1%g (from the $M_L = 4.7$ magnitude, March 11, 1998 earthquake). Modal analysis of these earthquake records has revealed that the structure's average time-invariant fundamental periods (frequencies) are 0.19 sec (5.2 Hz) in the NS direction and 0.22 sec (4.6 Hz) in the EW direction. The average of the time-invariant fundamental damping ratios obtained from each set of records was 12.0% in the NS direction and 11.8% in the EW direction. Plots of the recorded and predicted response time histories for selected channels are given in Appendix B (Figures B.1 through B.4).

Windowing analysis (breaking up the records into 6 second windows) showed that the natural frequencies and damping ratios change throughout the earthquake excitation (see Figure 3.2 where time-invariant values are solid lines). The fundamental frequencies were generally lowest at the time of strongest shaking and returned to

a higher value as shaking subsided. With few exceptions (due to the uncertainty in damping estimates), these damping ratios were generally highest at the time of strongest shaking and returned to a lower value as shaking subsided. Figure 3.3 shows the windowing analysis results as functions of peak roof drift ratios, illustrating the amplitude dependence of the building frequency and damping. Note that the fundamental frequency values were generally lower at the larger peak roof drift values, while the damping ratios were generally highest at the larger peak roof drifts (although there were a few exceptions due to uncertainty in the damping estimates as mentioned above).

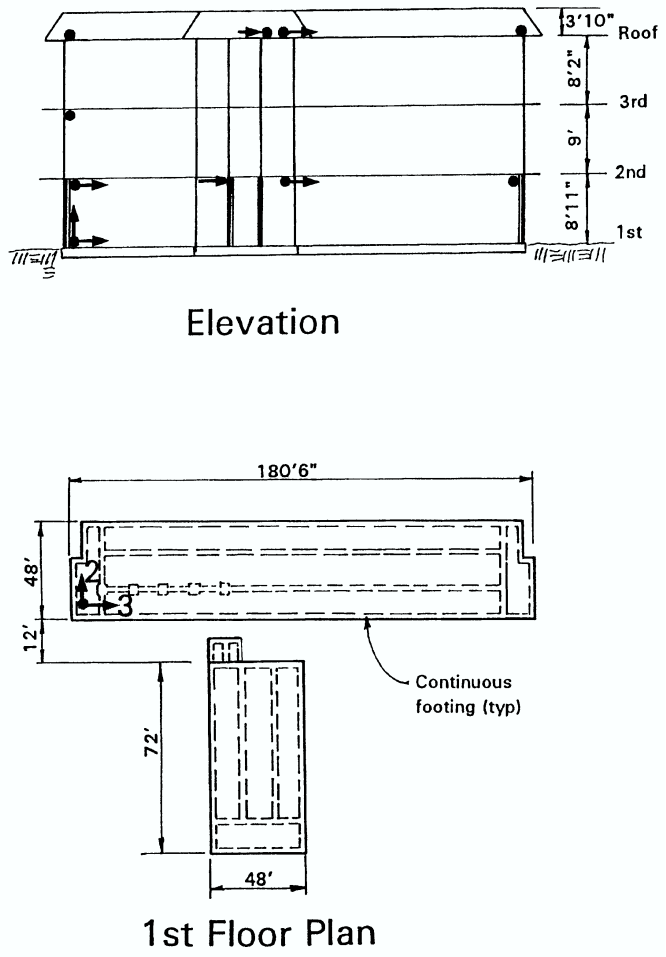

Figure 3.1: San Bernardino 3-Story Motel

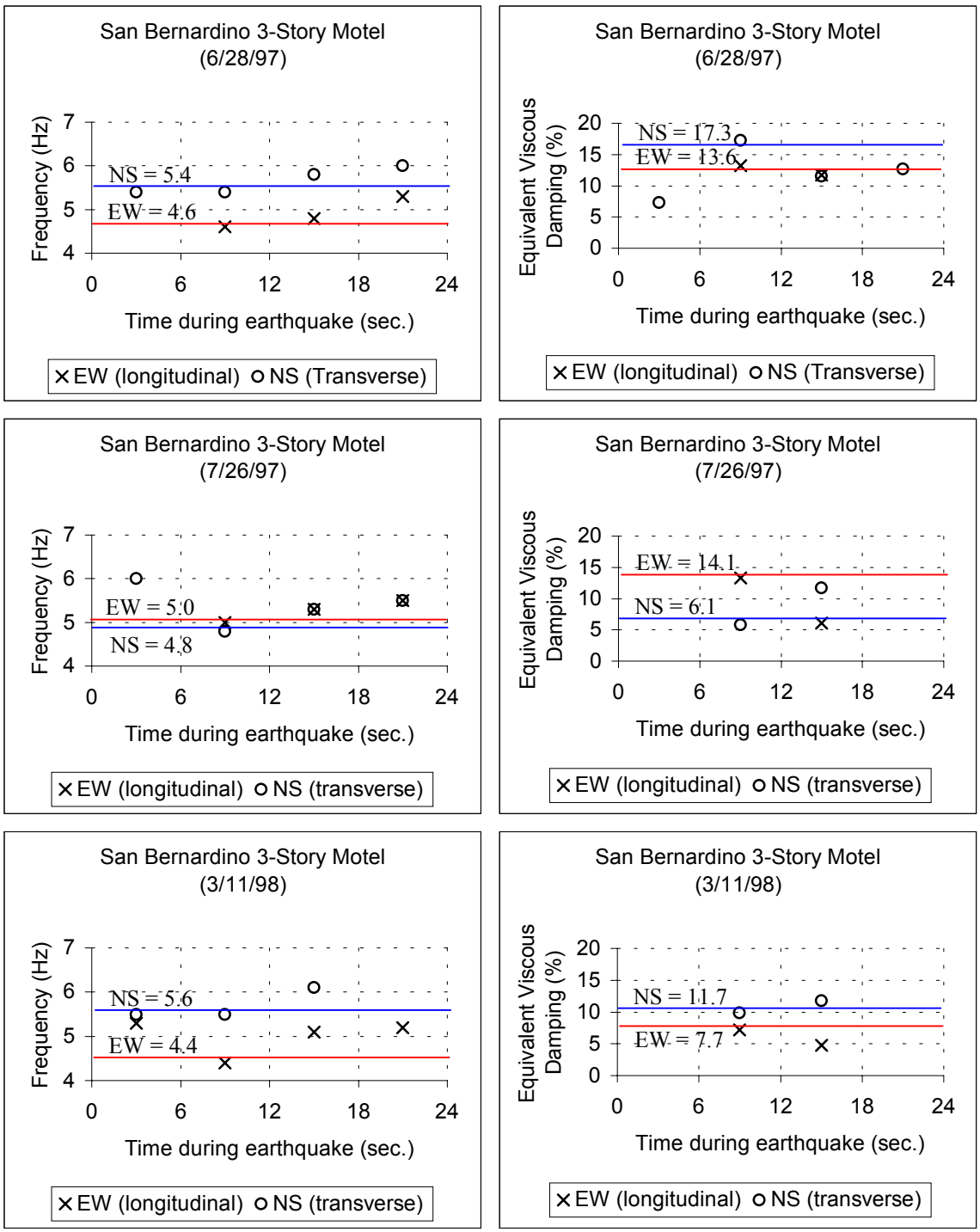

Figure 3.2: MODE-ID Results vs. Time for San Bernardino 3-Story Motel

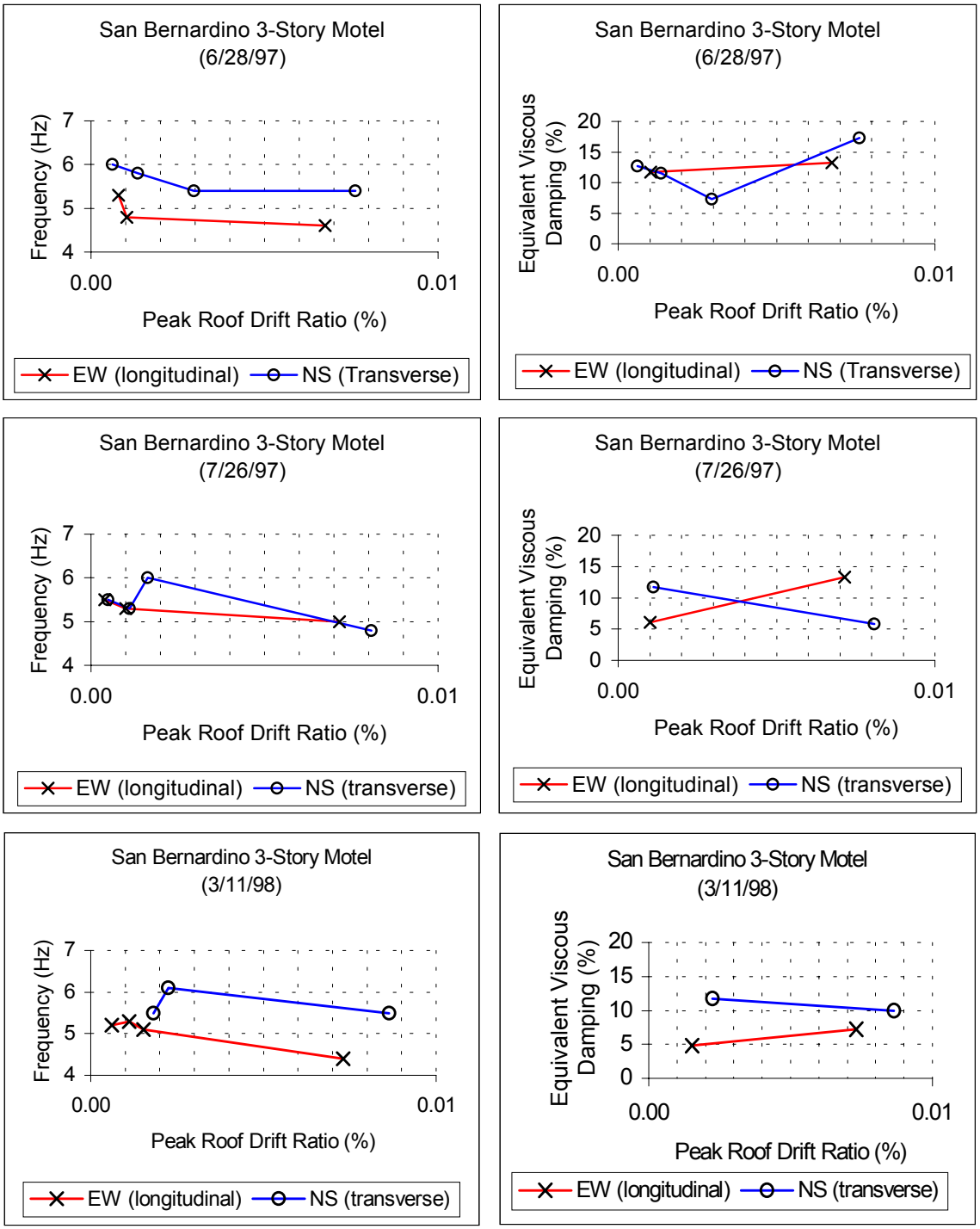

Figure 3.3: MODE-ID Results vs. Drift for San Bernardino 3-Story Motel

3.2.2 Parkfield – 1-Story Elementary School

Two sets of earthquake records obtained at this site were analyzed. This is a 1-story, rectangular building built in 1949, with plywood shear walls in the longitudinal direction. There were three channels in the NS (transverse) direction and three in the EW (longitudinal) direction. Channels 3 and 6 were taken as the excitation when using MODE-ID (See Figure 3.4).

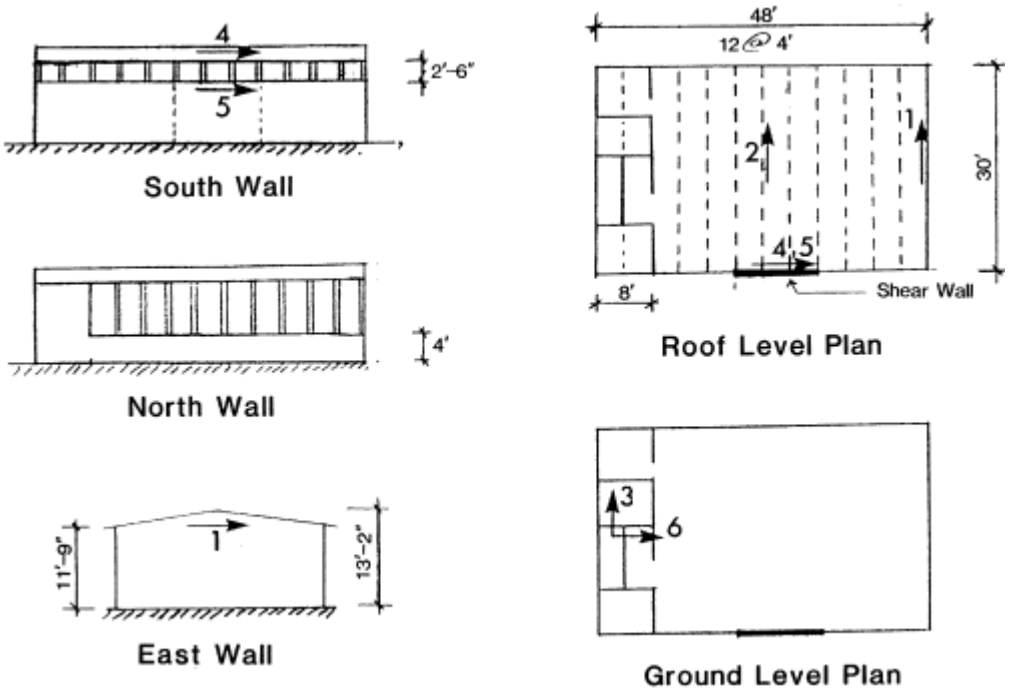

Figure 3.4: Parkfield 1-Story Elementary School

The two earthquakes were both within 10 km from the site. The horizontal maximum accelerations generated in the structure were 12.3%g (from the $M_L = 4.2$ magnitude, April 4, 1993 earthquake) and 20.1%g (from the $M_L = 4.7$ magnitude, December 20, 1994 earthquake). Modal analysis of these earthquake records has revealed that the structure's average time-invariant fundamental periods (frequencies) are 0.12 sec (8.3 Hz) in the NS direction and 0.14 sec (6.9 Hz) in the EW direction. The average of the time-invariant fundamental damping ratios was 14.7% in the NS direction and 11.2% in the EW direction. Plots of the recorded and predicted

response time histories for selected channels are given in Appendix B (Figures B.5 through B.8).

Windowing analysis (breaking up the records into 6 second windows) showed that the natural frequencies of vibration for this building change throughout the earthquake excitation (see Figure 3.5, where time-invariant values are solid lines). These frequencies were lowest at the time of strongest shaking (first window in NS direction and second window in EW direction) and returned to a higher value as shaking subsided. Damping ratios were highest at the time of strongest shaking (first window in NS direction and second window in EW direction) and returned to a lower value as shaking subsided.

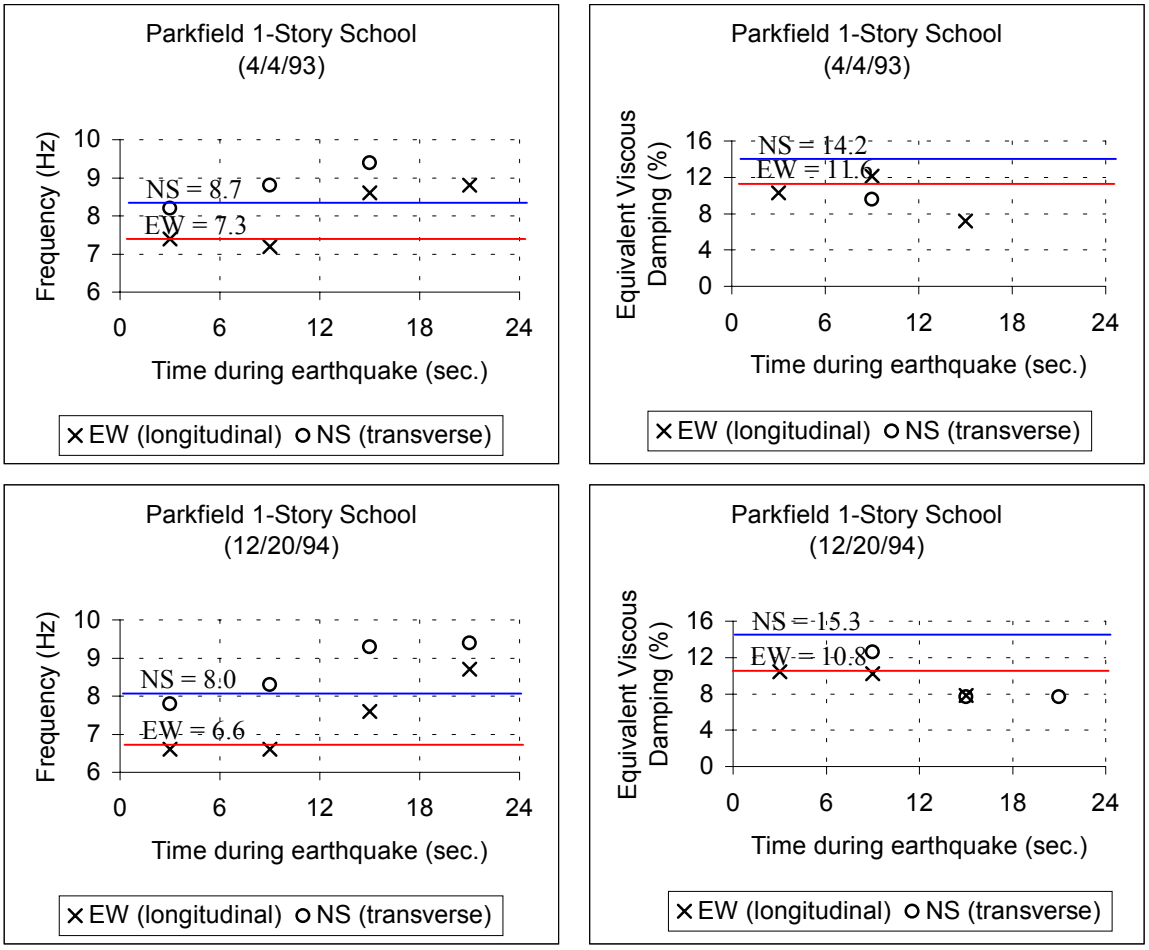

Figure 3.5: MODE-ID Results vs. Time for Parkfield 1-Story School

Figure 3.6 shows the windowing analysis results as functions of peak roof drift ratios, illustrating the amplitude dependence of the building stiffness and damping. Note that the fundamental frequencies and damping ratios generally decreased and increased, respectively, with increasing drift ratios, although this was not the trend for the higher drift ratios corresponding to low acceleration response (as shaking subsided). This suggests the frequencies and dampings for woodframe buildings may best correlate with acceleration amplitude than with drift.

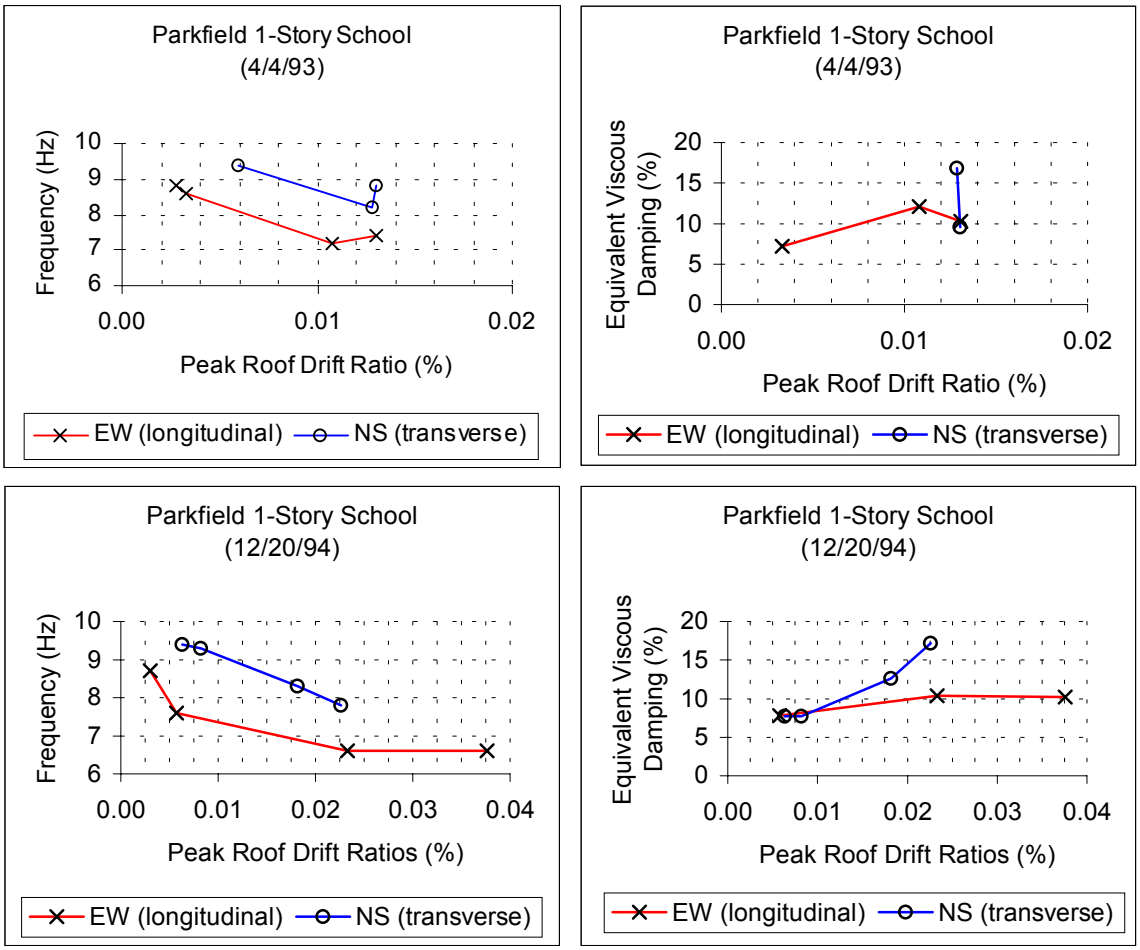

Figure 3.6: MODE-ID Results vs. Drift for Parkfield 1-Story School

3.2.3 Bishop – 1-Story Fire Station

One set of earthquake records obtained at this site was analyzed. This site is a 1-story, rectangular fire station with large door openings on both NS walls. Built in 1983, the structure has plywood shear walls along building perimeter with gypsum board interior finish. There were three channels in the NS (transverse) direction and three in the EW (longitudinal) direction. Channels 1 and 2 were taken as the input when using MODE-ID (See Figure 3.7).

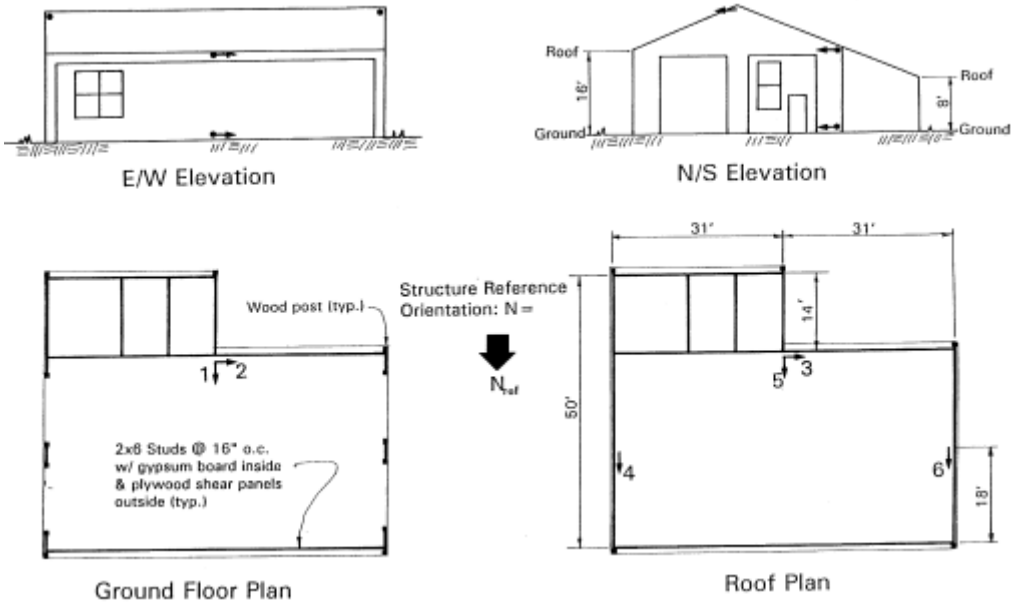

Figure 3.7: Bishop 1-Story Fire Station

The earthquake of May 17, 1993, recorded at this site, had magnitude $M_L = 6.0$. The horizontal maximum acceleration generated in the structure was 4.4%g. Modal analysis of this earthquake record has revealed that the structure's time-invariant fundamental periods (frequencies) are 0.18 sec (5.6 Hz) in the NS direction and 0.11 sec (8.7 Hz) in the EW direction. Note that the longer period is in the NS direction, which has considerably less shear walls than the EW direction. The time-invariant damping ratio is 7.0% in the NS direction and 12.2% in the EW direction. Note that the higher damping ratio is in the EW direction, which has considerably more shear

wall length. Plots of the recorded and predicted response time histories for selected channels are shown in Figure 3.8 and in Appendix B (Figures B.9 and B.10).

Windowing analysis (breaking up the records into 6 second windows) showed that the natural frequencies and damping ratios change throughout the earthquake excitation (see Figure 3.9, where time-invariant values are solid lines). These frequencies were lowest at the time of strongest shaking (second window) and returned to their initial value as shaking subsided. Figure 3.10 shows the windowing analysis results as functions of peak roof drift ratios, illustrating the amplitude dependence of the building frequencies and damping ratios. Note that the peak roof drift values in the longitudinal direction were considerably lower than in the transverse direction. The transverse direction fundamental frequencies and damping ratios showed some variation with drift and were generally lower and higher, respectively, at the larger peak roof drift values.

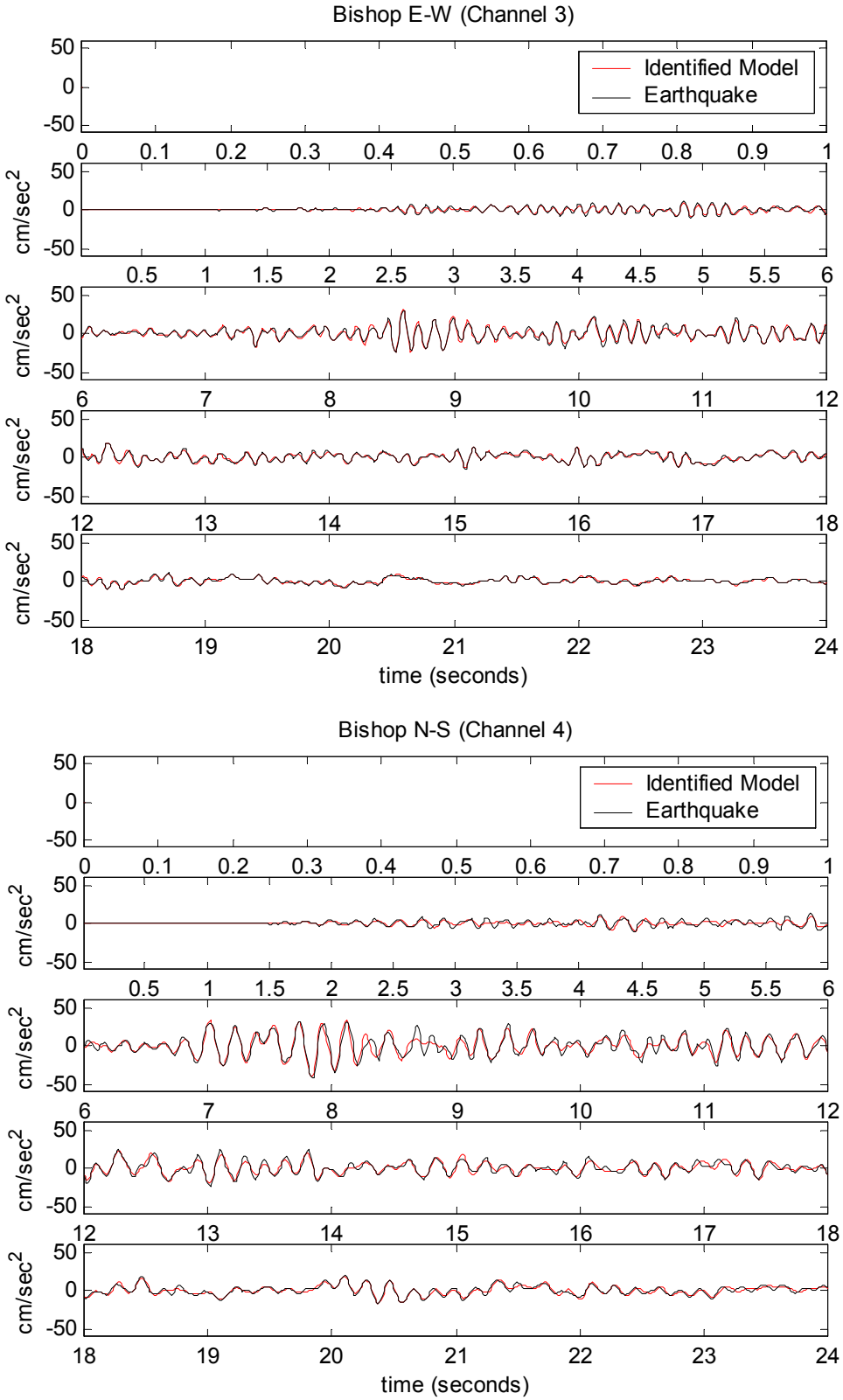

Figure 3.8: Predicted Response Using MODE-ID Time-Invariant Results (Bishop 1-story firestation channels 3 and 4)

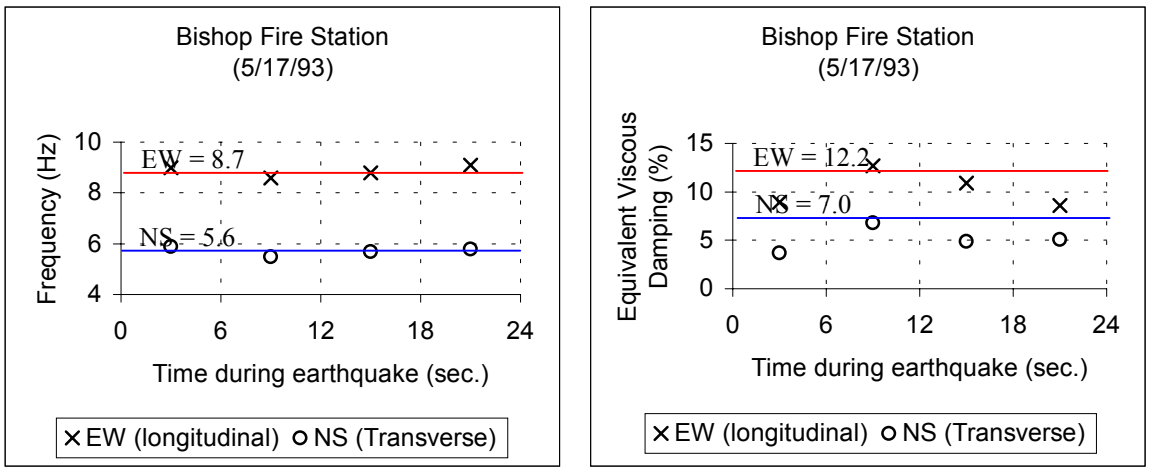

Figure 3.9: MODE-ID Results vs. Time for Bishop 1-Story Firestation

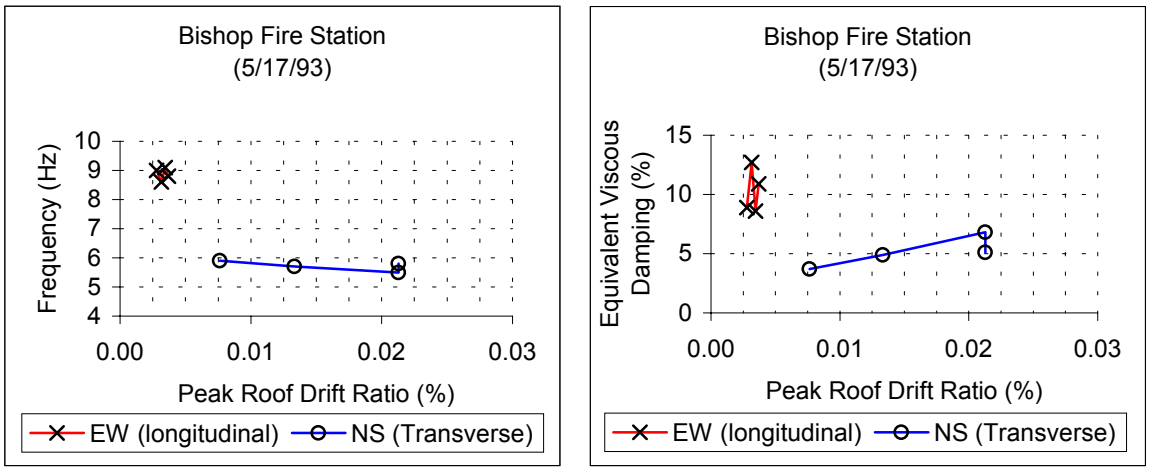

Figure 3.10: MODE-ID Results vs. Drift for Bishop 1-Story Firestation

3.2.4 Eureka – 2-Story Office Building

One set of earthquake records obtained at this site was analyzed. This site is a 2-story building built in 1992 with plywood shear walls along perimeter walls and at interior wall on first floor, and with gypsum board interior wall on second floor. There were three channels in the NS (longitudinal) direction and three in the EW (transverse) direction. Channels 2 and 3 were taken as the input when using MODE-ID (See Figure 3.11).

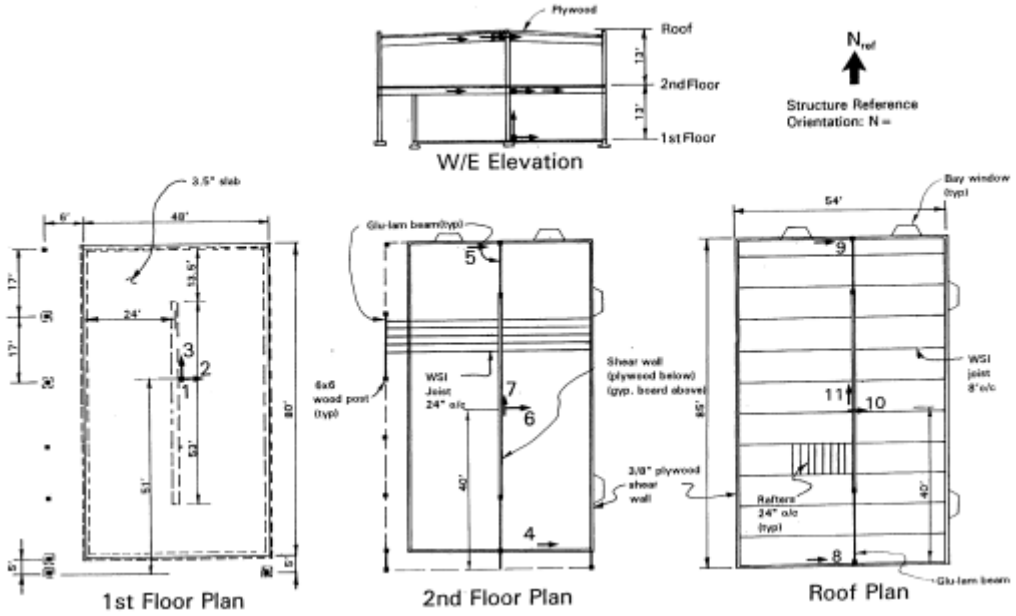

Figure 3.11: Eureka 2-Story Office Building

The earthquake of February 8, 1995, recorded at this site, had magnitude $M_L = 3.9$. The horizontal maximum acceleration generated in the structure was 6.2%g. Modal analysis of this earthquake record has revealed that the structure's time-invariant fundamental periods (frequencies) are 0.17 sec (5.8 Hz) in the NS direction and 0.20 sec (4.9 Hz) in the EW direction. Note that the longer period is in the EW direction, which has less shear walls than the NS direction. The time-invariant damping ratio is 16.5% in the NS direction and 14.9% in the EW direction. Note that the higher damping ratio is in the NS direction, which has more shear wall length

than the EW direction. A sample plot of the recorded and predicted response time histories for a selected channel is given in Appendix B (Figure B.11).

Windowing analysis (breaking up the records into 6 second windows) showed that the natural frequencies and damping ratios change throughout the earthquake excitation (see Figure 3.12, where time-invariant values are solid lines). These frequencies were lowest at the time of strongest shaking (first window) and returned to a higher value as shaking subsided. Figure 3.13 shows the windowing analysis results as functions of peak roof drift ratios, illustrating the amplitude dependence of the building stiffness and damping. The fundamental frequencies and damping ratios were generally lower and higher, respectively, at the larger peak drift values.

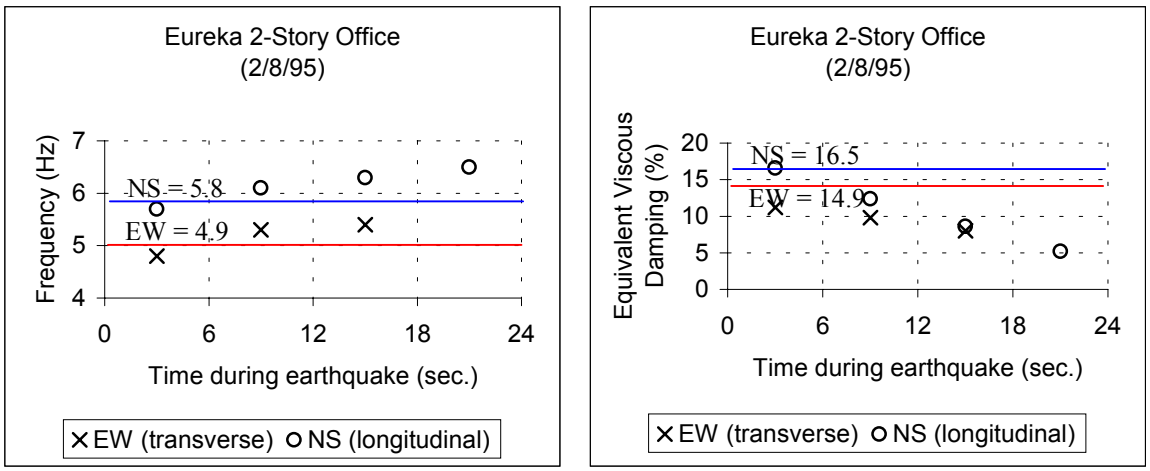

Figure 3.12: MODE-ID Results vs. Time for Eureka 2-Story Office Building

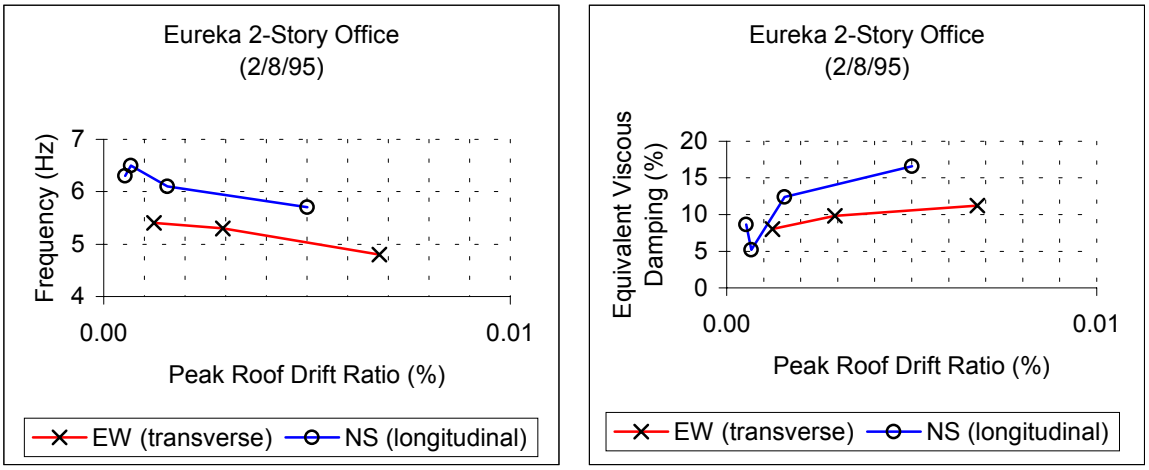

Figure 3.13: MODE-ID Results vs. Drift for Eureka 2-Story Office Building

3.2.5 Indio – 1-Story Hospital

One set of earthquake records obtained at this site was analyzed. This site is a 1-story building built in 1981 with plywood shear walls distributed along the first floor. There were three channels in the NS direction and three in the EW direction. Channels 1 and 2 were taken as the input when using MODE-ID (See Figure 3.14).

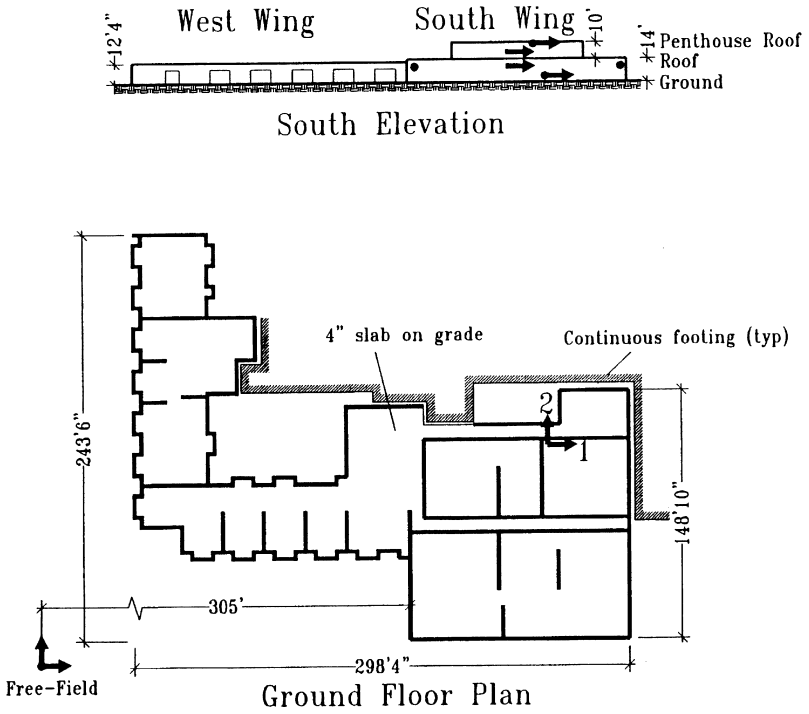

Figure 3.14: Indio 1-Story Hospital

The earthquake of July 25, 1997, recorded at this site, had magnitude $M_L = 4.9$. The horizontal maximum accelerations generated in the structure were 8.3%g. Modal analysis of this earthquake record has revealed that the structure's time-invariant fundamental periods (frequencies) are 0.14 sec (7.1 Hz) in the NS direction and 0.13 sec (7.9 Hz) in the EW direction. The time-invariant damping ratio was 6.3% in the NS direction and 8.9% in the EW direction. Plots of the recorded and predicted response time histories for selected channels are given in Appendix B (Figures B.12 and B.13).

Windowing analysis (breaking up the records into 6 second windows) showed that

the natural frequencies of vibration for this building change throughout the earthquake excitation (see Figure 3.15, where time-invariant values are solid lines). These frequencies were lowest at the time of strongest shaking (second window) and returned to a higher value as shaking subsided. Figure 3.16 shows the windowing analysis results as functions of peak roof drift ratios, illustrating the amplitude dependence of the building stiffness and damping. The fundamental frequencies and damping ratios were generally lower and higher, respectively, at the larger peak roof drift values.

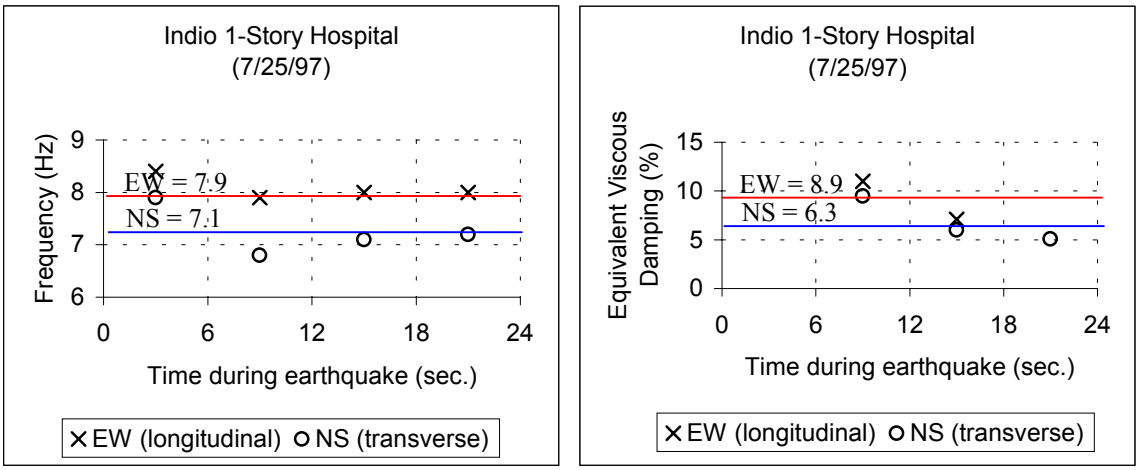

Figure 3.15: MODE-ID Results vs. Time for Indio 1-Story Hospital

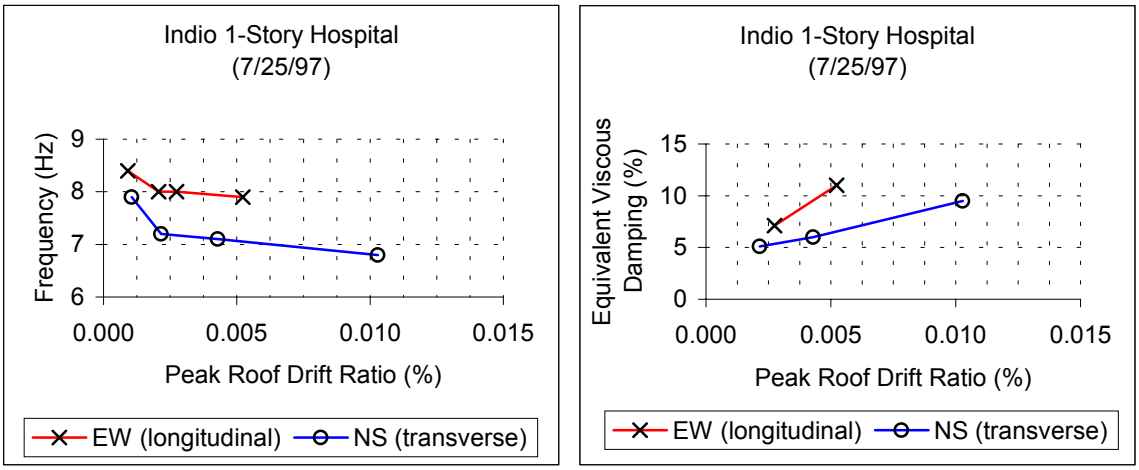

Figure 3.16: MODE-ID Results vs. Drift for Indio 1-Story Hospital

3.3 Discussion of Results

The time-invariant results from the MODE-ID analysis of the 8 sets of building records are summarized in Table 3.1. The normalized mean squared error (NMS Error), defined as $J(\underline{a})$ in equation 3.4 divided by the mean square response (which corresponds to the same expression as $J(\underline{a})$ in Equation 3.4 but with all the x_i's equal to zero), is also given as Jnorm in Table 3.1 for each set of records analyzed. Note that the values of Jnorm for the analysis of the San Bernardino 3-story motel are considerably higher than those for all other buildings (fit is not as good). Another way to evaluate the fit is to compare the recorded time histories to the response of a model with the modal properties identified by MODE-ID. Appendix B shows plots of recorded and predicted time histories at selected channels for every building analyzed.

Table 3.1: Summary of Building Dynamic Characteristics from Earthquake Records

		San Bernardino			Parkfield		Bishop	Indio	Eureka
Building Height (Top of Roof)		30'			13'		17'	14'	26'
Length	(Longit.)	180'			48'		62'	298'	80'
	(Transv.)	132'			30'		50'	148'	54'
Date of Earthquake		6/28 1997	7/26 1997	3/11 1998	4/4 1993	12/20 1994	5/17 1993	7/25 1997	2/8 1995
Peak Response (%g)		9.2	7.8	7.1	12.3	20.1	4.4	8.2	6.2
Total Drift (mm)	(Longit.)	0.7	0.7	0.8	0.5	0.9	1.1	0.4	0.4
(Roof w.r.t. Base)	(Transv.)	0.6	0.7	0.7	0.5	1.5	0.2	0.2	0.5
Periods (sec)	(Longit.)	0.22	0.20	0.23	0.14	0.15	0.11	0.13	0.17
(First Mode)	(Transv.)	0.19	0.21	0.18	0.11	0.13	0.18	0.14	0.20
Frequency (Hz)	(Longit.)	4.6	5.0	4.4	7.3	6.6	8.7	7.9	5.8
(First Mode)	(Transv.)	5.4	4.8	5.6	8.7	8.0	5.6	7.1	4.9
Damping Ratio (%)	(Longit.)	13.6	14.1	7.7	11.6	10.8	12.2	8.9	16.5
(First Mode)	(Transv.)	17.3	6.9	11.7	14.2	15.3	7.0	6.3	14.9
Jnorm	(Longit.)	0.337	0.458	0.148	0.058	0.081	0.063	0.143	0.083
(NMS Error)	(Transv.)	0.495	0.733	0.621	0.136	0.150	0.127	0.181	0.259

The fundamental frequency estimates for the different earthquakes recorded at the San Bernardino and Parkfield buildings are quite consistent, since the drifts are at similar levels and the uncertainty in the estimates of the fundamental frequencies is relatively small if the drift levels are comparable from test to test. The periods listed in Table 3.1 have been used in developing the period regression formula based on structural height that is presented later in this report (see Chapter 6).

The damping ratios shown in Table 3.1 are quite high, and these values are close to those from the time windows with the highest shaking amplitudes. This occurs because the prediction error minimized in MODE-ID places more weight on the higher amplitude sections of the record. The damping ratios obtained are consistent with the damping levels exhibited in the UCSD shaking table tests of Task 1.1.1, described in section 5.1 (also, see Fischer et al., 2001). The fundamental damping estimates vary significantly for the San Bernardino building for different earthquake records. This could be partly because the instrumentation layout, with input channels located only at the north building at one end, may not capture well the excitation of the structure, resulting in the poorer fit (higher values of Jnorm) observed. However, the uncertainty in the damping estimates is generally larger than for the natural frequencies even when the excitation is well defined, partly because the assumed linear viscous damping may not be a good model for the actual damping mechanisms and partly because the seismic response of the model is not nearly as sensitive to changes in the damping level as it is to changes in the natural frequencies.

Chapter 4

Field Tests

Several woodframe buildings were tested during the course of this research. This section describes the method used for system identification using ambient and forced vibration tests, and it also details the five buildings that were tested using an eccentric-mass shaker. The results are summarized in section 4.3 at the end of this chapter.

4.1 Ambient Vibration Surveys

Ambient vibration tests were performed on a number of houses and apartment buildings in the Los Angeles area. These tests measured naturally occurring ambient vibrations induced by wind, traffic, or other sources. The testing procedure consisted of placing Ranger seismometers throughout the structure and recording the response of the building for three minutes.

Analysis of ambient vibration data consisted of examining the Fast Fourier Transform of the recorded time histories and then processing the cross-correlated data using MODE-ID. The FFT method provided information regarding the frequency content of the data and was especially helpful in setting up for the forced vibration tests. To use MODE-ID, first the data were cross-correlated with a reference channel because the theoretical cross-correlations for a linear system satisfy the equation of motion for free vibrations with the time lag as the pseudo-time (Beck et al., 1995). Then MODE-ID was used to analyze the cross-correlated data as if they were free vibrations.

The results from the ambient vibration surveys are summarized in Table 4.1. Figure 4.1 shows an example of ambient vibration Fast Fourier Transform plots. See Figure 4.2 for a sample plot of empirical and identified (i.e., best fit) cross-correlation functions. It should be noted that, at longer time lags, theoretical cross-correlation functions are poor estimates of the empirical ones.

Table 4.1: Building Dynamic Characteristics from Ambient Vibration Tests

Test Site	Building Height	Test Date	1st Mode Frequency (Hz)	
			Transv.	Longit.
1-Story House (South Pasadena)	13'	02-May-00	10.9	11.8
1-Story House 95th st. (Los Angeles)	10'	09-May-00	13.0	15.0
			12.5	N/a
1-Story House/Office (Los Angeles)	10'	09-May-00	12.7	N/a
			13.5	15.0
1-Story House 99th st. (Los Angeles)	10'	11-May-00	12.7	15.5
2-Story House (South Pasadena)	20'	25-Apr-00	9.0	10.7
			9.0	10.5
			9.2	10.4
2-Story House: S. Catalina Ave. (Pasadena)	20'	23-Jun-00	6.5	7.8
3-Story Townhouse (Pasadena)	30'	13-Apr-00	5.1	5.2
			N/a	5.2
3-Story Apartment Building (Pasadena)	30'	07-Jul-00	4.5	5.5

The fundamental frequencies obtained from analysis of the ambient vibration surveys were considerably higher than those obtained from the earthquake records (see Chapter 3) as well as from the forced vibration tests (see section 4.2), even at very low shaking amplitudes. This illustrates the strong amplitude dependence of the periods of woodframe buildings. Since the period formula from regression (see Chapter 6) is intended to represent stronger motion behavior of these buildings, the ambient vibration survey results were excluded from the period database used in the regression analysis.

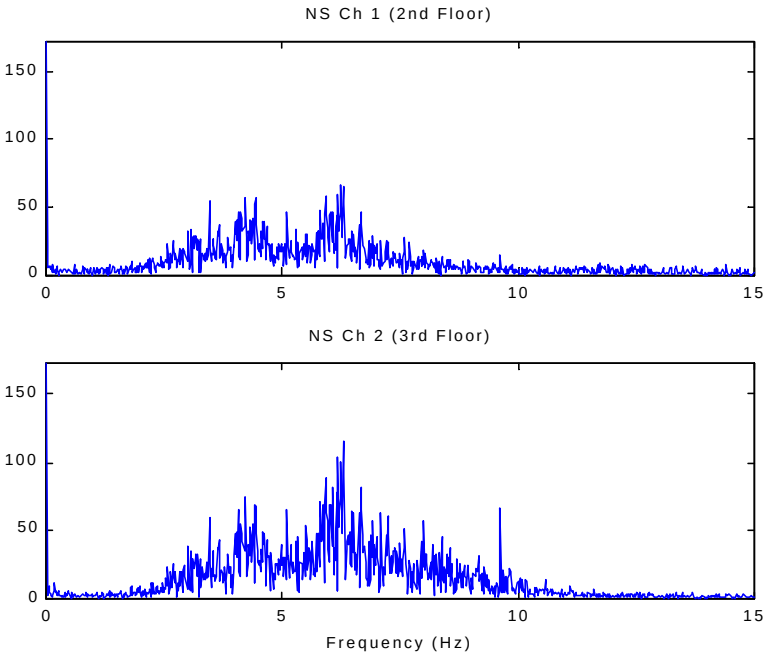

Figure 4.1: 3-Story Townhouse Ambient Vibration Survey FFT

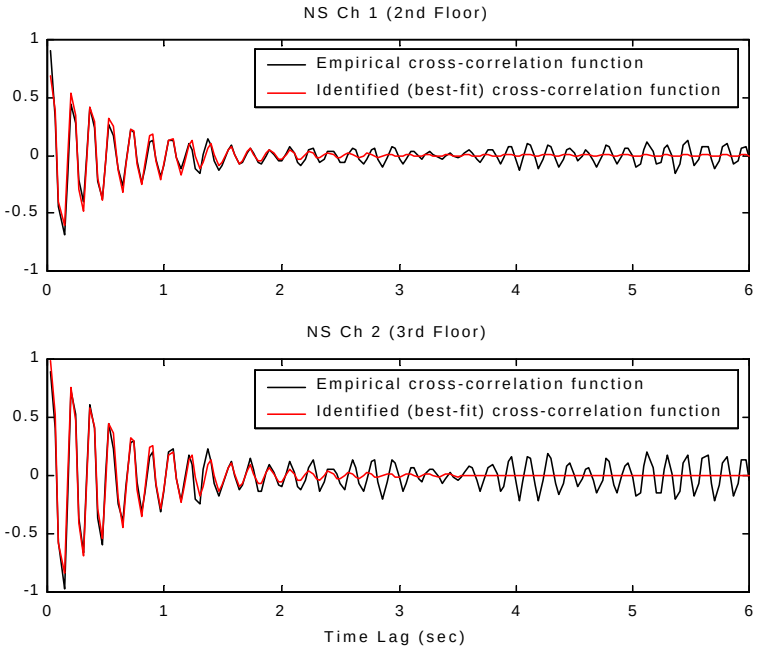

Figure 4.2: 3-Story Townhouse Cross-Correlation Function

4.2 Forced Vibration Tests

The purpose of the forced vibration tests was to fill gaps in the data obtained from the analysis of the earthquake records, providing a more reliable regression analysis result. These tests measured harmonic vibrations induced by a shaking machine borrowed from Harvey Mudd College (HMC), which has a much lower geometrical profile and therefore presented significantly less rocking than the Caltech shaker, making it easier to hold down on wooden floors.

The force delivered by the shaking machine is generated by the centrifugal acceleration of the masses which are attached to the two rotating shafts (see Figure 4.3 for detail). The amplitude of this harmonic force is proportional to mass eccentricity times the frequency squared:

$$F = 98\ e\ f^2 \tag{4.1}$$

where

$$\begin{aligned} F &= \text{ force delivered by shaker, } lbs \\ e &= \text{ eccentricity (weight overlap), between 0 and 1} \\ f &= \text{ shaker frequency, } Hz \end{aligned}$$

Seismometers (output proportional to velocity response), accelerometers (output proportional to acceleration response), or both were used to sample the building response at each driving frequency, then a sinusoidal curve was fit to the time history data to obtain the best (least-squares) approximation to the response amplitude, frequency and phase shift (amplitudes were normalized by the driving frequency squared to account for the increase in force between frequency samplings). Finally, by plotting the frequency-response curves for all data channels, the modal frequencies of the building were identified. The damping ratios were obtained using a curve-fitting approach involving non-linear least-squares matching of the theoretical and empirical frequency response curves, since the half-power bandwidth method cannot accurately estimate damping values from overlapping resonant peaks of the amplitude response

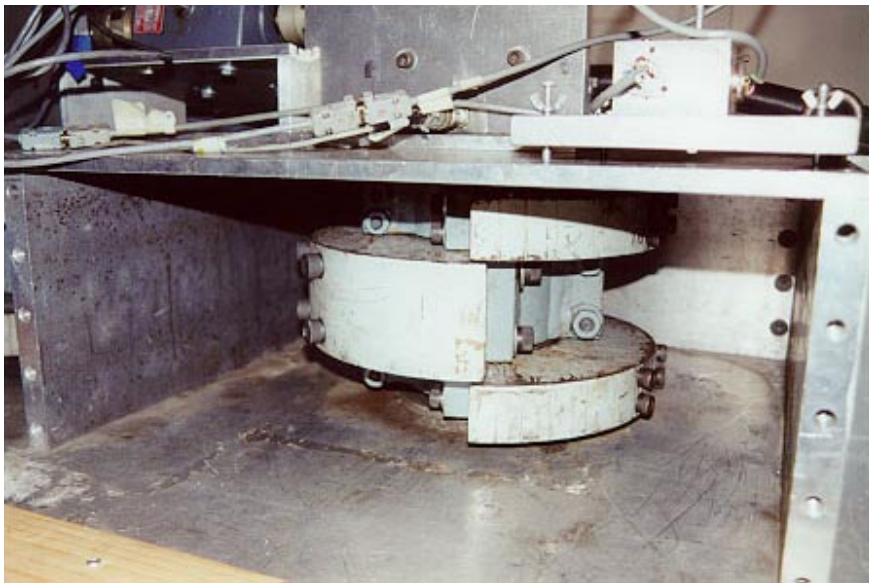

Figure 4.3: Harvey Mudd College Shaker Detail (weights at 2.5% eccentricity)

curves (which occurs when the natural frequencies are close together and damping is large). This curve fitting was performed using a simple *Matlab* routine using the function *fmins* to minimize the expression for the normalized squared error shown in Equation 4.2, where $\widehat{A}_{i,j}$ is the amplitude of the building response recorded at channel i due to shaking at frequency ω_j, $A_{i,j}(\underline{a})$ is the response amplitude (computed using modal parameters $\underline{a}$) at the location of channel i due to shaking at frequency ω_j, N_i is the number of data channels used and N_j is the number of frequencies sampled.

$$J_{norm} = \frac{\sum_{i=1}^{N_i} \sum_{j=1}^{N_j} |\widehat{A}_{i,j} - A_{i,j}(\underline{a})|^2}{\sum_{i=1}^{N_i} \sum_{j=1}^{N_j} |\widehat{A}_{i,j}|^2} \tag{4.2}$$

Finding buildings suitable for forced vibration testing was not an easy task because of the potential for some cosmetic damage. Test candidates were limited to buildings scheduled for demolition or buildings whose owners were not concerned about any cosmetic damage that might occur. The best-suited test candidates were offered by the California Institute of Technology, which owns several buildings in the vicinity of the campus. Test results are described in sections 4.2.1 through 4.2.5 and plots of the raw data are given in Appendix C (Figures C.1 through C.53).

4.2.1 2-Story House on S. Catalina Ave., Pasadena

This 2-story house, owned by the California Institute of Technology and located in the vicinity of the campus, was being used as an undergraduate dormitory at the time of testing on June 23 and 27, 2000 (see Figure 4.4). It was built circa 1940, with first floor over cripple walls and 2000 square feet in plan. It has two brick fireplaces, which have been seismically retrofitted and anchored to the roof. There is a stairway leading to the roof attic. The building has exterior wood shingles, the interior finish is plaster, and the original hardwood floors are still in place.

This building was shaken successfully using the Harvey Mudd shaker. The equipment was setup at the second floor level, placing the shaker at the top of the main stairway over a sheet of plywood and wedged between planks of wood, which were then screwed into the plywood below (see Figure 4.5). The intent was to avoid any damage to the carpeting beneath, so the assembly could not be bolted to the floor. Instead, the shaker assembly was fixed between the landing walls by squeezing it into place, in order to provide maximum shear transfer to the building. Six seismometers and ten accelerometers were located as shown in Figures 4.6 and 4.7, respectively.

Ambient vibration tests were performed prior to the shaking in order to determine the frequency range to be used and also to observe any shift in fundamental frequency due to loss of non-structural stiffness at stronger shaking amplitudes. A frequency scan was also performed, where the shaker winds down from high shaking frequencies while the response time histories are monitored in order to visually identify the resonant frequencies. Analysis of the data obtained from the ambient vibration surveys and frequency scans consisted of taking the Fast Fourier Transform (FFT) of the measured time histories, in order to observe the frequency content of the building response. This analysis was done during the testing, and it helped determine the frequency range for the shaking. See Figure 4.8 for a plot of the ambient vibration survey FFT, which can be compared with the corresponding frequency scan FFT in Figure 4.9 (note the shift in frequency content that can be observed in all the channels).

Figure 4.4: 2-Story House on S. Catalina Ave., Pasadena

Figure 4.5: Experimental Setup

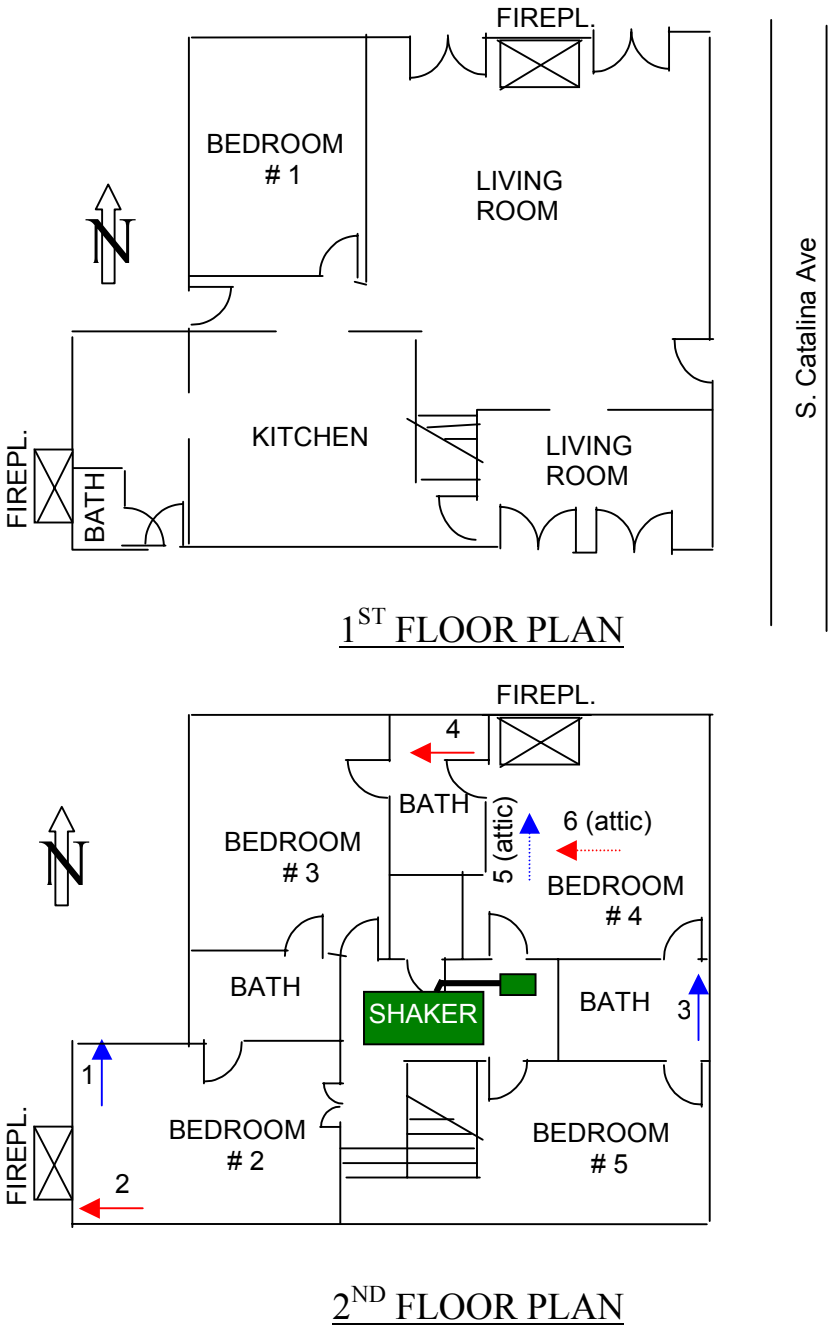

Figure 4.6: Seismometer Locations

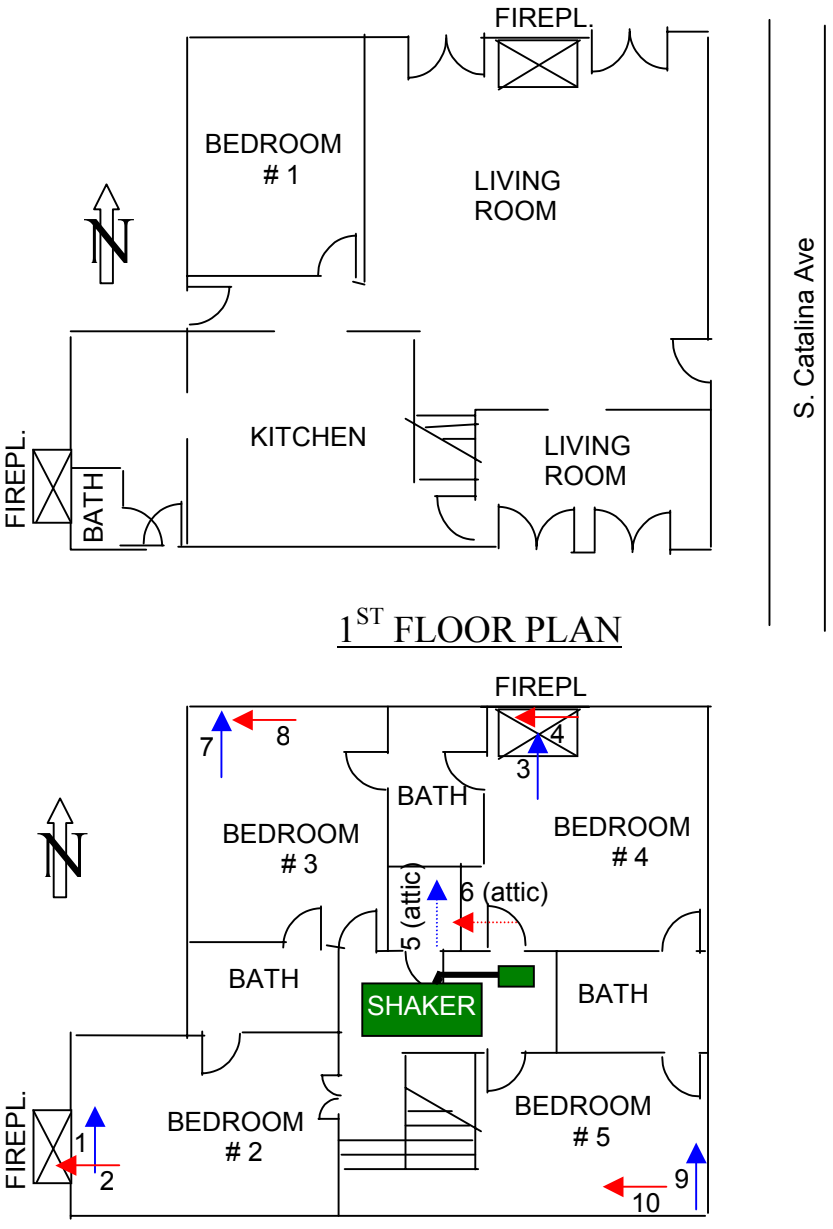

Figure 4.7: Accelerometer Locations

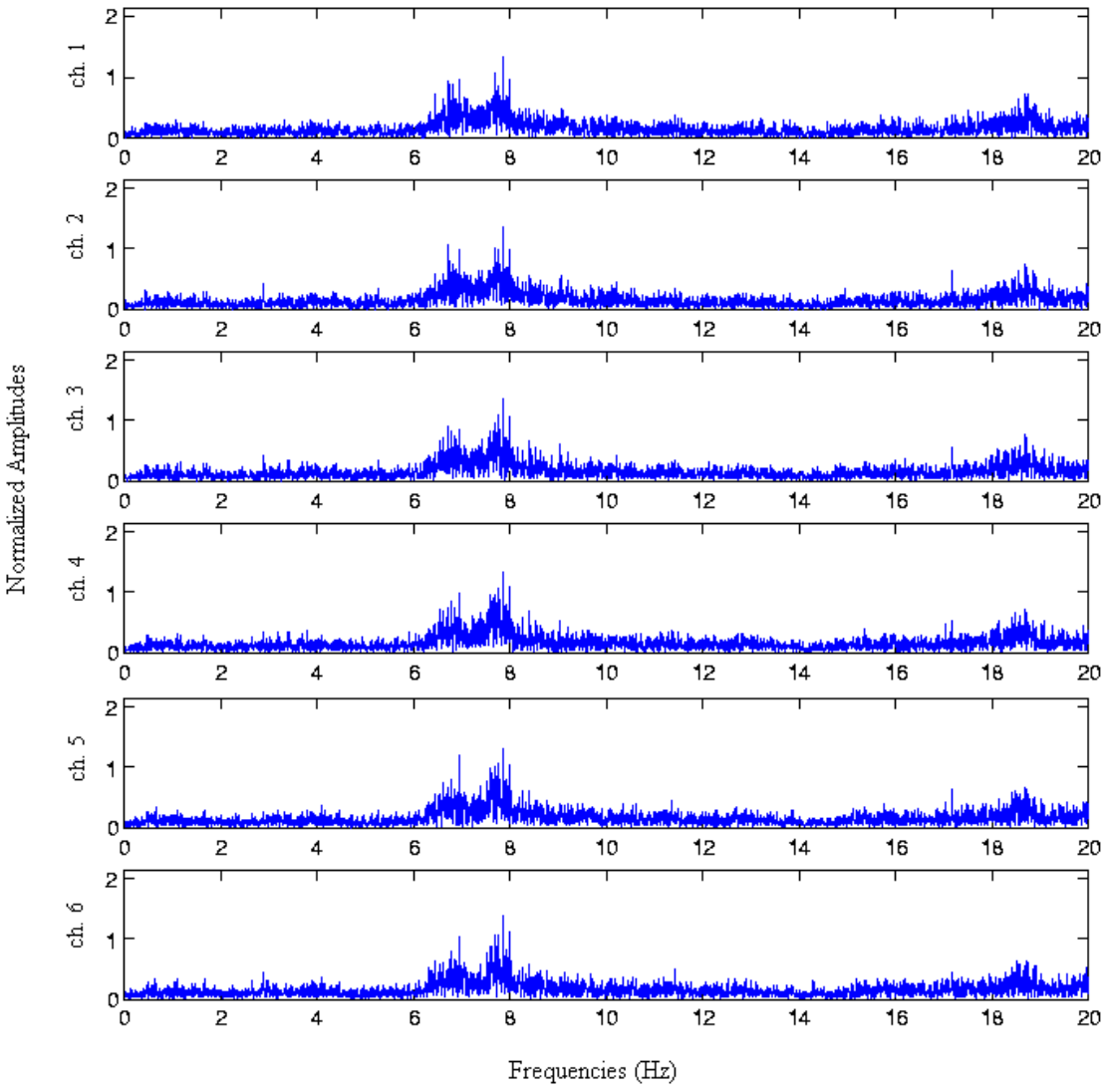

Figure 4.8: Ambient Vibration Survey FFT

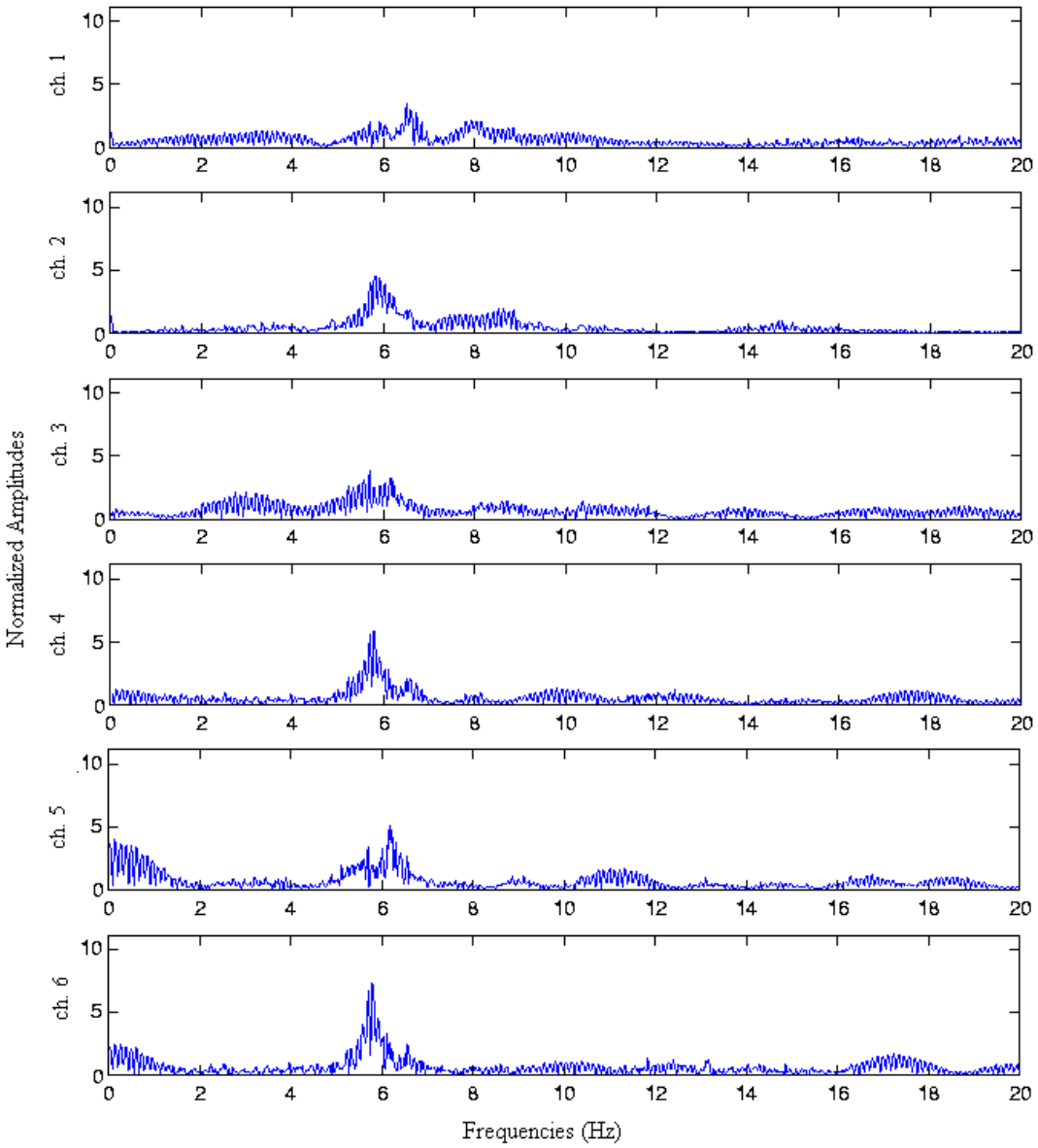

Figure 4.9: Frequency Scan FFT

During the first day of testing, the shaker weights were placed at 2.5% eccentricity. The building response was recorded for shaking in the EW direction between 5.0 Hz and 12.6 Hz, at 0.2 Hz increments, and between 4.6 Hz and 10.0 Hz for the NS direction, also at 0.2 Hz increments. During the next day of testing, the building was again shaken at 2.5% eccentricity and the building response was re-recorded for shaking between 4.5 Hz and 10.0 Hz in each direction, this time at 0.1 Hz increments. Next, the shaker eccentricity was raised to 10% to increase the force levels by a factor of 4, and the building was shaken in the frequency range between 4.0 Hz and 7.0 Hz in the EW direction. Finally, the shaker eccentricity was raised to 20%, a further doubling of the force levels, and the response was recorded for shaking between 4.0 Hz and 7.0 Hz also in the EW direction and with 0.1 Hz increments. Each recording was taken for 5 seconds at 1000 Hz sampling frequency. Plots of the ranger seismometer data for shaking at the resonant frequencies are given in Appendix C, Figures C.1 through C.7 (note the smooth sinusoidal response).

Plots of the test results can be found in Figures 4.10 and 4.11, where the vertical axes are proportional to velocity normalized by the square of the frequency to account for the frequency dependence of the shaker force. Figure 4.12 shows sketches of the floor response at the identified resonant frequencies during EW and NS shaking at selected eccentricities. Figure 4.13 shows a sample of the comparison of the identified model and test frequency-response curves. The identified fundamental modal frequencies and damping ratios are listed in Table 4.2 along with the ambient vibration survey (AVS) results. The maximum drift computed at this structure was 0.14mm at channel W4 for EW shaking at 20% eccentricity.

The identified EW and NS fundamental frequencies are very close together, and Figures 4.10 and 4.11 show that these modes are coupled: all channels are excited in both modes as observed from the double peaks, one at each resonant frequency. Note that shaking in each direction excites all EW and NS channels, and that seismometer channels N1 (NS) and W4 (EW), which were placed near the west and north fireplaces, respectively, show a resonant peak at 6.4 Hz that does not show up in the other channels (see Figure 4.10). This peak may be the fundamental frequency of the

west and north chimneys. The identified transverse and longitudinal fundamental frequencies of 5.5 Hz and 5.7 Hz at 2.5% eccentricity are significantly lower than the corresponding fundamental frequency of 6.5 Hz and 7.8 Hz identified from the ambient vibration survey. Figure 4.11 shows the downward shift in fundamental frequencies with increasing force amplitude, as stronger shaking reduces stiffness in the non-structural components. It should be noted that the amplitude of shaking in the NS direction did not increase significantly as the shaker eccentricity increased from 10% to 20% (see Figure 4.11), indicating that the shaker force did not transfer completely due to sliding and rocking of the shaker observed during NS shaking (shaker transverse direction, see Figure 4.5) at 20% eccentricity.

Table 4.2: Summary of 2-Story House on S. Catalina Ave. Results

Test Date	Shaking Direction	Eccentr.	1st NS		1st EW	
			Freq. (Hz)	Damp.	Freq. (Hz)	Damp.
June 23, 2000	–	AVS	7.8	–	6.5	–
	EW	2.5%	5.7	5.2%	5.5	2.6%
	NS	2.5%	5.6	4.9%	–	–
June 27, 2000	NS	2.5%	5.5	5.0%	–	–
	EW	2.5%	5.7	4.8%	5.5	2.9%
	EW	10%	5.2	6.0%	5.1	2.9%
	EW	20%	5.2	4.1%	4.9	2.7%

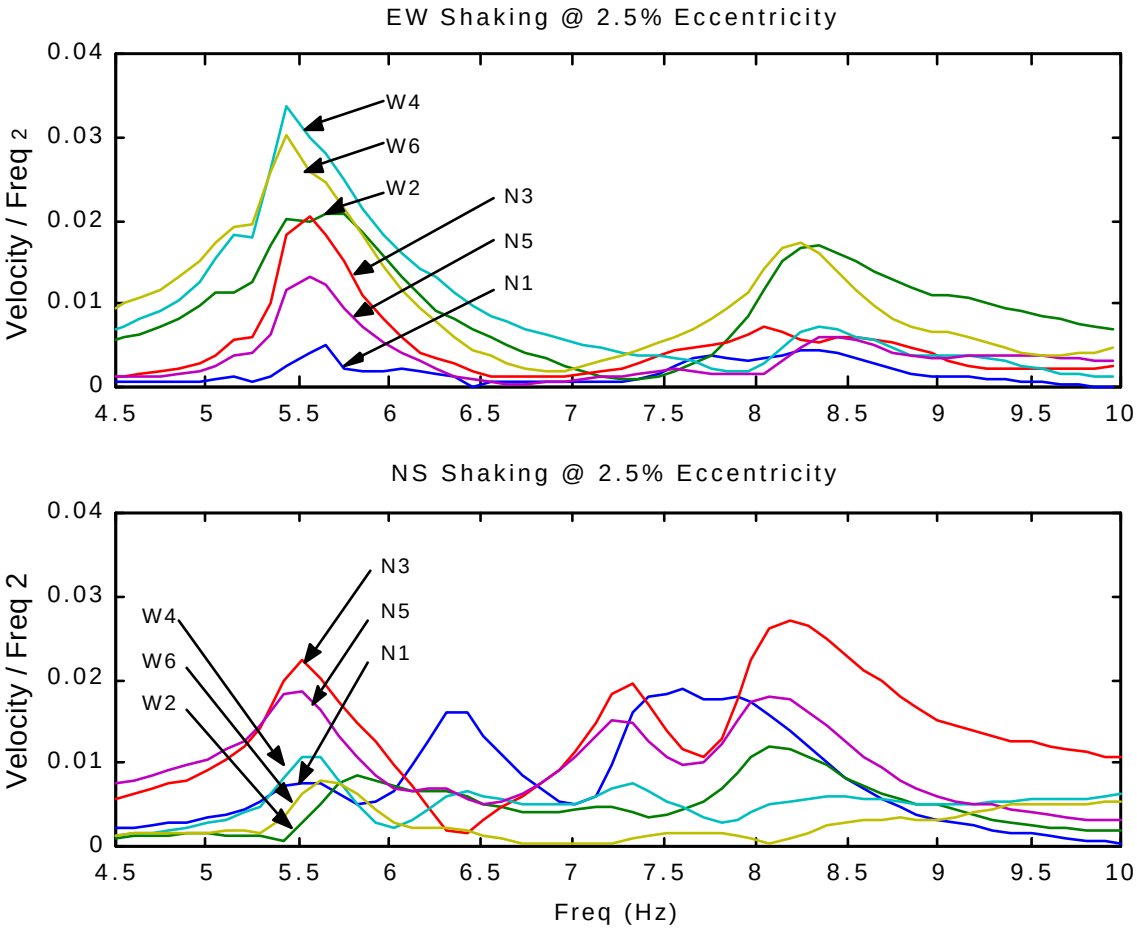

Figure 4.10: Forced Vibration Tests (seismometer results)

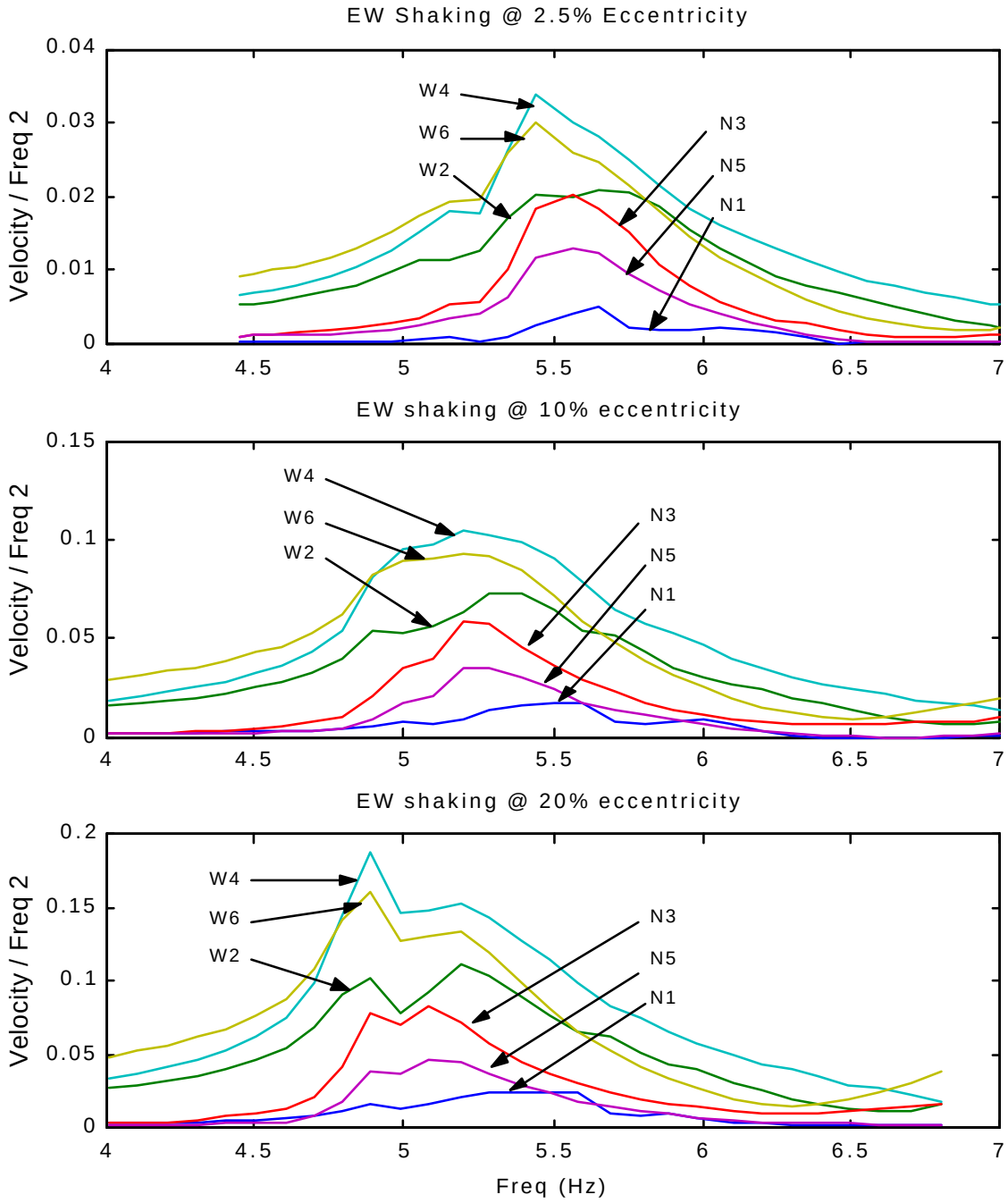

Figure 4.11: Fundamental Frequency Drop with Increased Shaking Force

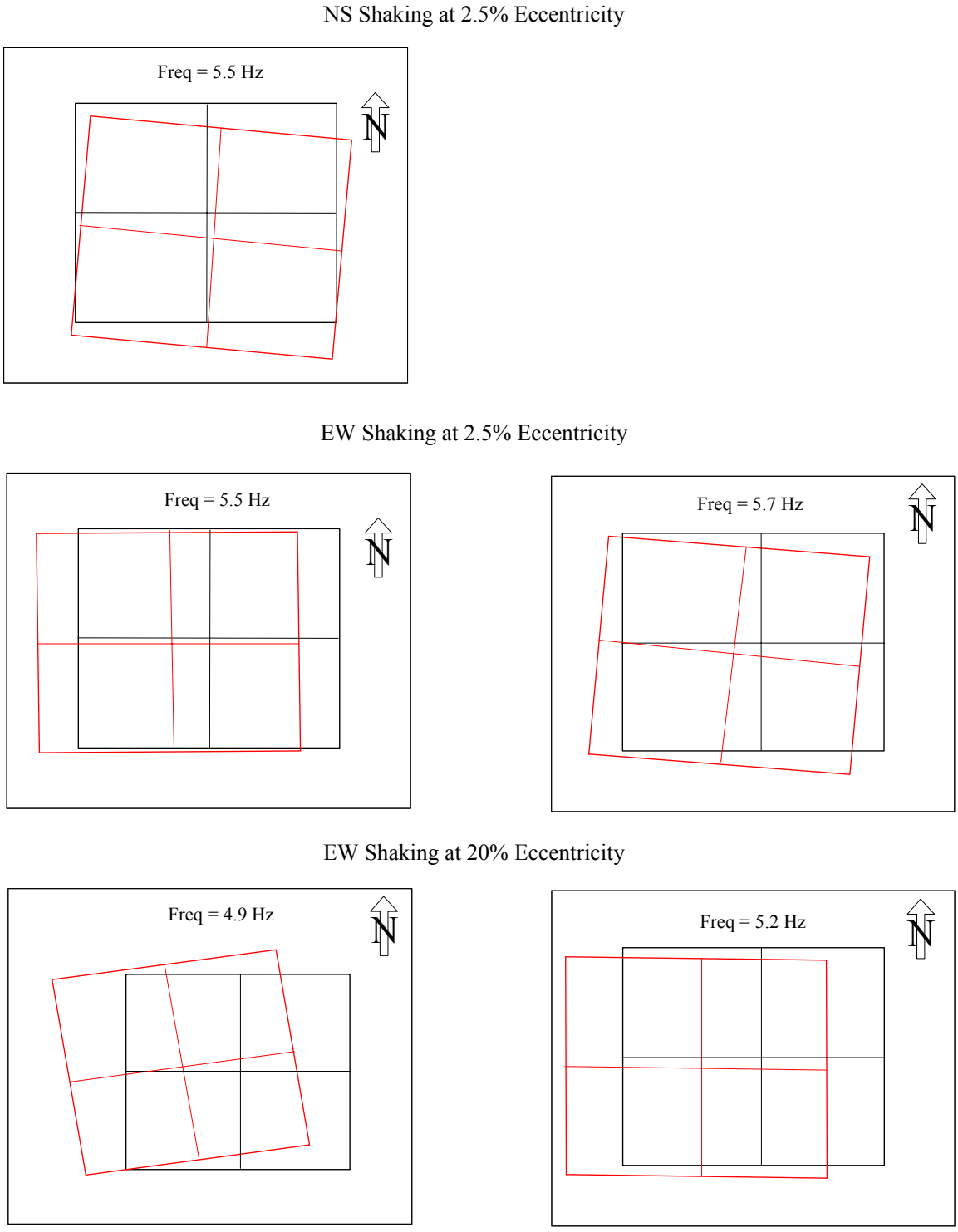

Figure 4.12: 2-Story House 2nd Floor Response During Forced Vibration Tests

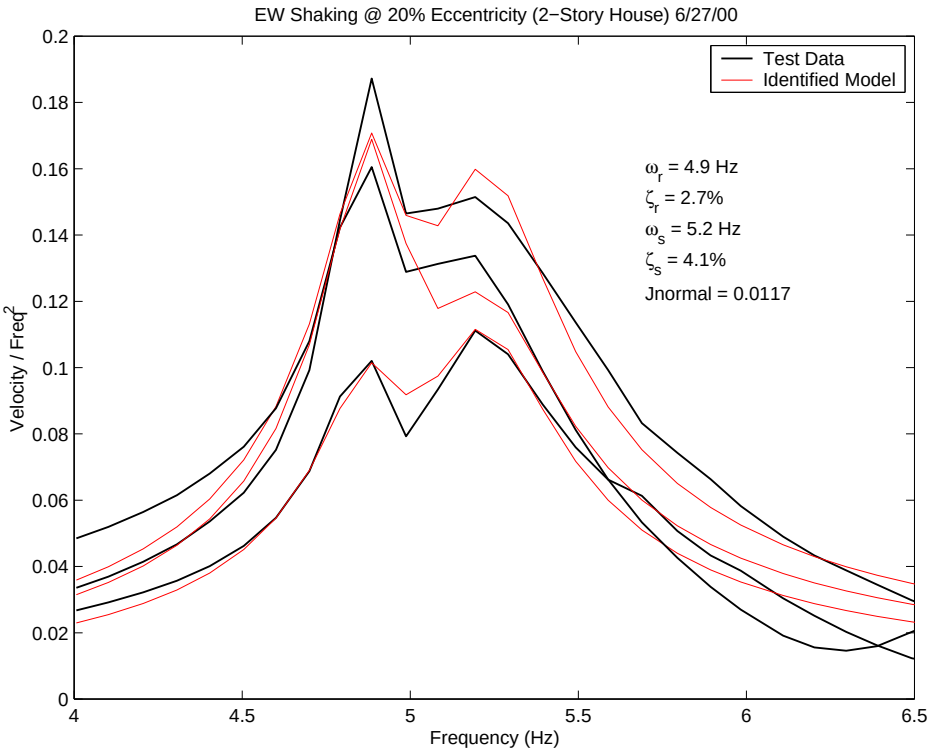

Figure 4.13: Amplitude Response Curves (model and test data)

4.2.2 3-Story Building on E. Del Mar Ave., Pasadena

This apartment building is owned by the California Institute of Technology and is located near the campus (see Figure 4.14). It is currently being used as graduate student apartments. It was built circa 1960. There is an underground parking garage with concrete shear walls below ground level around three sides and the east side of the garage is open. The first floor plan area is approximately 5000 square feet, with an aspect ratio of approximately 3:1. The student apartments are located at the first and second floor levels, and there is a penthouse apartment occupying the third floor. The exterior wall finish is stucco, the interior finish is plaster on drywall, and the flooring is a soundproofing topping (probably lightweight concrete) over sheathing.

This building was shaken successfully using the Harvey Mudd shaker, which was placed at the third floor over a sheet of plywood and wedged between wood planks which were secured to the floor deck below using nails and screws. See Figure 4.15 for a picture of the experimental setup and Figure 4.16 for the seismometer locations.

During the first day of testing, the shaker weights were placed at 2.5% eccentricity. The building response was recorded for shaking between 3.6 Hz and 13.0 Hz, at 0.2 Hz increments, in each direction. During the next day of testing, the building was again shaken at 2.5% eccentricity and the building response was re-recorded for shaking between 4.5 Hz and 10.0 Hz in each direction, this time at 0.1 Hz increments. Next, the shaker eccentricity was raised to 10% and the building was shaken in the frequency range between 4.0 Hz and 7.0 Hz in the EW direction. Finally, the shaker eccentricity was raised to 20% and response recorded for shaking between 4.0 Hz and 7.0 Hz also in the EW direction, again with 0.1 Hz increments. Each recording was taken for 5 seconds at 1000 Hz sampling frequency. Plots of the ranger seismometer data for shaking at the resonant frequencies are given in Appendix C, Figures C.8 through C.14 (note the smooth sinusoidal response).

Figure 4.14: 3-Story Apartment Building on E. Del Mar Ave., Pasadena

Figure 4.15: Experimental Setup

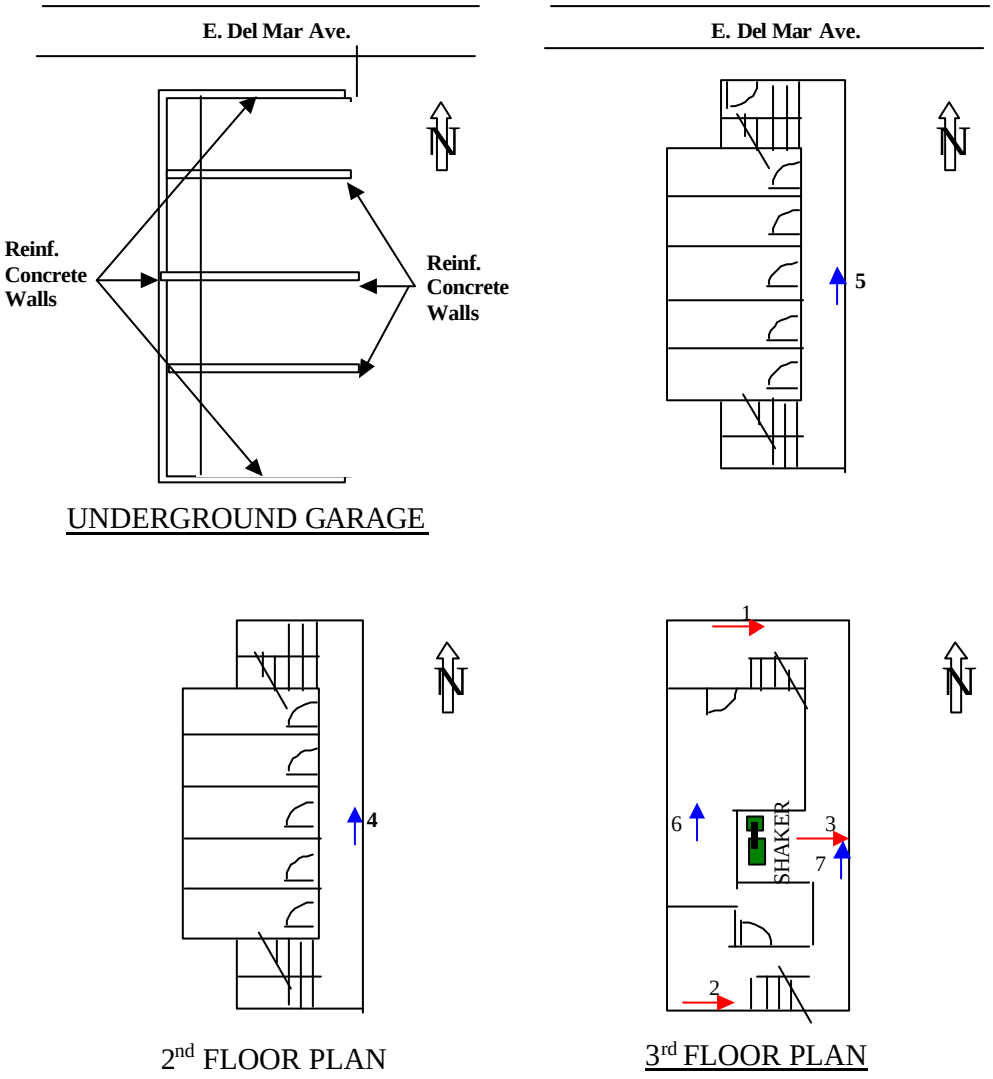

Arrows indicate seismometer locations with corresponding channel numbers

Figure 4.16: Seismometer Locations

Figure 4.17 shows a plot of the ambient vibration survey FFTs. Plots of the results from the forced vibration tests are shown in Figures 4.18 and 4.19 for shaking between 3.6 and 7.0 Hz , and Figure 4.20 shows a sample of the comparison of the theoretical and empirical frequency-response curves. The vertical axes are proportional to velocity normalized by the square of the frequency to account for the frequency dependence of the shaker force. The identified fundamental modal frequencies and damping ratios are listed in Table 4.3 along with the ambient vibration survey (AVS) results. Figure 4.21 shows sketches of the floor response at the identified resonant frequencies during EW and NS shaking at 20% eccentricity.

The maximum drift computed at this structure was 0.13mm at channel N7 for NS shaking at 20% eccentricity. This building showed strong torsional behavior when shaken in the NS direction due to the lack of walls on the east side of the parking garage. Figures 4.18 and 4.19 show that under shaking in the NS direction, both NS and EW channels have peak amplitudes at the NS fundamental frequency (i.e., there is a strong torsional component to that mode). This shows that the floor diaphragm is undergoing almost pure torsion rigidly as it translates in the NS direction in the first NS mode. Note on Figure 4.19 that the ratio of N7 (east wall) to N6 (west wall) motion in the NS mode is large because of the torsional component of the modeshape and because of the lower stiffness of the east wall compared with that of the west wall. This ratio is reduced as the shaker eccentricity is increased from 2.5% to 20%. The fundamental EW modeshape has the highest component of EW motion at the mid-span of the building (channel E3, top of Figure 4.18), which indicates that the floor is bending in plane. The EW modeshape also has a torsional component since channels E1 and E2 have significantly different amplitudes. The difference in diaphragm behavior for shaking in the EW and NS directions is most likely due to the aspect ratio of the floor diaphragm (3:1 in this building). The identified transverse and longitudinal fundamental frequencies of 4.4 Hz and 5.3 Hz at 2.5% eccentricity are close to the corresponding frequencies of 4.5 Hz and 5.5 Hz identified from the ambient vibration survey. Note that the fundamental frequencies of this building lowered as the shaking amplitude increased (see Figure 4.19).

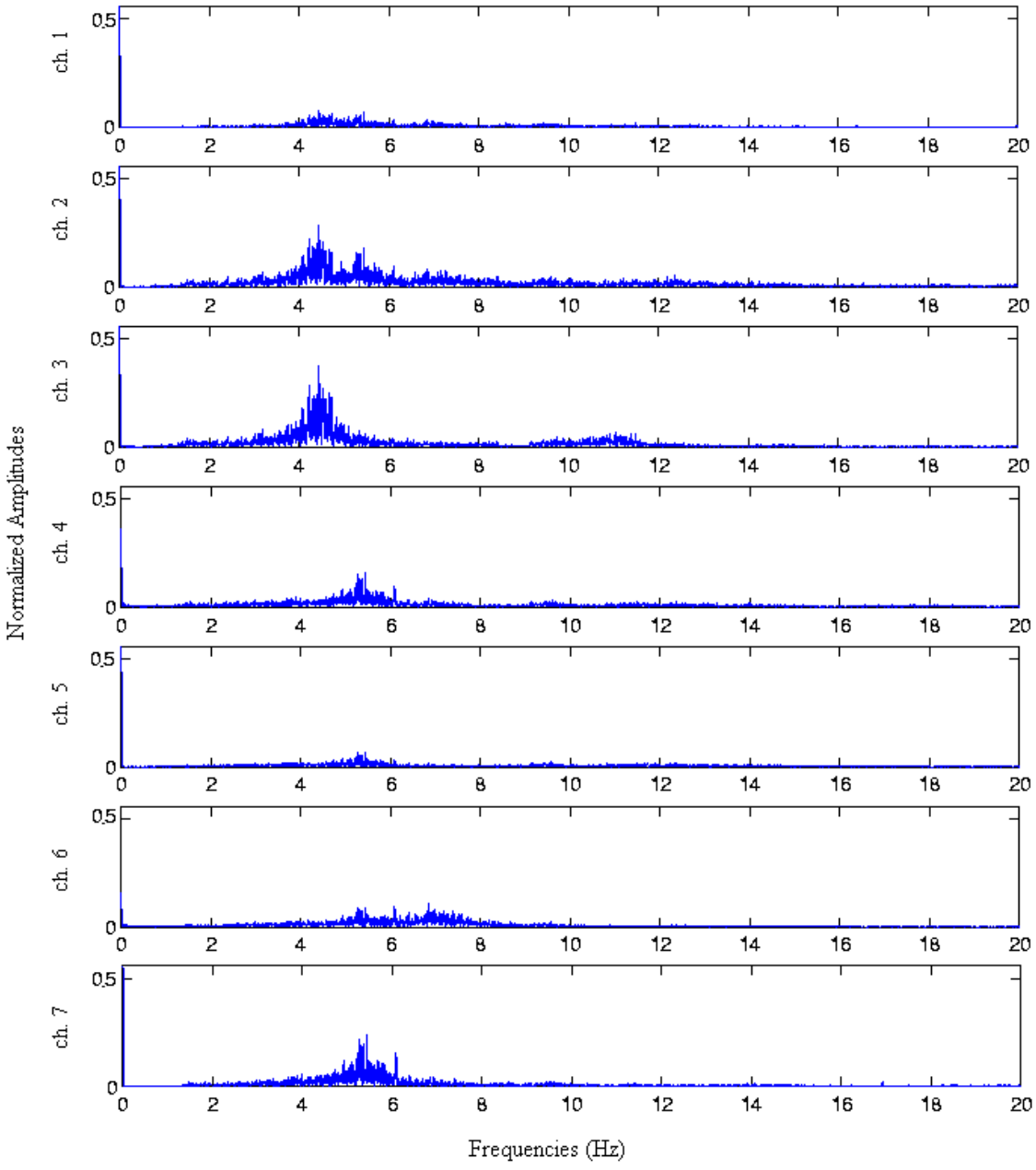

Figure 4.17: Ambient Vibration Survey FFT

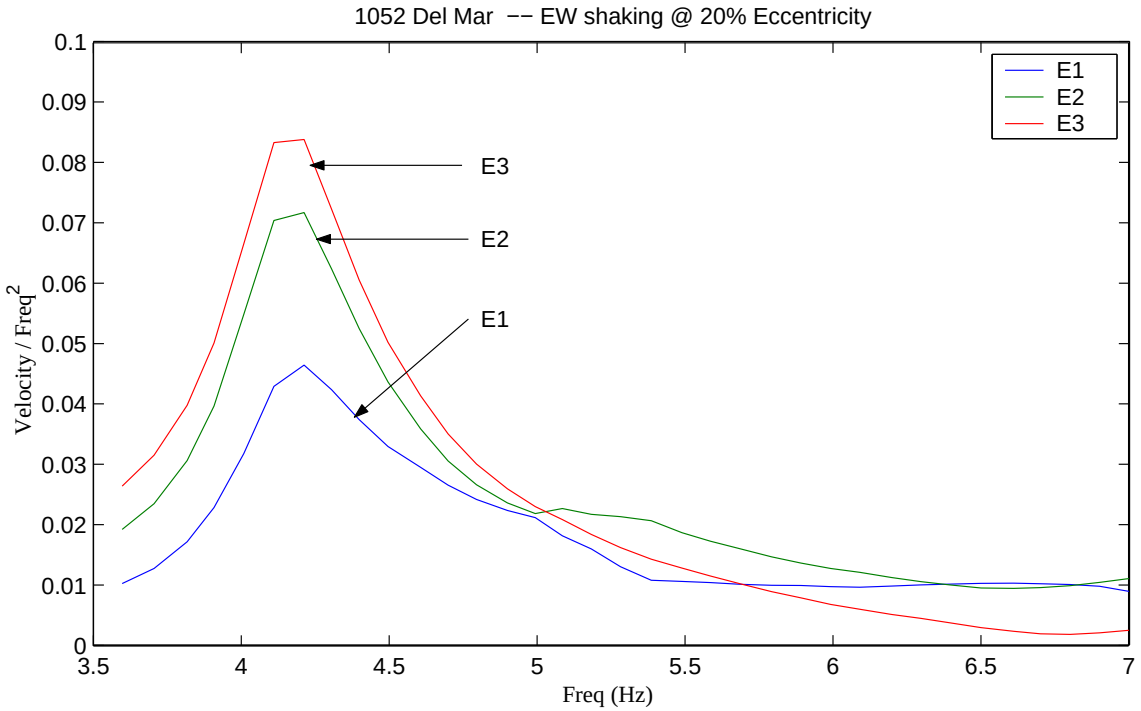

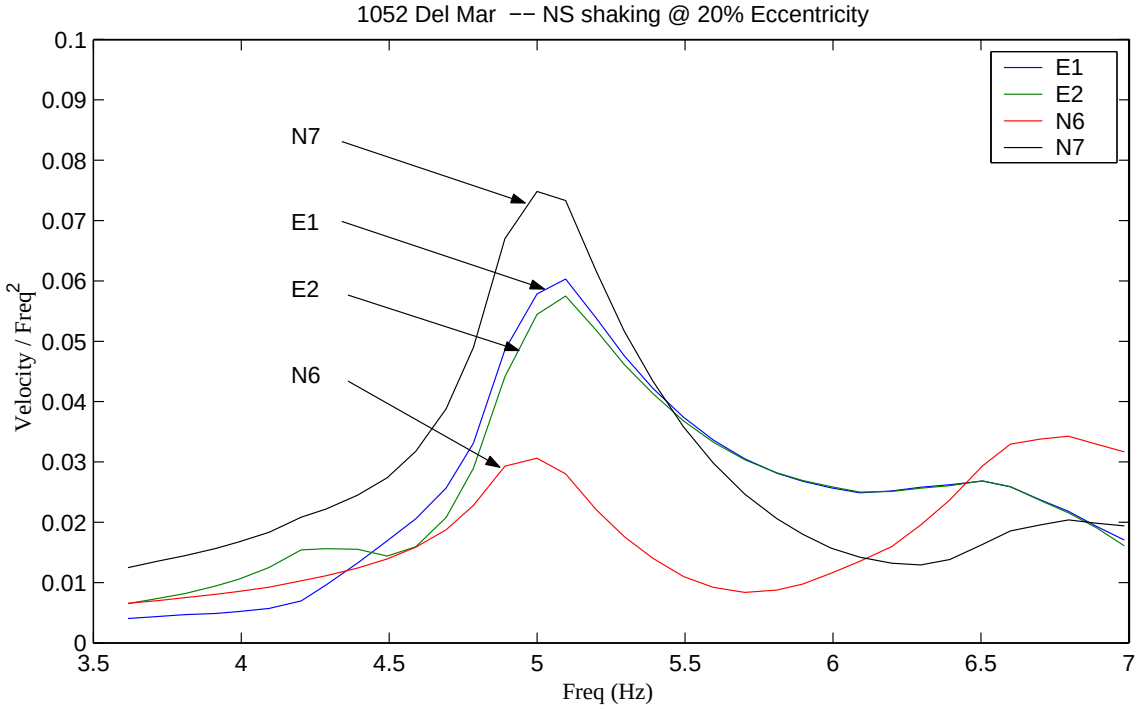

Figure 4.18: Forced Vibration Tests (seismometer results)

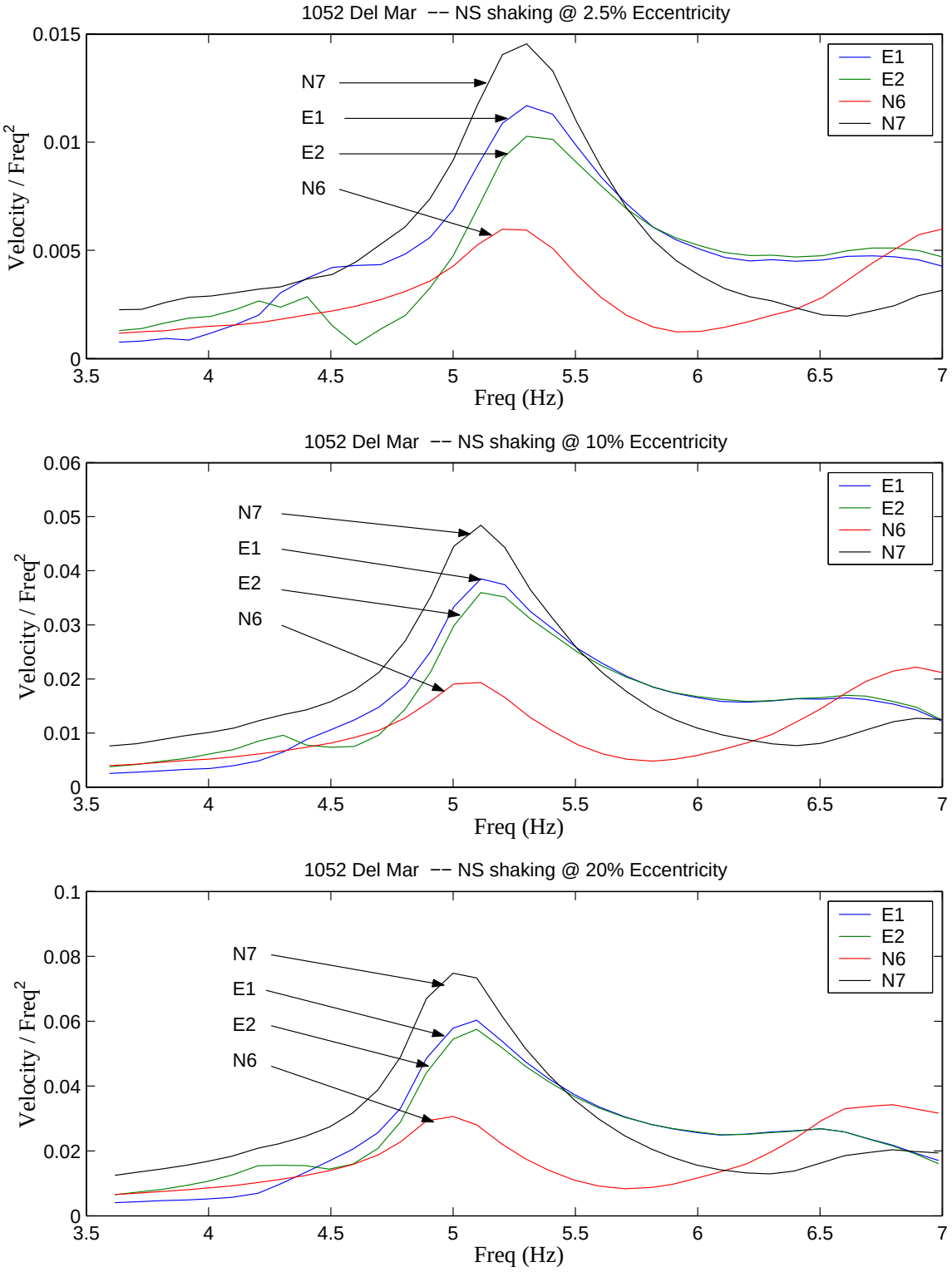

Figure 4.19: Fundamental Frequency Drop with Increased Shaking Force

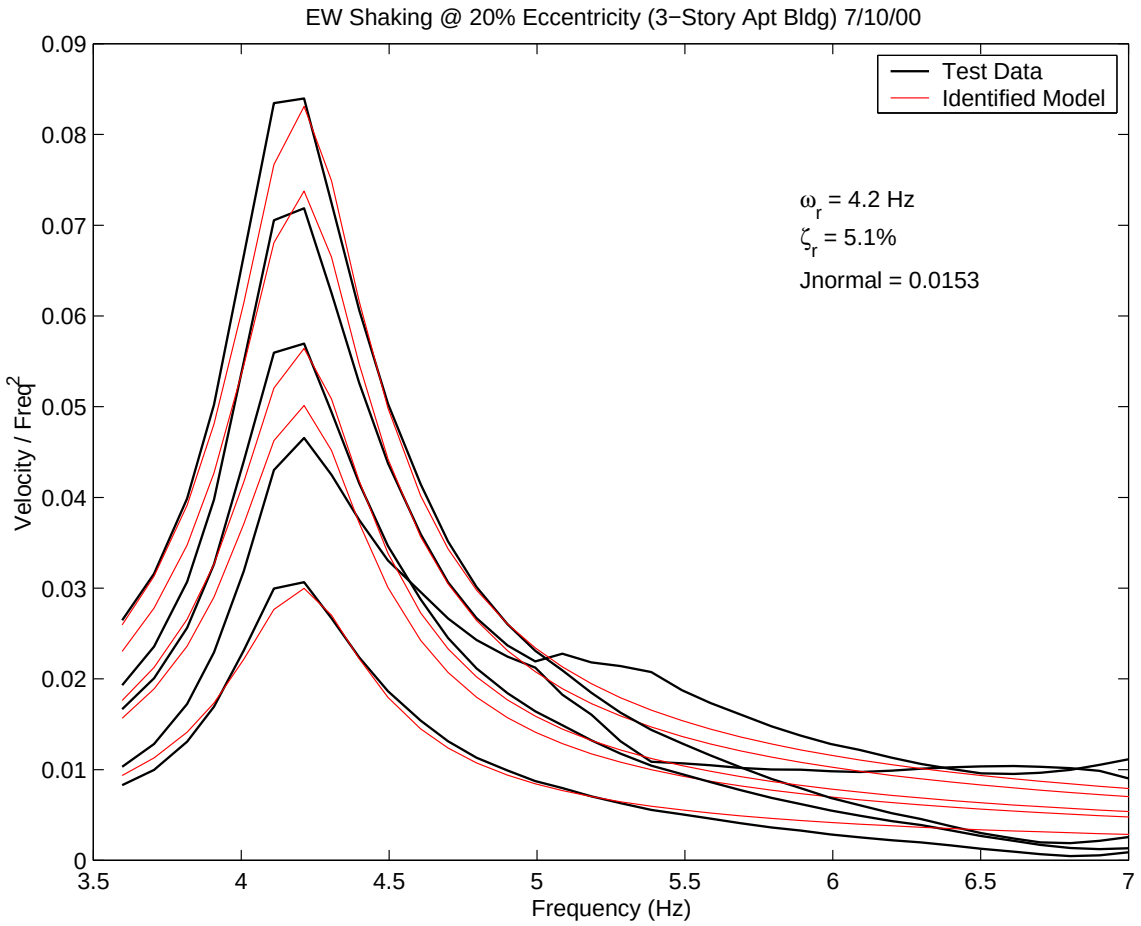

Figure 4.20: Amplitude Response Curves (model and test data)

Table 4.3: Summary of 3-Story Building on E. Del Mar Ave. Results

Test Date	Shaking Direction	Eccentr.	1st NS		1st EW	
			Freq. (Hz)	Damp.	Freq. (Hz)	Damp.
July 7, 2000	–	AVS	5.5	–	4.5	–
	NS	2.5%	5.3	4.7%	–	–
	EW	2.5%	–	–	4.4	4.7%
July 10, 2000	NS	2.5%	5.3	4.4%	–	–
	EW	2.5%	–	–	4.4	4.6%
	NS	10%	5.2	4.6%	4.3	–
	NS	20%	5.1	4.9%	4.2	–
	EW	20%	–	–	4.2	5.1%

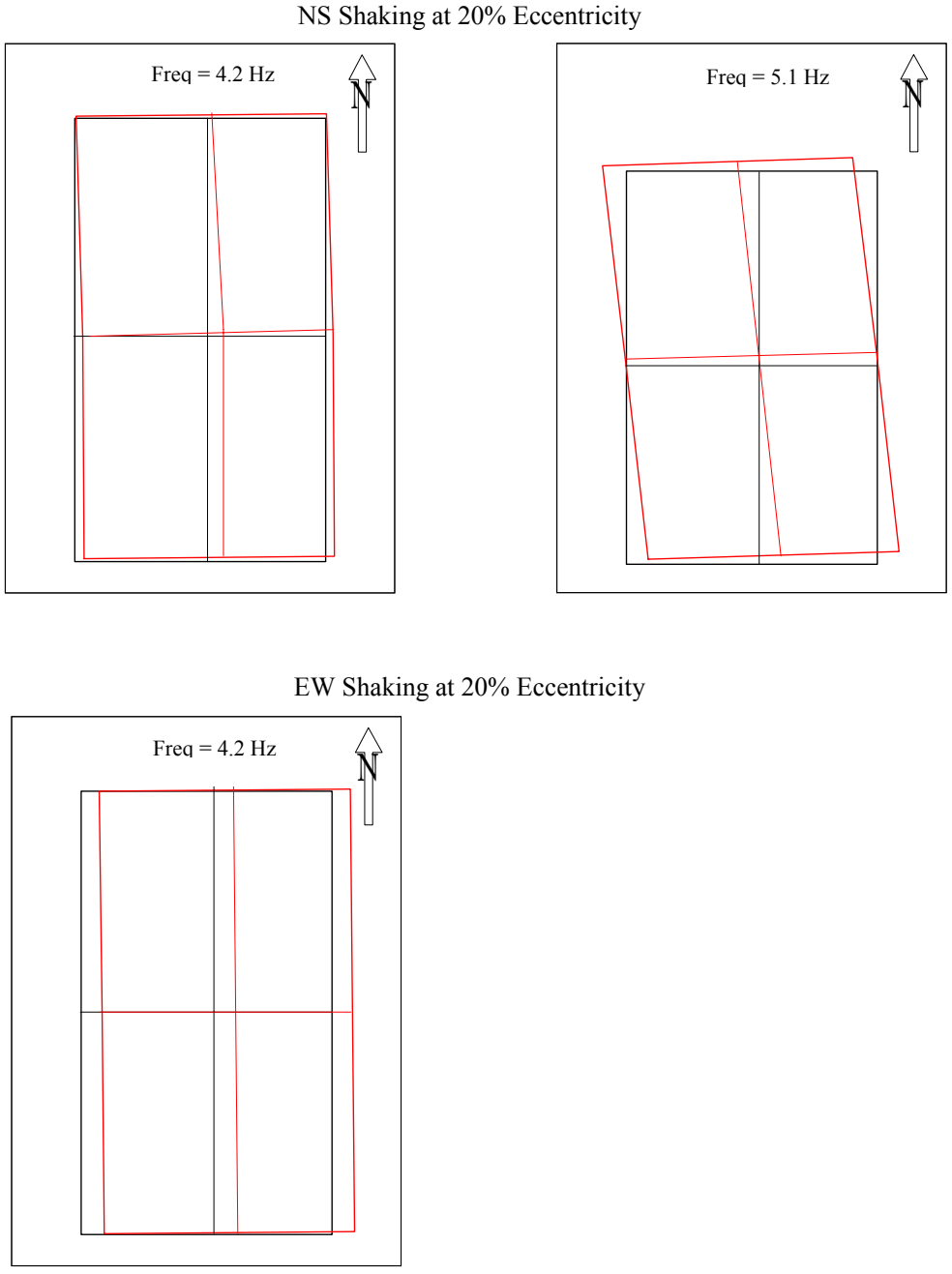

Figure 4.21: 3-Story Building 3rd Floor Response During Forced Vibration Tests

4.2.3 2-Story Office on S. Chester Ave., Pasadena

This building is owned by the California Institute of Technology and is located near the campus (see Figure 4.22). It was under construction at the time of the testing, with all plywood sheathing, asphalt and tile roofing, and concrete flooring in place, but no interior or exterior finishes (no drywall or stucco at time of testing). This is a rectangular building with steel ridge beam and center columns, and a small steel moment frame supporting the east end of the ridge beam due to window openings. There are no interior shear walls (all interior walls are drywall partitions on metal studs). The first floor plan area is approximately 5600 square feet (140'x40').

Figure 4.22: 2-Story Office Building on S. Chester Ave., Pasadena

The Harvey Mudd shaker was placed at the second floor, over the bare concrete flooring with enough weights over the shaker to prevent sliding and rocking, since the shaker could not be bolted to the floor in order to minimize damage. See Figure 4.23 for a sketch of the floor plan and seismometer locations. During the first day of testing, the shaker weights were placed at 5% eccentricity. The building response was recorded for shaking in the NS direction (transverse direction), for a frequency range between 4.5 Hz and 13.0 Hz, at 0.1 Hz increments. During the next day of testing, a few channels were lost due to damage to one of the signal conditioners, and

the testing had to be finished with only 3 out of 7 channels working properly. The building was shaken at 5% eccentricity in the EW direction (longitudinal direction) for the same frequency range, and then the shaker eccentricity was increased to 10% and the building was shaken between 4.5 Hz and 7.6 Hz in the EW direction with 0.1 Hz increments. Each recording was taken for 5 seconds at 1000 Hz sampling frequency.

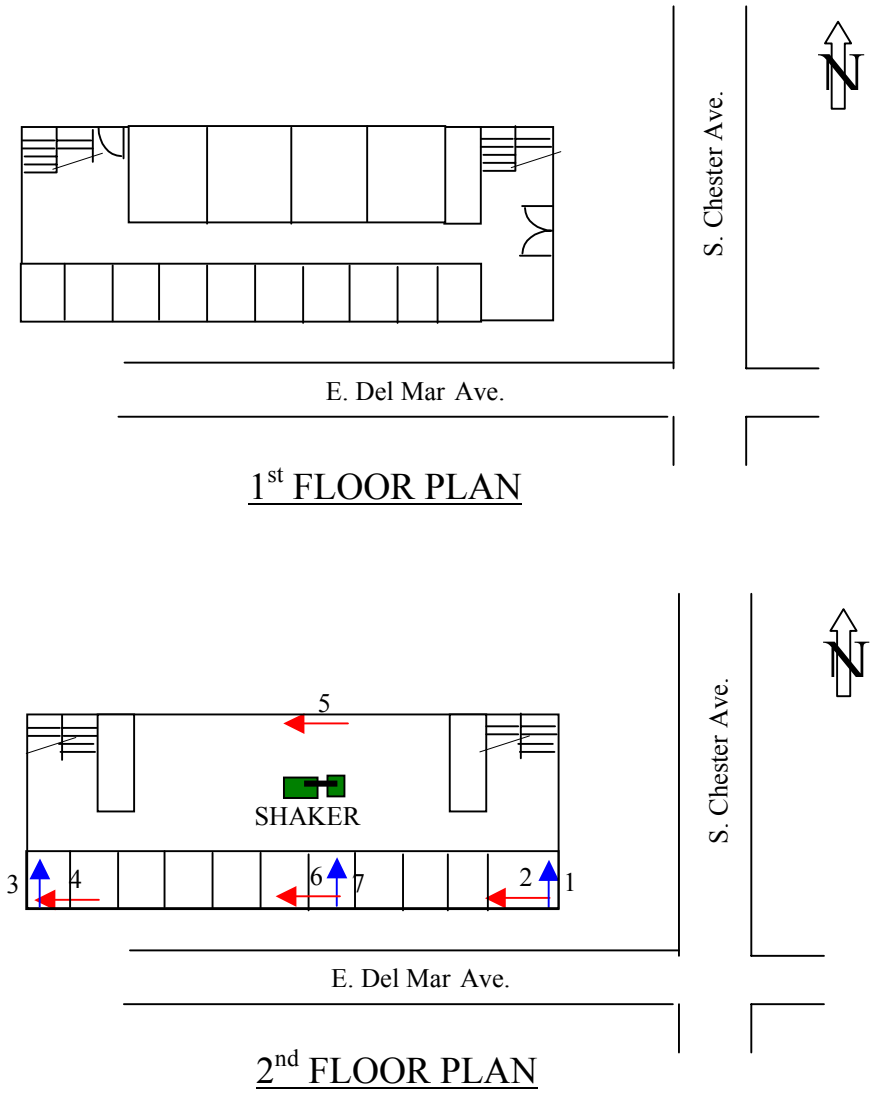

Figure 4.23: Seismometer Locations

Plots of the ranger seismometer data for shaking at the resonant frequencies are given in Appendix C (Figures C.15 through C.19), where it should be noted the response is smooth at all the channels during NS shaking and at channels E6 and E7 for EW shaking (since all other channels malfunctioned). Figures 4.24 and 4.25 show plots of the results, where the vertical axes are proportional to velocity normalized by the square of the frequency to account for the frequency dependence of the shaker force. The identified fundamental modal frequencies and damping ratios are listed in Table 4.4. Results show that the first NS mode has substantial in-plane bending and rotation of the second floor (see Figure 4.24), as shown by the large amplitude at the NS channel 7 (located at the mid-span of the building). In contrast, in the first EW mode, there is very little rotation of the second floor. In Figure 4.25, the downward shift in fundamental frequencies with increasing force amplitude is noticeable. Unfortunately, on the second day of testing there were problems with the instrumentation used and many of the channels malfunctioned, so only the data from three of the seismometers could be used. Also, because the shaker could not be fastened to the floor, the shaker eccentricity was limited to 10% or less. Due to the limited data available from the forced vibration tests of this structure, it was difficult to identify the modal properties, specially the modeshapes since the response was only known at three locations for the EW (longitudinal) shaking of this building. The identified natural frequencies of 7.2Hz and 6.7 Hz at 5% eccentricity are significantly higher than those of the 2-story houses discussed in sections 4.2.1 and 4.2.5. It is possible that fastening the plywood to aluminum framing members may produce stiffer walls than those using conventional woodframe construction, but additional research would be necessary to make any conclusions.

Table 4.4: Summary of 2-Story Office on S. Chester Ave. Results

Test Date	Shaking Direction	Eccentr.	1st NS		1st EW	
			Freq. (Hz)	Damp.	Freq. (Hz)	Damp.
Sept 9, 2000	NS	5%	7.2	4.8%	–	–
Sept 10, 2000	EW	5%	7.2	–	6.7	6.8%
	EW	10%	7.0	–	6.6	6.4%

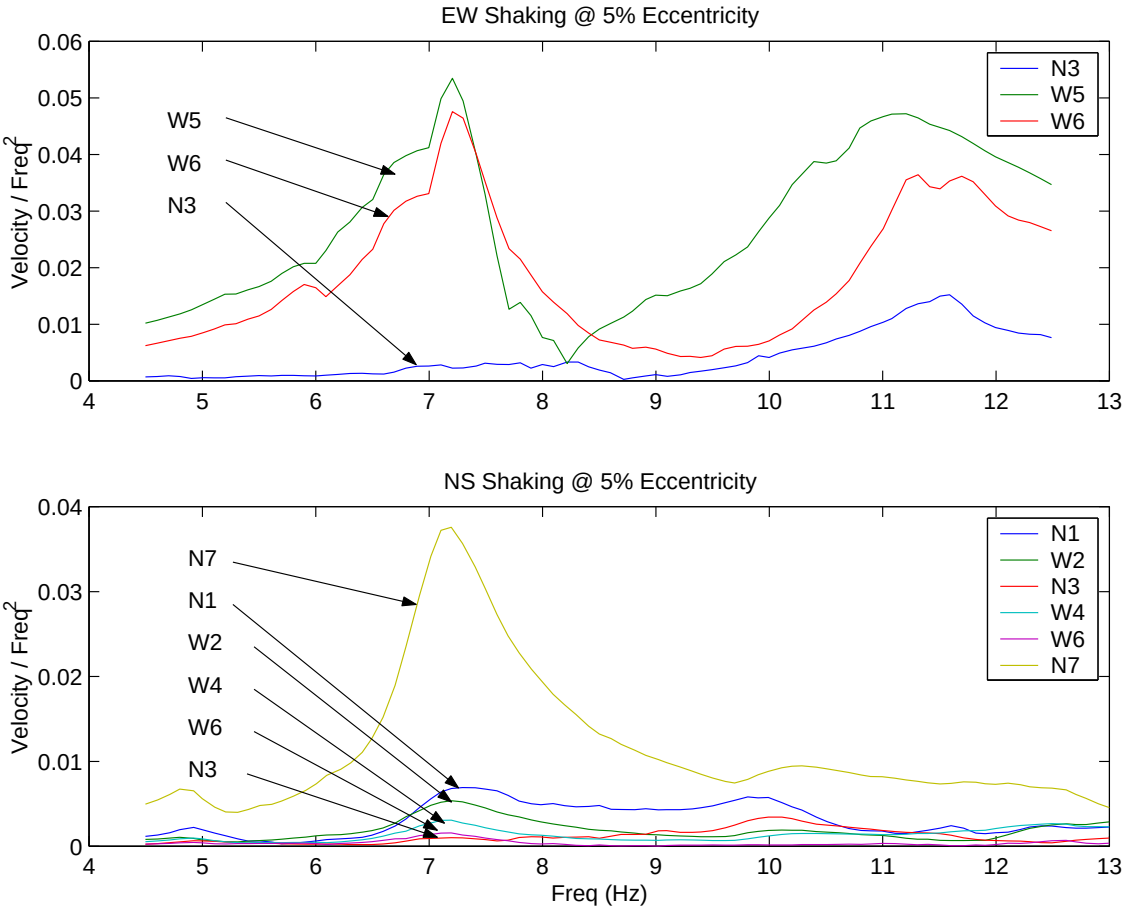

Figure 4.24: Forced Vibration Tests (seismometer results)

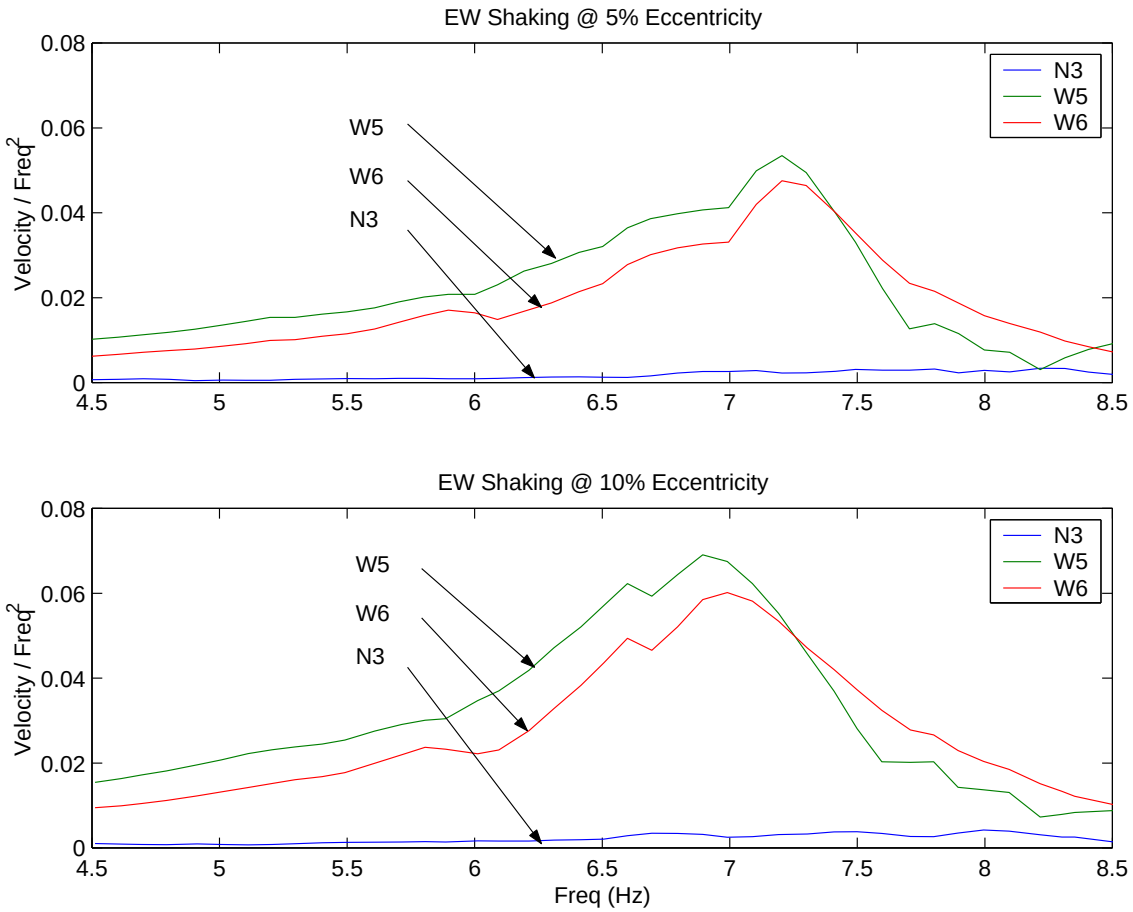

Figure 4.25: Fundamental Frequency Drop with Increased Shaking Force

4.2.4 2-Story Garage on S. Hill Ave., Pasadena

This three-car garage is located in the back of a property owned by the California Institute of Technology and located in the vicinity of the campus (see Figure 4.26). Built circa 1920, this building has wood siding exterior finish and no interior wall finish. The first floor plan area is approximately 900 square feet, with an aspect ratio of approximately 1:1.

Figure 4.26: 2-Story Garage on S. Hill Ave., Pasadena

The shaker and all accelerometers were placed at the second floor. This building was shaken using the Harvey Mudd shaker, which was bolted to the floor diaphragm using tension rods. Screws then were driven through the planks, the plywood and the floor deck below to secure the shaker assembly. The building response was recorded using seven accelerometers belonging to Harvey Mudd College, since the stronger shaking of this building were causing the Ranger seismometer signals to be clipped. See Figure 4.27 for the accelerometer locations and Figure 4.28 for a picture of the experimental setup.

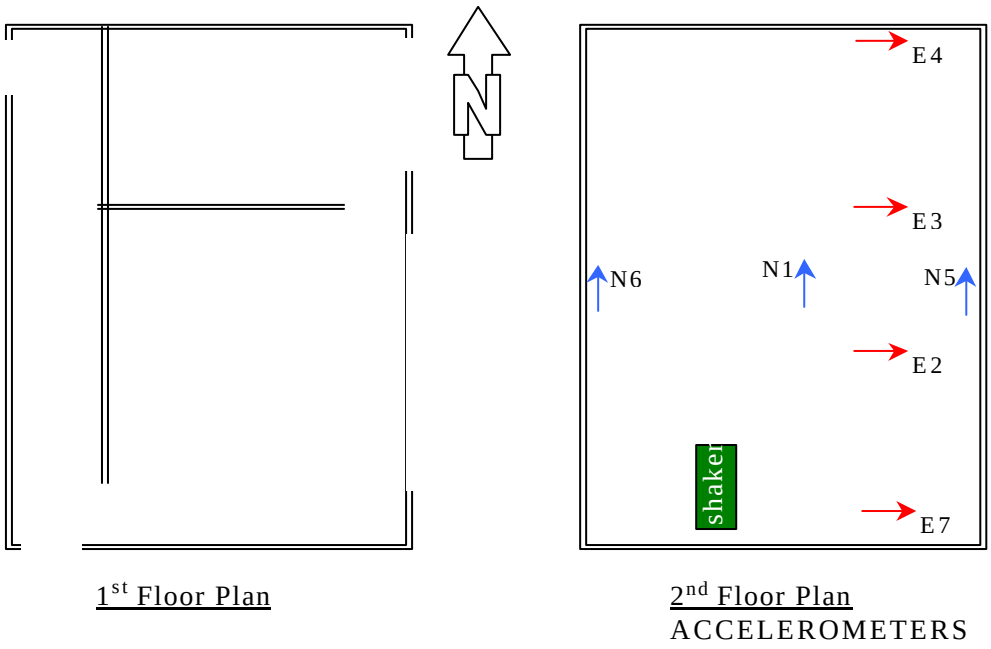

Figure 4.27: Accelerometer Locations

Figure 4.28: Experimental Setup

During the first day of testing, the shaker weights were placed at 5% eccentricity. The building response was recorded for shaking between 2.0 Hz and 4.8 Hz, at 0.2 Hz increments, in each direction. During the next few days of testing, the building was shaken in each direction at 5%, 20% (EW only), 50% and 100% eccentricity. The frequencies were sampled every 0.1 Hz, and each recording was taken for 5 seconds at 1000 samples per second. The frequency ranges varied, from between 2.0Hz and 6.0Hz at 5% eccentricity to between 1.4Hz and 3.5Hz at 100% eccentricity (back to 1.4Hz during NS shaking). Plots of the accelerometer data for shaking at the resonant frequencies are given in Appendix C (Figures C.20 through C.33), where it should be noted the response is generally not sinusoidal at any of the channels. Also, channel E2 appears to have some high frequencies coming through (beats) for shaking at the lower eccentricities.

The identified modal frequencies and damping ratios are listed in Table 4.5. Plots of the results obtained are shown in Figures 4.29 and 4.30, where the vertical axes are proportional to velocity (acceleration divided by the frequency) and normalized by the square of the frequency to account for the frequency dependence of the shaker force. Figure 4.29 shows results for the forward and backward frequency sweep, where the forward sweep (solid lines) shows a higher fundamental frequency than the backward sweep (dashed lines). Figure 4.31 shows sketches of the floor response at the identified resonant frequencies during EW and NS shaking at 100% eccentricity.

The EW, NS and torsional modes of this 2-story garage are very close together. Figure 4.30 shows that the NS fundamental mode does not have a strong torsional component since only the NS channels were excited by shaking in the NS direction, which differs from the behavior observed during the tests of the Del Mar 3-story apartment building described in section 4.2.2, even though both buildings have no shear walls on the east side at the first level. This may be due to the location of the shaker near the NS shear wall, since the shaker force would be transmitted directly into the NS shear wall without exciting significant torsional response. Shaking in the EW direction excites both the EW and NS fundamental modes, since the location of the shaker introduces a torsional component in the building response, but the channels

did not have double peaks indicating the EW and NS modes are not coupled. It should also be noted that Figure 4.30 shows a peak at a fourth resonant frequency, where the response of the building was significantly stronger. These peaks had the largest component of motion near the center of the diaphragm for shaking in each direction, which indicates that these peaks are the in-plane diaphragm modes. All fundamental frequencies were lowered as the shaking amplitude increased, as seen in Figure 4.30. Figure 4.29 shows how these frequencies shift during the frequency scans, as can be seen from the change in resonant frequencies from the upwards sweep (solid lines) to the downwards sweep (dashed lines). This occurs because the shaker force increases with the square of the frequency, leading to additional loss of stiffness as the shaker force is thus increased.

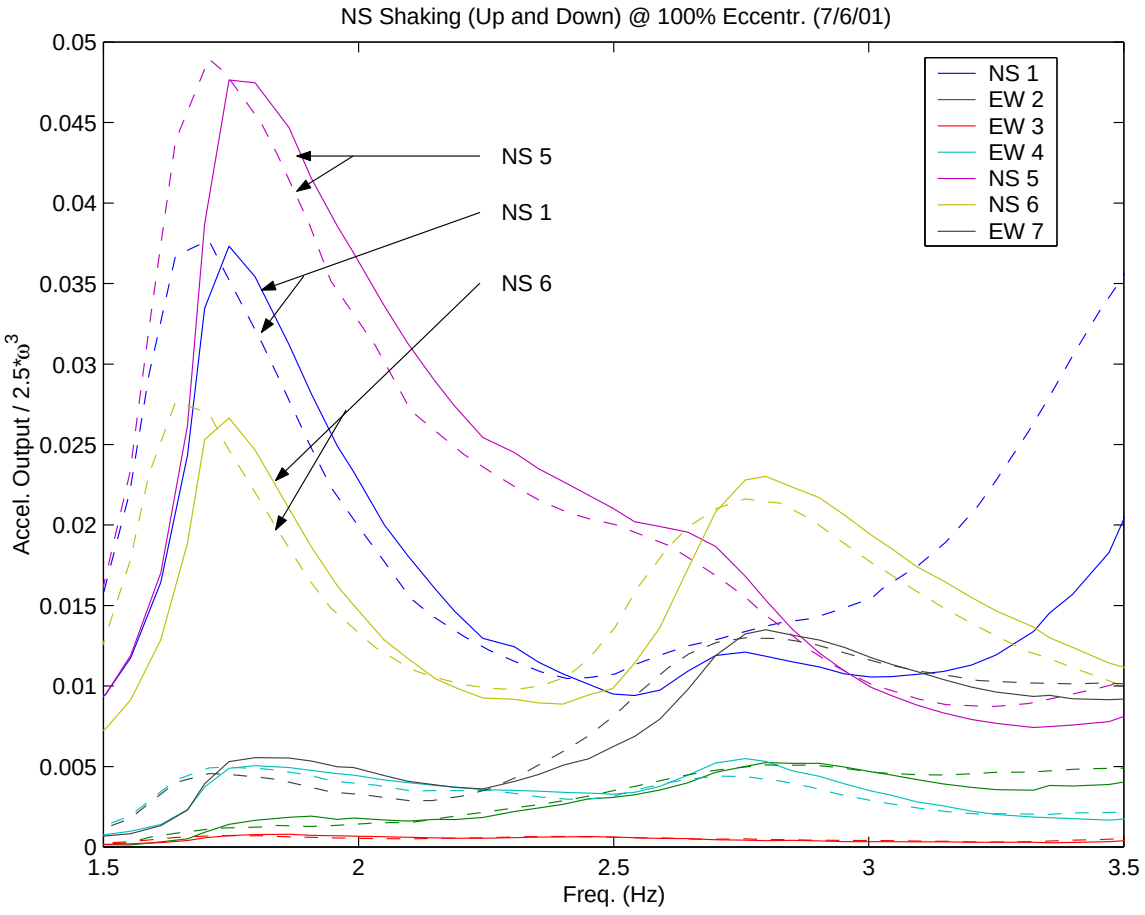

Figure 4.29: Forward and Backward Frequency Sweep

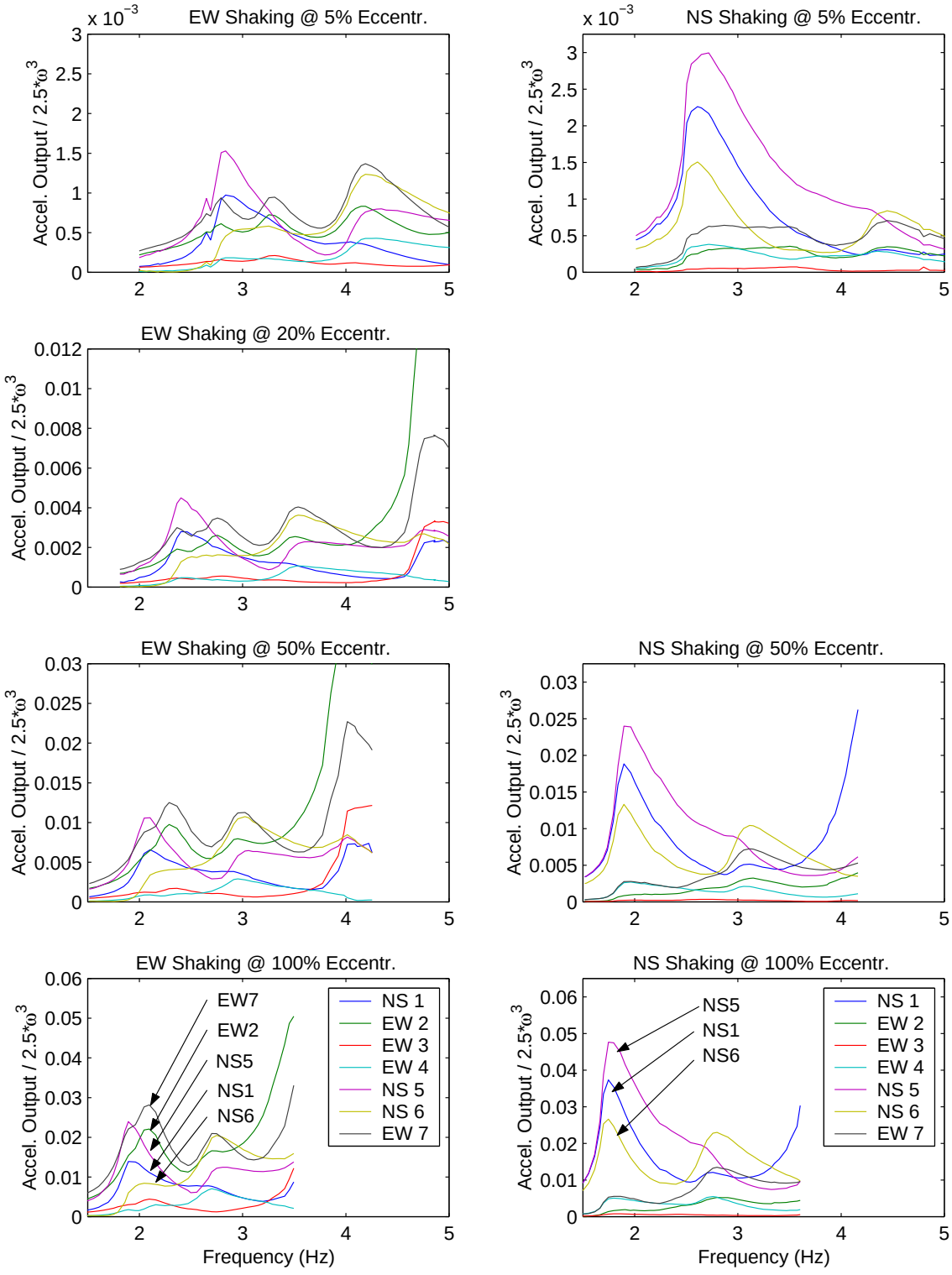

Figure 4.30: Forced Vibration Tests (accelerometer results)

Table 4.5: Summary of 2-Story Garage on S. Hill Ave. Results

Shaking Direction	Eccentr.	1st NS		1st EW	
		Freq. (Hz)	Damp.	Freq. (Hz)	Damp.
NS	5%	2.7	6.2%	3.0	5.2%
	50%	2.0	6.1%	2.2	8.3%
	100%	1.8	5.8%	2.0	6.4%
EW	5%	2.8	6.2%	3.2	6.3%
	20%	2.4	7.3%	2.7	7.1%
	50%	2.1	6.4%	2.3	6.7%
	100%	1.9	6.0%	2.1	6.1%

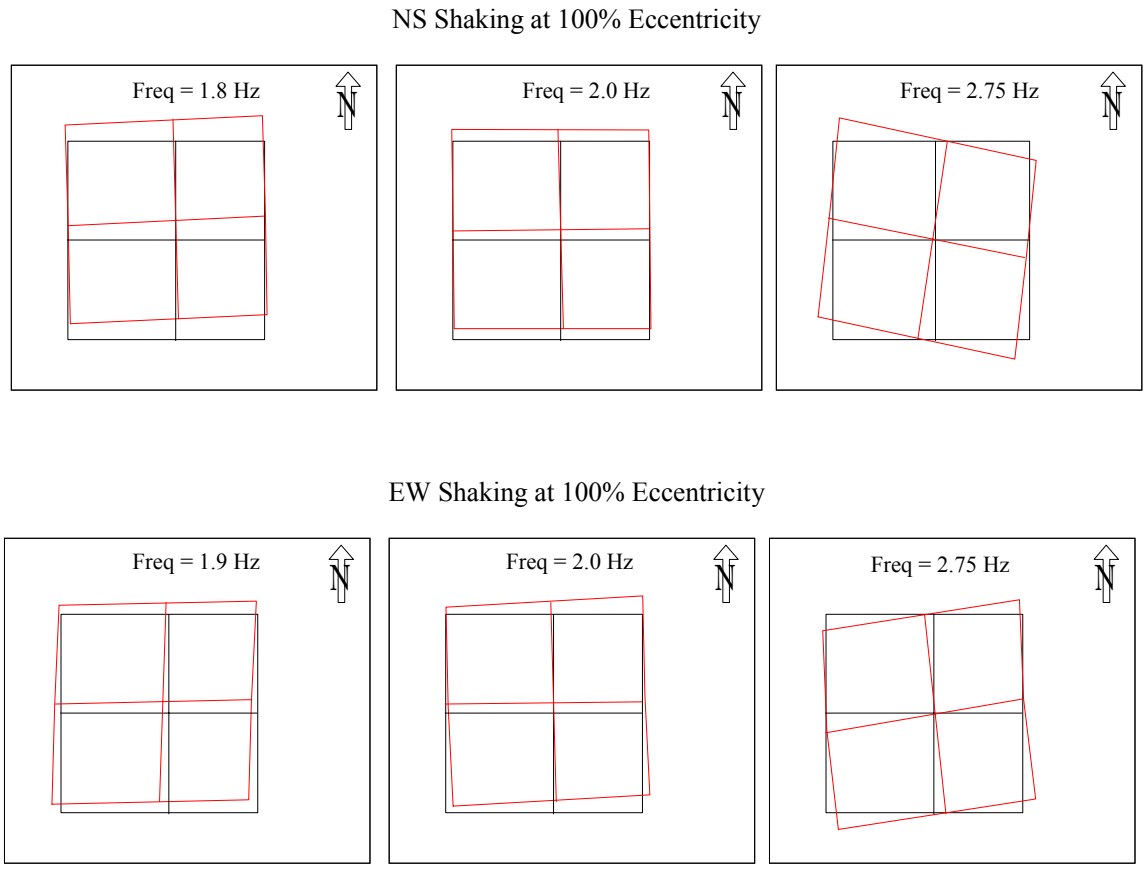

Figure 4.31: 2-Story Garage 2nd Floor Response During Forced Vibration Tests

4.2.5 2-Story House on S. Hill Ave., Pasadena

This 2-story house is owned by the California Institute of Technology (see Figure 4.32). It is on the same lot as the 2-story garage described in section 4.2.4. Built circa 1920, this building has wood siding exterior finish and plaster interior wall finish. The first floor plan area is irregular, approximately 2000 square feet with a fireplace at middle of the south wall of the building.

Figure 4.32: 2-Story House on S. Hill Ave., Pasadena

This building was shaken successfully using the Harvey Mudd shaker, which was securely bolted to the floor diaphragm at the second level. Screws then were driven through the planks, the plywood and the floor deck below to secure the shaker assembly. The first set of tests was recorded using six Ranger seismometers, but since shaking at 100% eccentricity was causing the signals to be clipped, a second set of tests was performed with FBA-11 accelerometers placed adjacent to each seismometer and two additional accelerometers placed in the attic (roof level). See Figure 4.33 for the experimental setup and instrument locations.

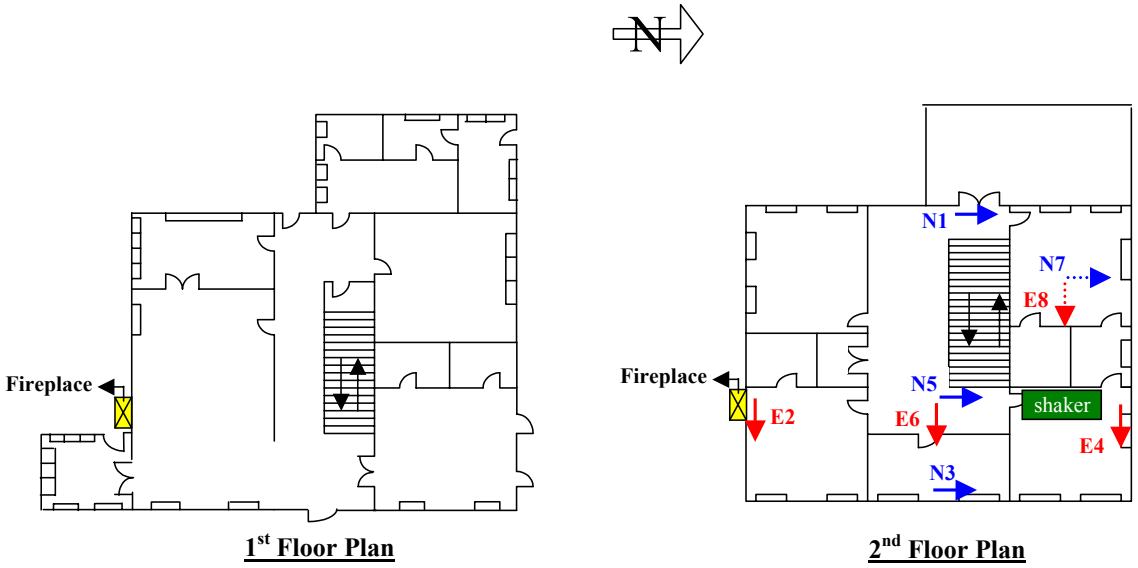

Figure 4.33: Accelerometer Locations

During the first set of tests using Ranger seismometers to record the building motion, the shaker weights were placed at 5%, 20%, 50% and 100% eccentricity. The building response was recorded for shaking between 3.0Hz and 8.0Hz, at 0.1 Hz increments, in each direction. The frequency ranges varied, from between 4.0Hz and 8.0Hz at 5% eccentricity in EW direction to between 3.0Hz and 5.0Hz at 100% eccentricity in NS direction. Each recording was taken for 5 seconds at 1000 samples per second. The second set of tests was performed using Ranger seismometers and also FBA-11 accelerometers, and was identical to the original setup. The frequency ranges and shaker eccentricities used during the second set of tests were the same. Plots of the seismometer and accelerometer data for shaking at the resonant frequencies are given in Appendix C (Figures C.34 through C.53). It should be noted that the seismometer output is generally smooth sinusoidal, unless clipping is observed. The accelerometer output is generally harmonic, and the signal is considerably noisier than the seismometer output.

The identified fundamental modal frequencies and damping ratios are listed in Table 4.6. Plots of the results obtained from the first set of tests are shown in Figure 4.34. The results from the second set of tests are shown in Figures 4.35 and 4.36, where the vertical axes are proportional to velocity (acceleration divided by the frequency) and normalized by the square of the frequency to account for the frequency dependence of the shaker force. It should be noted that the first set of response curves (Figure 4.34) shows higher fundamental frequencies than the second and third sets of response curves (Figures 4.35 and 4.36). The strong shaking at 100% eccentricity during the first set of tests may have damaged the building and therefore the subsequent test showed lower resonant frequencies than those originally recorded. The maximum drift computed at this structure was 1.24mm for EW and NS shaking at 100% eccentricity. The maximum drift for shaking at 20% eccentricity was 0.30mm at channel E8 (roof attic) and 0.25mm at channels E4 and N3.

Table 4.6: Summary of 2-Story House on S. Hill Ave. Results

Test Date	Shaking Direction	Eccentr.	1st NS		1st EW		1st Tors.	
			Freq. (Hz)	Damp.	Freq. (Hz)	Damp.	Freq. (Hz)	Damp.
Jul 24 2001	NS	5%	5.0	4.1%	–	–	–	–
		20%	4.7	4.7%	–	–	–	–
		50%	4.2	5.0%	–	–	–	–
	EW	5%	–	–	5.5	3.9%	6.4	5.5%
		20%	–	–	5.1	4.0%	5.8	6.3%
		50%	–	–	4.7	4.0%	5.3	6.8%
Aug 23 2001	NS	5%	4.8	4.2%	–	–	–	–
		20%	4.4	4.7%	–	–	–	–
		50%	4.0	4.8%	–	–	–	–
		100%	3.7	5.3%	–	–	–	–
	EW	5%	–	–	5.3	4.0%	6.2	7.5%
		20%	–	–	4.8	3.9%	5.5	8.2%
		50%	–	–	4.4	3.8%	5.0	7.4%
		100%	–	–	4.2	3.9%	4.7	8.8%

The response curves in Figures 4.34 and 4.35 show that the output of the Ranger seismometers was clipped when shaker eccentricity was at 100%. Note that the natural frequencies in Figure 4.34 are significantly higher than those shown in Figure 4.35, due to the prolonged strong shaking of the structure during the first series of tests.

Figure 4.36 shows the response curves from the second series of forced vibration tests recorded using FBA-11 accelerometers normalized so that curves are proportional to seismometer outputs, and these normalized curves are identical to those obtained using Ranger seismometers, with the exception of the 100% eccentricity curves where the Ranger seismometer signals were clipped. Both series of tests show that increasing the shaker eccentricity results in lower resonant frequencies, since the higher shaking forces cause the building to lose some of its non-structural stiffness. Some of this reduction in stiffness is permanent, as seen by the lower natural frequencies obtained from the second set of tests after severe shaking during the first set of tests. Some of the non-structural stiffness is recovered, as seen by the fact that the natural frequencies obtained from the second set of tests were identical to those from the first set of tests, even though the frequencies shifted during each set of tests when the shaker eccentricity was increased.

Figure 4.37 shows sketches of the floor response at the identified resonant frequencies during EW and NS shaking at 100% eccentricity. Note that the NS fundamental mode has strong torsional component to its modeshape and the floor is acting as a rigid diaphragm, with the motion at the EW channels near the outer walls comparable to that of the NS channel farthest from the shaker. The EW mode has a slight torsional component and the EW modeshape indicates the floor moves rigidly with the strongest response at the channel nearest the shaker and the smallest response at the channel farthest from the shaker (near the fireplace). The torsional mode was excited by shaking in the EW direction but not by shaking in the NS direction, due to the location of the shaker with respect to the building center of rigidity.

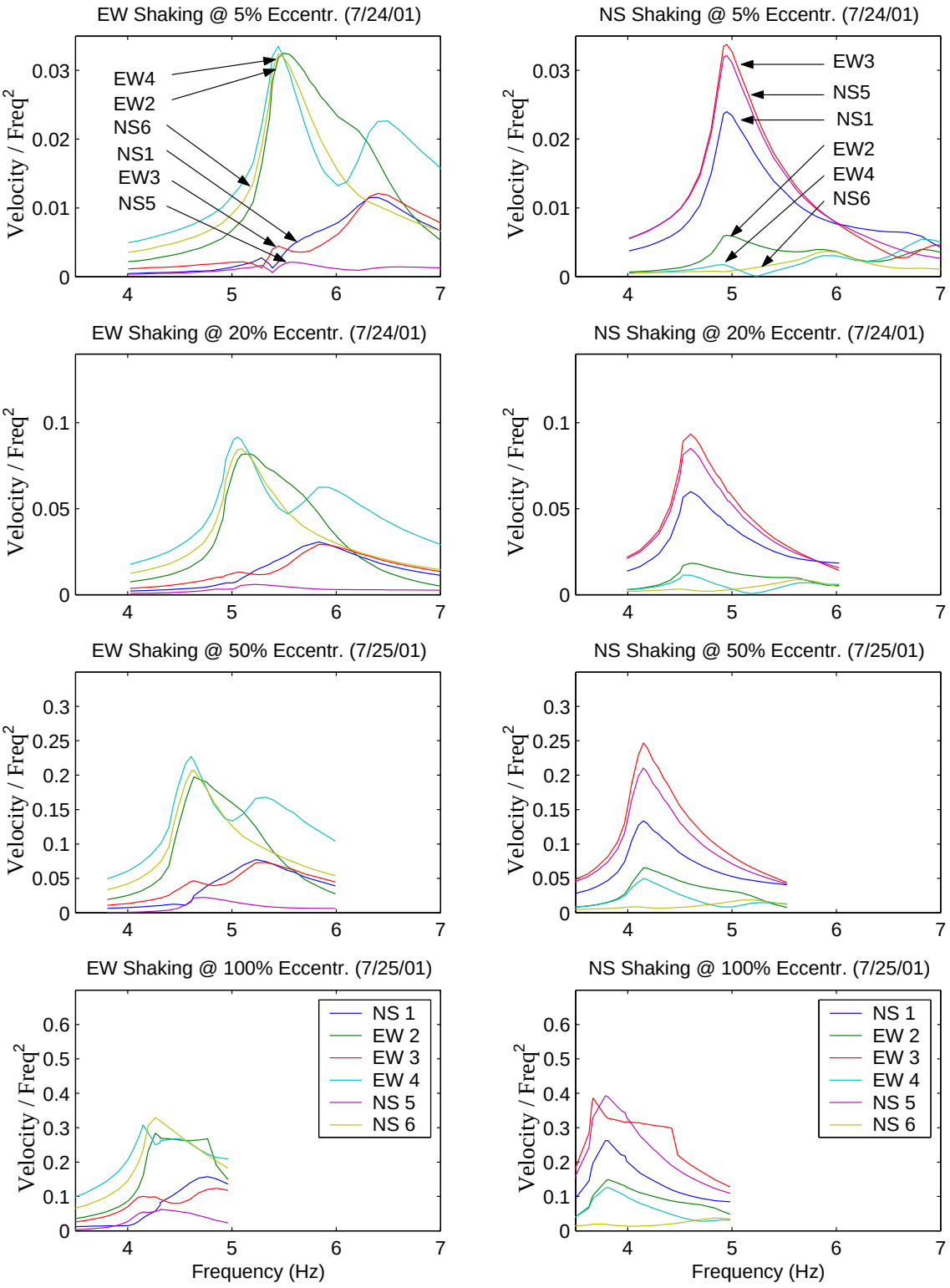

Figure 4.34: 1st Forced Vibration Tests (seismometer results)

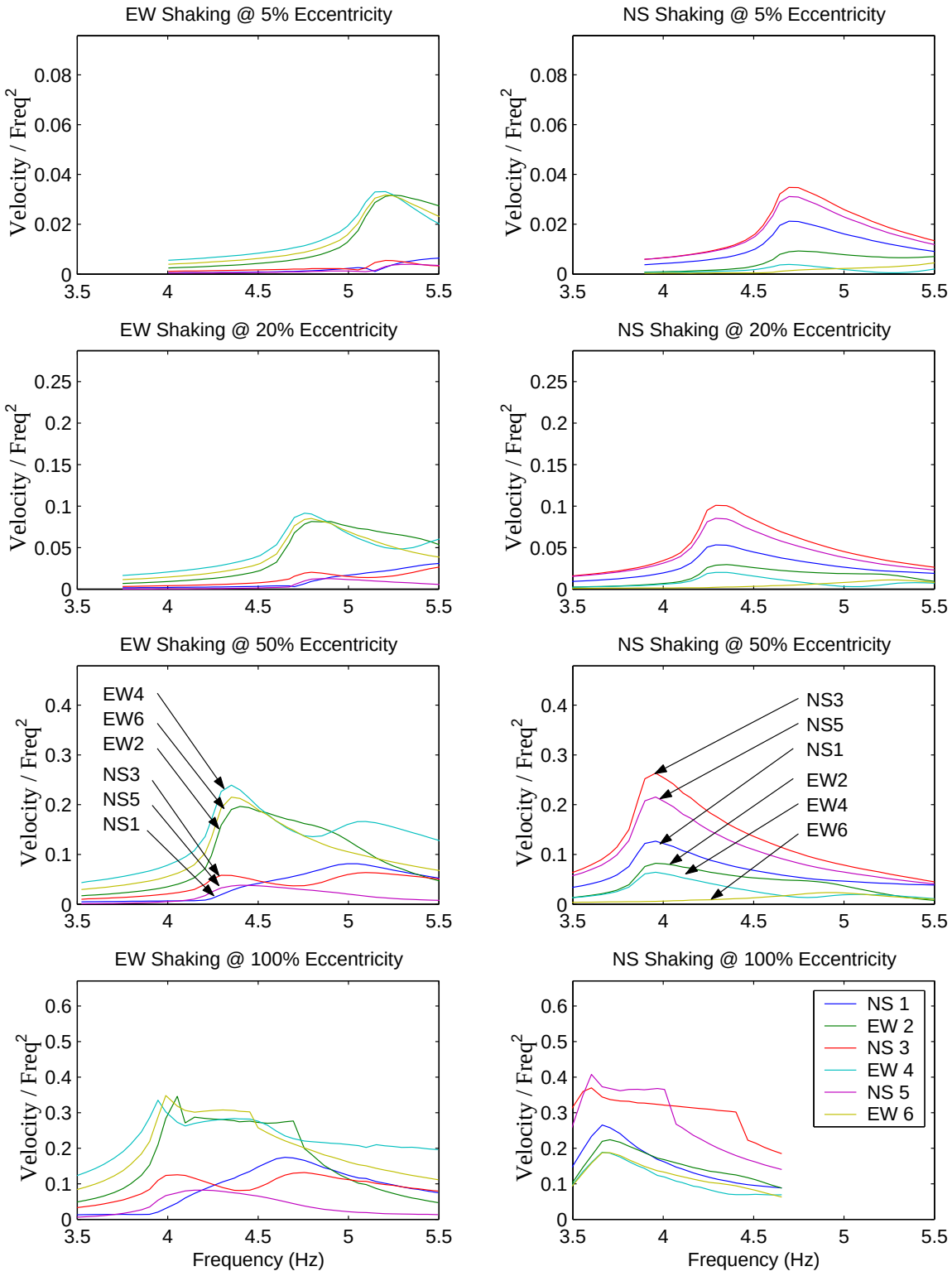

Figure 4.35: 2nd Forced Vibration Tests (seismometer results)

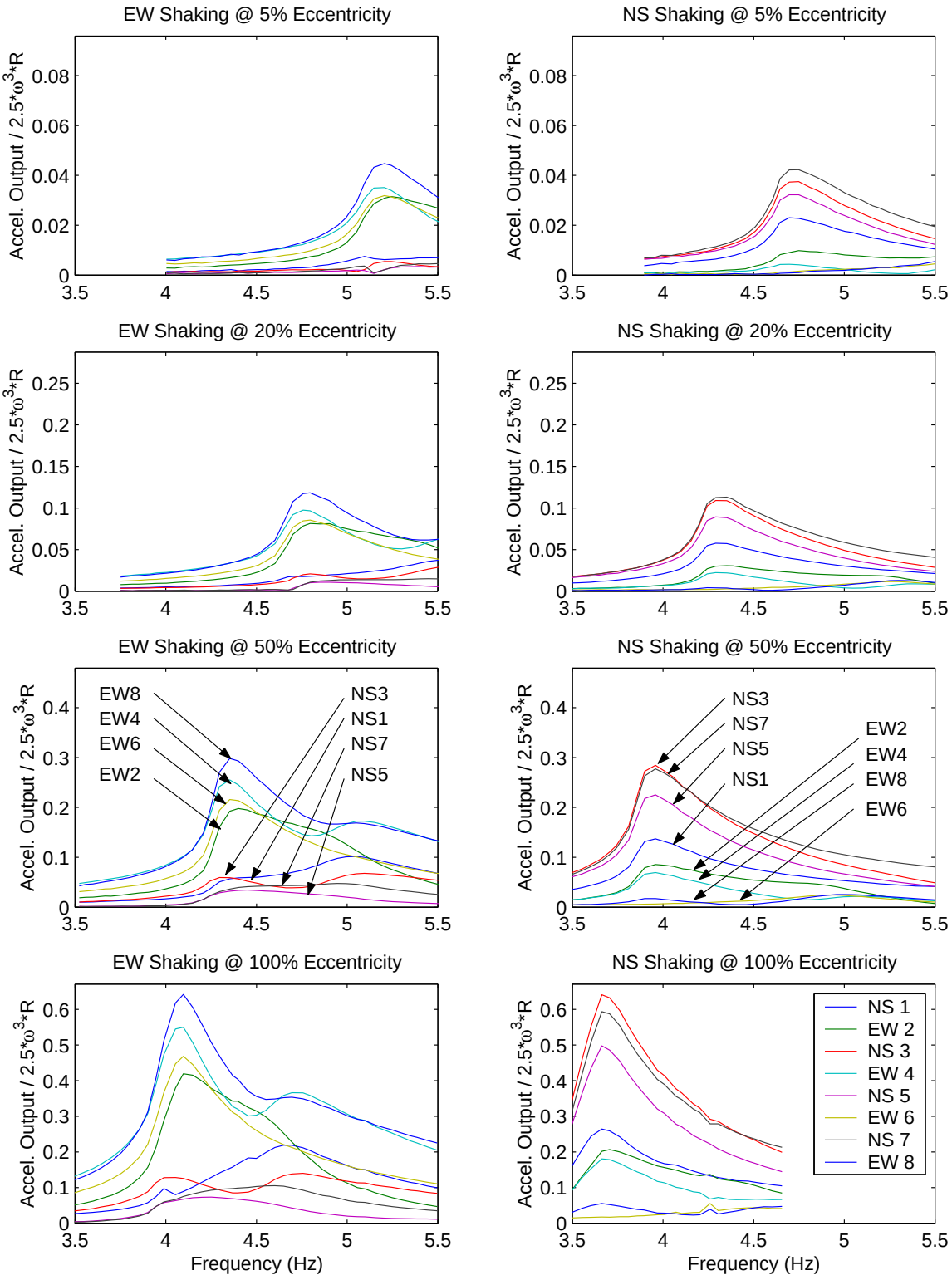

Figure 4.36: 2nd Forced Vibration Tests (accelerometer results)

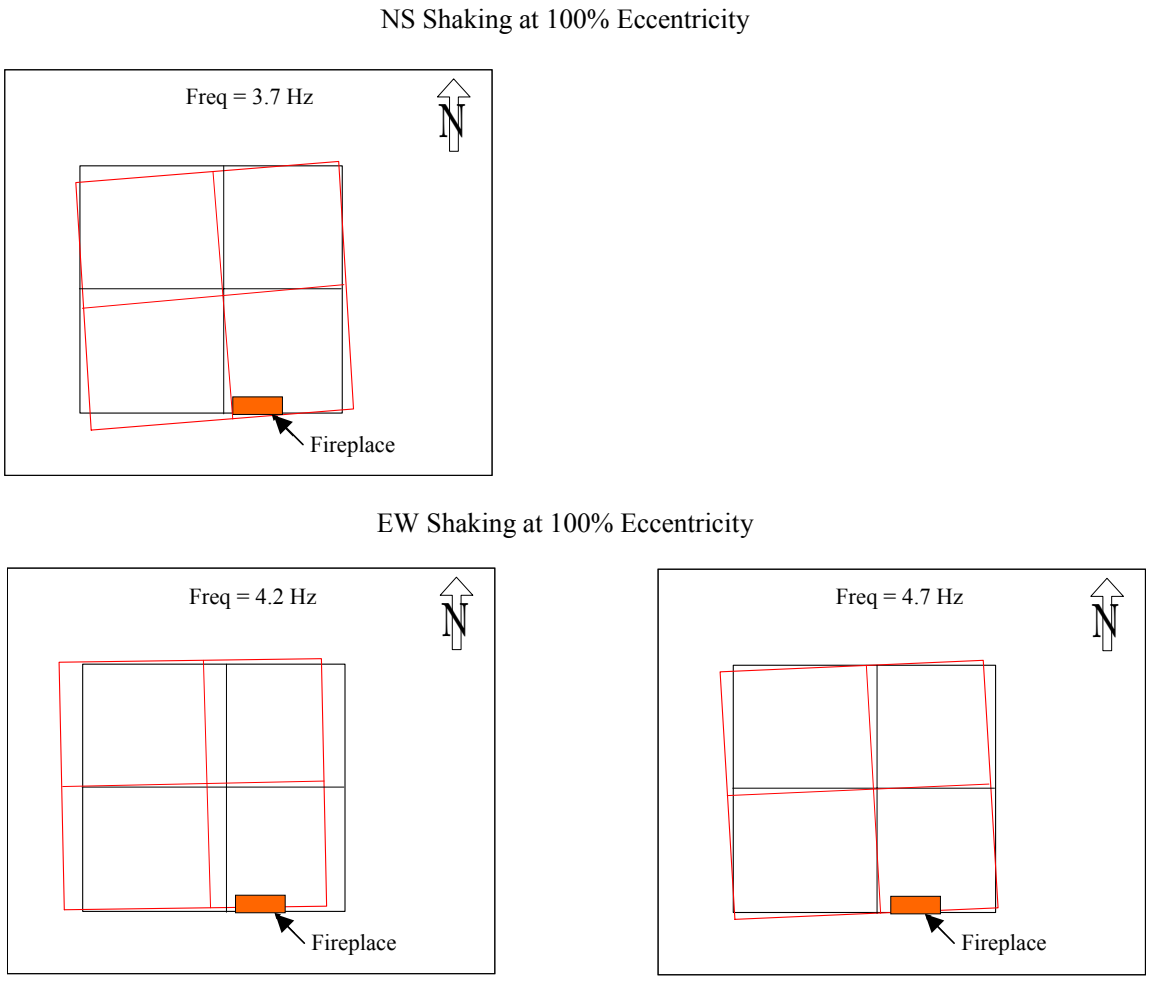

Figure 4.37: 2-Story House 2nd Floor Response During Forced Vibration Tests

4.3 Discussion of Results

The frequencies obtained from the forced vibration tests are consistent with those obtained from analysis of the earthquake records, with the exception of the 2-story garage since there were no records from a building without stucco, plaster or dry-wall finish materials. The dynamic characteristics obtained from ambient vibration testing were significantly different from those obtained from forced vibration testing of the buildings, illustrating the amplitude dependence of the periods and dampings. Therefore, the periods obtained from ambient vibration testing were not used to derive the design period formula by regression, and only the earthquake data and the forced vibration test data at 20% eccentricity were used (see Chapter 6). This is not to say that ambient vibration tests are not useful in other applications, such as structural health monitoring. The data for forced vibration testing at 20% eccentricity was selected for use in the regression analysis since it was the highest eccentricity used in the testing of most of the buildings, and since the periods at 50% and 100% eccentricity are dramatically different than those at 20% eccentricity. The maximum total drifts for some of the forced vibration tests were computed using the calibrated accelerometer data and the results are shown in Table 4.7. These drift values are comparable to the drifts produced by the earthquakes in the database (Chapter 3).

Table 4.7: Forced Vibration Tests Drift Ratios

Building	Shaking Direction	Ecc.	Drift (mm)	Channel	Height (m)	Drift Ratio
2-Story House on S. Catalina Ave.	EW	20%	0.14	W4	3	0.005%
3-Story Building on E. Del Mar Ave.	NS	20%	0.13	N7	6	0.002%
2-Story House on S. Hill Ave.	EW	20%	0.30	E8	6	0.004%
	EW/NS	20%	0.25	E4/N3	3	0.008%
	NS	100%	1.24	N3	3	0.04%

The damping values obtained from the forced vibration tests should have been higher than those obtained from earthquake records due to additional energy dissipated by soil-structure interaction expected in forced vibration tests (note that in the analysis of the earthquake records, the input channel is taken at the base of the

structure, and therefore the input motion already accounts for the soil-structure interaction), but all forced vibration test damping results were considerably lower than the damping values obtained from the earthquake records. Since the system is really nonlinear, perhaps the damping estimation based on a linear model assumption is not appropriate. Note that the upwards and backwards sweep curves shown in Figure 4.29 have different widths, indicating that the damping values may be affected by changes in the structural stiffness as the force amplitude changes. Another possibility is that this difference may be due to the fact that the buildings tested differ significantly from those from which the earthquake records were obtained.

Figure 4.38 shows how the periods shifted as a function of the shaking force (periods and forces were normalized by the values at resonance during 10% eccentricity shaking). Note that the 2-story garage has much steeper curves than any of the other buildings tested, while the 3-story apartment building has the shallowest slope (neglecting the 2-story house on Catalina Avenue shaking at 20%, since the shaker force was not completely transmitted into the building due to sliding and rocking). This may indicate that wall finish materials have an effect on the period elongation observed during stronger shaking, since the 2-story garage has no interior wall finishes and wood-siding exterior finish while all other buildings have stucco, plaster or at least plywood sheathing on the walls. This effect may also be due to the fact that the garage is a much lighter and more flexible building than all others tested (it is small in plan and has no additional mass and stiffness due to wall finishes), and therefore the shaker is better able to excite its drift response than the larger buildings (such as the 3-story apartment building on Del Mar Avenue).

It should be noted that approximating the building response with sinusoidal curves is generally a reasonable assumption, but this may not be the case for the 2-story garage (see data in Appendix C, Figures C.20 through C.33), where the response is not sinusoidal. Since fitting a sinusoidal curve allows for comparison of the response amplitude at different shaking frequencies, it is still a useful tool for that purpose, but not for describing the general response of the building. Since the 2-story garage is the only building with significantly non-sinusoidal response, this suggests that the

wall finish materials may affect the general character of the building response as well as the overall building stiffness. The non-sinusoidal response could also be due to shaker stick-slip behavior, where the shaker overcomes friction at higher force levels and starts sliding until it comes to a stop (perhaps by hitting the tension rods securing it), although the shaker assembly appeared to be well-secured and no slippage was visible during testing of the garage.

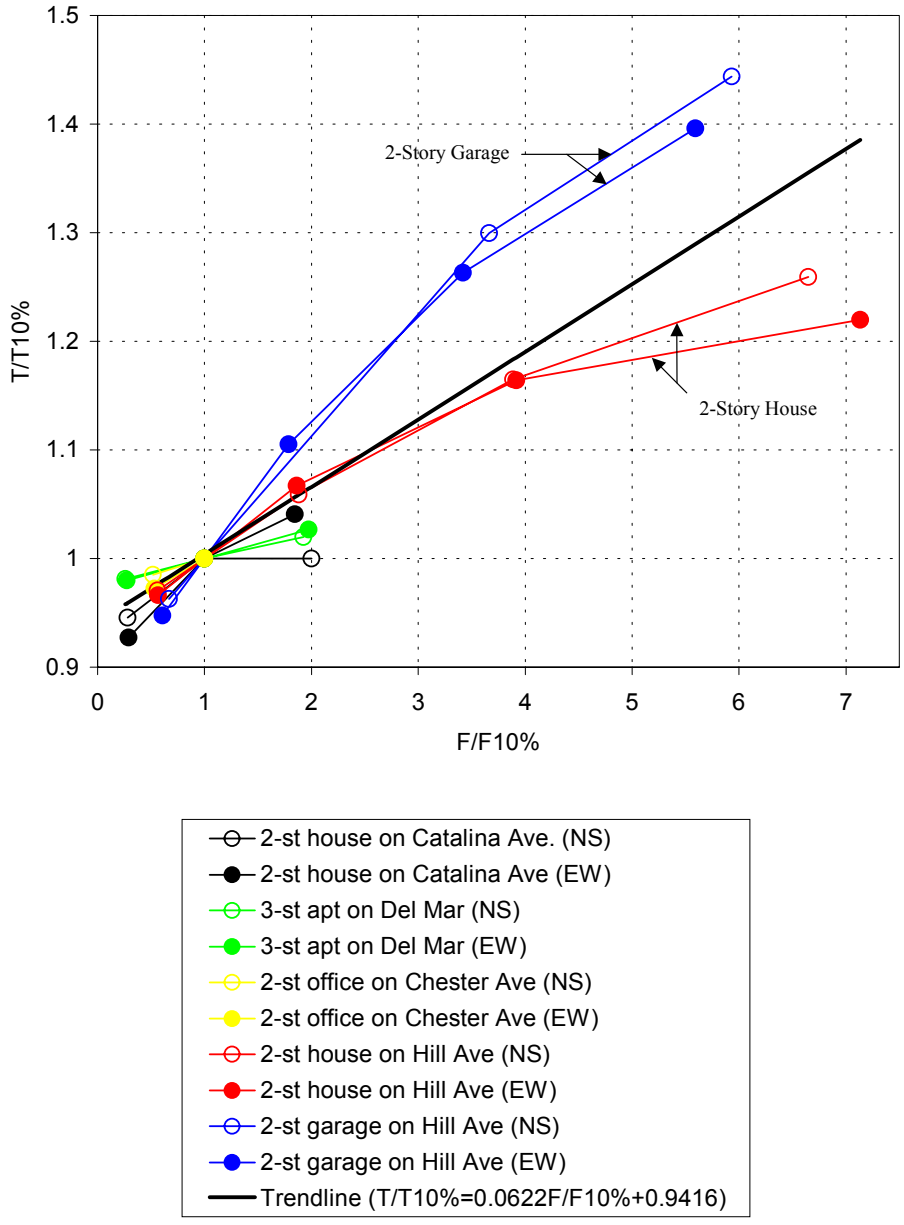

Figure 4.38: Period as a Function of Shaking Force

Chapter 5

Shake-Table Tests

Two full-scale shake-table tests of woodframe buildings were performed under the CUREE-Caltech Woodframe Project: a 2-story house at UC San Diego and a 3-story apartment building with tuck-under parking at UC Berkeley. Data obtained from these shake-table tests were used to validate the period formula by regression. Forced vibration tests of the UC Berkeley structure before and after each set of shake-table tests showed how the dynamic characteristics of that building changed due to damage. This chapter describes the details of the analysis of the UC San Diego data, and the forced vibration testing and analytical modelling of the UC Berkeley test structure.

5.1 UC San Diego 2-Story House

A full-scale 2-story house was tested on a shake-table at UC San Diego under Task 1.1.1 of the CUREE-Caltech Woodframe Project. The structure was shake-table tested using the 1994 Northridge, Canoga Park record, scaled at increasing levels of peak accelerations (level 1 to 4, 0.05g to 0.5g) as well as the Rinaldi record (level 5, 0.89g). If a shake-table test caused peak transient drift ratios between 0.5% to 1.0%, it was repeated once (level 3r, etc.). Each shake-table test was followed by a frequency evaluation test using white noise base input (0.025g to 0.04g RMS), and by a damping evaluation test using an impulse as input (0.05g peak response at roof).

Records from the shake-table tests during Phase 9 and Phase 10 were selected to be analyzed using MODE-ID. The records selected correspond to seismic tests at

levels 1, 2, 3, 3r, 4 and 5 for Phase 9 testing (no stucco, see Figure 5.1), and at levels 1, 2, 3, 4, 4r, 5 and 5r for Phase 10 testing (exterior stucco, see Figure 5.2). Channels D1, D2, D3 (NS), E1 and E3 (EW) were taken as input in the MODE-ID analysis (see Appendix D, Figures D.1 through D.10 for the acceleration time-histories recorded at the shake-table level). The output channels selected were D9, D11, D13 in NS direction and E4, E6 in EW direction at 2nd floor, and D14, D16, D18 in NS direction and E7, E9 in EW direction at roof. See Figure 5.3 for channel locations.

Figure 5.1: Phase 9

Figure 5.2: Phase 10

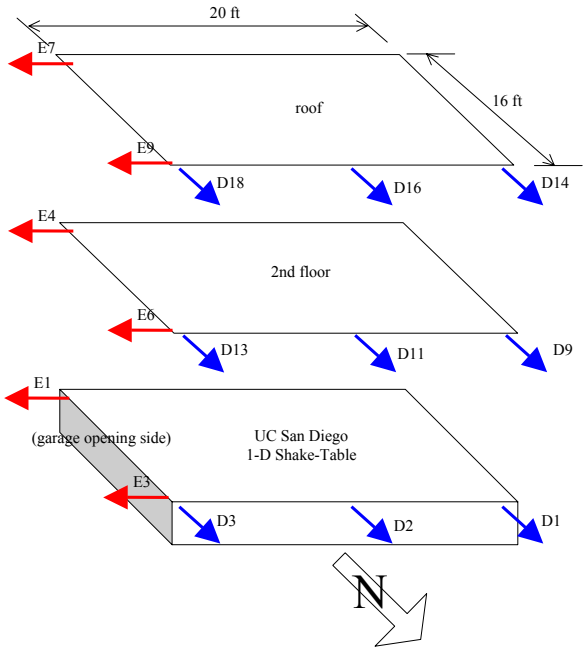

Figure 5.3: UCSD 2-Story House, Location of Channels Used in MODE-ID Analysis

Results from the MODE-ID analysis were then compared to the frequencies and dampings obtained from the low-amplitude frequency and damping tests performed by UCSD. The damping values from the UCSD damping tests were computed using the logarithmic decrement method. Although both the MODE-ID and the UCSD equivalent viscous damping values for the structure account for hysteretic damping, the UCSD damping values are for much smaller amplitude levels (roof response less than 0.05g) and therefore the hysteretic damping contribution will be smaller.

Figures 5.4 and 5.5 show a comparison between the frequencies and dampings obtained from MODE-ID analysis of the shake-table data (labeled MODE-ID) and those obtained from the low-amplitude frequency and damping tests performed by UCSD (labeled UCSD) for the Phase 9 and 10 structures, respectively. These figures also show plots of the MODE-ID results versus peak shake-table accelerations and peak drift ratios. It should be noted that the UCSD frequency and damping values were obtained from vibrations at smaller amplitudes than those observed during the seismic tests. Also, the UCSD values used for comparison were obtained after each level of testing was concluded. It is expected that the MODE-ID identified frequencies for stronger shaking would be lower than those obtained from low-level white noise shaking, as was observed during the windowing analysis in sections 3.2.1 through 3.2.5. Note that, in Figure 5.4, the MODE-ID identified frequencies are lower than the UCSD frequencies found by white-noise light shaking after the shake-table tests for all test levels except at test level 1. Similarly, Figure 5.5 shows that the MODE-ID frequencies for test levels 4, 4r, 5 and 5r are lower than the UCSD frequencies after the shake-table tests, but the MODE-ID frequencies for test levels 1, 2 and 3 are higher than the UCSD values. The higher MODE-ID values at the lighter shaking levels is probably due to the methodology used in computing the fundamental frequencies from the white-noise data. As expected, the shake-table tests performed using the same input time history after the drift threshold of 0.5% to 1% was exceeded (3 and 3r during Phase 9, 4 and 4r, 5 and 5r during Phase 10) yield lower fundamental frequency values, which can presumably be attributed to cumulative damage (i.e., permanent loss of stiffness) that occurs in both tests. Figures 5.4 and 5.5 also show

that the MODE-ID identified damping ratios are considerably higher at stronger shaking. The lower MODE-ID values at lighter shaking levels seen in Figure 5.5 levels 1 and 2 is probably due to the methodology used in computing the damping ratios (logarithmic decrement method).

Summaries of the results from the MODE-ID analyzes are given in Tables 5.1 and 5.2. The normalized mean squared error (NMS Error) is given for each set of records analyzed, and is defined as $J(\underline{a})$ in equation 3.4 divided by the mean square response (which corresponds to the same expression as $J(\underline{a})$ in Equation 3.4 but with all the x_i's equal to zero).

Figures 5.6 through 5.10 compare the motion recorded at channel D16 (middle of roof) to the predicted response based on the frequency and damping estimates obtained using MODE-ID and those estimates obtained from low-level white-noise shaking of the structure (performed at UCSD before and after each set of shake-table tests). In Figures 5.6 through 5.10, it is important to emphasize once again that the dynamic characteristics obtained from the white-noise shaking and the impulse tests performed at UCSD before and after each shake-table tests were at low levels of shaking, and the dynamic characteristics obtained from MODE-ID using the shake-table test data are for considerably higher levels of shaking. Therefore, the parameters obtained using MODE-ID give a better estimate for the dynamic characteristics of the building during strong shaking of the structure, and these frequency and damping values can change significantly throughout the shaking of the building, as shown in Figures 5.4 and 5.5.

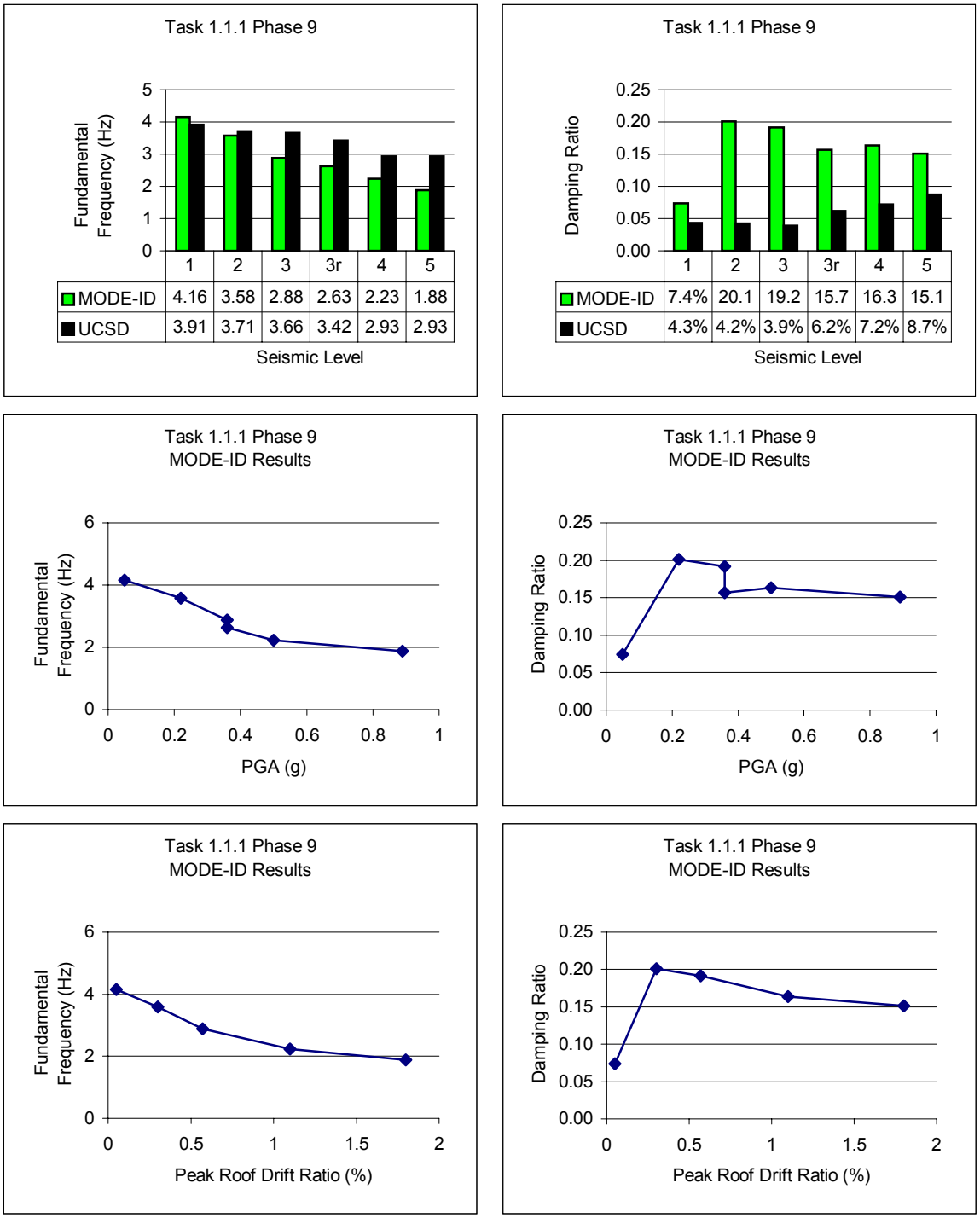

Figure 5.4: Fundamental Frequencies and Dampings, Phase 9

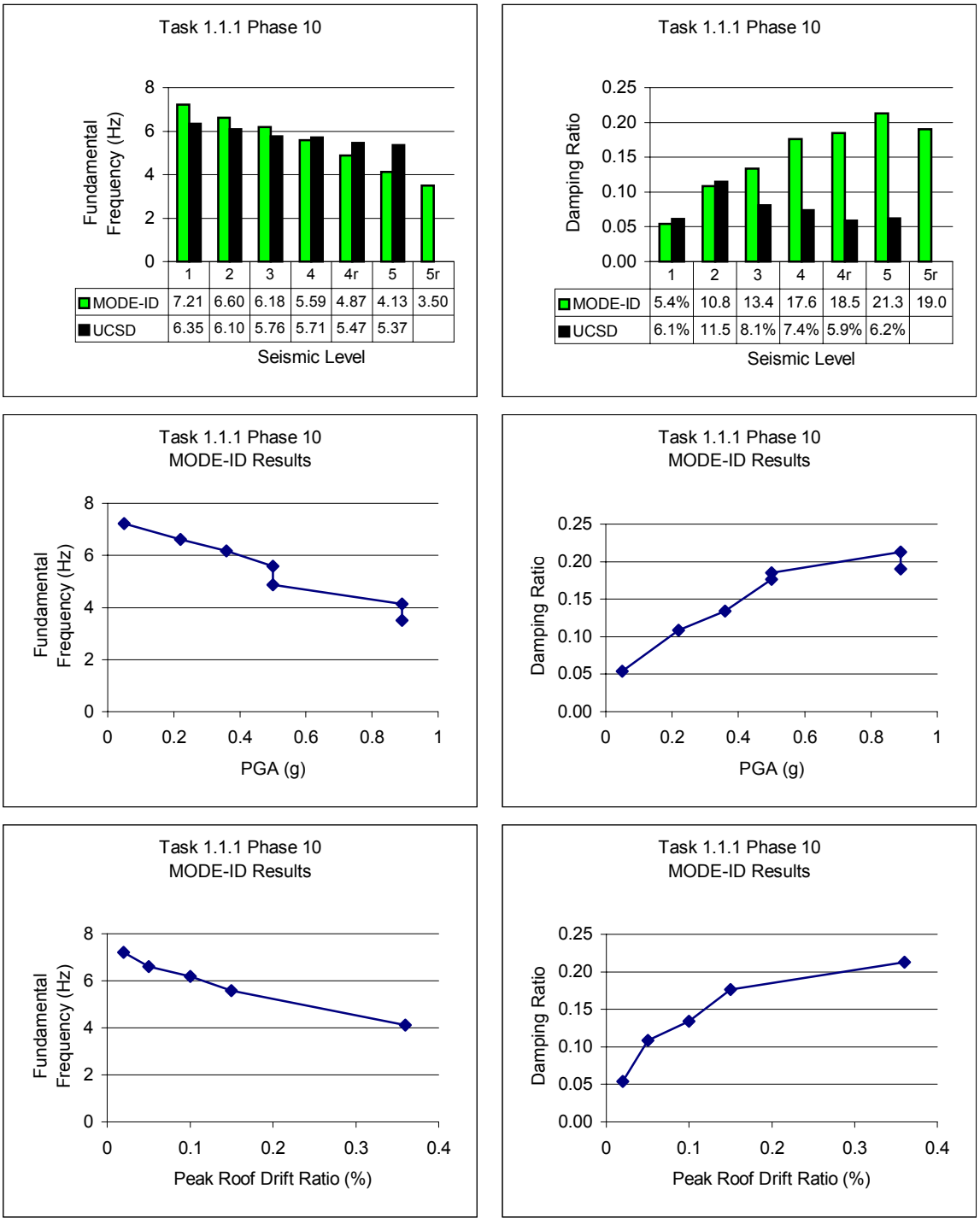

Figure 5.5: Fundamental Frequencies and Dampings, Phase 10

Table 5.1: MODE-ID Analysis of UCSD Phase 9 Data

Test Level	1	2	3	3r	4	5
PGA (g)	0.05	0.22	0.36	0.36	0.50	0.89
Peak Roof Drift Ratio	0.05%	0.30%	0.57%	–	1.1%	1.8%
MODE-ID Freq. (Hz)	4.16	3.58	2.88	2.63	2.23	1.88
MODE-ID Damp. Ratio	7.4%	20.1%	19.2%	15.7%	16.3%	15.1%
NMS Error (J)	0.226	0.161	0.144	0.111	0.128	0.112
UCSD Freq. (Hz)	3.91	3.71	3.66	3.42	2.93	2.93
UCSD Damp. Ratio	4.3%	4.2%	3.9%	6.2%	7.2%	8.7%

Table 5.2: MODE-ID Analysis of UCSD Phase 10 Data

Test Level	1	2	3	4	4r	5	5r
PGA (g)	0.05	0.22	0.36	0.50	0.50	0.89	0.89
Peak Roof Drift Ratio	0.02%	0.05%	0.10%	0.15%	–	0.36%	–
MODE-ID Freq. (Hz)	7.21	6.60	6.18	5.59	4.87	4.13	3.50
MODE-ID Damp. Ratio	5.4%	10.8%	13.4%	17.6%	18.5%	21.3%	19.0%
NMS Error (J)	0.066	0.046	0.55	0.074	0.086	0.096	0.092
UCSD Freq. (Hz)	6.35	6.10	5.76	5.71	5.47	5.37	–
UCSD Damp. Ratio	6.1%	11.5%	8.1%	7.4%	5.9%	6.2%	–

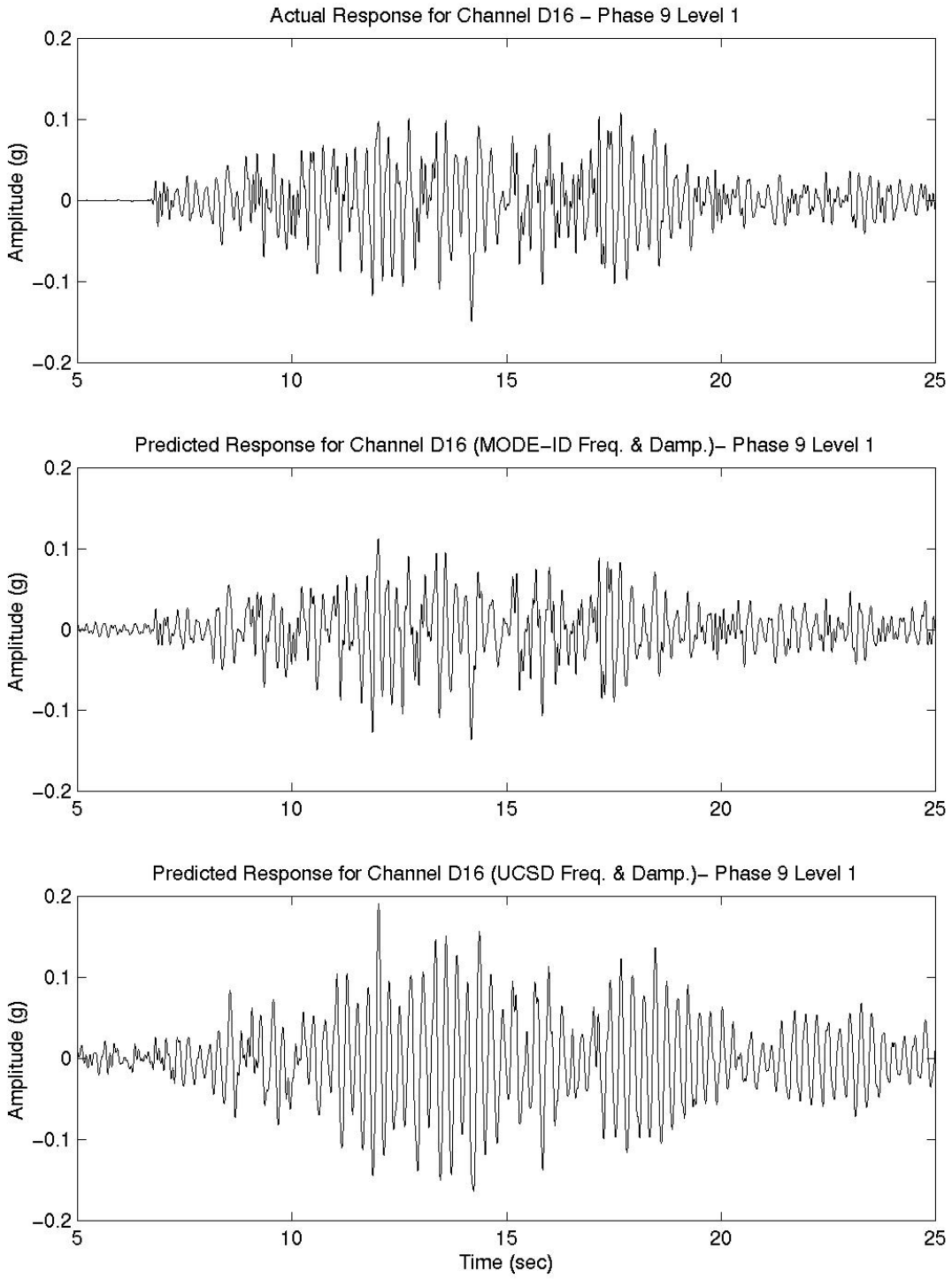

Figure 5.6: Recorded and Predicted Response at Channel D16 (Phase 9 Level 1)

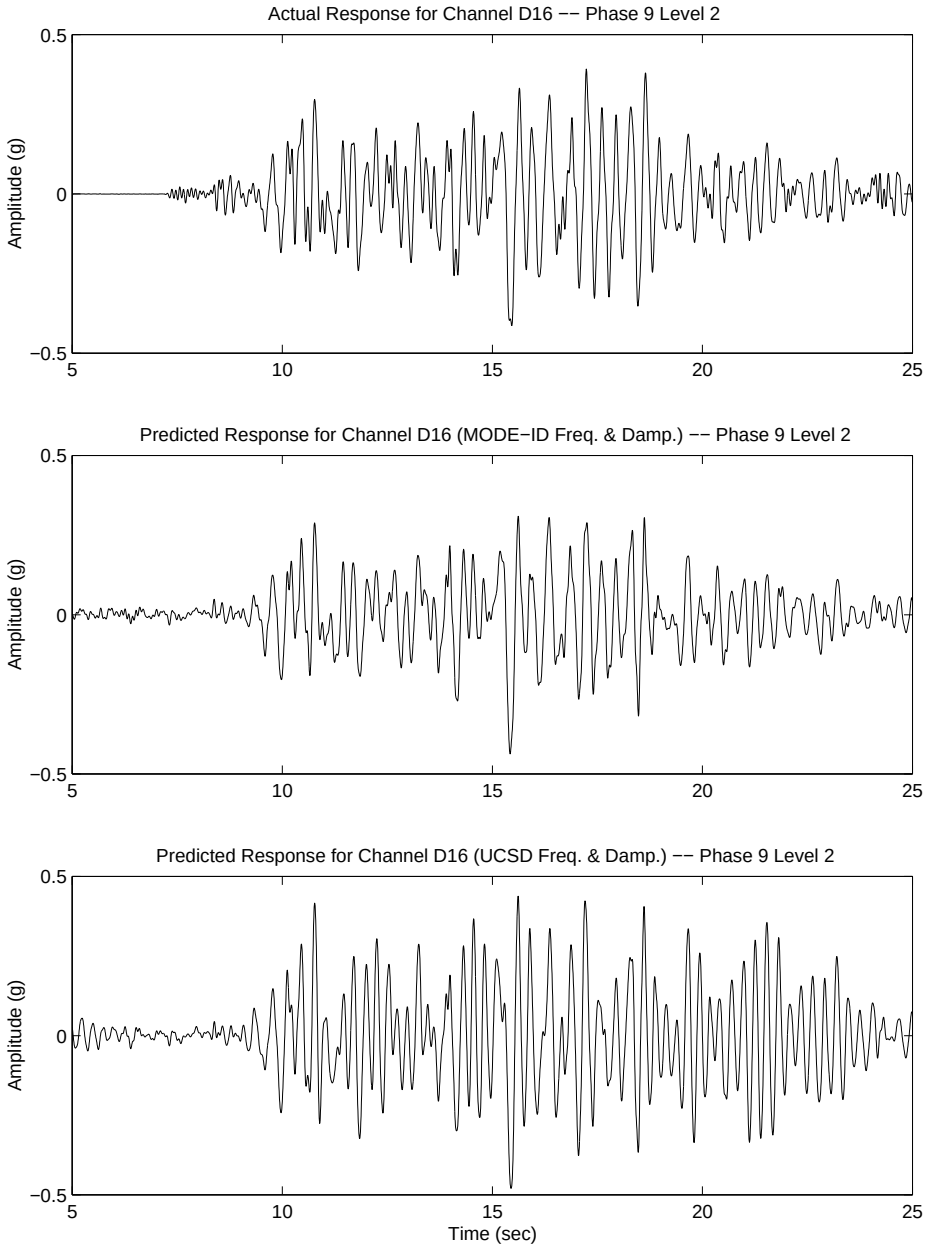

Figure 5.7: Recorded and Predicted Response at Channel D16 (Phase 9 Level 2)

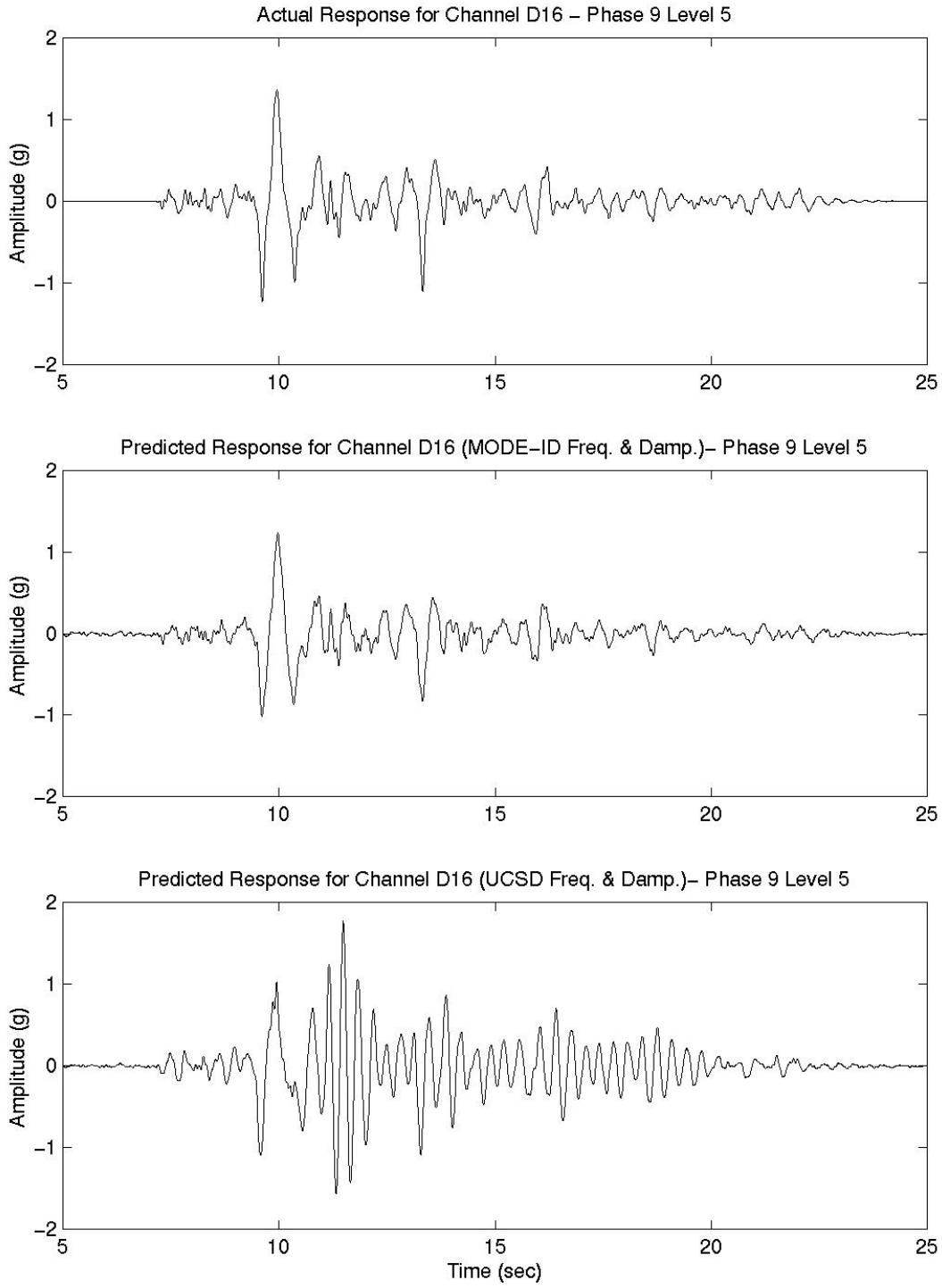

Figure 5.8: Recorded and Predicted Response at Channel D16 (Phase 9 Level 5)

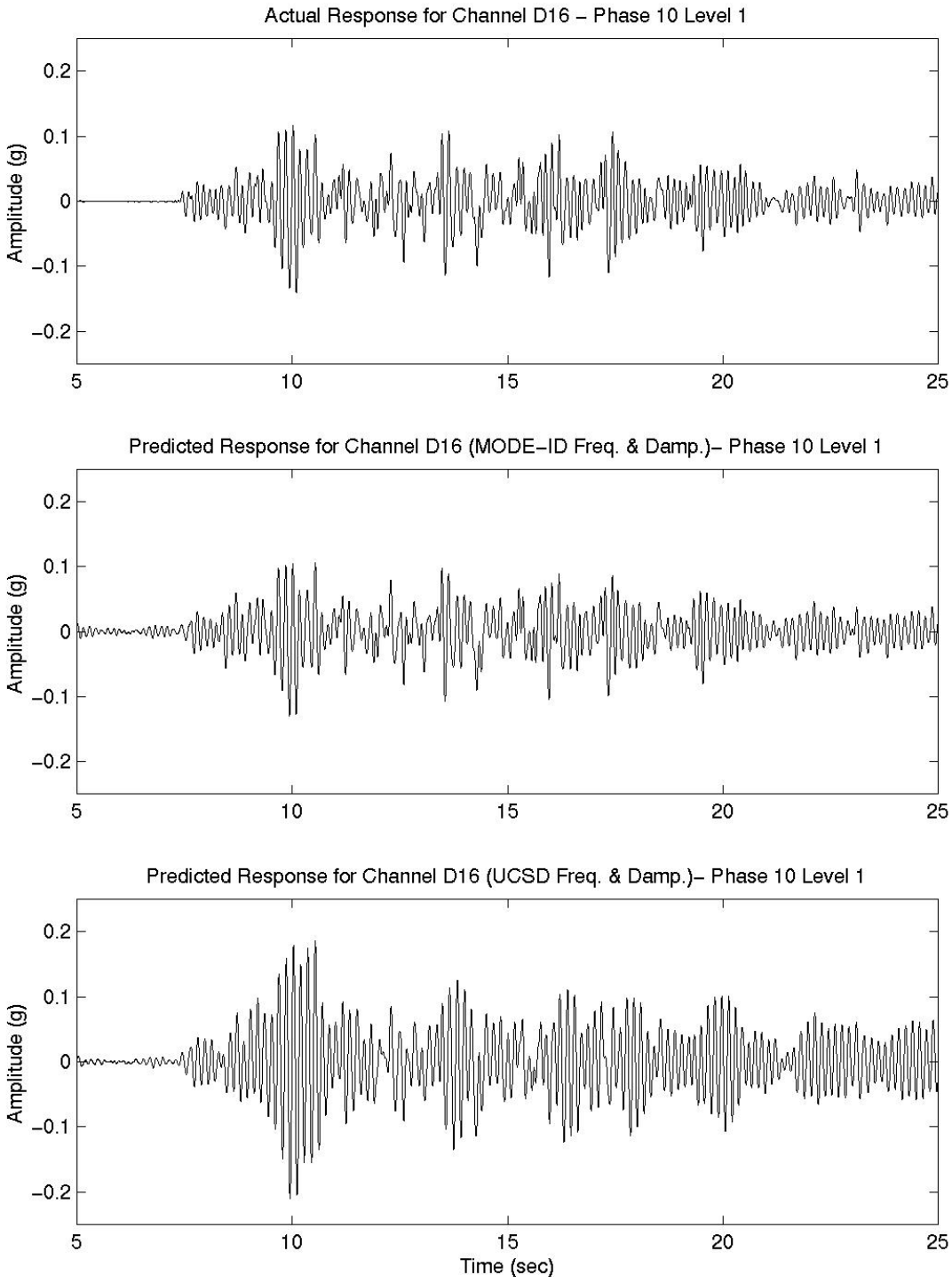

Figure 5.9: Recorded and Predicted Response at Channel D16 (Phase 10 Level 1)

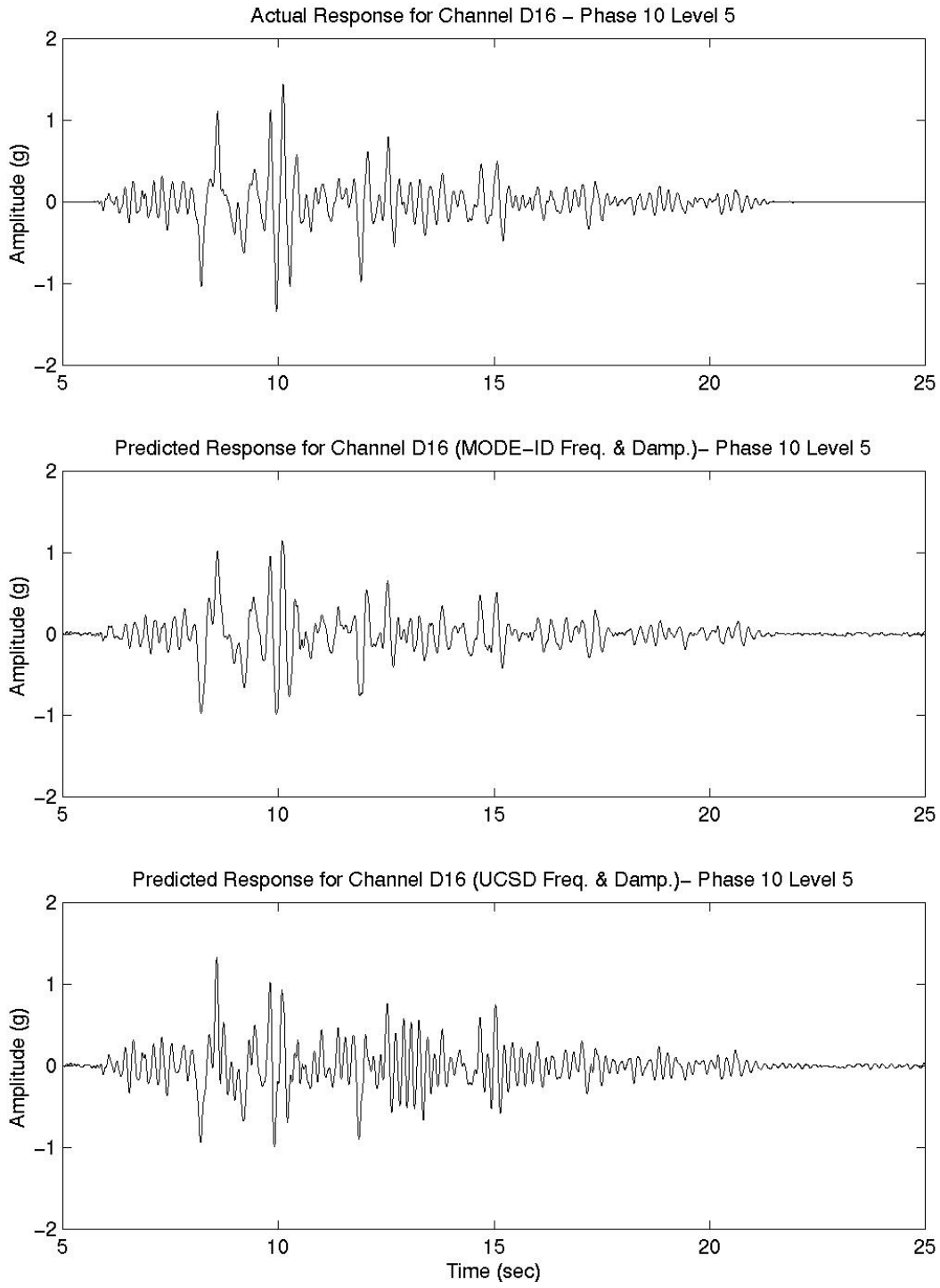

Figure 5.10: Recorded and Predicted Response at Channel D16 (Phase 10 Level 5)

5.2 UC Berkeley 3-Story Apartment Building

A 3-story woodframe building with tuck-under parking was tested under Task 1.1.2 of the CUREE-Caltech Woodframe Project. The test specimen was full-scale with respect to height, but the shake-table limited the building dimensions to 16'x32'. The prototype was shake-table tested during three main phases of construction: Phase I - no wall finish materials, no retrofit scheme (see Figure 5.11); Phase II - wall finishes installed, retrofitted structure; Phase III - wall finishes installed, no retrofit scheme (see Figure 5.12). For complete testing details, see Mosalam et al., 2002.

The Harvey Mudd shaker was placed at the third floor level of the structure and forced vibration tests were performed before and after each phase of shake-table testing to identify the modal properties of the building before and after damage. A model of the building using masses and springs was then used to produce frequency response curves that were best fit to the forced vibration data, allowing the damage observed to be described in terms of stiffness loss and changes in mode shapes. The modal properties identified by forced vibration tests of the undamaged structures were also used to verify the period formula by regression.

Figure 5.11: Phase I

Figure 5.12: Phase III

5.2.1 Forced Vibration Tests

The Harvey Mudd shaker was installed at the third floor of the structure, where it remained throughout all the phases of shake-table testing. The shaker was fastened to the floor diaphragm using tension rods (see Figures 5.13 and 5.14), and the remaining equipment (motor, controller) was secured during the shake-table tests using metal straps. The building response was recorded using two FBA-11 accelerometers at the roof, six FBA-11 accelerometers at the third floor, and six Ranger seismometers at the second floor. Because stronger shaking of the building caused clipping of the seismometer signals, only the accelerometer data (channels 1 through 8) were used to obtain the frequencies and dampings of the structure. See Figure 5.15 for the instrument locations.

Figure 5.13: Shaker Setup (third floor)

Figure 5.14: Shaker Setup (view of second floor ceiling)

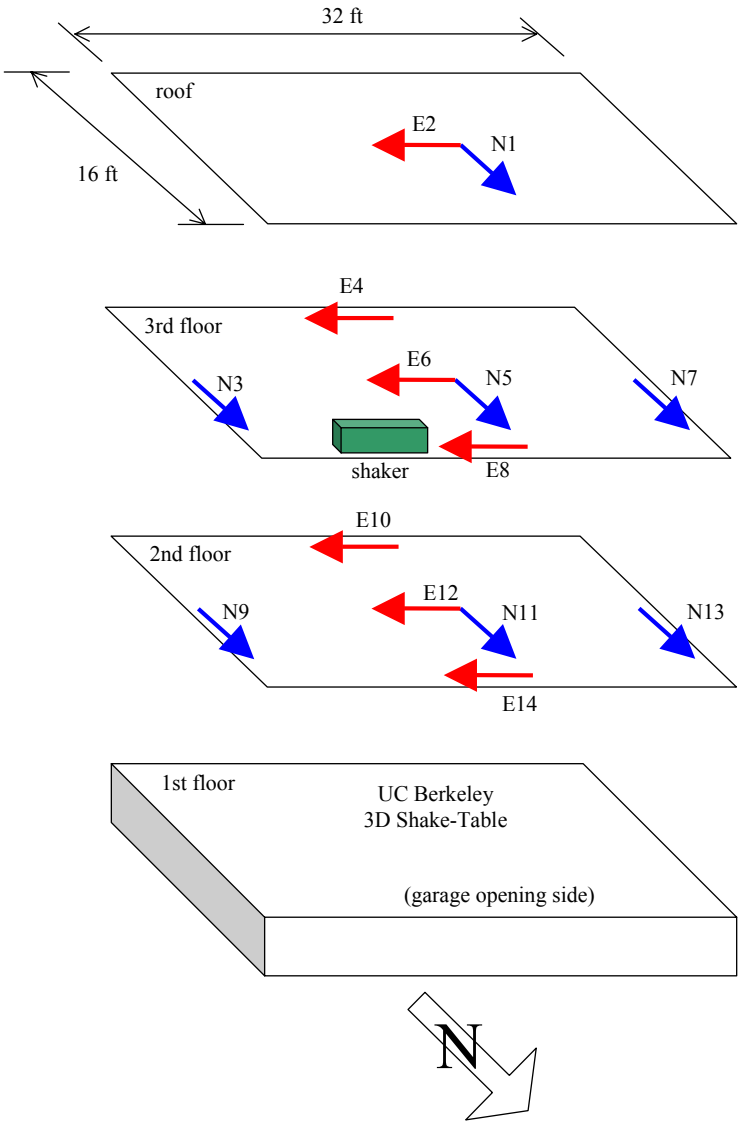

Figure 5.15: Instrument Locations

5.2.2 Analytical Model for System Identification Study

The data obtained from the 20% eccentricity forced vibration tests were used to identify a simple analytical shear model (no bending) of the building using twelve translational degrees of freedom, masses lumped at each floor, and twelve springs, one at each wall. The number of parameters to be identified was reduced by introducing constraints, and the selected model had six independent spring stiffnesses, K1 to K6 (see Figure 5.16, where the numbered degrees of freedom are in the direction of the arrows). The diaphragm rigidity was taken into account by adding diaphragm shear stiffness at each level, denoted GP2, GP3 and GPR for the second floor, third floor, and roof diaphragms, respectively. Solving the eigenvalue problem for the model using specified values for the masses and stiffnesses gives the modal frequencies and modeshapes for this building. The first four modes of the building were extracted and used, along with specified values for equivalent damping ratios, to compute the model response (in the frequency domain) due to a harmonic load at the shaker location.

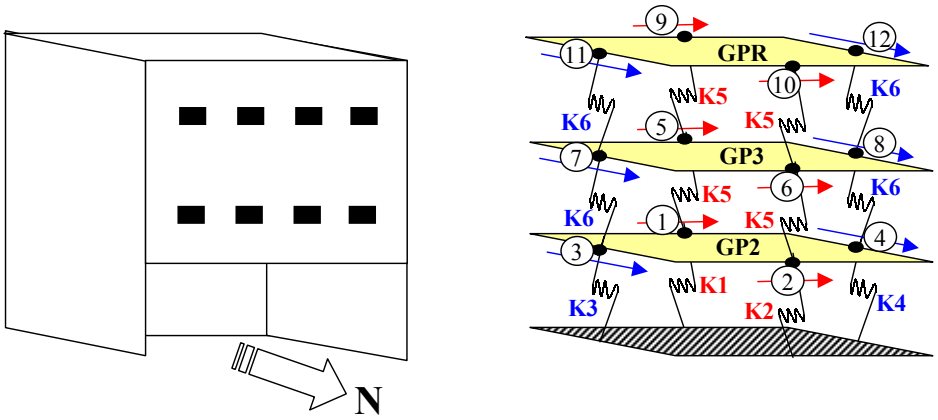

Figure 5.16: Analytical Shear Model

The effects of diaphragm stiffness and mass distribution were first studied using a symmetric test model with no garage opening and with wall story stiffnesses fixed at 1.0E+6 and 1.5E+6 lbs/in along the entire height of the walls in the transverse (NS: K3, K4, K6) and longitudinal (EW: K1, K2, K5) directions, respectively. The diaphragm behaves as nearly rigid as long as its stiffness value is of similar or greater

order of magnitude as those of the spring stiffnesses. As the diaphragm shear stiffness is reduced, the motion at the degrees of freedom perpendicular to the direction of shaking is reduced and approaches zero when the diaphragm is fully flexible. Also, when the diaphragm stiffness approached zero, the model response had an antisymmetric mode in each direction instead of a torsional mode involving all degrees of freedom. The NS and EW fundamental frequencies remained the same regardless of the diaphragm stiffness. Therefore, the diaphragm stiffness should be selected so the torsional frequency of the model as well as the amplitude of the response match the experimental data obtained.

Regarding the effects of the mass distribution, it was observed that a diagonal mass matrix produces dramatically different results from those obtained using a non-diagonal consistent mass matrix. The diagonal mass matrix comes from lumping of the wall and diaphragm masses at each degree of freedom (each of the four degrees of freedom in a floor has half the floor mass, the entire mass of the wall at its location, plus half of the wall masses corresponding to perpendicular degrees of freedom on that level, so the total mass in the mass matrix equals twice the total mass of the model), while the non-diagonal mass matrix comes from assuming a finite-element consistent mass distribution. The diagonal mass matrix results in torsional fundamental frequencies that are considerably lower (by a factor of $\sqrt{3}$) than the torsional frequencies produced by assuming the consistent mass distribution (non-diagonal matrix). The amplitude of the response of the torsional mode under harmonic excitation is also lower when the mass matrix is diagonal. The NS and EW fundamental frequencies remained the same regardless of the mass distribution. See Appendix E for the response curves and modal frequencies of this test model using different diaphragm stiffnesses and mass matrices.

The mass matrix selected for the identification model of the 3-story building was the sum of a diagonal matrix based on lumping the tributary wall masses at each degree of freedom and a non-diagonal consistent mass matrix based on a continuous distribution of the remaining mass at each level (floor diaphragm, partition walls). These masses were computed using unit weights for plywood, lumber, stucco and

drywall found in *Design of Wood Structures* (Breyer, 1993), plus the weights added at each level during each phase of shake-table testing (see Mosalam et al., 2002). The added weights accounted for the mass of components that would be present in a real building, such as the wall finishes that were not present in the Phase I structure, insulation, HVAC/plumbing/electrical systems, walkways, etc. Table 5.3 shows the computed weights at each floor and at each node for the Phase I structure (no wall-finish materials). Table 5.4 shows the computed weights at each floor and at each node for the Phase III structure (stucco and drywall installed). See Appendix F for details in the computation of these weights.

Table 5.3: Phase I Weights

Consistent Mass					
2nd Floor Weights (lbs)		3rd Floor Weights (lbs)		Roof Weights (lbs)	
Wood =	3,101	Wood =	3,101	Wood =	2,266
Added =	9,400	Added =	11,000	Added =	7,600
TOTAL =	12,501	TOTAL =	14,101	TOTAL =	9,866

Nodal Weights – Wood (lbs)			
W1 = 900	W2 = 1,081	W3 = 450	W4 = 450
W5 = 814	W6 = 814	W7 = 407	W8 = 407
W9 = 407	W10 = 407	W11 = 203	W12 = 203

Total Building Weight (lbs) = 43,101 lbs

Table 5.4: Phase III Weights

Consistent Mass					
2nd Floor Weights (lbs)		3rd Floor Weights (lbs)		Roof Weights (lbs)	
Wood + Finish =	5,601	Wood + Finish =	5,601	Wood + Finish =	3,866
Added =	2,000	Added =	2,000	Added =	2,600
TOTAL =	7,601	TOTAL =	7,601	TOTAL =	6,466

Nodal Weights – Wood + Finish (lbs)			
W1 = 4,680	W2 = 2,971	W3 = 2,340	W4 = 2,340
W5 = 4,594	W6 = 4,594	W7 = 2,297	W8 = 2,297
W9 = 2,297	W10 = 2,297	W11 = 1,148	W12 = 1,148

Total Building Weight (lbs) = 54,670 lbs

The model parameters $\underline{a}$ to be updated included the spring and diaphragm stiffnesses, damping ratios, and an amplitude scaling constant (c). This constant allows for uncertainty in the mass, shaker force and/or signal processing, and it is simply a multiplier of the equations of motion (see Equation 5.1).

$$M\underline{\ddot{x}} + C\underline{\dot{x}} + K\underline{x} = \frac{1}{c}\underline{F} \tag{5.1}$$

where M, C and K are the mass, damping and stiffness matrices and $\underline{x}$ and $\underline{F}$ are the displacement response and excitation force, respectively, at each degree of freedom. Classical modes of vibration were assumed, i.e., $KM^{-1}C = CM^{-1}K$.

A minimization routine was used to best-fit the model frequency-response curves to the experimental data for six channels (N1, E2, N3, E4, N7 and E8, see Figure 5.15) in a least-squares sense. This simple routine used the $Matlab$ function $fmins$ to minimize the expression for the normalized squared error shown in Equation 5.2, where $\widehat{A}_{i,j}$ is the amplitude of the building response recorded at channel i due to EW or NS shaking at frequency ω_j, $A_{i,j}(\underline{a})$ is the model response amplitude (computed using parameters $\underline{a}$) at the location of channel i due to EW or NS shaking at frequency ω_j, N_i is the number of data channels used and N_j is the number of frequencies sampled.

$$J_{norm}(\underline{a}) = \left.\frac{\sum_{i=1}^{N_i}\sum_{j=1}^{N_j}|\widehat{A}_{i,j} - A_{i,j}(\underline{a})|^2}{\sum_{i=1}^{N_i}\sum_{j=1}^{N_j}|\widehat{A}_{i,j}|^2}\right|_{EW} + \left.\frac{\sum_{i=1}^{N_i}\sum_{j=1}^{N_j}|\widehat{A}_{i,j} - A_{i,j}(\underline{a})|^2}{\sum_{i=1}^{N_i}\sum_{j=1}^{N_j}|\widehat{A}_{i,j}|^2}\right|_{NS} \tag{5.2}$$

Constraints were used to reduce the number of variables to be found, reducing the computational effort and improving the convergence properties of the minimization routine. They also allow easy correlation between the parameters for the undamaged and damaged building. The springs at the second and third floor levels representing walls of the same length and nailing patterns were constrained to have the same stiffness values, since only the walls at the first floor level experienced significant damage. This resulted in six independent spring values. Also, all spring stiffnesses for the damaged building models were constrained to remain the same as or less than

their respective undamaged values. The diaphragm stiffness was constrained to one value at the second and third floors and to 60% of that value at the roof (to account for the different plywood thickness of 3/8" at the roof versus 5/8" at the floors), resulting in one independent diaphragm shear stiffness value. The amplitude scaling constant was also estimated during identification of the undamaged Phase I and Phase III structures and then constrained to remain the same during the identification of the damaged structures, since any discrepancy in the calculated mass, force or signals recorded was expected to remain the same before and after damage.

The sensitivity of the normalized squared error (Jnorm, Equation 5.2) to the model diaphragm stiffness (GP) was examined by finding the best-fit model parameters assuming a diaphragm stiffness fixed at a given value. Plots of the resulting spring stiffnesses and normalized squared error (Jnorm) are given in Figures 5.17 through 5.21.

In Figures 5.17 through 5.21, the horizontal axis represents the specified values of diaphragm stiffness (a logarithmic scale was used), the left axis represents values for the normalized squared error (Jnorm) and the right axis represents the best-fit spring stiffness values. These plots show that higher values of diaphragm stiffness have a minimal effect on the best fit spring stiffnesses and on Jnorm, but small changes in diaphragm stiffness at lower values have a significant effect on the best-fit spring stiffnesses.

It was necessary to investigate whether the diaphragm stiffness should be estimated or held at a nearly rigid value. Allowing diaphragm flexibility in the identification model does not give meaningful results for wall stiffnesses. The relative values of the spring stiffnesses corresponding to the best-fit diaphragm stiffnesses are not realistic, as can be seen in Figure 5.17, where the selected stiffness for spring K4 is considerably higher than that of spring K1 even though the wall corresponding to spring K1 is twice as long and has more closely spaced nails than the wall corresponding to spring K4, and therefore it would be expected that the spring stiffness K1 would be greater than K4. Also, selecting different diaphragm stiffnesses before and after the shake-table tests would not allow for the comparison of spring stiffness

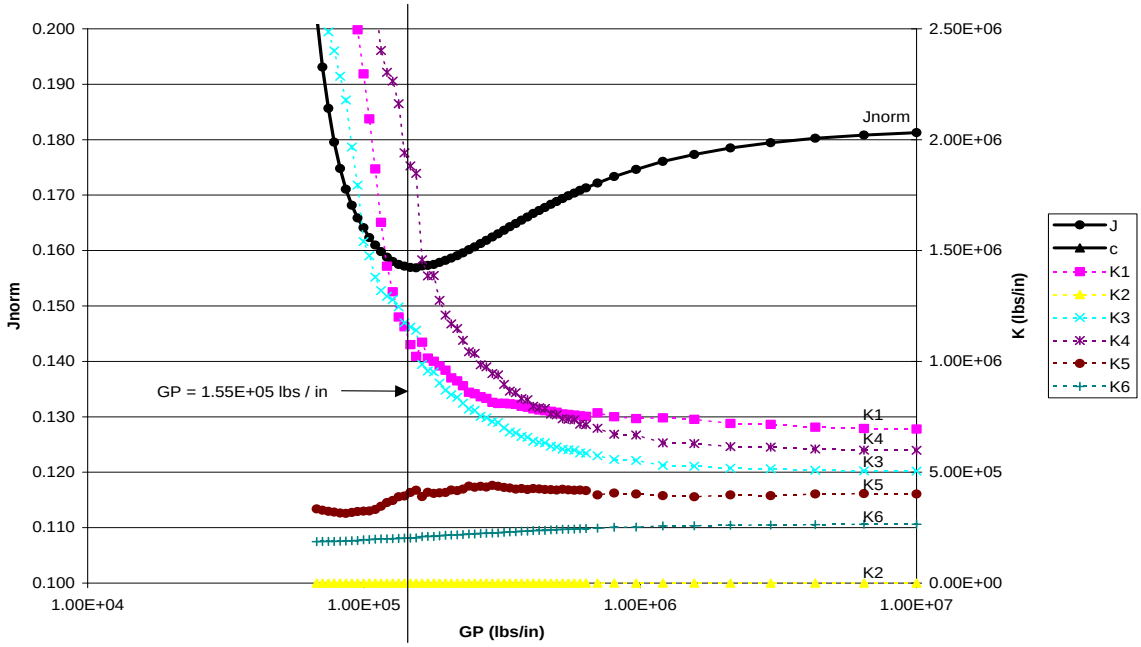

Figure 5.17: Model Sensitivity to Diaphragm Stiffness (before Phase I)

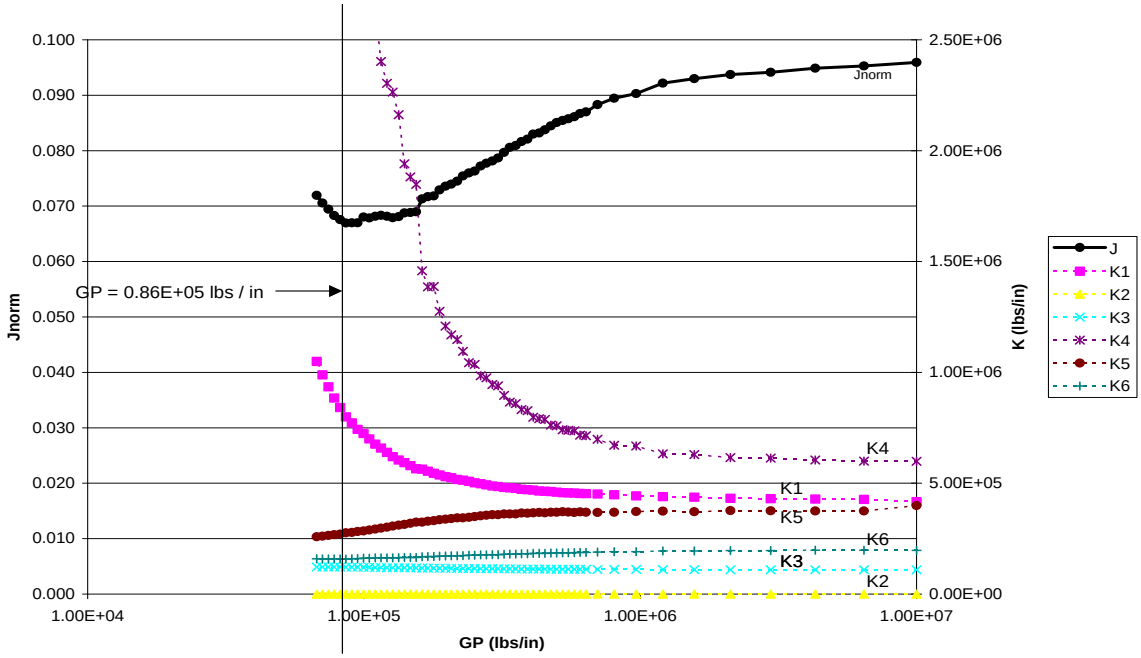

Figure 5.18: Model Sensitivity to Diaphragm Stiffness (after Phase I)

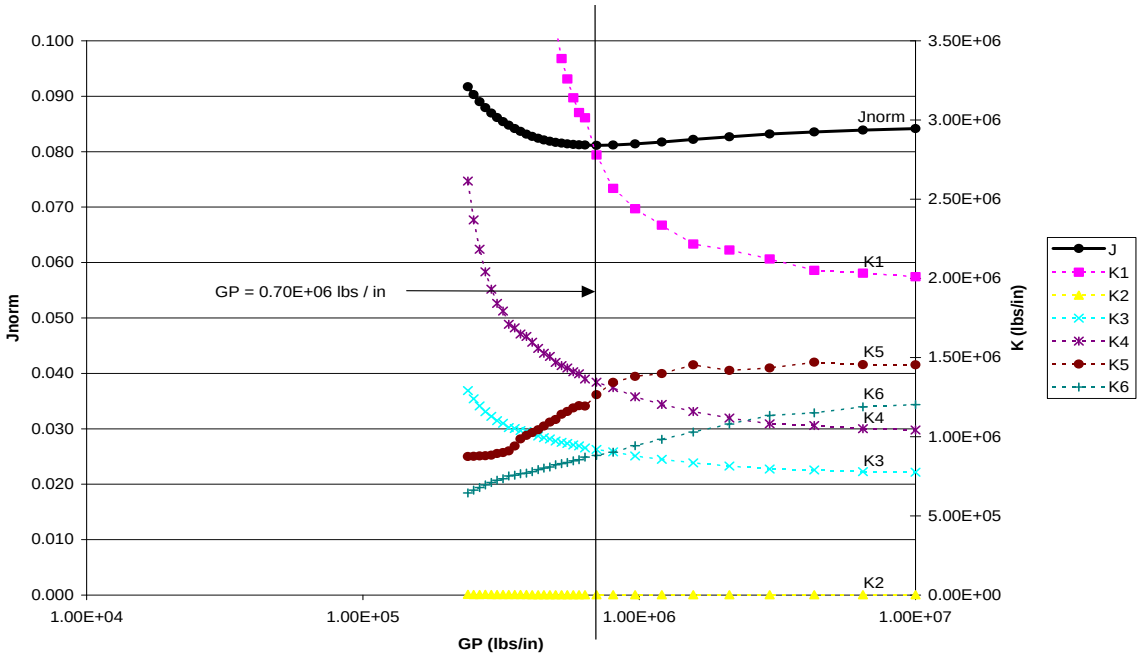

Figure 5.19: Model Sensitivity to Diaphragm Stiffness (before Phase III)

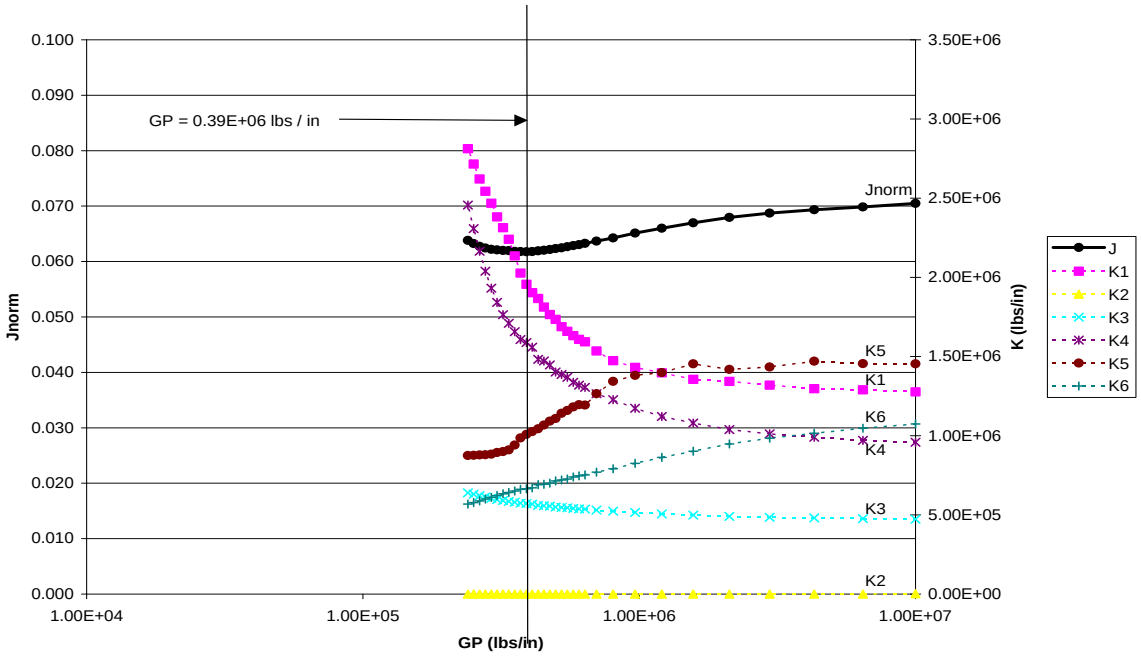

Figure 5.20: Model Sensitivity to Diaphragm Stiffness (after Phase III)

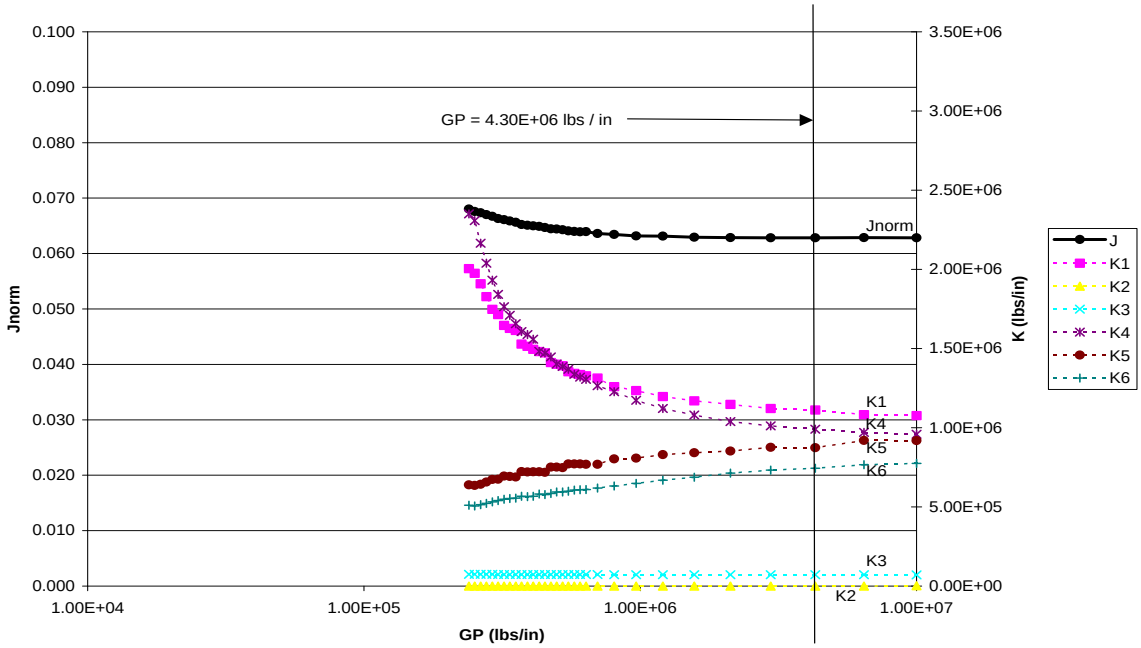

Figure 5.21: Model Sensitivity to Diaphragm Stiffness (after repeated shaking)

values before and after damage, even though the diaphragm stiffness is expected to drop during the shake-table tests. For example, before Phase I shake-table tests, the best-fit value for K4 is 1.8E+06 lbs/in at GP = 1.55E+05 lbs/in, while the corresponding value for K4 after damage at GP = 0.86E+05 lbs/in would be over 2.5E+06 lbs/in (see Figures 5.17 and 5.18). Therefore, the rigid diaphragm model corresponding to GP = 1.0E+7 was selected and used to compute the stiffness drop as a result of damage from the shake-table tests. The results are discussed in the following sections.

5.2.3 Phase I Structure: No Wall Finish

The Phase I structure had no wall finish, only the exterior wall sheathing was in place (see Figure 5.11). To avoid damaging the building, the forced vibration tests were performed with shaker weights restricted to 5%, 10%, 15%, and 20% eccentricity before the Phase I shake-table tests. After the shake-table tests, the building was also shaken at 50% and 100% eccentricity. The building response was recorded for harmonic shaking between 1.5Hz and 5.5Hz, at 0.1Hz increments, in each direction. Each recording was taken for 5 seconds at 1000 samples per second.

After the Phase I shake-table tests, there was severe damage to the east wall at the lower level of the building, where some of the sheathing had separated from the studs due to some of the nails pulling through the sheathing or shearing off. There was also evidence that a few of the nails on the east wall (at least three or four nails) had not been properly fastened to the studs during construction of the test structure and either missed the stud completely or just barely made it in, which could help explain the concentration of damage observed at the east wall.

5.2.3.1 Forced Vibration Test Results

Because stronger shaking of the building caused clipping of the seismometer signals, only the accelerometer data (channels 1 through 8) were used to obtain the frequencies and dampings of the structure. Plots from forced vibration tests performed before Phase I shake-table testing are shown in Figure 5.22, and a summary of these results is shown in Table 5.5. Plots from forced vibration tests performed after Phase I shake-table testing are shown in Figure 5.23, and a summary of these results is shown in Table 5.6. All the curves shown are from the accelerometers at the roof and third floor (see Figure 5.15), and the vertical axes are proportional to velocity (acceleration divided by the frequency) and normalized by the square of the frequency to account for the frequency dependence of the shaker force.

The frequencies and damping ratios given in Tables 5.5 and 5.6 were obtained using a curve-fitting approach involving least-squares matching of the theoretical

and experimental frequency response curves (see section 4.2 for details of the forced vibration data analysis). Because the first two natural frequencies of the undamaged Phase I building were uncoupled, shaking in the NS and EW directions excited mostly the corresponding mode in that direction and it was not possible to identify the NS frequency using the EW shaking data and viceversa (see dashed lines in Table 5.5). The building response is nonlinear, since the increase of the response curve amplitudes is not proportional to the shaker force increase and increasing the shaker force lowers the natural frequencies (see Figures 5.22 and 5.23).

Table 5.5: Experimental Results Before Phase I (no wall finish)

Test Date	Shaking Direction	Eccentr.	1st Mode		2nd Mode	
			Freq. (Hz)	Damp.	Freq. (Hz)	Damp.
Sep 21, 2001	NS	2.5%	–	–	3.09	2.6%
	EW	2.5%	2.85	2.3%	–	–
Sep 23, 2001	NS	5%	–	–	3.10	2.7%
		10%	–	–	3.02	2.8%
		15%	–	–	3.00	3.1%
		20%	–	–	2.96	3.4%
	EW	5%	2.86	2.6%	–	–
		10%	2.82	3.1%	–	–
		20%	2.76	4.0%	–	–

Table 5.6: Experimental Results After Phase I (no wall finish)

Test Date	Shaking Direction	Eccentr.	1st Mode		2nd Mode	
			Freq. (Hz)	Damp.	Freq. (Hz)	Damp.
Oct 13, 2001	NS	5%	1.95	5.1%	2.56	2.9%
		10%	1.87	5.5%	2.50	3.2%
		15%	1.82	6.0%	2.46	3.4%
		20%	1.80	6.1%	2.44	3.5%
		50%	1.62	6.8%	2.29	5.3%
		100%	1.45	6.3%	n/a	n/a
	EW	5%	1.94	5.0%	2.59	3.0%
		10%	1.87	6.0%	2.52	3.7%
		15%	1.84	5.8%	2.48	4.0%
		20%	1.81	5.9%	2.46	4.6%

5.2.3.2 Modelling Results

Many models were considered, each with a set of constraints to reduce the number of springs to be found, and the simplest model (fewest springs) able to capture the experimental behavior was selected. For each model, the selected spring stiffnesses were those that resulted in frequency response curves that best-fit the experimental data for EW and NS shaking at 20% eccentricity. A six-spring model was chosen to represent the structure with no wall finish materials (see Figure 5.16).

Figure 5.24 shows a plot of the response curves obtained prior to the Phase I shake-table tests (for shaking in EW and NS directions at 20% eccentricity). Although in theory the east and west walls should have the same stiffnesses (according to the building plans), the asymmetry in the experimental response curves is best captured by the six-spring model allowing different spring stiffness values for the east and west walls (see Figure 5.25). These different stiffnesses can perhaps be explained by the faulty nailing which was observed after Phase I tests were concluded. The best-fit model parameters for the six-spring model are summarized in Table 5.7 and discussed in section 5.3. The model modeshapes for the first three modes are shown in Figure 5.26.

Figure 5.27 shows a plot of the response curves obtained after the Phase I shake-table tests (for shaking in EW and NS directions at 20% eccentricity). Although constraining the damage to occur only on the south and east walls gives a reasonable fit of the experimental data, the model allowing all springs to be damaged gives a better fit and therefore this was the model selected (see Figure 5.28). This is reasonable since a moderate amount of damage is expected to have occurred throughout the building even though the most severely damaged walls were the south and east walls. The results are summarized in Table 5.8 and discussed in section 5.3. The model modeshapes for the first three modes are shown in Figure 5.29.

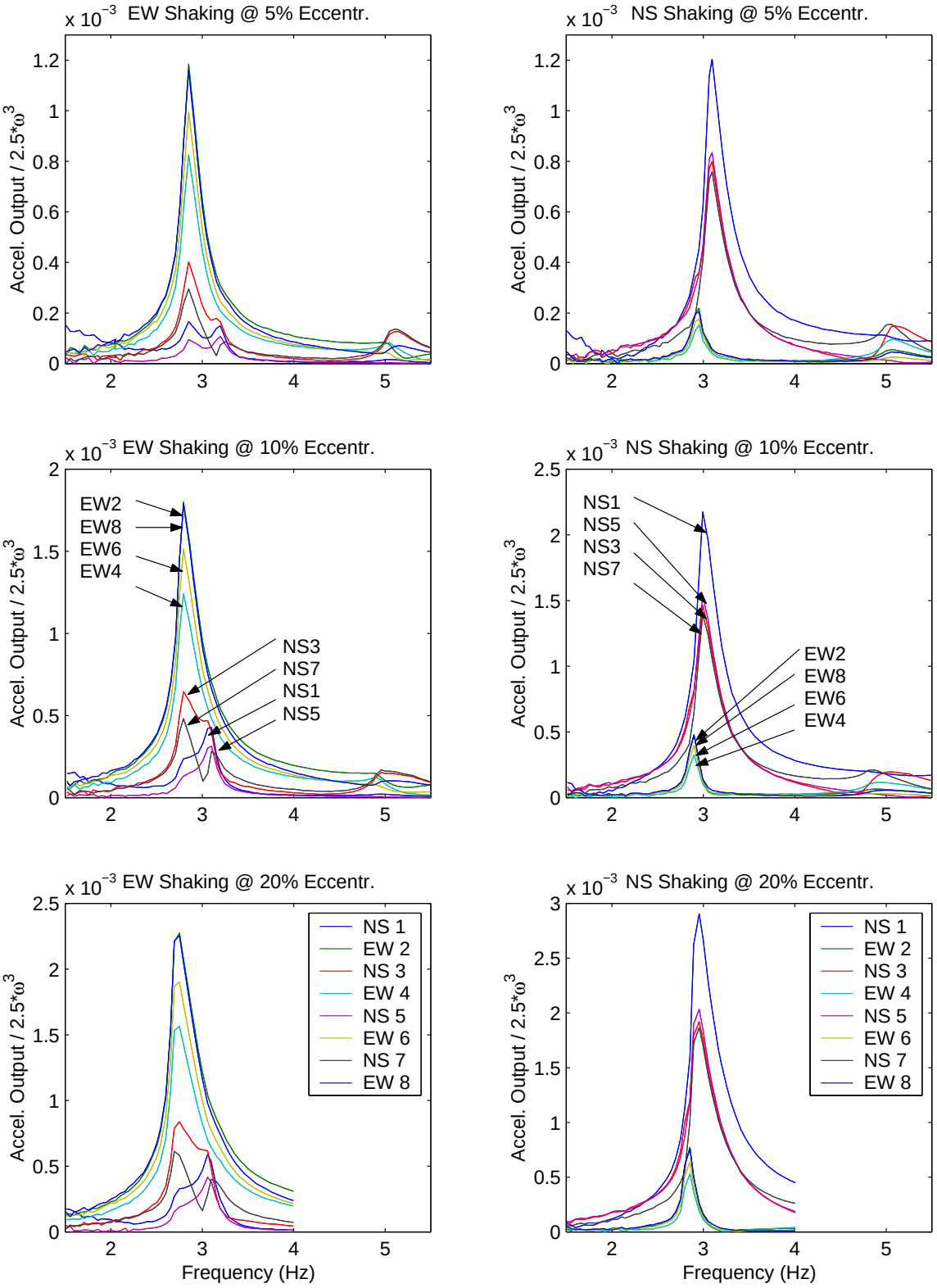

Figure 5.22: Experimental Results Before Phase I (no wall finish)

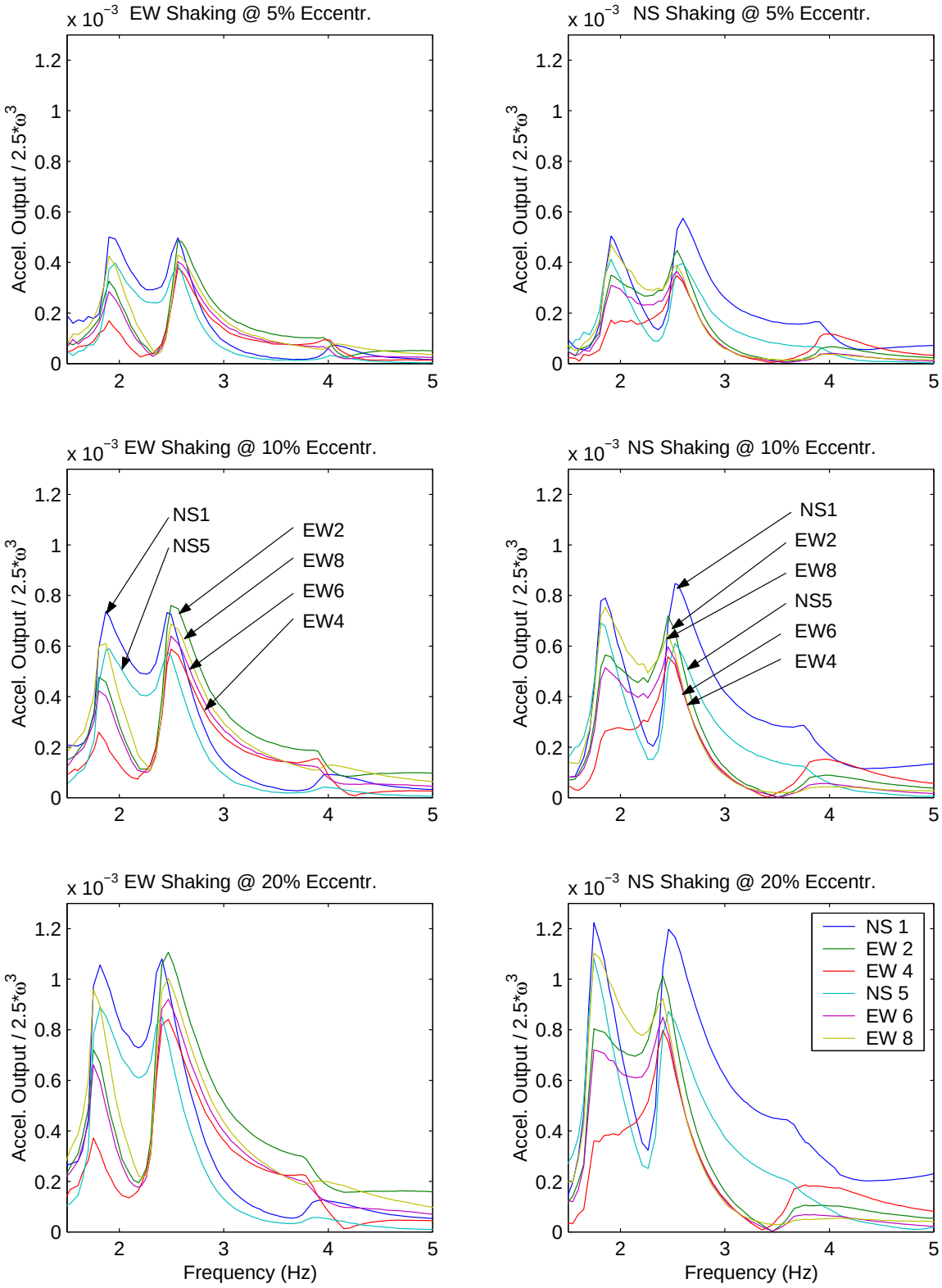

Figure 5.23: Experimental Results After Phase I (no wall finish)

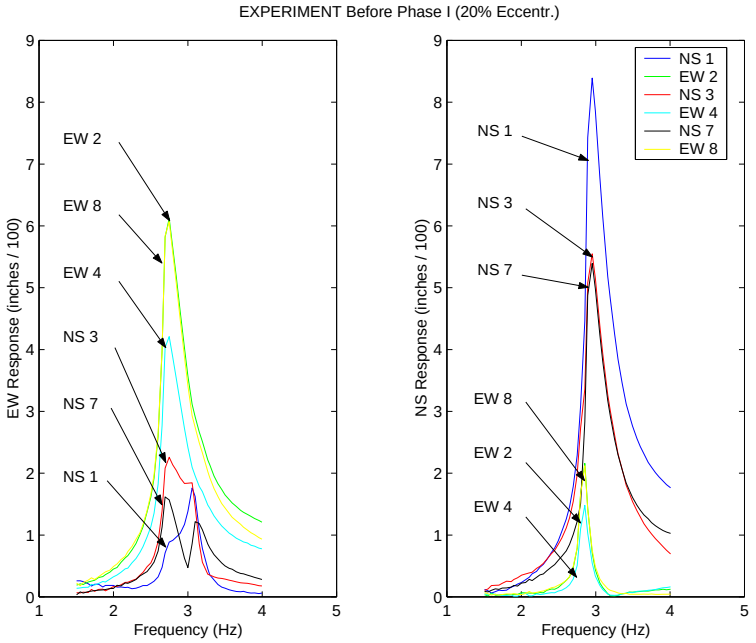

Figure 5.24: Experimental Data (before Phase I testing)

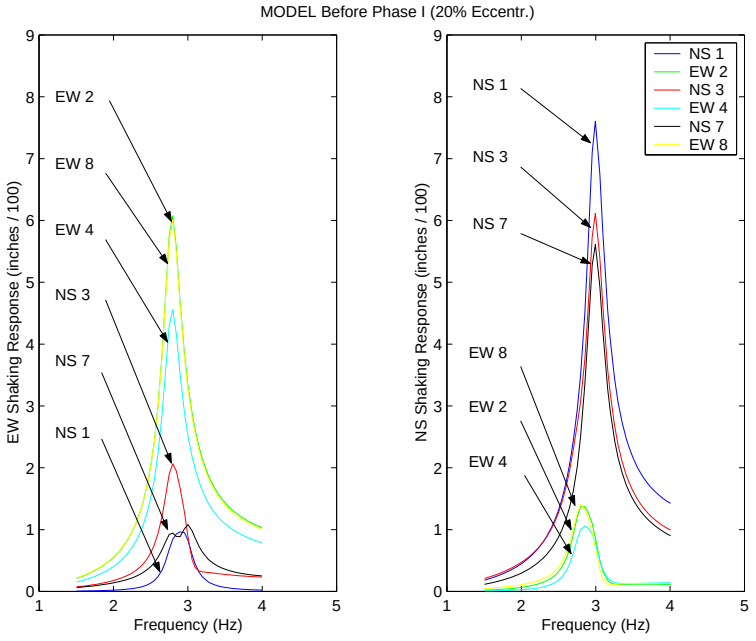

Figure 5.25: Model Response (before Phase I testing)

Table 5.7: Model Results from Tests Before Phase I

Diaphragm Stiffness	Scaling Constant	Jnorm
0.10E+8 lbs/in	1.170	0.1813

Spring Stiffnesses (lbs/in)					
K1	K2	K3	K4	K5	K6
0.69E+6	0.00E+6	0.50E+6	0.60E+6	0.40E+6	0.27E+6

Modal Properties		
$\omega_1 = 2.79$ Hz	$\omega_2 = 2.99$ Hz	$\omega_3 = 4.97$ Hz
$\zeta_1 = 4.3\%$	$\zeta_2 = 3.7\%$	$\zeta_3 = --$

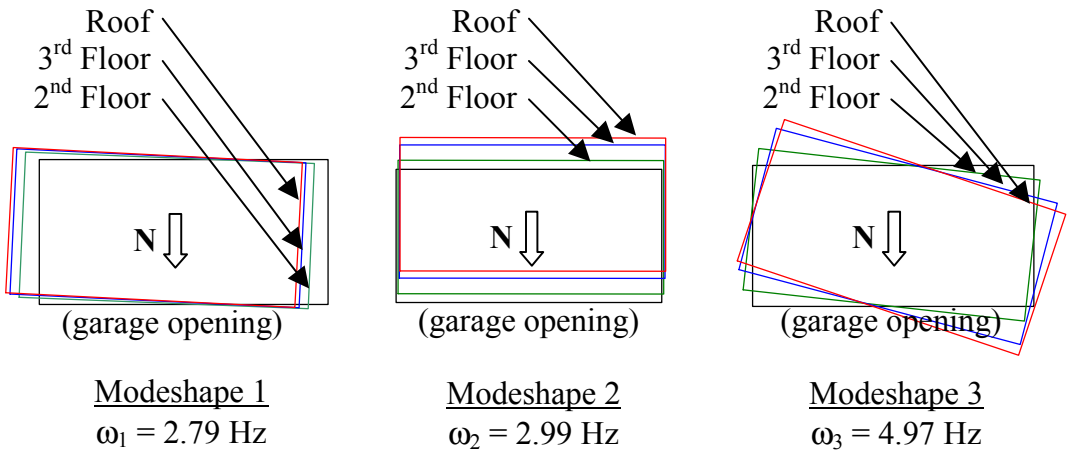

Figure 5.26: Modeshapes (before Phase I testing)

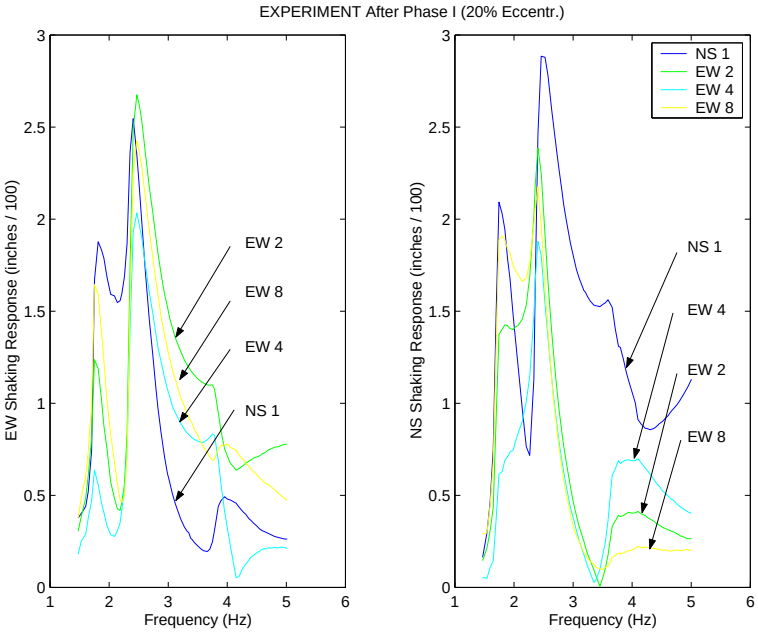

Figure 5.27: Experimental Data (after Phase I testing)

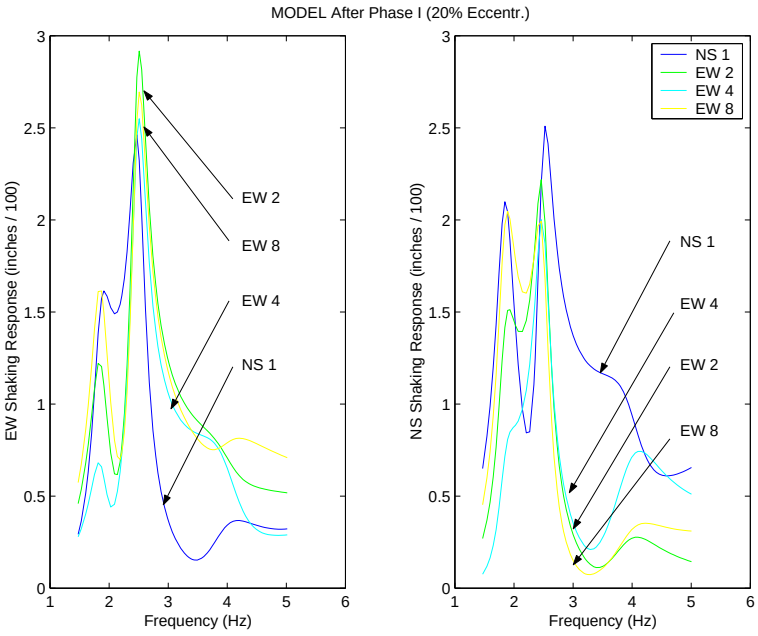

Figure 5.28: Model Response (after Phase I testing)

Table 5.8: Model Results from Tests After Phase I

Diaphragm Stiffness	Scaling Constant	Jnorm
0.10E+8 lbs/in	1.170	0.0959

Spring Stiffnesses (lbs/in)					
K1	K2	K3	K4	K5	K6
0.42E+6	0.00E+6	0.11E+6	0.60E+6	0.39E+6	0.20E+6

Modal Properties		
$\omega_1 = 1.86$ Hz	$\omega_2 = 2.49$ Hz	$\omega_3 = 3.99$ Hz
$\zeta_1 = 8.6\%$	$\zeta_2 = 5.3\%$	$\zeta_3 = 10.6\%$

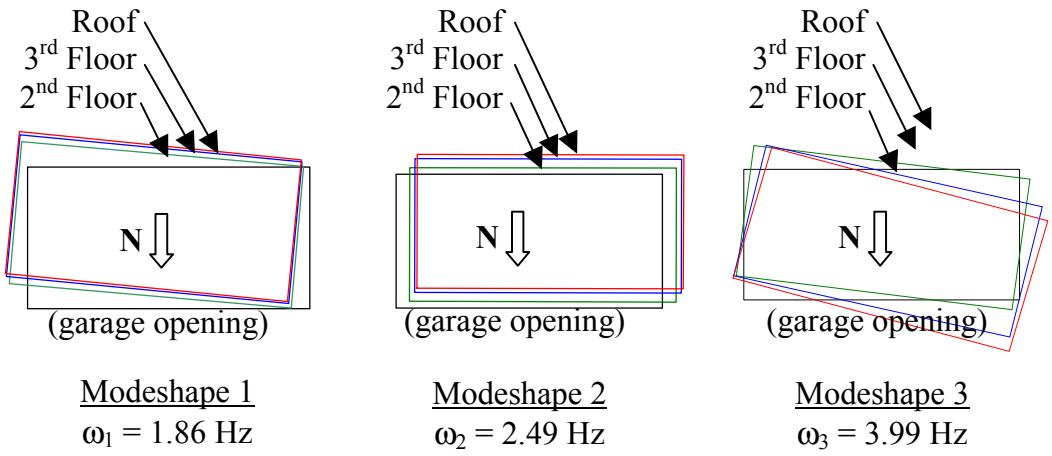

Figure 5.29: Modeshapes (after Phase I testing)

5.2.4 Phase III Structure: Wall Finishes Installed

After repairs to Phase I damage were completed (sheathing was replaced where deemed necessary), all finish materials, such as exterior stucco on metal lath and interior drywall, were installed. Then a retrofit scheme comprised of a steel moment resisting frame was bolted to the girder at the garage opening and the Phase II shake-table tests were performed. No significant damage was observed after the Phase II tests, except for a few minor hairline cracks. Therefore, no repairs were done prior to the Phase III tests, only the steel moment-resisting frame and retrofit scheme were removed (see Figure 5.12). To avoid damaging the building, the forced vibration tests prior to the Phase III tests were limited to 5%, 10%, and 20% shaker weight eccentricity. After the Phase III shake-table tests were completed, the shaker weights were also placed at 50% and 100% eccentricity, since damage to the structure was no longer a concern. The building response was recorded for shaking between 2.0Hz and 6.0Hz, at 0.1Hz increments, in each direction. Each recording was taken for 5 seconds at 1000 samples per second.

After the Phase III shake-table tests, there was considerable cracking of the stucco all throughout the building and there was some spalling at the north edge of the east wall, although the damage observed did not appear to be severe.

After the conclusion of all Task 1.1.2 testing (Phases I through III), one additional set of shake-table tests was designed to further damage the structure and perhaps initiate a collapse mechanism. The ground motions used were from the 1994 Northridge and 2000 Turkey earthquakes. There was considerable deterioration of the east wall, with the stucco completely separating from the sheathing along the first floor level, but there was no indication of imminent collapse. After all shake-table tests were concluded, forced vibration tests were performed placing the shaker weights at 5%, 10%, 20%, 50% and 100% eccentricity. The building response was recorded for shaking between 1.0Hz and 4.5Hz, at 0.1Hz increments, in each direction. Each recording was taken for 5 seconds at 1000 samples per second.

5.2.4.1 Forced Vibration Test Results

Because stronger shaking of the building caused clipping of the seismometer signals, only the accelerometer data (channels 1 through 8) were used to obtain the frequencies and dampings of the structure. Plots from forced vibration tests performed before Phase III shake-table testing are shown in Figure 5.30, and a summary of these results is shown in Table 5.9. Plots from forced vibration tests performed after Phase III shake-table testing are shown in Figure 5.31, and a summary of these results is shown in Table 5.10. Plots from forced vibration tests performed after repeated shake-table testing using strong ground motions as input are shown in Figure 5.32, and a summary of these results is shown in Table 5.11. All the curves shown are from the accelerometers at the roof and third floor, and the vertical axes are proportional to velocity (acceleration divided by the frequency) and normalized by the square of the frequency to account for the frequency dependence of the shaker force. Note that there is significant noise in signals from the severely damaged structure at low amplitude of shaking (lower weight eccentricity or lower frequencies), but as the shaker force increases (higher weight eccentricity or higher frequencies), the relative amount of noise in the signals is reduced. The frequencies and damping ratios given in Tables 5.9 and 5.11 were obtained using the same curve-fitting approach described in section 4.2. Because the first two natural frequencies of the undamaged Phase III building were so close together, only the first mode frequency and damping was found using the EW shaking data (see dashed lines in Table 5.9). The building response is nonlinear, since the increase of the response curve amplitudes is not proportional to the shaker force increase and increasing the shaker force lowers the natural frequencies (see Figures 5.30 through 5.32).

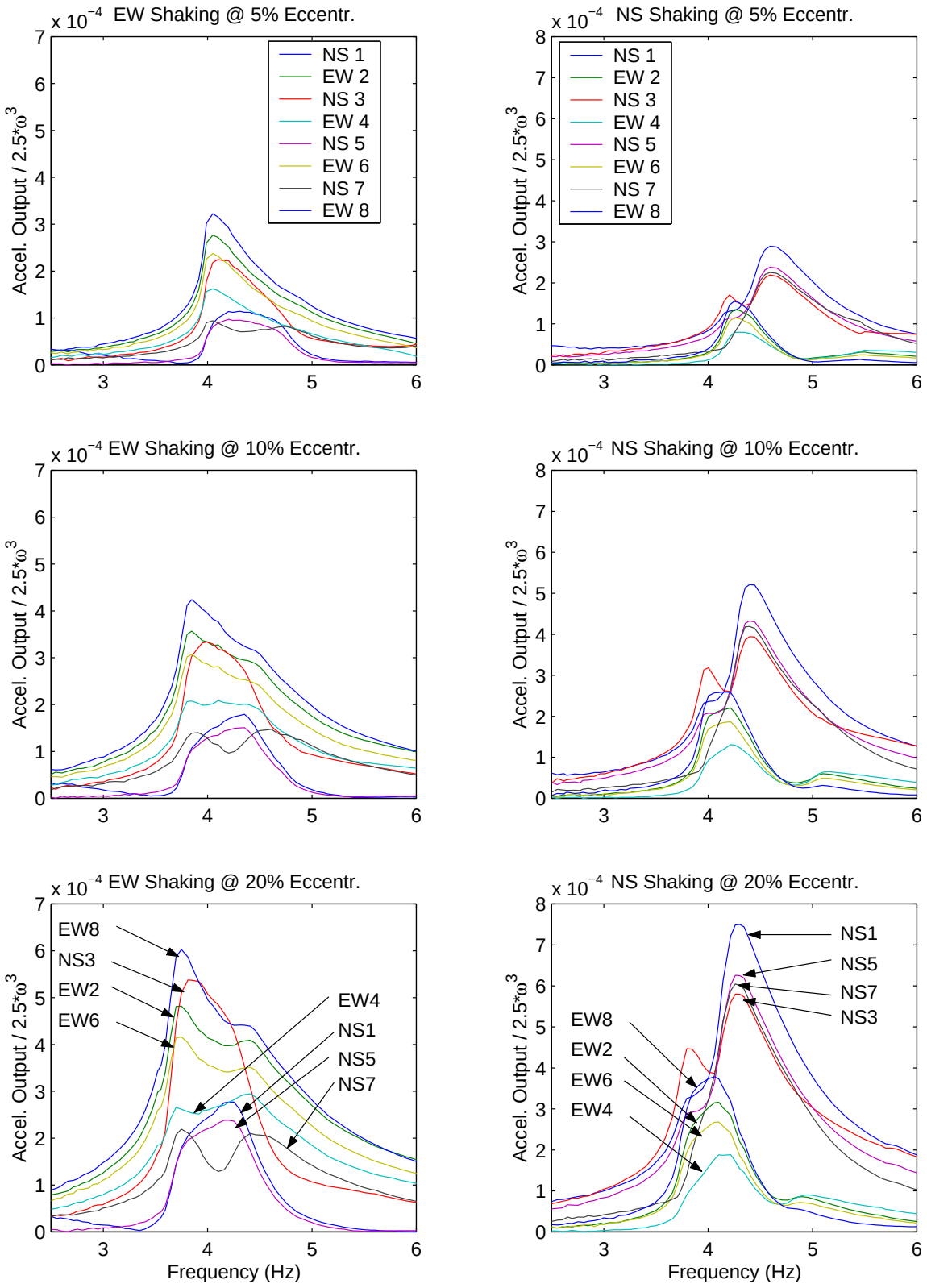

Figure 5.30: Experimental Results Before Phase III (wall finishes installed)

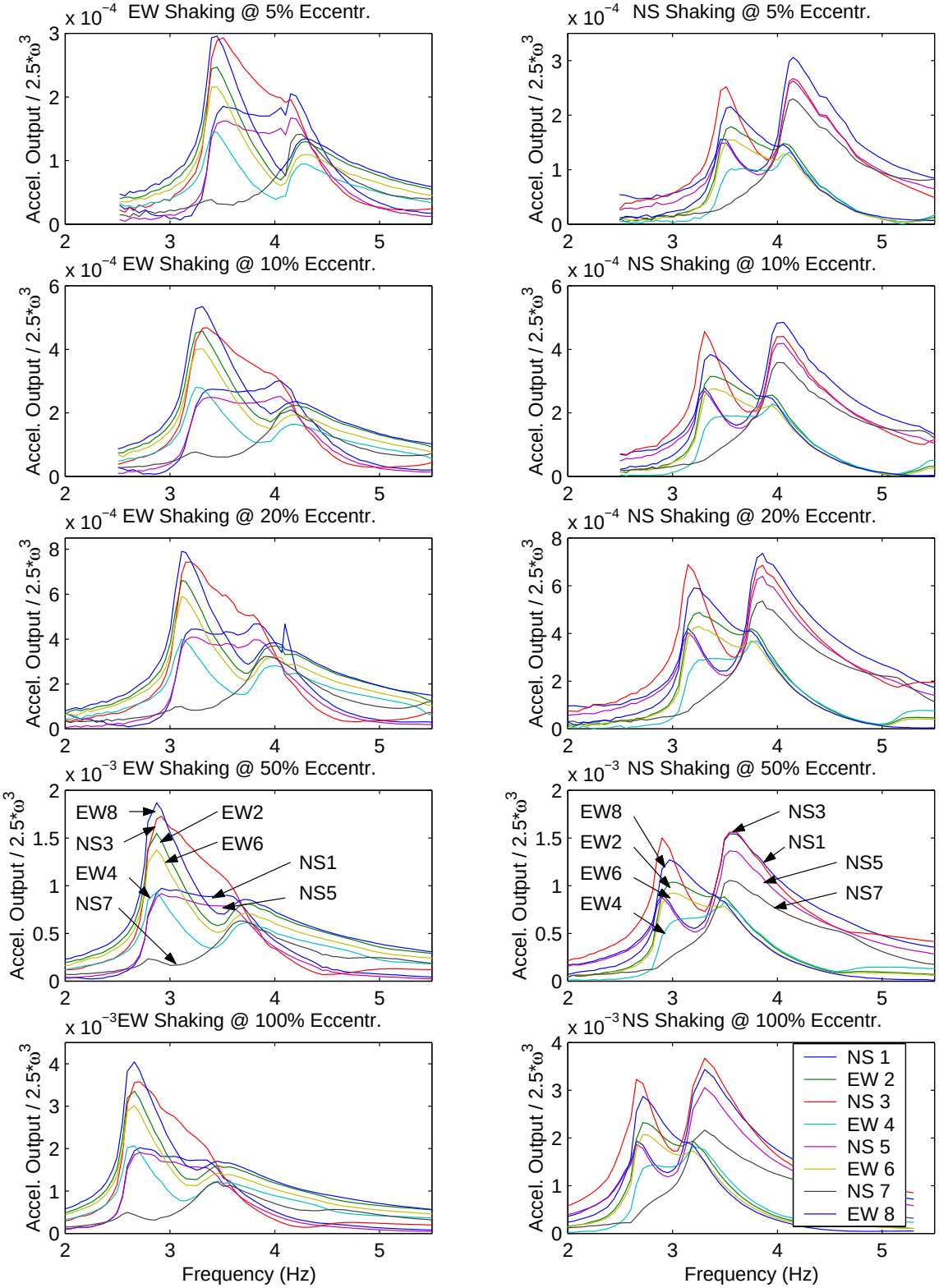

Figure 5.31: Experimental Results After Phase III (wall finishes installed)

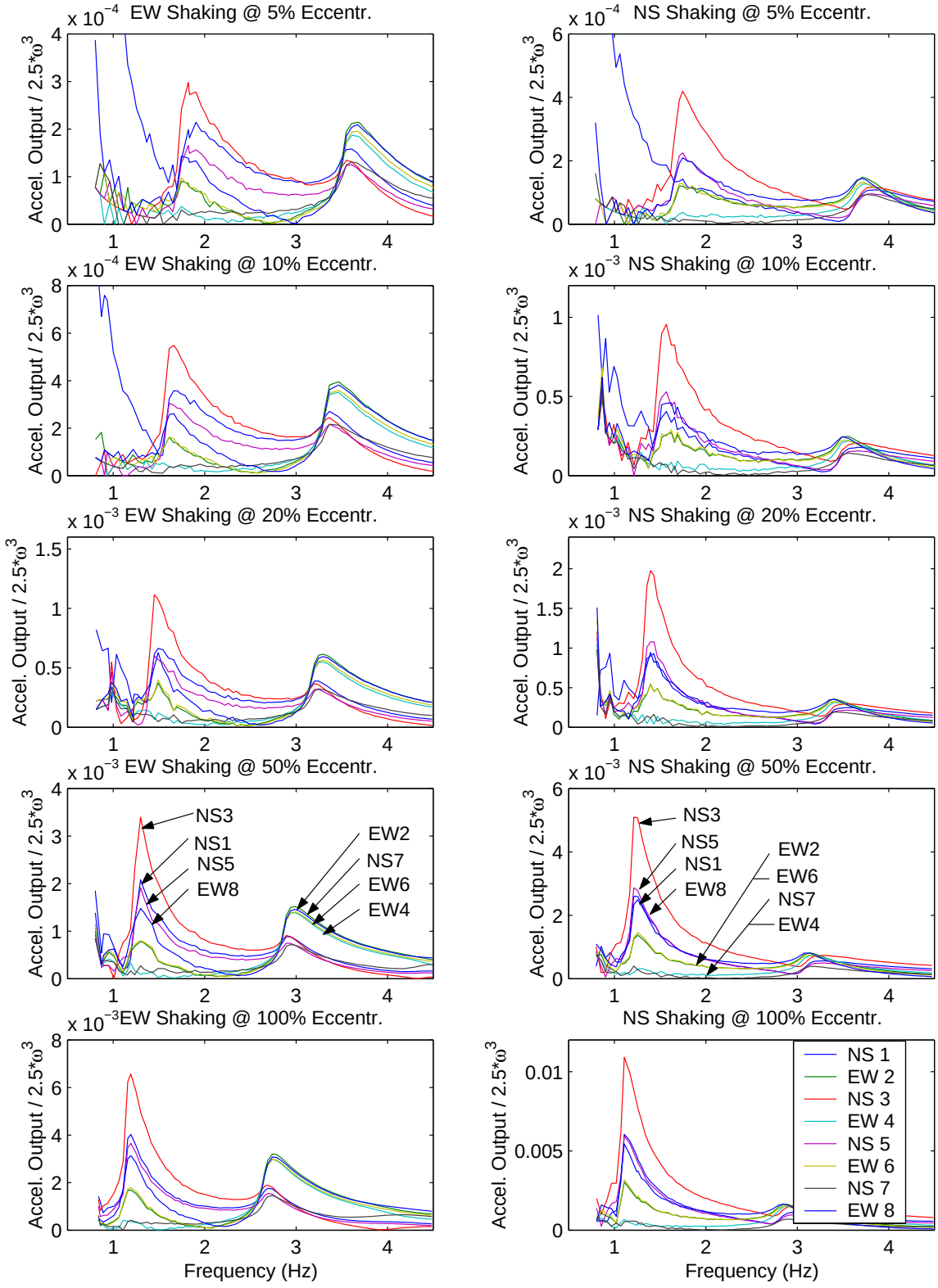

Figure 5.32: Experimental Results After Repeated Strong Shaking

Table 5.9: Experimental Results Before Phase III (wall finishes installed)

Test Date	Shaking Direction	Eccentr.	1st Mode		2nd Mode	
			Freq. (Hz)	Damp.	Freq. (Hz)	Damp.
Dec 19, 2001	NS	5%	4.27	3.6%	4.60	3.2%
		10%	4.07	3.8%	4.46	5.9%
		20%	3.89	4.4%	4.35	6.4%
	EW	5%	4.08	2.5%	–	–
		10%	3.89	3.8%	–	–
		20%	3.80	5.5%	–	–

Table 5.10: Experimental Results After Phase III (wall finishes installed)

Test Date	Shaking Direction	Eccentr.	1st Mode		2nd Mode	
			Freq. (Hz)	Damp.	Freq. (Hz)	Damp.
Dec 21, 2001	NS	5%	3.57	3.9%	4.20	4.9%
		10%	3.39	4.2%	4.05	5.6%
		20%	3.23	4.2%	3.89	5.9%
		50%	2.97	4.5%	3.60	6.7%
		100%	2.74	5.0%	3.32	6.9%
	EW	5%	3.49	4.7%	4.25	4.2%
		10%	3.35	5.5%	4.10	6.5%
		20%	3.20	5.3%	3.91	6.5%
		50%	2.93	5.6%	3.64	7.8%
		100%	2.71	5.5%	3.37	8.1%

Table 5.11: Experimental Results After Repeated Strong Shaking

Test Date	Shaking Direction	Eccentr.	1st Mode		2nd Mode	
			Freq. (Hz)	Damp.	Freq. (Hz)	Damp.
Jan 7, 2002	NS	5%	1.81	8.8%	3.65	4.0%
		10%	1.59	8.1%	3.48	3.1%
		20%	1.42	6.6%	3.35	3.9%
		50%	1.27	6.6%	3.12	4.1%
		100%	1.16	6.8%	2.80	–
	EW	5%	1.88	8.5%	3.71	6.0%
		10%	1.71	8.4%	3.51	6.5%
		20%	1.52	6.9%	3.35	6.5%
		50%	1.33	6.4%	3.04	6.5%
		100%	1.21	6.7%	2.80	6.1%

5.2.4.2 Modelling Results

Many models were considered, each with a set of constraints to reduce the number of springs to be found, and the simplest model (fewest springs) able to capture the experimental behavior was selected. For each model, the selected spring stiffnesses were those that resulted in frequency response curves that best-fit the experimental data for EW and NS shaking at 20% eccentricity. A six-spring model was chosen to represent the structure with all finish materials installed (see Figure 5.16).

Figure 5.33 shows a plot of the response curves obtained prior to the Phase III shake-table tests (for shaking in EW and NS directions at 20% eccentricity). Note that the east wall response (channel NS 3) during EW shaking is much higher than that of the west wall (channel NS 7), almost as high as the response recorded at the garage opening (channel EW 8). For NS shaking, the responses of the EW and NS walls are at similar levels, indicating that there is little torsion in the NS mode of this building. The simple model selected has difficulty simulating the response of the east wall (NS 3), but the general behavior of the building is captured, as can be seen in Figure 5.34. The modelling results are summarized in Table 5.12 and discussed in section 5.3. The model modeshapes for the first three modes are shown in Figure 5.35.

Figure 5.36 shows a plot of the response curves obtained after the Phase III shake-table tests (for shaking in EW and NS directions at 20% eccentricity). Note that the EW resonant frequency has dropped more than the NS resonant frequency, resulting in EW and NS modes that are more separated than before. Figure 5.37 shows that the model is able to capture the response of the building quite well, including the response at the east wall (channel NS 3) that was not well captured before. The modelling results are summarized in Table 5.13 and discussed in section 5.3. The model modeshapes for the first three modes are shown in Figure 5.38.

Figure 5.39 shows a plot of the response curves obtained after the repeated shake-table tests using strong ground motion records (for shaking in EW and NS directions at 20% eccentricity). Note that the NS resonant frequency has dropped dramatically,

from 3.89Hz after Phase III to 1.42Hz, while the EW frequency drop was moderate, from 3.20Hz after Phase III to 3.04Hz, resulting in well separated EW and NS modes. Figure 5.40 shows that the model is able to capture the response of the building very well. The modelling results are summarized in Table 5.14 and discussed in section 5.3. The model modeshapes for the first three modes are shown in Figure 5.41.

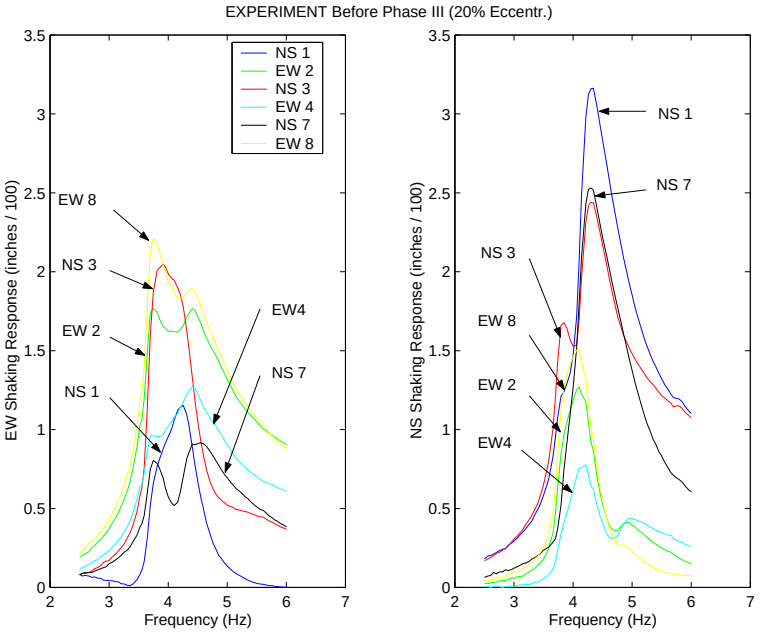

Figure 5.33: Experimental Data (before Phase III testing)

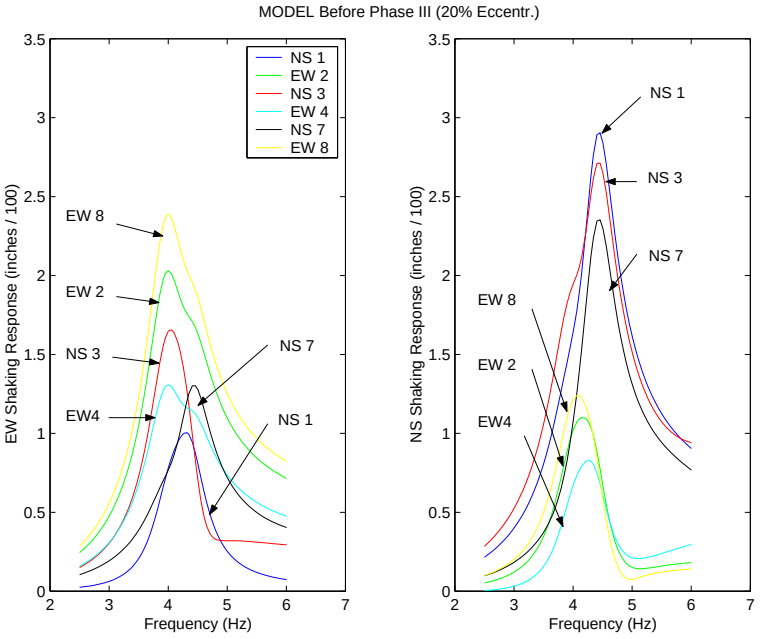

Figure 5.34: Model Response (before Phase III testing)

Table 5.12: Model Results from Tests Before Phase III

Diaphragm Stiffness	Scaling Constant	Jnorm
0.10E+8 lbs/in	1.113	0.0842

Spring Stiffnesses (lbs/in)					
K1	K2	K3	K4	K5	K6
2.01E+6	0.00E+6	0.78E+6	1.04E+6	1.45E+6	1.20E+6

Modal Properties		
$\omega_1 = 3.97$ Hz	$\omega_2 = 4.41$ Hz	$\omega_3 = 6.48$ Hz
$\zeta_1 = 8.8\%$	$\zeta_2 = 6.5\%$	$\zeta_3 = 26\%$

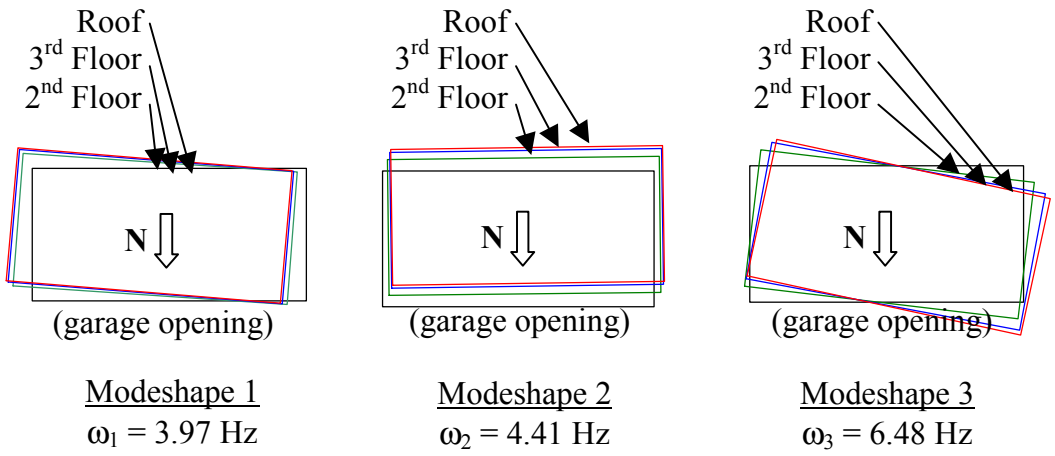

Figure 5.35: Modeshapes (before Phase III testing)

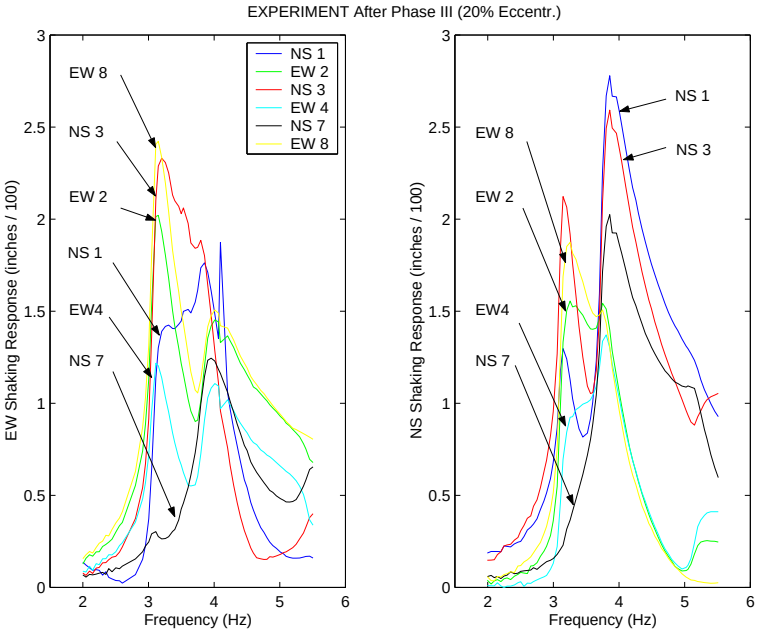

Figure 5.36: Experimental Data (after Phase III testing)

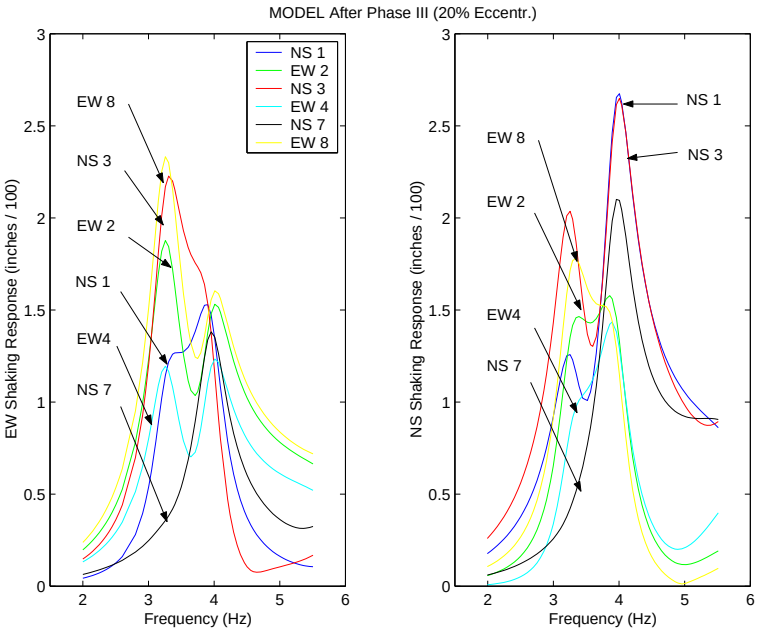

Figure 5.37: Model Response (after Phase III testing)

Table 5.13: Model Results from Tests After Phase III

Diaphragm Stiffness	Scaling Constant	Jnorm
0.10E+8 lbs/in	1.113	0.0705

Spring Stiffnesses (lbs/in)					
K1	K2	K3	K4	K5	K6
1.28E+6	0.00E+6	0.47E+6	0.96E+6	1.45E+6	1.07E+6

Modal Properties		
$\omega_1 = 3.26$ Hz	$\omega_2 = 3.95$ Hz	$\omega_3 = 5.83$ Hz
$\zeta_1 = 7.5\%$	$\zeta_2 = 5.8\%$	$\zeta_3 = 11\%$

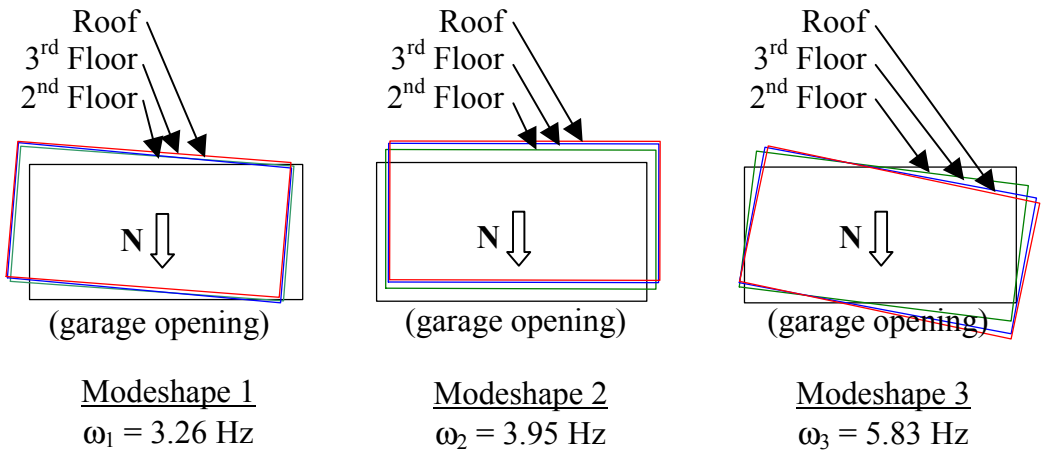

Figure 5.38: Modeshapes (after Phase III testing)

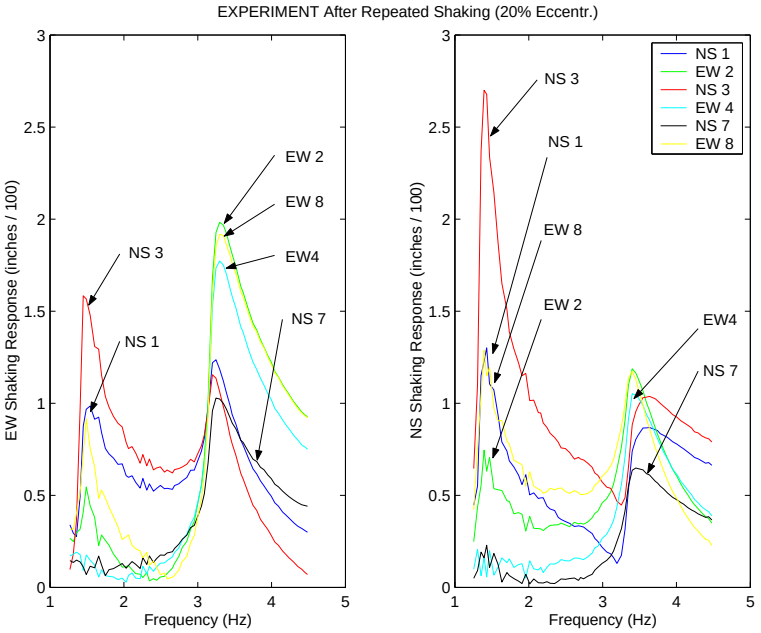

Figure 5.39: Experimental Data (after repeated shaking)

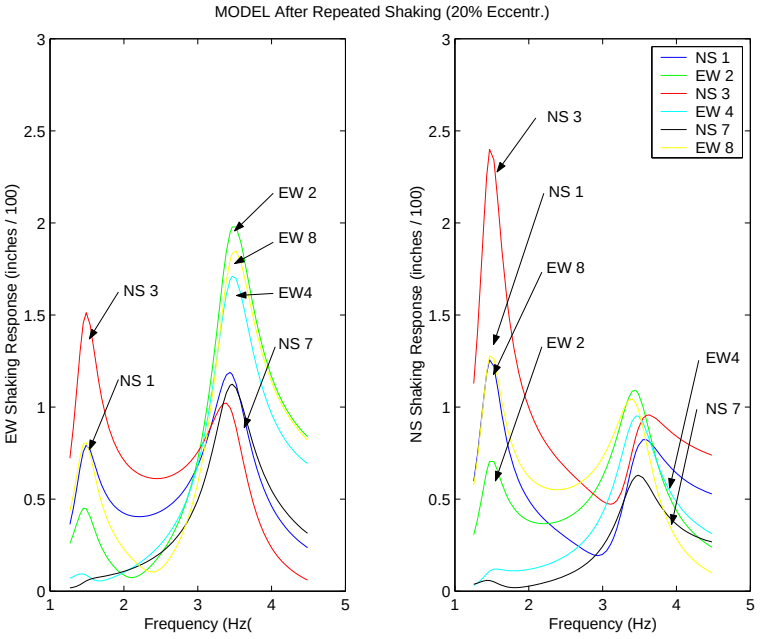

Figure 5.40: Model Response (after repeated shaking)

Table 5.14: Model Results from Tests After Repeated Shaking

Diaphragm Stiffness	Scaling Constant	Jnorm
0.10E+8 lbs/in	1.113	0.0628

Spring Stiffnesses (lbs/in)					
K1	K2	K3	K4	K5	K6
1.08E+6	0.00E+6	0.07E+6	0.96E+6	0.92E+6	0.77E+6

Modal Properties		
$\omega_1 = 1.47$ Hz	$\omega_2 = 3.45$ Hz	$\omega_3 = 5.08$ Hz
$\zeta_1 = 10\%$	$\zeta_2 = 7.8\%$	$\zeta_3 = 6.0\%$

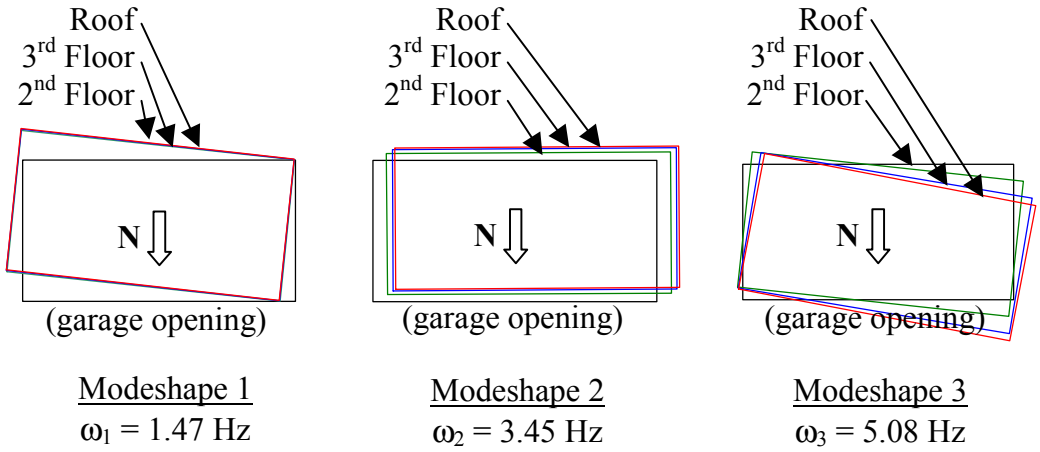

Figure 5.41: Modeshapes (after repeated shaking)

5.3 Discussion of Results

Table 5.15 shows the spring stiffnesses obtained for the models of the undamaged and damaged Phase I building, as well as the percent drop in the undamaged stiffness values after strong shaking of the building. Visual inspection of the building after all Phase I shake-table tests showed severe damage occurred at the east wall (corresponding to spring K3). All other walls showed minimal signs of damage.

Table 5.16 shows the spring stiffnesses obtained for the models of the undamaged and damaged Phase III building, as well as the cumulative percent drop in the undamaged stiffness values after the Phase III tests and the subsequent repeated strong shaking of the building. Inspection of the building after all Phase III shake-table tests showed some sign of damage, mainly cracking of the stucco throughout the building. After the repeated shaking of the structure using strong ground motions, there was severe damage to the east wall (corresponding to spring K3), and there was some additional cracking and spalling at the south wall door and window corners, with some visible shear cracking of the stucco between the windows.

It can be seen from Tables 5.15 and 5.16 that the severe damage observed at the east wall for Phase I and III corresponded to stiffness losses of 78% and 91%, respectively. The more moderate values of stiffness loss (of up to 46%) did not appear to be severe damage based on visual inspection.

Table 5.15: Loss of Stiffness from Phase I Testing

	Spring Stiffnesses (lbs/in)					
	K1	K2	K3	K4	K5	K6
Before Phase I Tests	0.69E+6	0.00E+6	0.50E+6	0.60E+6	0.40E+6	0.27E+6
After Phase I Tests	0.42E+6	0.00E+6	0.11E+6	0.60E+6	0.39E+6	0.20E+6
	Cumulative Stiffness Reduction (%)					
	ΔK1	ΔK2	ΔK3	ΔK4	ΔK5	ΔK6
After Phase I Tests	39%	0	78%	0	2.5%	26%

Table 5.16: Loss of Stiffness from Phase III Testing

	Spring Stiffnesses (lbs/in)					
	K1	K2	K3	K4	K5	K6
Before Phase III Tests	2.01E+6	0.00E+6	0.78E+6	1.04E+6	1.45E+6	1.20E+6
After Phase III Tests	1.28E+6	0.00E+6	0.47E+6	0.96E+6	1.45E+6	1.07E+6
After Severe Shaking	1.08E+6	0.00E+6	0.07E+6	0.96E+6	0.92E+6	0.77E+6
	Cumulative Stiffness Reduction (%)					
	ΔK1	ΔK2	ΔK3	ΔK4	ΔK5	ΔK6
After Phase III Tests	36%	0	40%	8%	0%	11%
After Severe Shaking	46%	0	91%	8%	36%	36%

For the undamaged Phase I structure, the ratios between the spring stiffnesses were as expected, with the south wall stiffness K1 higher than all other springs (nails are more closely spaced) and first floor level springs K3 and K4 are higher than second and third floor springs K6 (more closely spaced nails, wider studs at first floor). The model of the damaged Phase I structure showed that the stiffness loss occurred where expected, with most of the damaged concentrated in the east and south walls (springs K3 and K1). For the undamaged Phase III structure, the ratios between the spring stiffnesses were also as expected, with the south wall stiffness K1 about twice as large as all other springs and all other springs have similar stiffness values (the lower values of K3 and K4 may be due to minor damage occurring during the Phase II tests). Note that the stiffness values for the Phase III structure are considerably higher than those for the Phase I structure even after severe shaking (with the exception of the east wall corresponding to K3, where the stucco and plywood separated from the studs). The addition of stucco increased the Phase I spring values by about 1E+6 lbs/in (a factor of about 3) for the shorter upper walls (K5, K6), by about 1.3E+6 lbs/in (a factor of about 2) for the south wall (K1), and by 0.3E+6 and 0.4E+6 lbs/in (a factor of about 1.6) for the shorter lower walls (K3, K4). The smaller than expected increase in the values of the first floor springs K1, K3, K4 may be due to the minor damage experienced during the Phase II testing. The model of the damaged Phase III structure showed that the stiffness loss occurred where expected, with most of the damaged concentrated in the east and south walls (springs K3 and K1).

The model diaphragm was assumed to be essentially rigid in order to obtain realistic values of equivalent spring stiffnesses. The good correlation between the experimental data and the model response hints that the diaphragm behaves as nearly rigid, supporting the recommendation by the Woodframe Project Codes and Standards Committee to assume a rigid rather than flexible diaphragm in the design of woodframe buildings where significant torsion is expected to occur. The issue of flexible versus rigid diaphragm should be further investigated in future research.

The scaling constant that accounts for mass, force and/or signal processing inaccuracies was fitted for the undamaged models and found to be 1.17 for the Phase I building and 1.11 for the Phase III building. It should be noted that if this factor is an indication that the mass of the building was underestimated, the stiffness terms have also been underestimated by the same amount (this constant does not affect the fundamental frequencies identified). Therefore, when evaluating the effect of wall finish materials on the wall stiffnesses, this scaling factor could be taken into account and the equivalent stiffness values shown in Tables 5.15 and 5.16 could be multiplied by the appropriate factor of 1.17 and 1.11, respectively.

Chapter 6

Period Regression Analysis

6.1 Methodology

A maximum likelihood estimation method based on a lognormal distribution for the periods at each value of the selected regressor was used to determine a period formula. Thus, a period formula similar to Equation 2.1 is derived from a statistical model of the form:

$$\ln T = \ln c + \gamma \ln x + s_e^2 \varepsilon \tag{6.1}$$

where $\ln c$ and γ are parameters to be estimated, the regressor x is a structural characteristic, ε is a Unit Normal random variable (i.e., zero mean and unit variance) and s_e^2 is the variance in the predicted value of $\ln T$, taken to be independent of x.

The maximum likelihood estimates $\hat{c}$ and $\hat{\gamma}$ minimize $\sum_{i=1}^{N}[\ln T_i - (\ln c + \gamma \ln x_i)]^2$ and the standard error estimate $\hat{s}_e$ in $\ln T$ is calculated from:

$$\hat{s}_e = \sqrt{\frac{\sum_{i=1}^{N}[\ln T_i - (\ln \hat{c} + \hat{\gamma} \ln x_i)]^2}{(N-2)}} \tag{6.2}$$

where N = total number of data points (x_i, T_i) in the period database. The estimated relationship $\ln \hat{T} = \ln \hat{c} + \hat{\gamma} \ln x$ (or, equivalently, $\hat{T} = \hat{c} x^{\hat{\gamma}}$) gives the median period for the given regressor value.

Curves for the 84$^{\text{th}}$ and 16$^{\text{th}}$ percentiles can be obtained based on an amount s_e above and below, respectively, the logarithm of the median period (i.e., there is 84% and 16% probability that a period will lay below the respective curves). The equations for these curves are

$$T_{16} = \hat{T}\, e^{-\hat{s}_e} \tag{6.3}$$

$$T_{84} = \hat{T}\, e^{+\hat{s}_e} \tag{6.4}$$

6.2 Discussion of Results

The data obtained from the analysis of the earthquake records and the forced vibration tests (with the exception of the 2-story garage) were used to perform a regression analysis with respect to building height. It was felt that the number of data was insufficient to regress on additional structural characteristics, such as total area of shear walls in the direction of each building axis. Ambient vibration survey results were not used in developing this period formula since the natural periods are significantly lower due to the much smaller vibration amplitudes, and the interest has been in the behavior for stronger shaking of these buildings. The best-fit curve for the median period based on the earthquake records and the strongest shaking in the forced vibration tests can be represented by the following formula:

$$\hat{T} = 0.032\, h_n^{0.55} \tag{6.5}$$

where h_n is the building height, in feet. The periods found from the earthquake records and from forced vibration tests, as well as the curves given by equations 2.1, 2.6 and 6.5, are shown in Figure 6.1. The 16- and 84-percentile curves are given by 6.3 and 6.4, where $\hat{s}_e = 0.129$ is the standard error in $\ln T$. For comparison, the periods from ambient vibrations and shake-table tests are also shown in Figure 6.1, although these were not used in the regression analysis.

Figure 6.1 shows that the current UBC-97 period formula (Equation 2.1) gives

a reasonable approximation to the periods of the woodframe buildings examined throughout this project. It must be noted that these periods are for low amplitude of shaking only (drifts less than 0.1%) and also for structures with stiff wall finish materials such as drywall, plaster, stucco, or some combination. The periods for structures under strong shaking or for buildings without wall finish materials would be considerably longer than what is predicted using the UBC-97 formula or the formula found by regression analysis, as seen by the dramatic elongation of the periods of the unfinished shake-table structures at UC San Diego and UC Berkeley as shaking amplitude increased. It should also be noted that the periods given by the FEMA-273 simplified formula (Equation 2.6) are much too high and would underestimate the force demand in the structure. Even though the UBC-97 formula is for low amplitude of shaking, it provides a reasonably conservative estimate of the building period for design purposes, placing most woodframe buildings in the plateau region of the UBC design response spectrum, although these periods may underestimate the drift demand on these structures during stronger shaking.

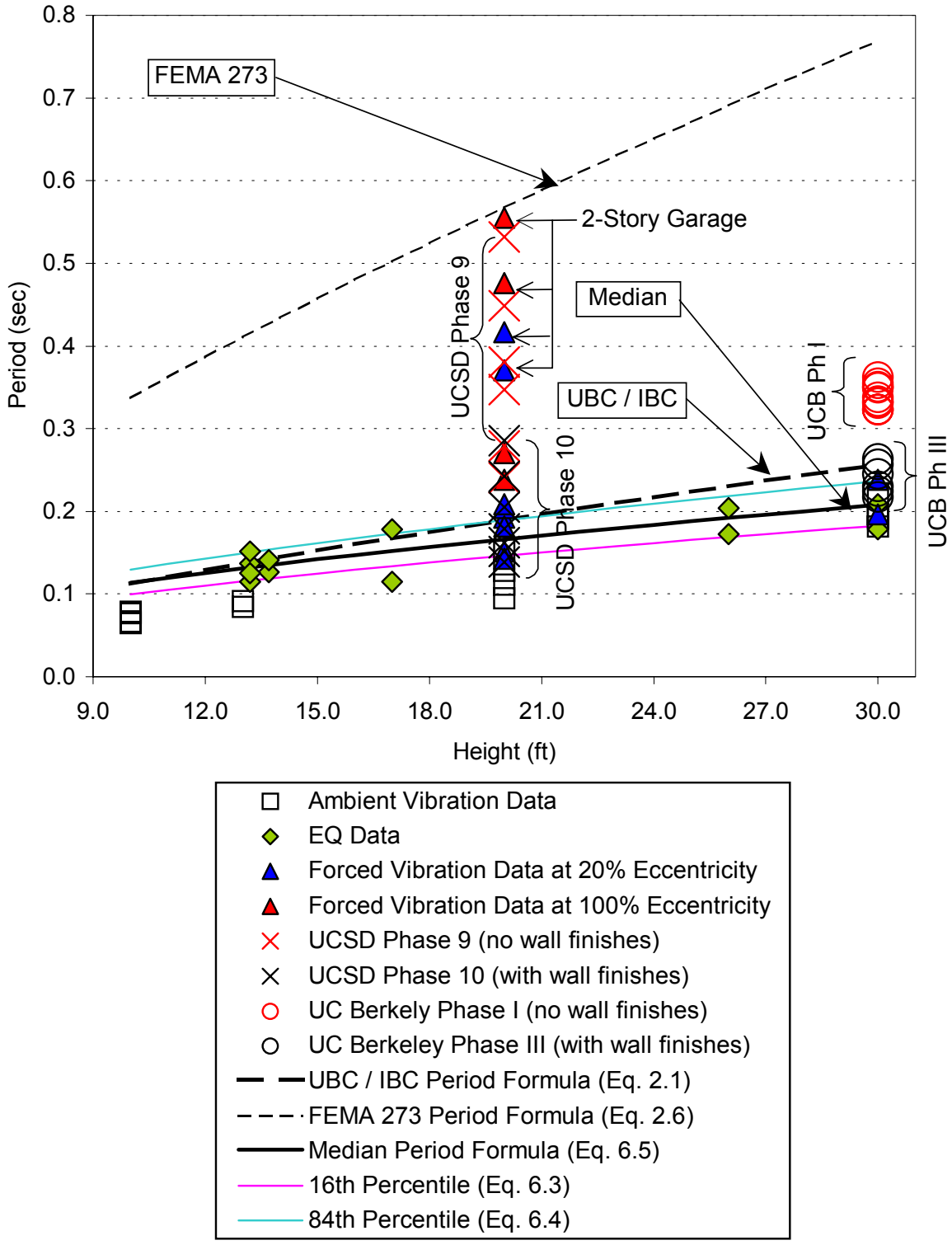

Figure 6.1: Period as a Function of Building Height

Chapter 7

Conclusions and Research Opportunities

Valuable insight was gained regarding the dynamic behavior of woodframe buildings, which showed natural periods between 0.56 and 0.24 sec (natural frequencies between 1.8 and 8.7 Hz) for one- to three-story buildings at low-amplitude shaking. A period formula was developed based on the data obtained from analysis of earthquake records and from dynamic tests of woodframe buildings. This new median period formula (Equation 6.5) is expected to represent the behavior of these structures more accurately than the current UBC/IBC formula (Equation 2.1) for miscellaneous woodframe/masonry buildings, and perhaps it is more realistic than the FEMA-273 period formula (Equation 2.6) for light to moderate shaking levels. The median period formula (Equation 6.5) was derived from low-amplitude shaking (drift ratios less than 0.1%), since strong earthquake shaking data is not currently available. The periods are expected to be significantly longer for stronger shaking of these structures (see, for example, the increase in fundamental period with increasing amplitude that is apparent in Figure 6.1 for UCSD shake-table test data). Instrumented woodframe structures will provide stronger motion data in future earthquakes and provide a valuable supplement to this database, since the building behavior changes significantly during strong shaking.

The damping ratios obtained from the earthquake records and forced vibration tests were high, averaging 7.2% and ranging from 2.6% to 17.3%. Those values ob-

tained from analysis of the earthquake records (11.6% mean, 3.4% standard deviation) were generally higher than those obtained from the forced vibration tests (4.9% mean, 1.1% standard deviation). These high damping ratios, when compared with the tests of structures with no wall finishes (see Chapter 2), suggest that plywood and wall finish materials (stucco, plaster, drywall, and wood siding) are major contributors to the damping in woodframe buildings, perhaps due to the energy dissipation mechanism inherent in the connection of these wall finishes to the wood frame (using nails or staples). The damping ratios also showed a strong amplitude dependence, increasing significantly with higher shaking amplitude, and perhaps the linear viscous damping assumption is not a good model for the actual damping mechanisms. Since the majority of the data obtained during this research was from low-level shaking (drift ratios less than 0.1%), it would be reasonable to use the average damping ratio of 7% as viscous damping when modelling woodframe buildings where no hysteretic energy dissipation is exhibited until the model drifts reach larger values than 0.1% or when using a linear model. If a more conservative value is desired, the minimum damping ratio found from all the low-level forced and shake-table tests was 2.6%.

Regarding the rigidity of woodframe diaphragms, the buildings tested during the course of this research were generally irregular and showed significant torsional behavior. A building with a fully flexible diaphragm would not be expected to have a torsional component in the response, but some diaphragm stiffness is expected even when the diaphragm is fairly flexible. The results of the system identification study in section 5.2 suggest that the diaphragm is best modelled as nearly rigid for the UC Berkeley 3-story building. The issue regarding the load distribution in the design of woodframe buildings should be addressed in future research, since woodframe buildings are currently designed assuming a flexible diaphragm even though the CUREE-Caltech Woodframe research to date shows that the diaphragm behaves as essentially rigid. This design assumption could have significant impact on the vulnerability of these buildings, and so is an important issue that should be further examined.

The data obtained from the forced vibration tests and from the shake-table test structures at UC San Diego and UC Berkeley illustrate the amplitude dependence of the building periods and damping ratios. Even small increases in the force amplitude result in the elongation of the identified fundamental periods. As long as the building is not damaged during the forced vibration tests, the periods generally return to their original values after the testing is concluded. The UC Berkeley test structure showed that even when these fundamental periods elongated permanently, indicating a permanent loss of stiffness, this loss sometimes corresponded to slight or no visible damage. The areas of the building where severe damage was observed had stiffness losses of over 75%. Therefore, the fundamental periods and modeshapes of a building may not be a reliable tool for quantifying the degree of damage in a building, but they could be used to identify areas where structural damage may have occurred. This correlation between stiffness loss and damage to woodframe buildings has potential structural health monitoring implications and should be further examined in future research. In particular, the relationship between damage and strength loss should be investigated, since stiffness losses of up to 40% were observed during the UC Berkeley shake-table tests (see Section 5.2) without initiation of a collapse mechanism or loss of the building's load carrying ability. Ambient vibration data may be a useful tool for structural health monitoring of these buildings, although a methodology should be developed which addresses the considerable period elongation observed even at low-amplitude shaking, and care must be taken so that testing of these structures is performed at the same excitation levels.

Appendix A

Earthquake Records

Station Name	Station Number	No. of Stories	Floor Dimension	Lateral Force Resisting System	Year of Construction	Date Instrumented	No. of Sensors
Parkfield – Elementary School	36531	1	48′ x 30′	plywood shear walls in longitudinal direction	1949	6/87	6+FF
Bishop - Fire Station	54545	1	62′ x 50′	Perimeter plywood shear walls	1983	9/88	6
Eureka – Office Building	89687	2	80′ x 48′	perimeter plywood shear walls	1992	2/95	11
Templeton – Hospital *	36695	1	87′ x 51′	distributed plywood shear walls	1977	6/94	9+FF
San Bernardino – Motel	23701	3	181′ x 48′	plywood shear walls in 1st story	1986	9/94	15
Fremont – Motel	57720	2	145′ x 38′	plywood shear walls in long. direction in the 1st story	1989	7/95	11
Indio - Hospital *	12759	1	298′ x 244′	distributed plywood shear walls	1981	6/97	8+FF

* Instrumented under OSHPD/CSMIP Hospital Instrumentation Project.

Figure A.1: CDMG/CSMIP Instrumented Woodframe Buildings as of May 1999

Date of Earthquake	Time (UTC) hr:min:sec	Magnitude (M_L)	Epicentral Distance (km)	Maximum Acceleration(g)	
				Ground	Structure
Parkfield – Elementary School					
04/04/93	05:21:25.3	4.2	7	7.5% H	12.3% H
12/20/94	10:27:47.2	4.7	4	8.9% H	20.1% H
Bishop – Fire Station					
05/17/93	23:20:48.8	6.0	61	1.8% H	4.4% H
Eureka – 2-story Office Building					
02/08/95	09:36:51.1	3.9	13	3.7% H, 0.8% V	6.2% H
San Bernardino – 3-story Motel					
06/28/97	21:45:25.1	4.2	1	6.4% H, 3.5% V	9.2% H
07/26/97	10:24:16.9	3.7	0	3.8% H, 2.7% V	7.8% H
03/11/98	12:18:51.8	4.5	18	2.3% H, 1.1% V	7.1% H
Indio – 1-story Hospital					
07/26/97	03:14:56.0	4.9	33	2.4% H	8.3% H

Figure A.2: Records from CDMG/CSMIP Instrumented Woodframe Buildings

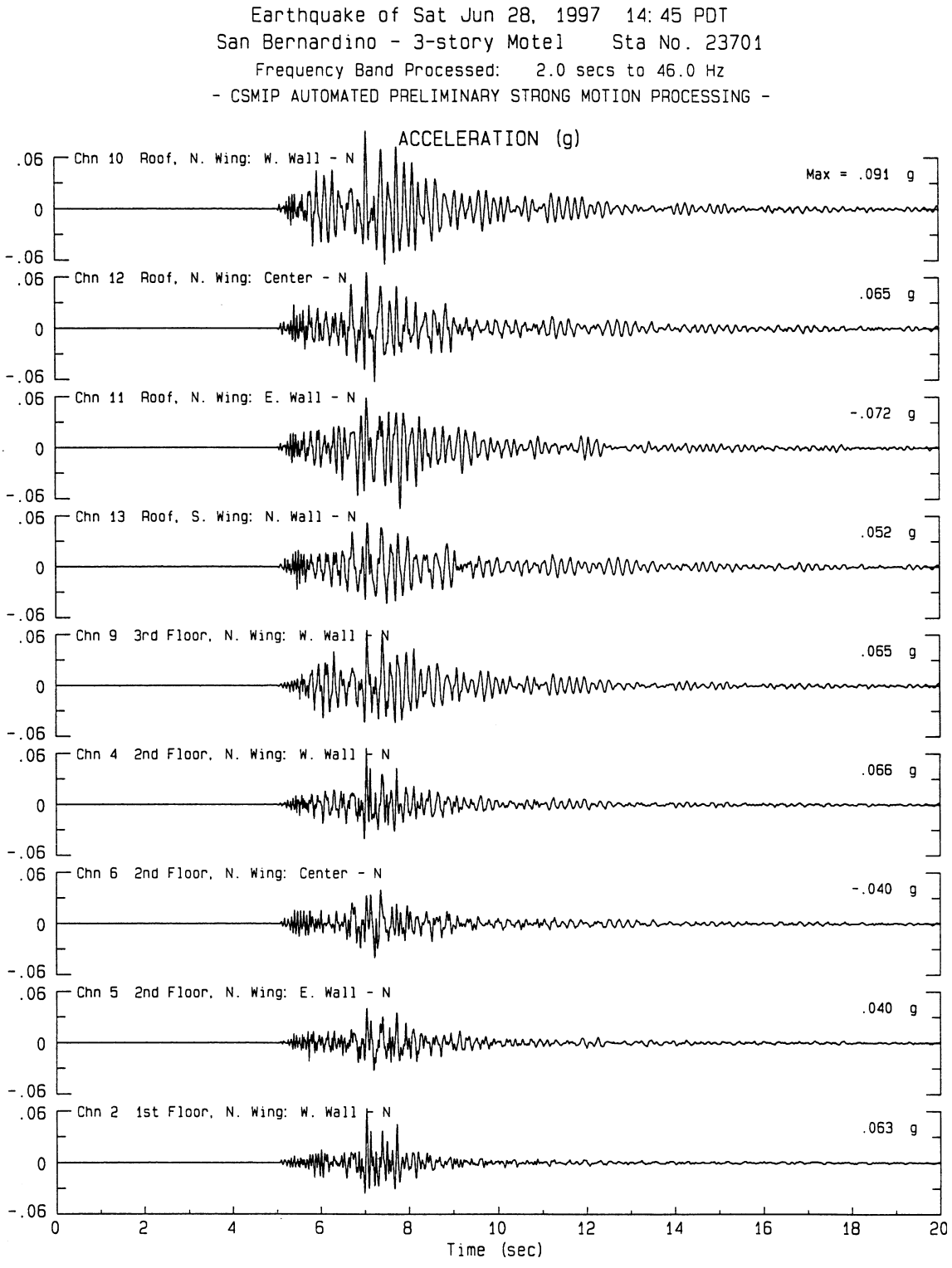

Figure A.3: San Bernardino 3-Story Motel, Records from 6/28/97 Earthquake

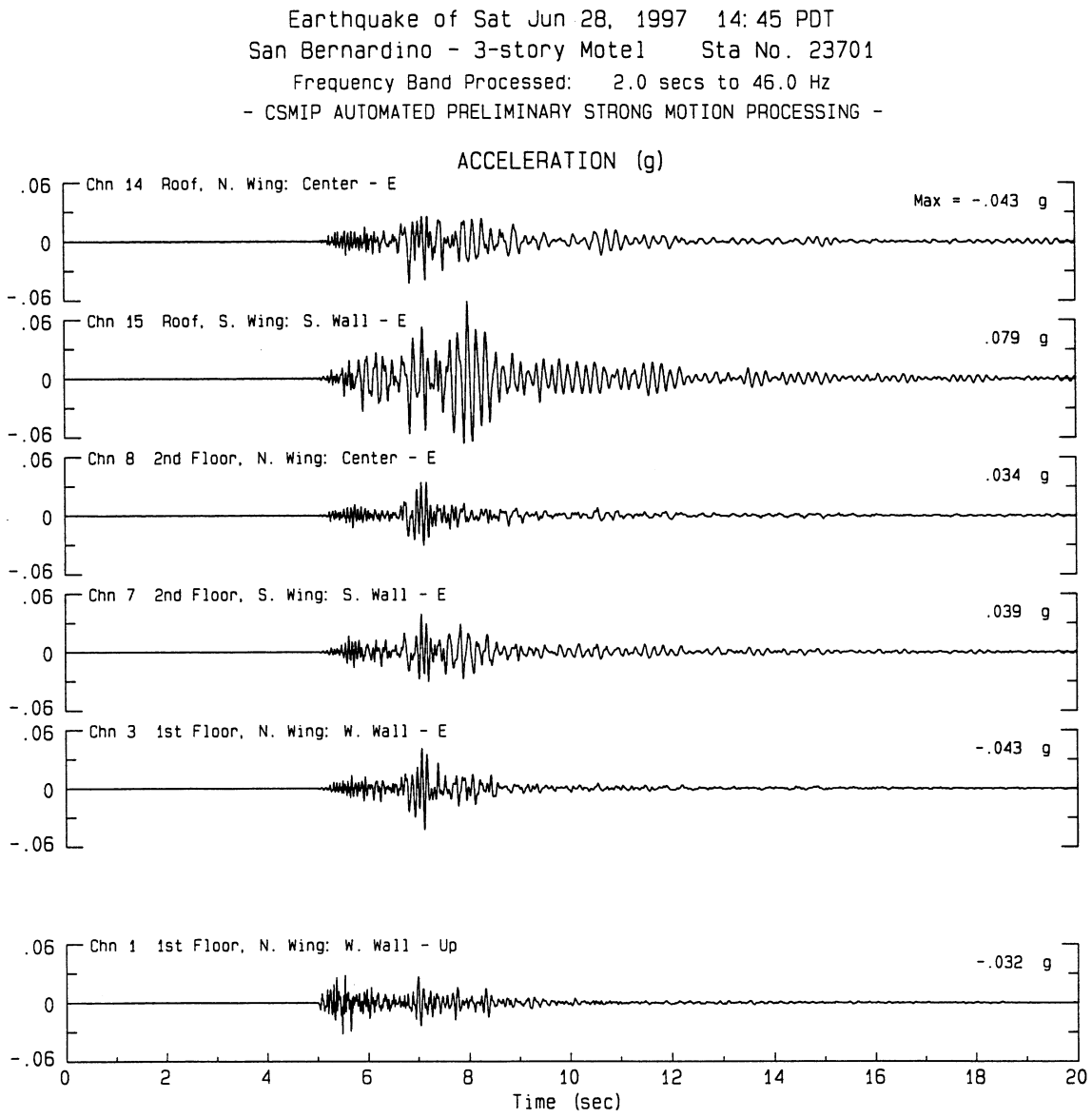
Earthquake of Sat Jun 28, 1997 14:45 PDT
San Bernardino - 3-story Motel Sta No. 23701
Frequency Band Processed: 2.0 secs to 46.0 Hz
- CSMIP AUTOMATED PRELIMINARY STRONG MOTION PROCESSING -
ACCELERATION (g)
Chn 14 Roof, N. Wing: Center - E
Max = -.043 g
Chn 15 Roof, S. Wing: S. Wall - E
.079 g
Chn 8 2nd Floor, N. Wing: Center - E
.034 g
Chn 7 2nd Floor, S. Wing: S. Wall - E
.039 g
Chn 3 1st Floor, N. Wing: W. Wall - E
-.043 g
Chn 1 1st Floor, N. Wing: W. Wall - Up
-.032 g
.06
0
-.06
0 2 4 6 8 10 12 14 16 18 20
Time (sec)

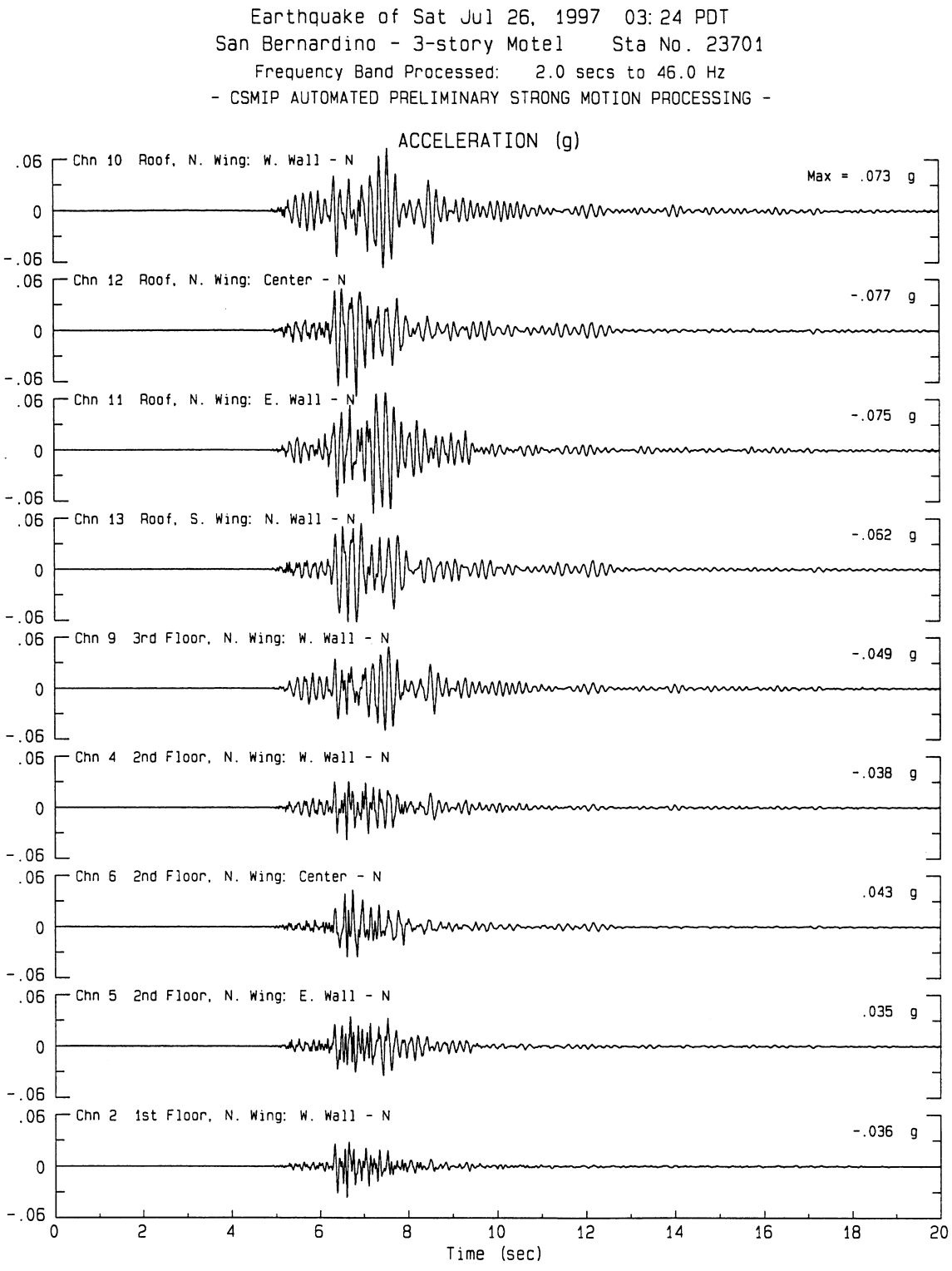

Figure A.4: San Bernardino 3-Story Motel, Records from 7/26/97 Earthquake

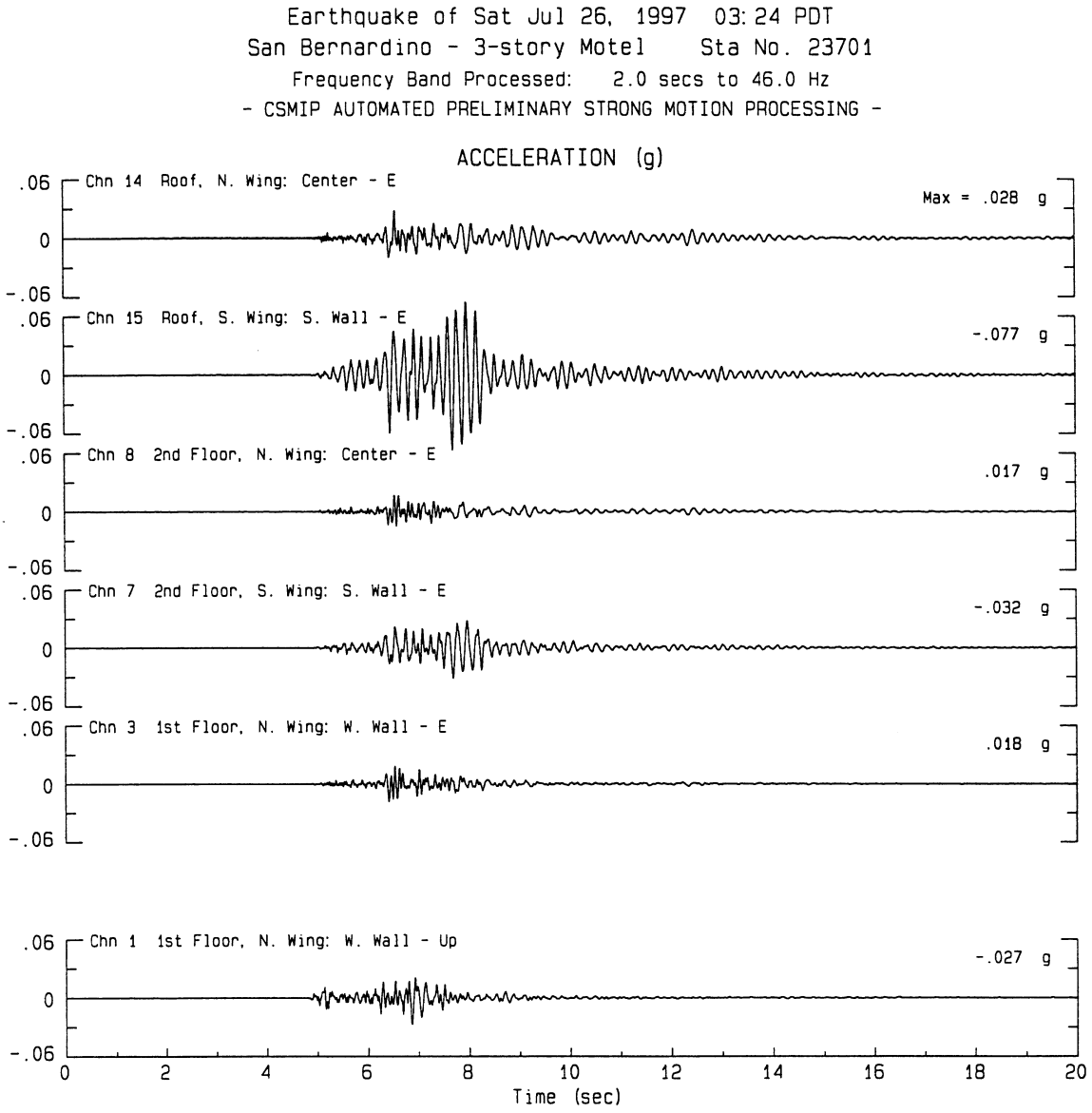
Earthquake of Sat Jul 26, 1997 03:24 PDT
San Bernardino - 3-story Motel Sta No. 23701
Frequency Band Processed: 2.0 secs to 46.0 Hz
- CSMIP AUTOMATED PRELIMINARY STRONG MOTION PROCESSING -
ACCELERATION (g)
Chn 14 Roof, N. Wing: Center - E
Max = .028 g
Chn 15 Roof, S. Wing: S. Wall - E
-.077 g
Chn 8 2nd Floor, N. Wing: Center - E
.017 g
Chn 7 2nd Floor, S. Wing: S. Wall - E
-.032 g
Chn 3 1st Floor, N. Wing: W. Wall - E
.018 g
Chn 1 1st Floor, N. Wing: W. Wall - Up
-.027 g
.06
0
-.06
0 2 4 6 8 10 12 14 16 18 20
Time (sec)

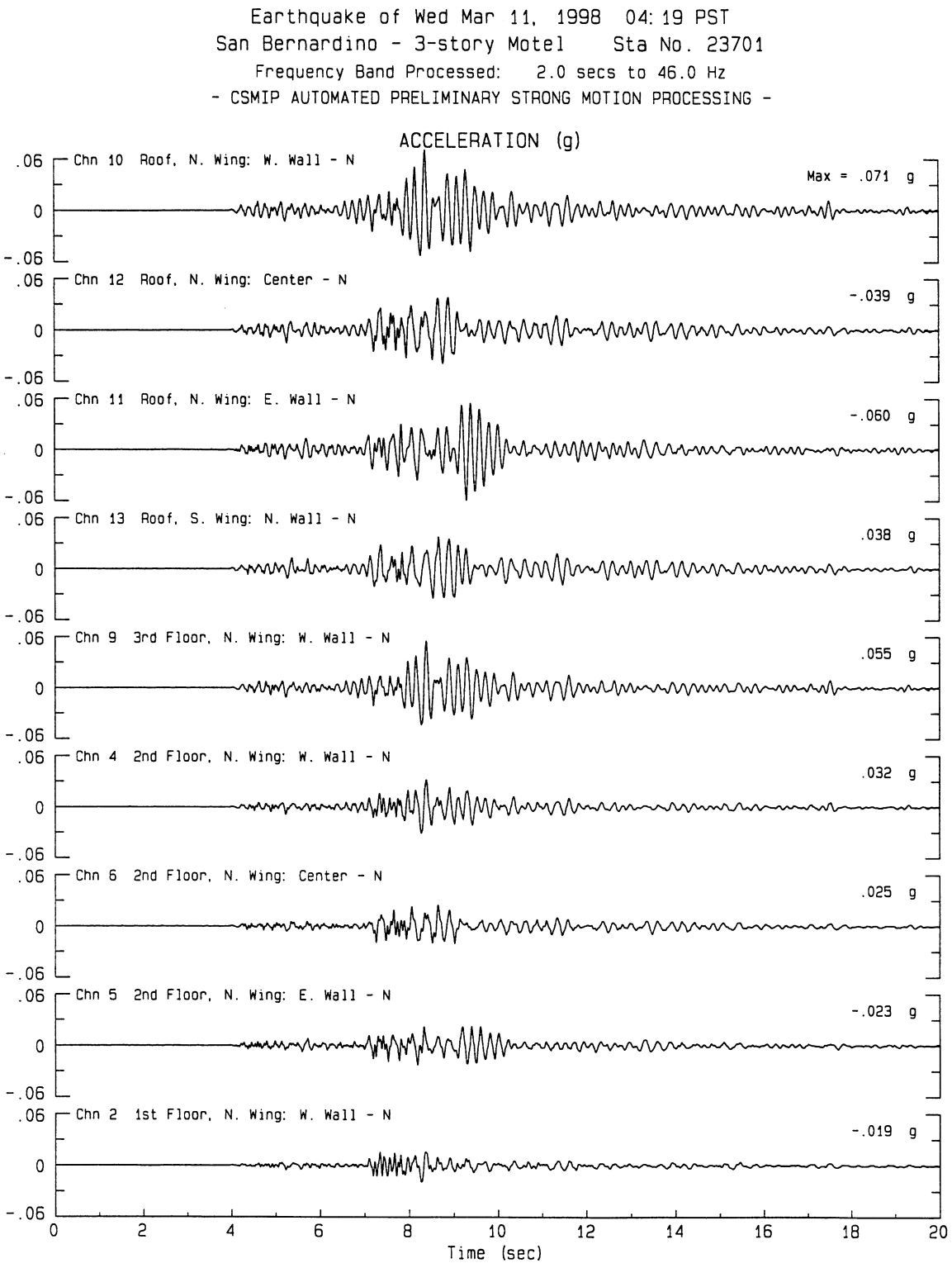

Figure A.5: San Bernardino 3-Story Motel, Records from 3/11/98 Earthquake

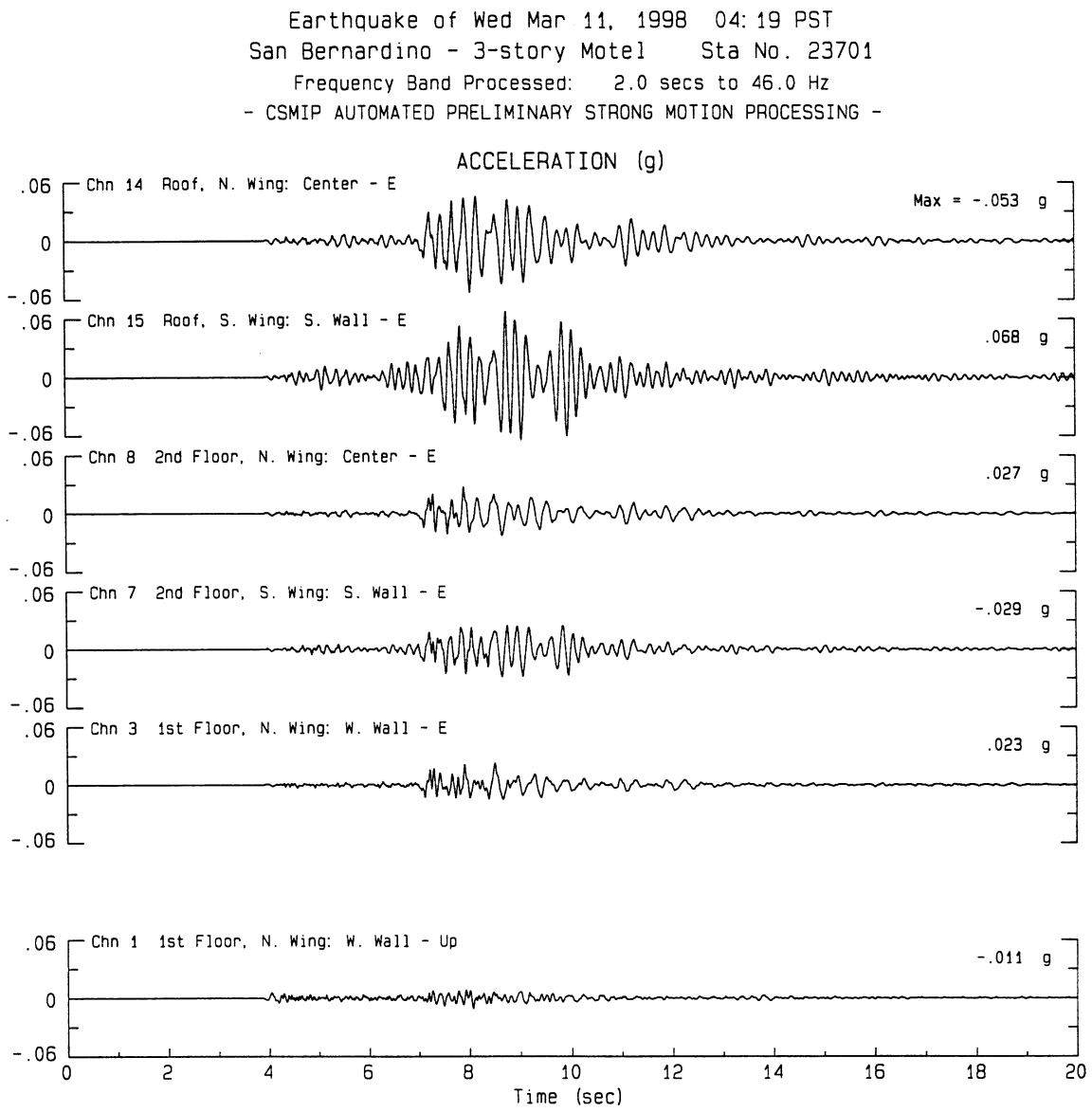
Earthquake of Wed Mar 11, 1998 04:19 PST
San Bernardino - 3-story Motel Sta No. 23701
Frequency Band Processed: 2.0 secs to 46.0 Hz
- CSMIP AUTOMATED PRELIMINARY STRONG MOTION PROCESSING -
ACCELERATION (g)
Chn 14 Roof, N. Wing: Center - E
Max = -.053 g
Chn 15 Roof, S. Wing: S. Wall - E
.068 g
Chn 8 2nd Floor, N. Wing: Center - E
.027 g
Chn 7 2nd Floor, S. Wing: S. Wall - E
-.029 g
Chn 3 1st Floor, N. Wing: W. Wall - E
.023 g
Chn 1 1st Floor, N. Wing: W. Wall - Up
-.011 g
.06
0
-.06
0 2 4 6 8 10 12 14 16 18 20
Time (sec)

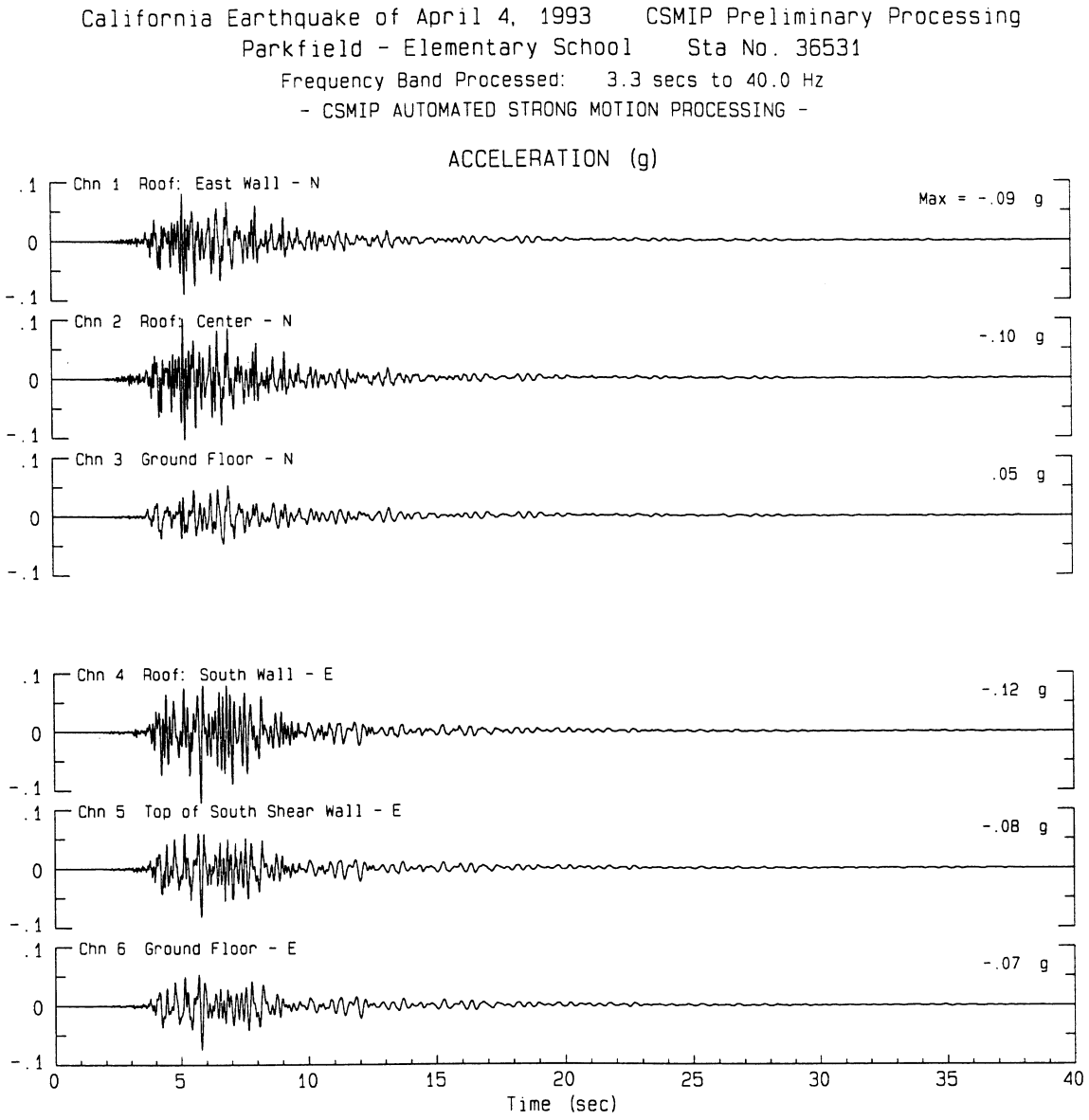

Figure A.6: Parkfield 1-Story School, Records from 4/4/93 Earthquake

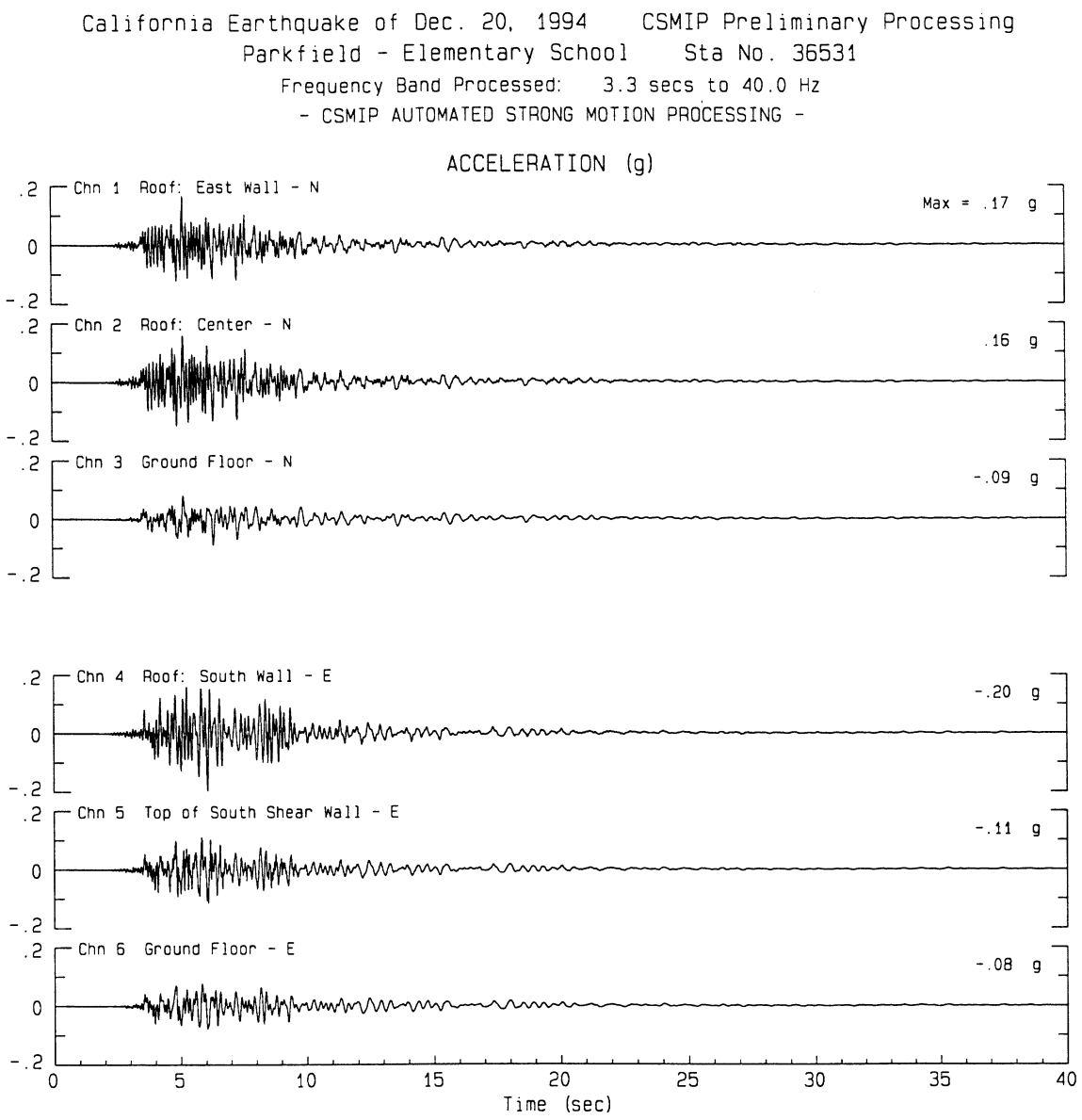

Figure A.7: Parkfield 1-Story School, Records from 12/20/94 Earthquake

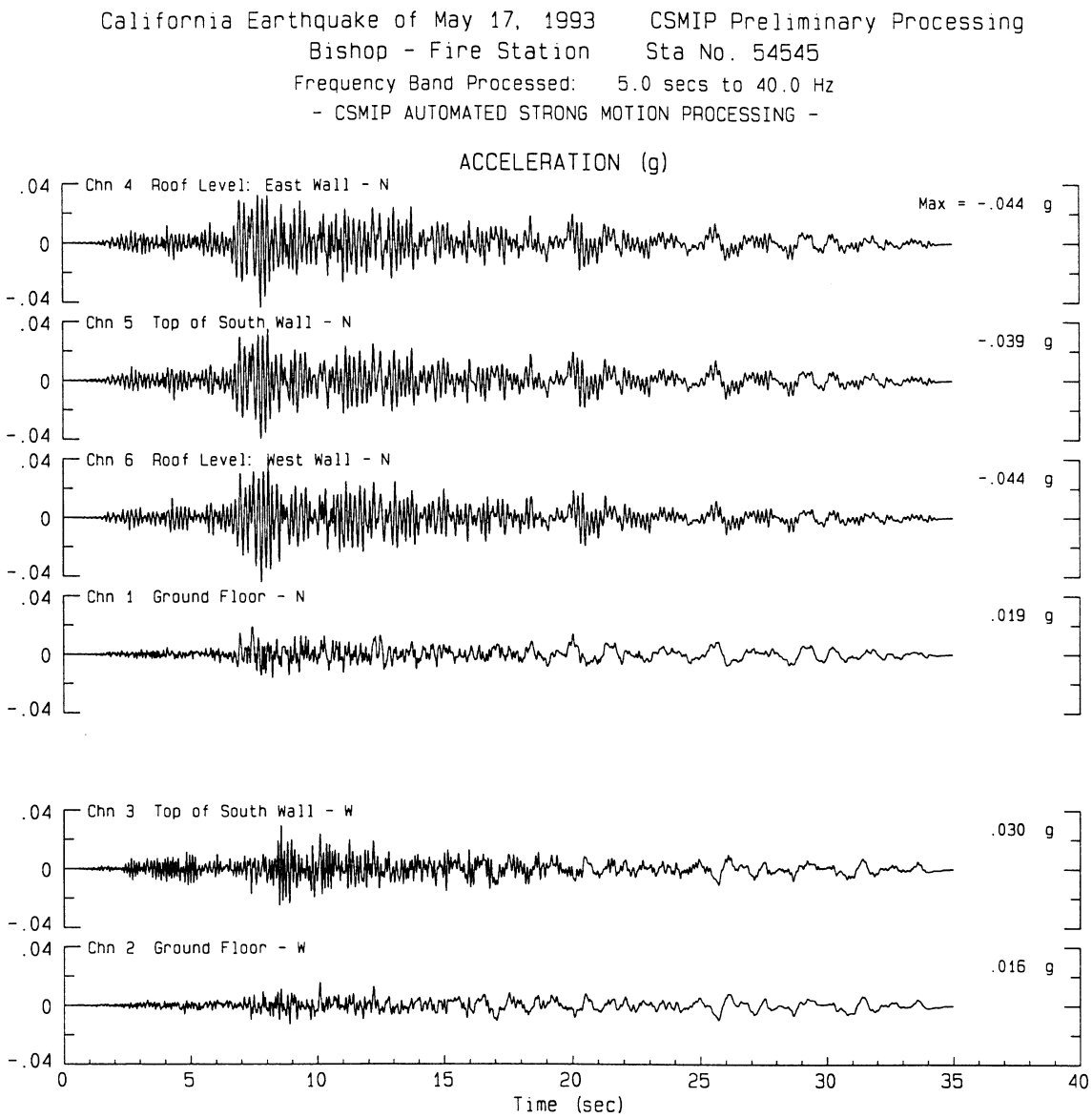

Figure A.8: Bishop 1-Story Fire Station, Records from 5/17/93 Earthquake

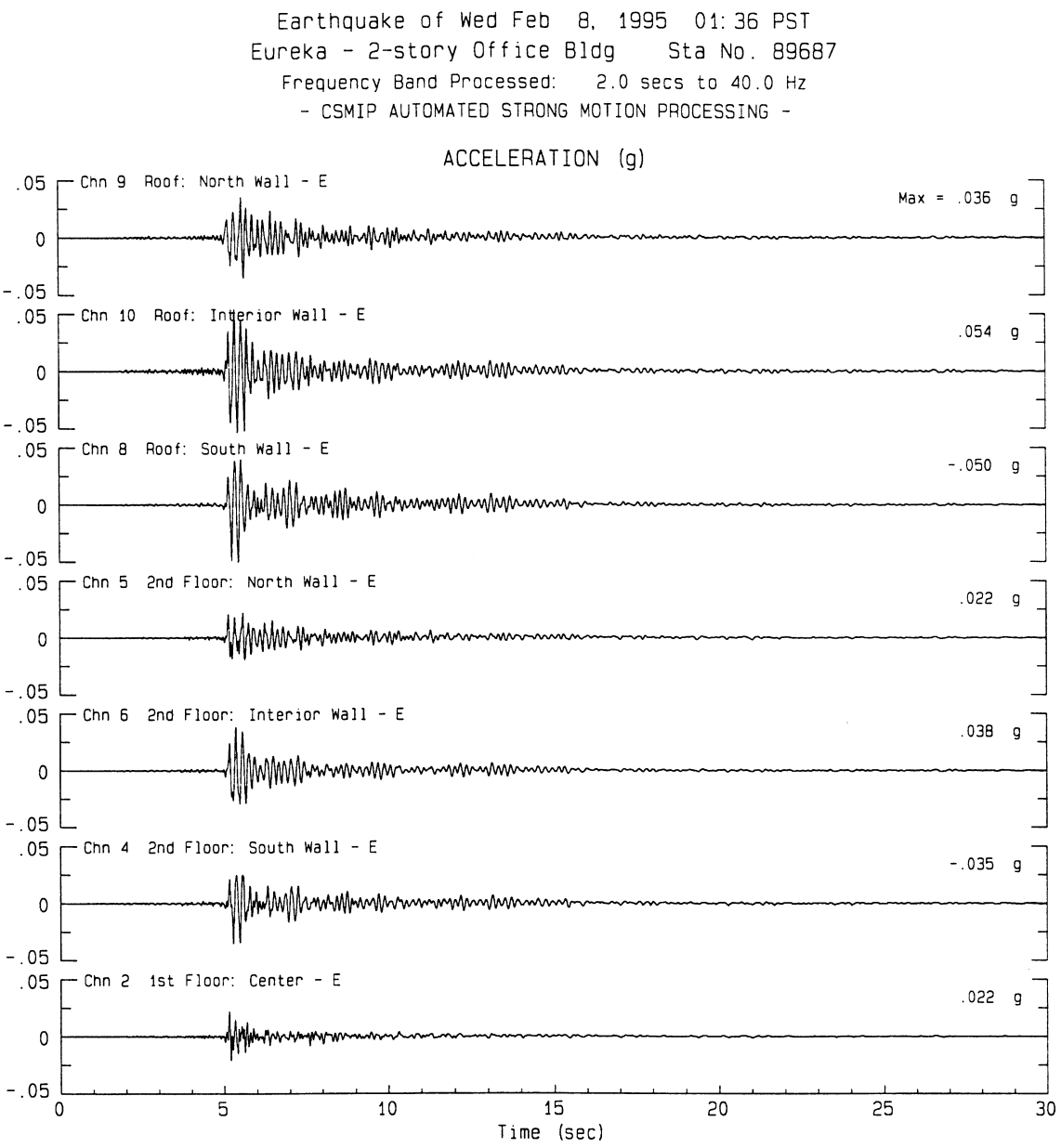

Figure A.9: Eureka 2-Story Office, Records from 2/8/95 Earthquake

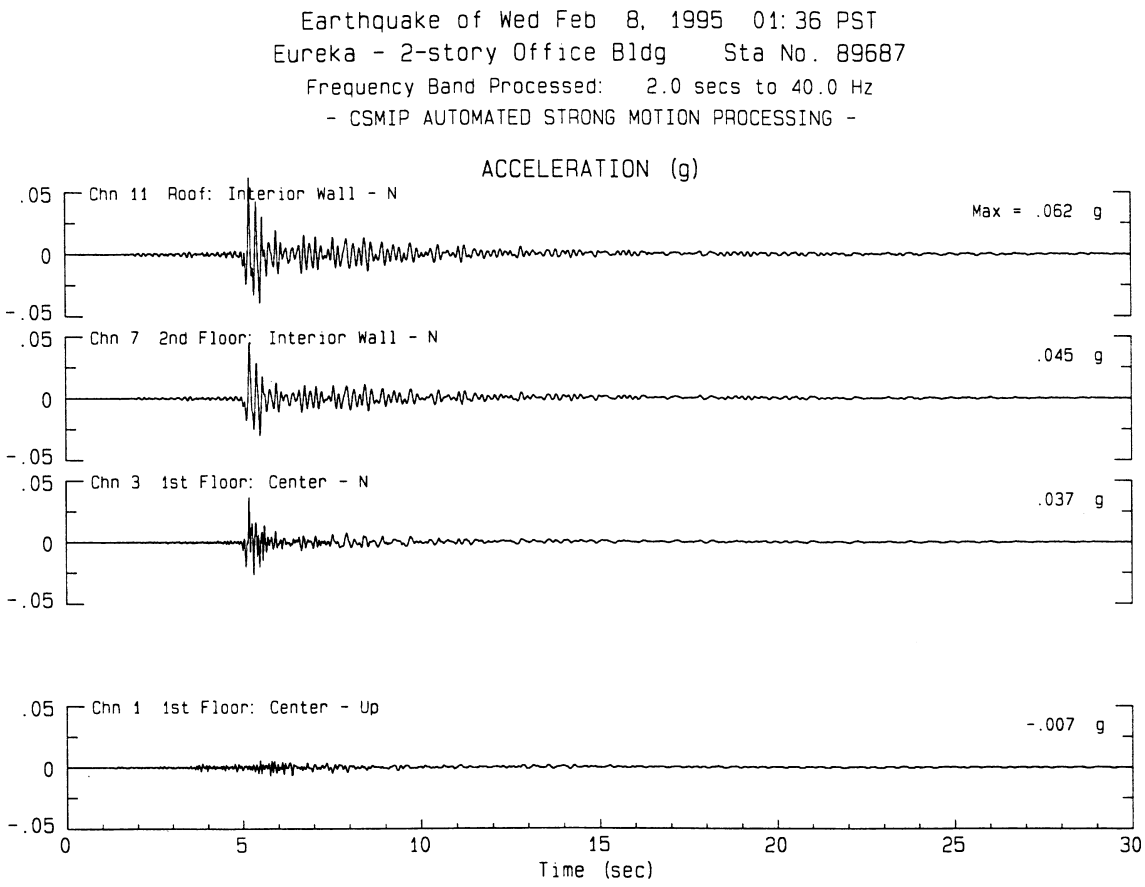
Earthquake of Wed Feb 8, 1995 01:36 PST
Eureka - 2-story Office Bldg Sta No. 89687
Frequency Band Processed: 2.0 secs to 40.0 Hz
- CSMIP AUTOMATED STRONG MOTION PROCESSING -
ACCELERATION (g)
Chn 11 Roof: Interior Wall - N
Max = .062 g
Chn 7 2nd Floor: Interior Wall - N
.045 g
Chn 3 1st Floor: Center - N
.037 g
Chn 1 1st Floor: Center - Up
-.007 g
.05
0
-.05
0
5
10
15
20
25
30
Time (sec)

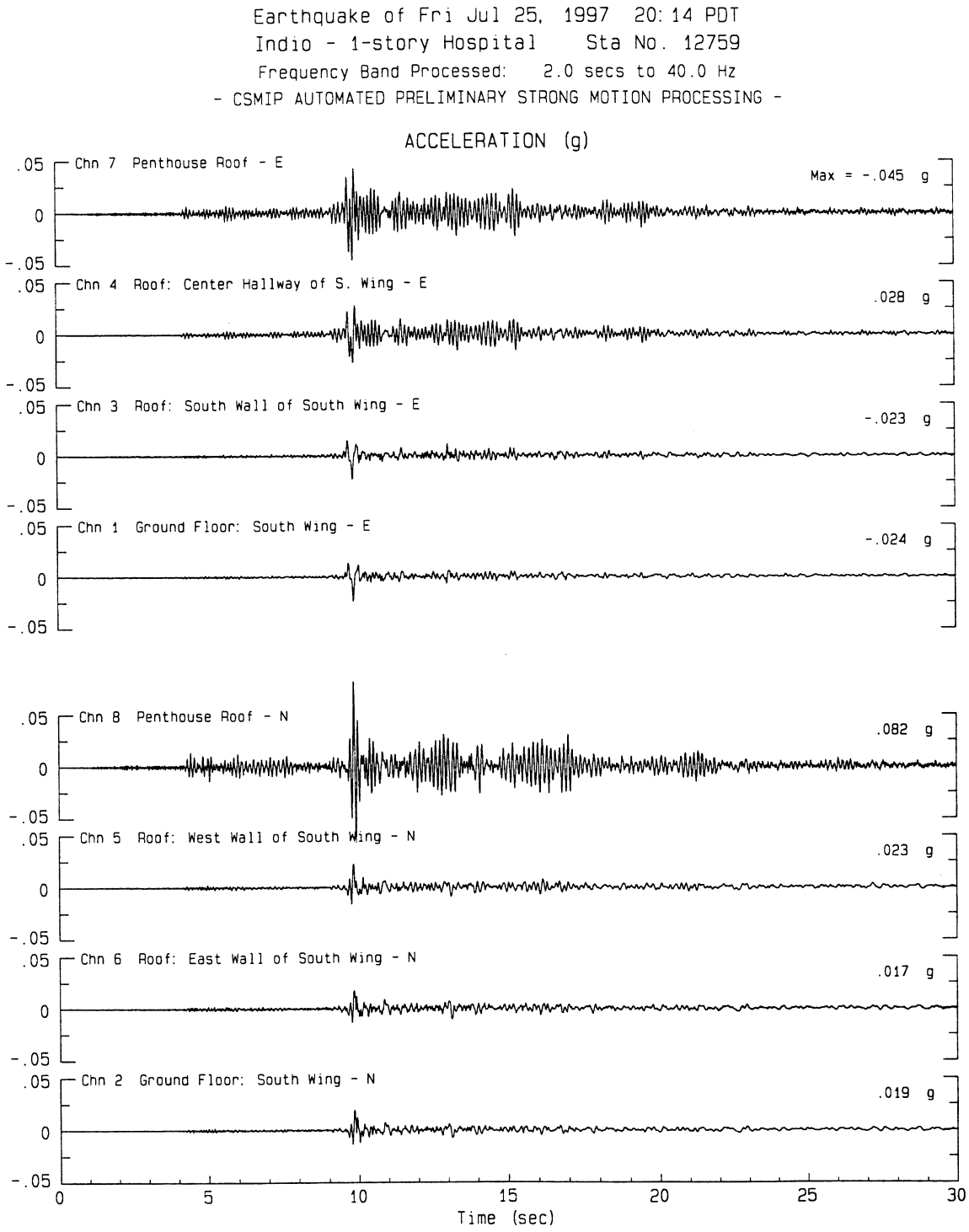

Figure A.10: Indio 1-Story Hospital, Records from 7/25/97 Earthquake

Appendix B

MODE-ID Results, Analysis of EQ Records

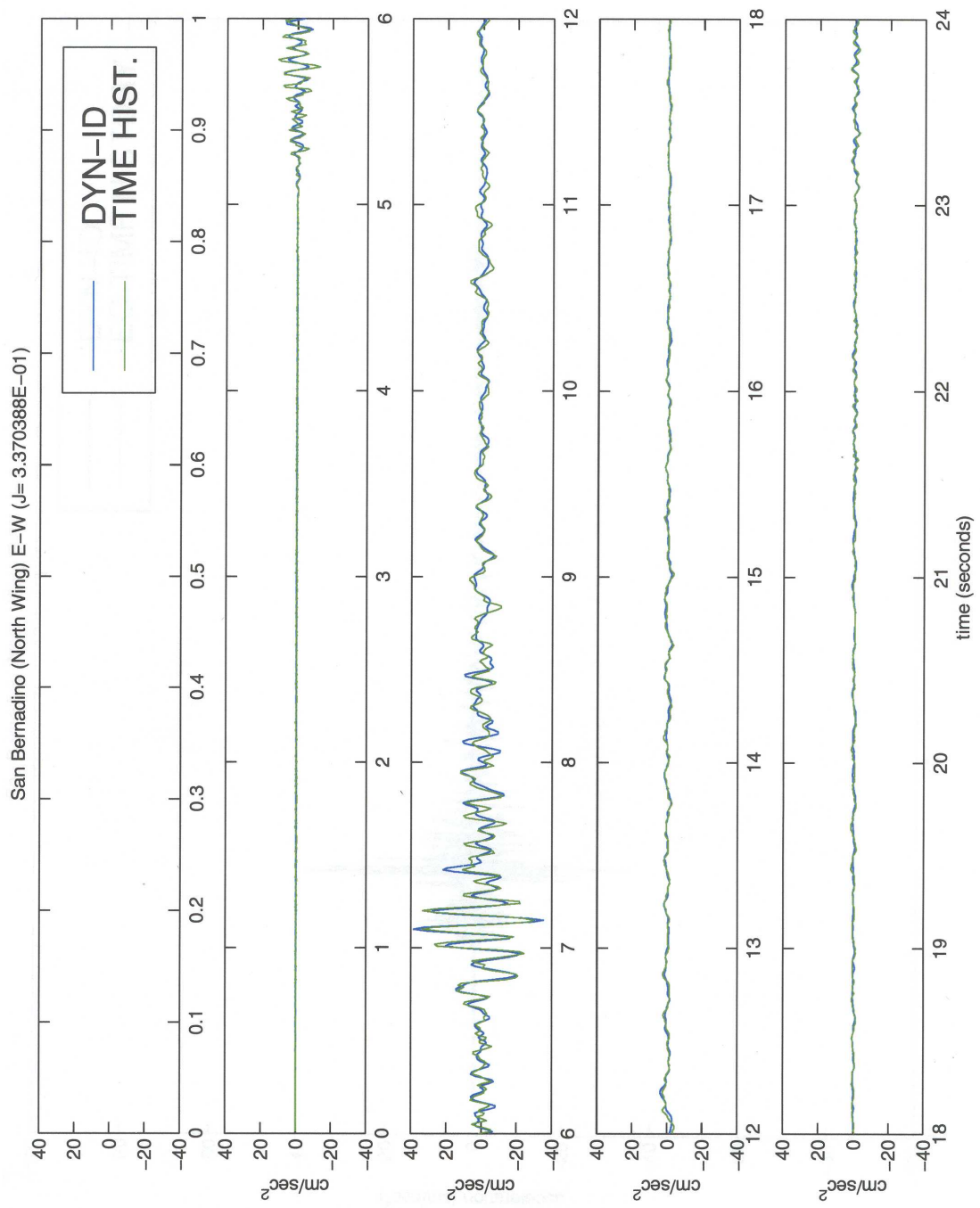

Figure B.1: Predicted Response Using MODE-ID Time-Invariant Results
San Bernardino 3-Story Motel, 06/28/97
(EW channel 8, 2nd floor, N. wing, center)

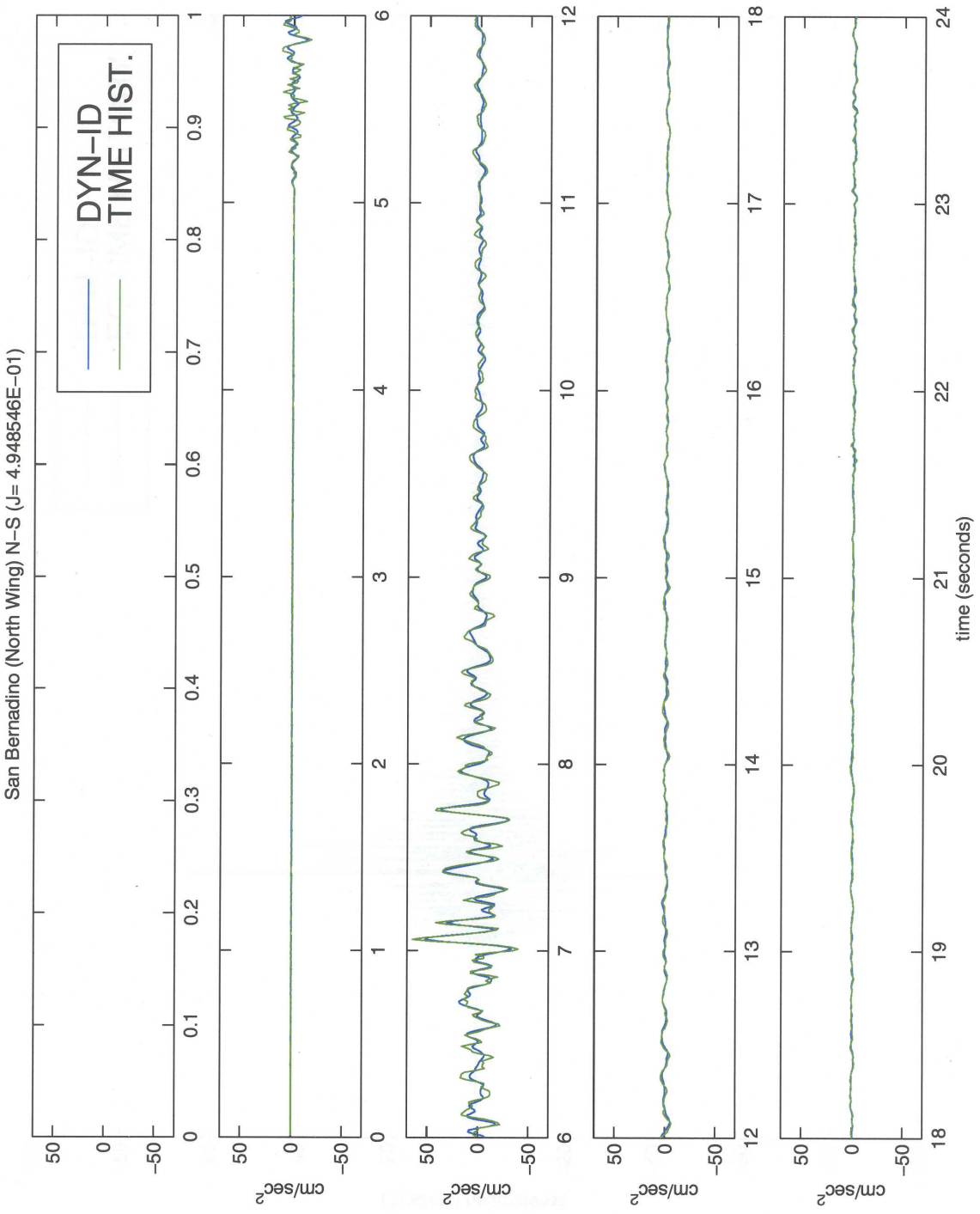

Figure B.2: Predicted Response Using MODE-ID Time-Invariant Results
San Bernardino 3-Story Motel, 06/28/97
(NS channel 4, 2nd floor, N. wing, W. wall)

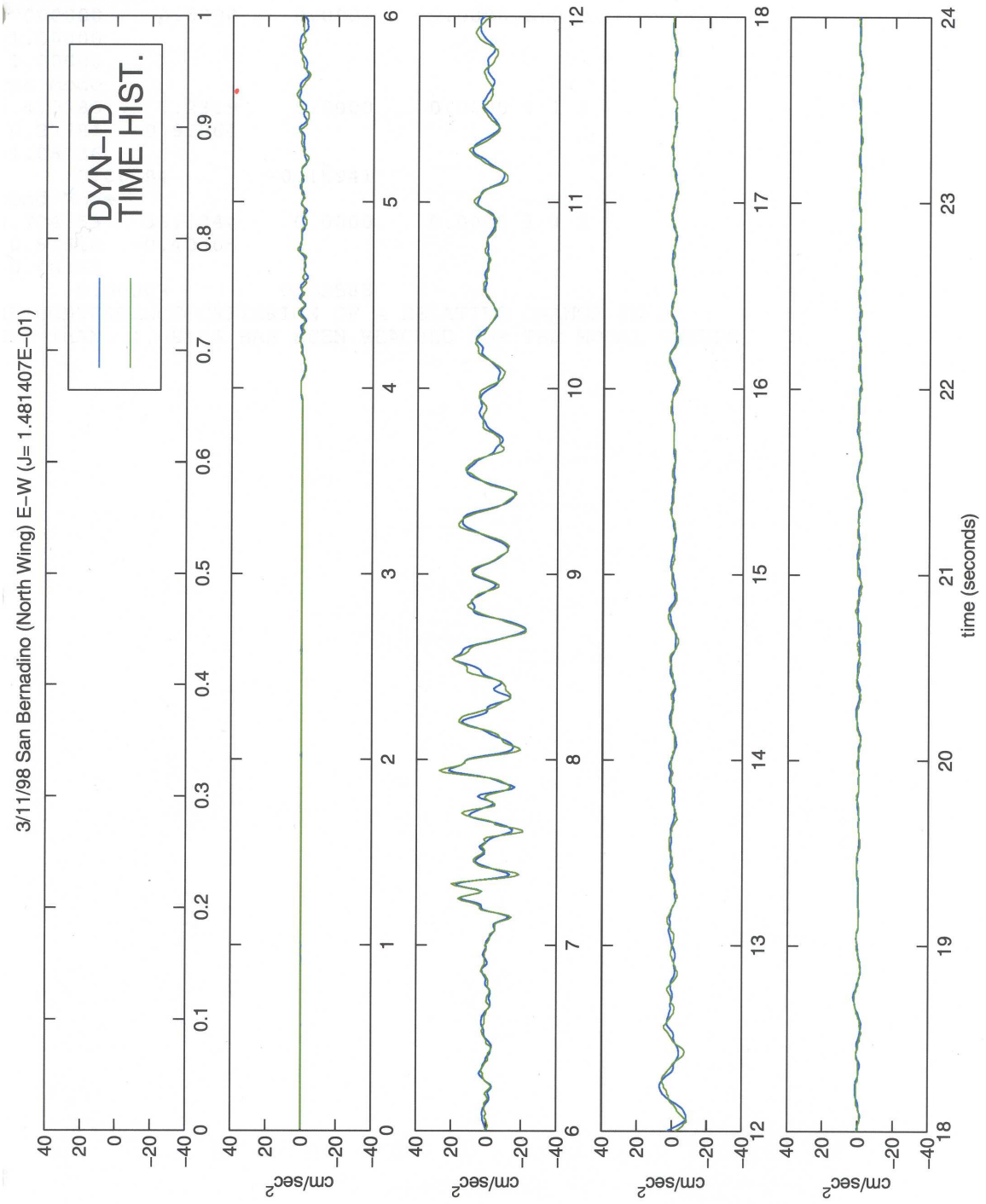

Figure B.3: Predicted Response Using MODE-ID Time-Invariant Results
San Bernardino 3-Story Motel, 03/11/98
(EW channel 4, 2nd floor, N. wing, W. wall)

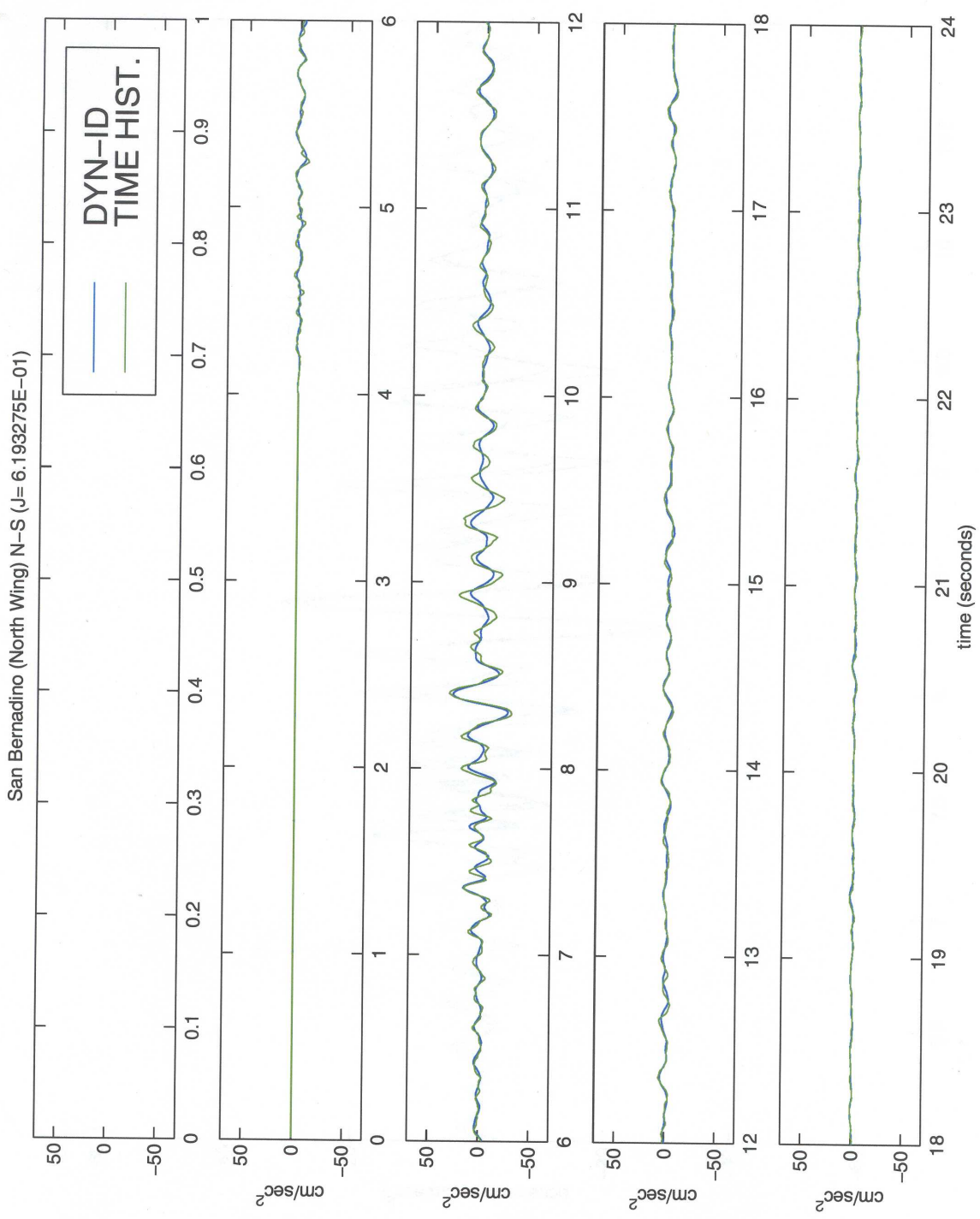

Figure B.4: Predicted Response Using MODE-ID Time-Invariant Results
San Bernardino 3-Story Motel, 03/11/98
(NS channel 4, 2nd floor, N. wing, W. wall)

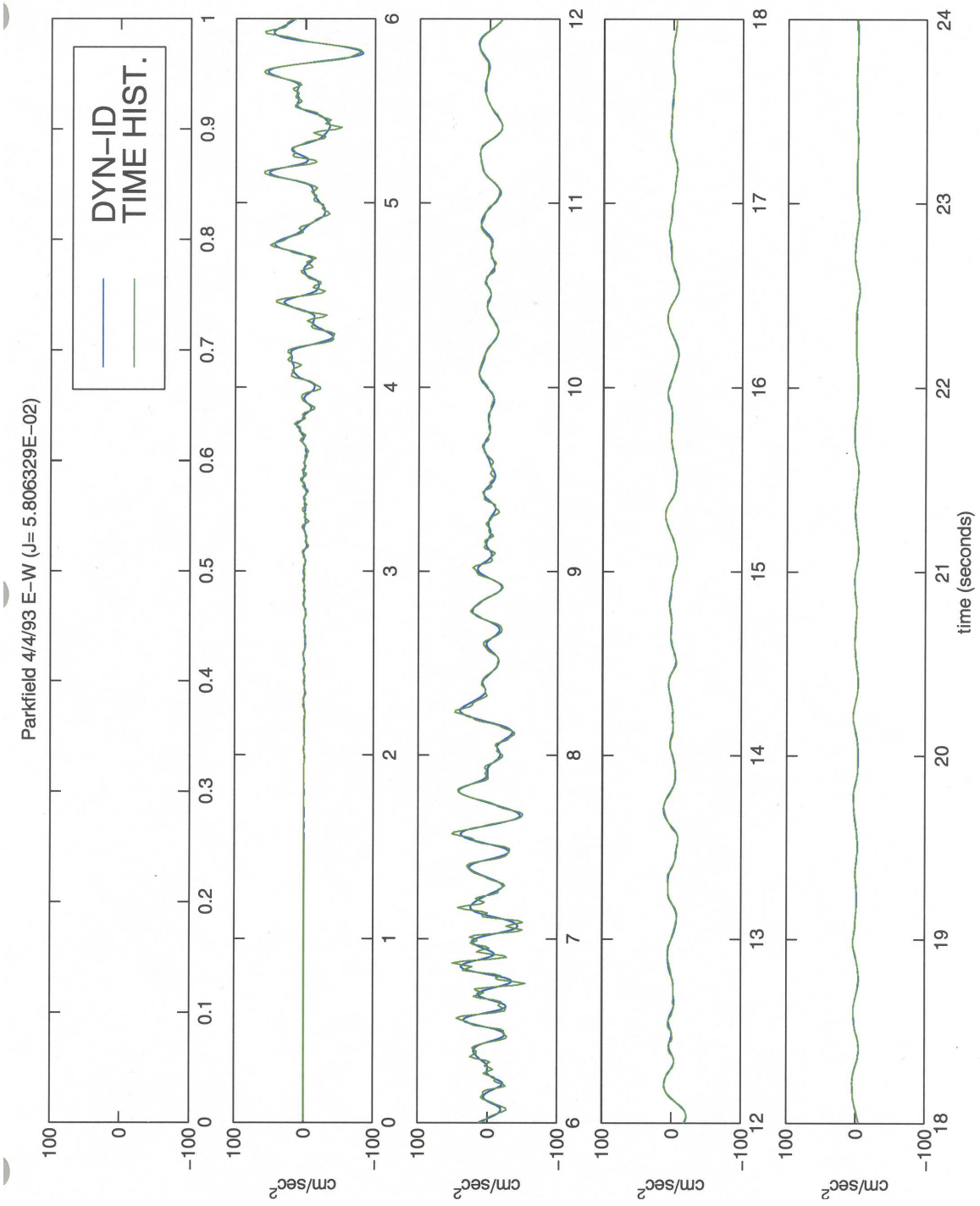

Figure B.5: Predicted Response Using MODE-ID Time-Invariant Results
Parkfield 1-Story School, 04/04/93
(EW channel 5, top of south shear wall)

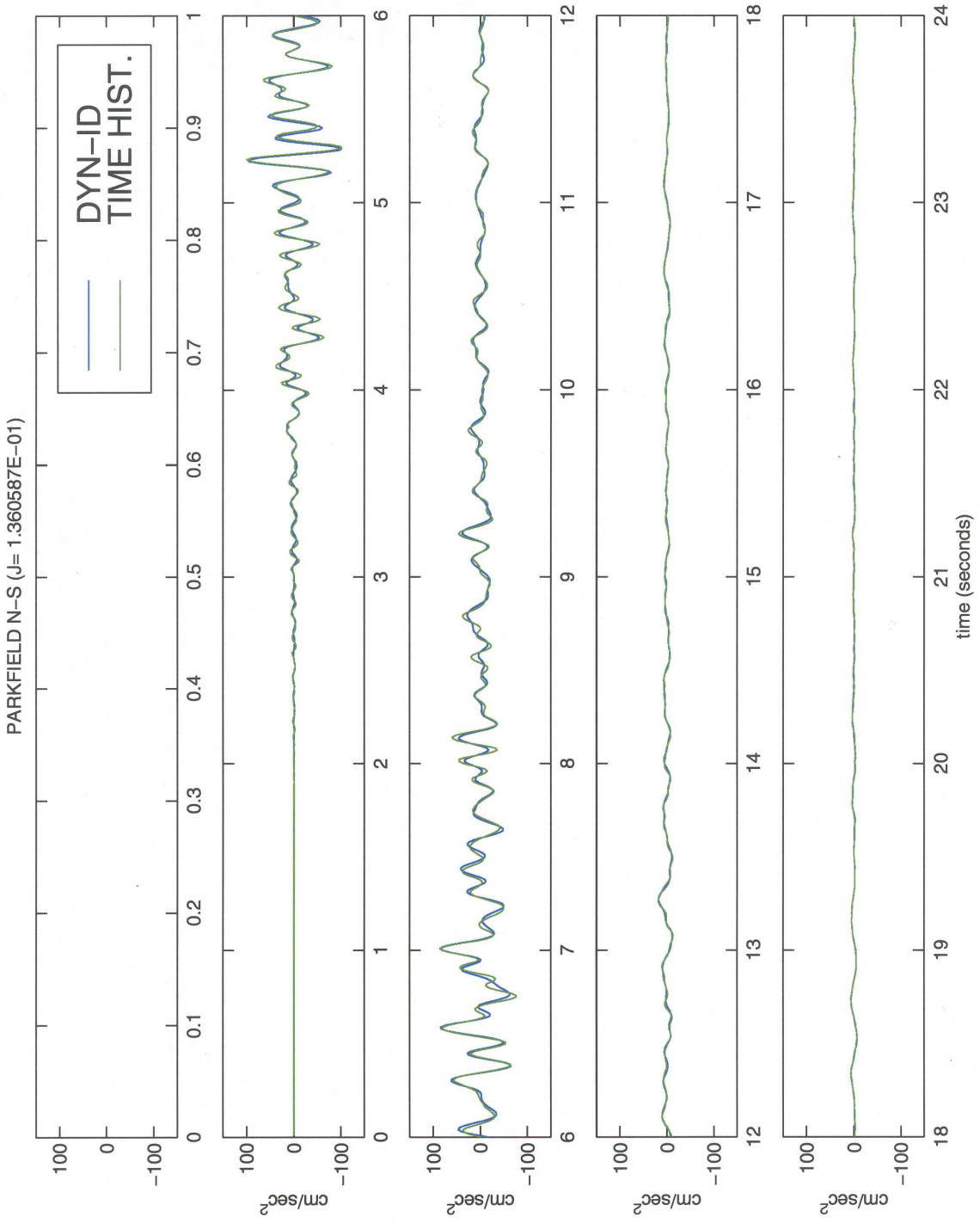

Figure B.6: Predicted Response Using MODE-ID Time-Invariant Results
Parkfield 1-Story School, 04/04/93
(NS channel 2, center of roof)

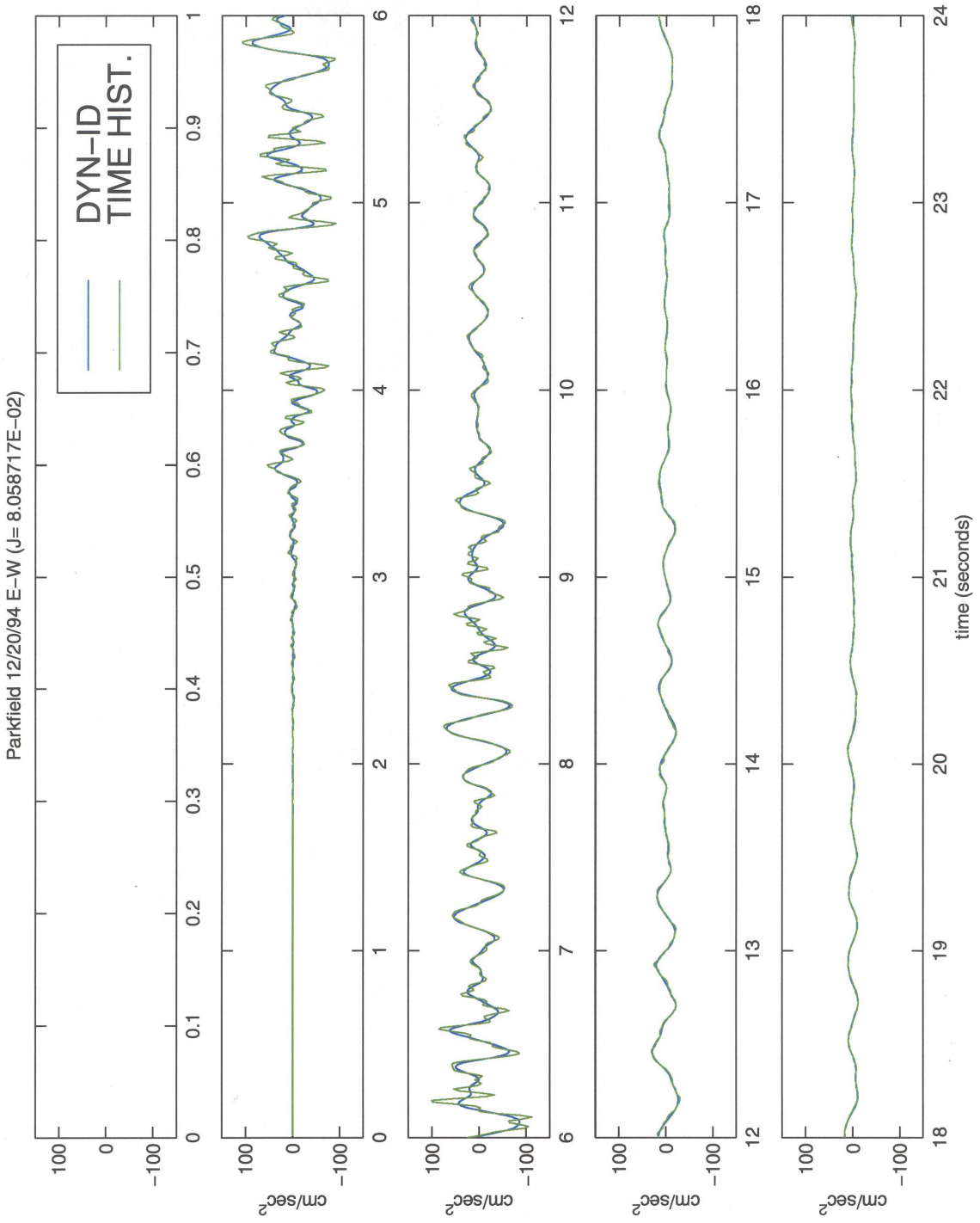

Figure B.7: Predicted Response Using MODE-ID Time-Invariant Results
Parkfield 1-Story School, 12/20/94
(EW channel 5, top of south shear wall)

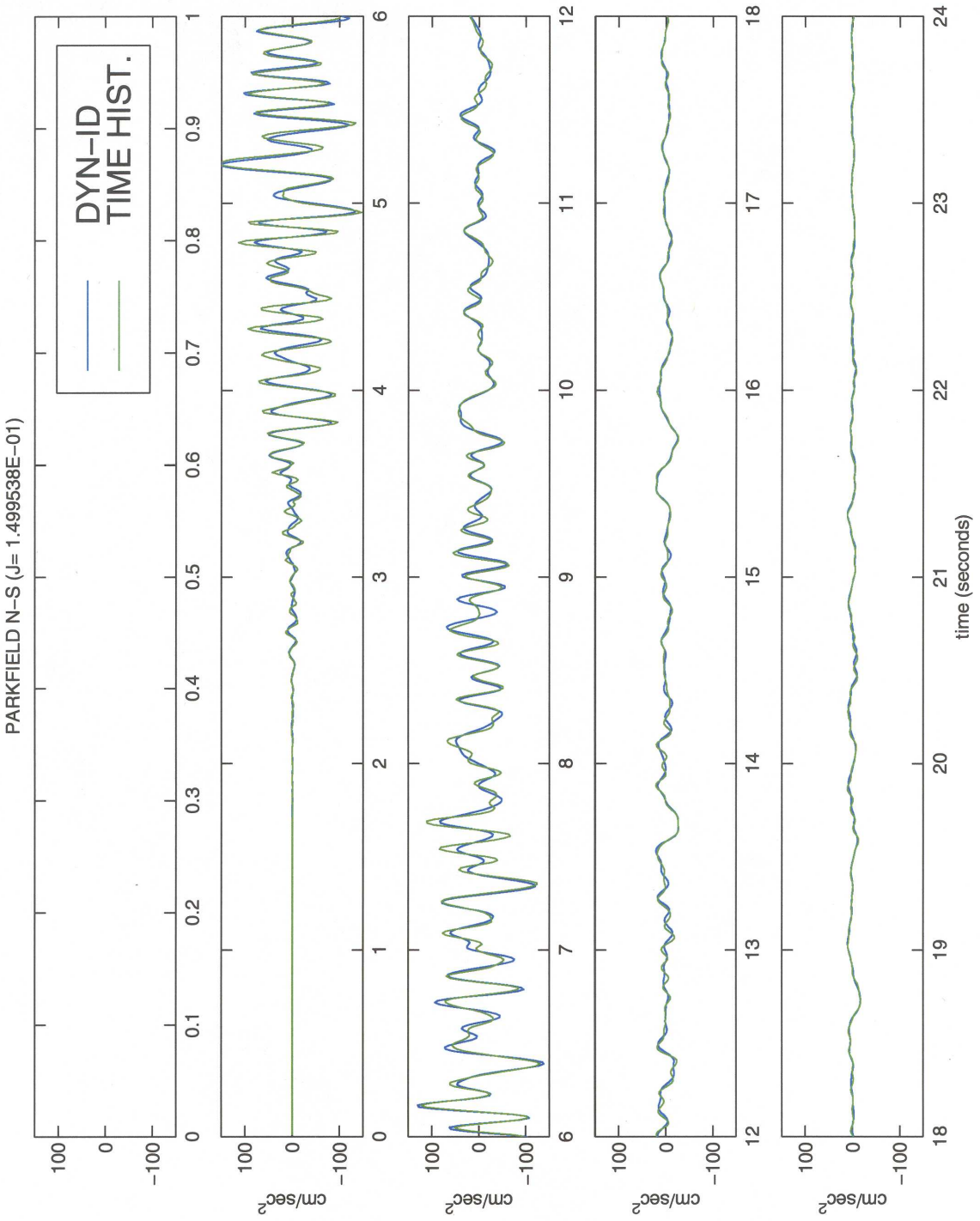

Figure B.8: Predicted Response Using MODE-ID Time-Invariant Results
Parkfield 1-Story School, 12/20/94
(NS channel 2, center of roof)

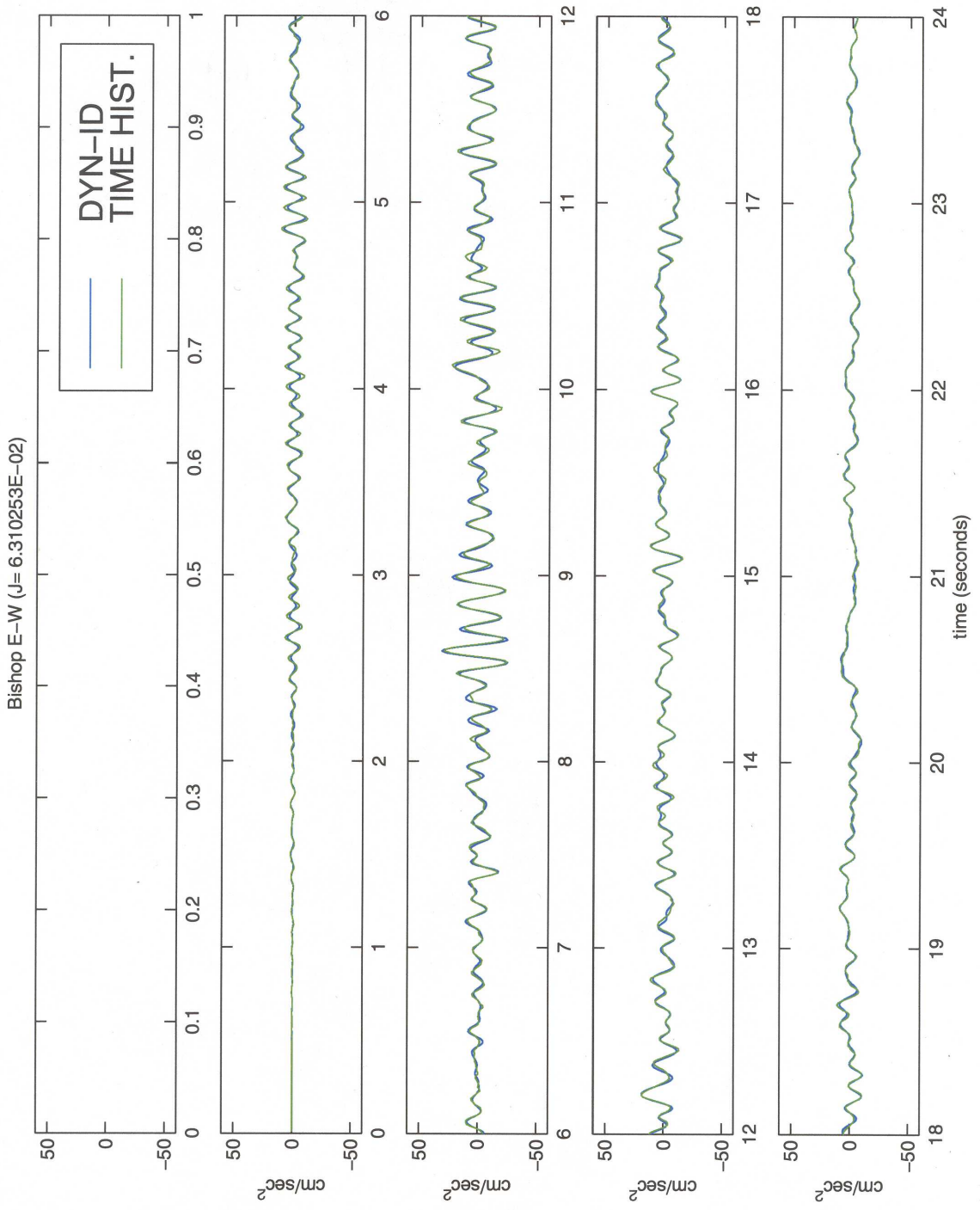

Figure B.9: Predicted Response Using MODE-ID Time-Invariant Results
Bishop 1-Story Firestation
(EW channel 3, top of south wall)

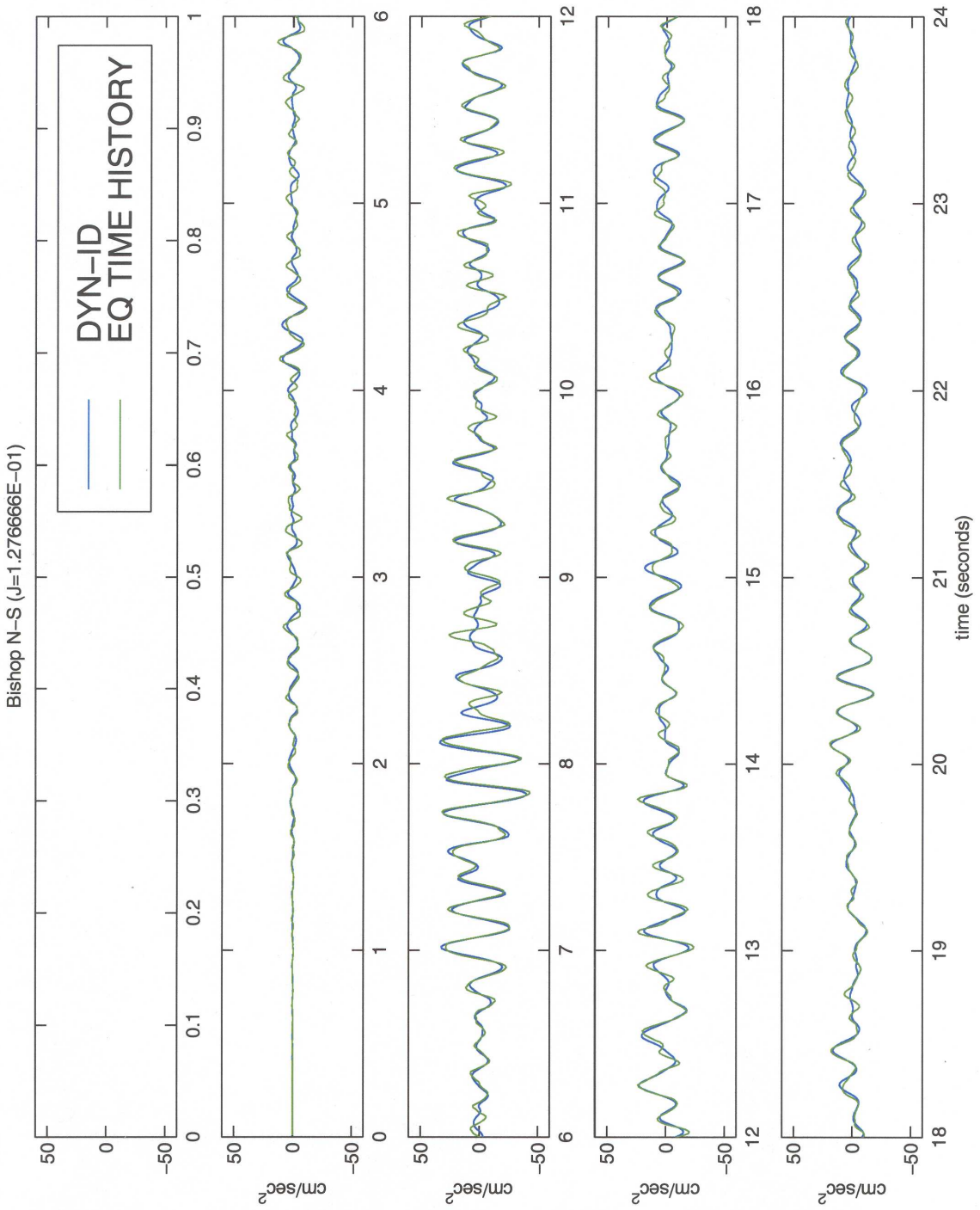

Figure B.10: Predicted Response Using MODE-ID Time-Invariant Results
Bishop 1-Story Firestation
(NS channel 4, roof at west wall)

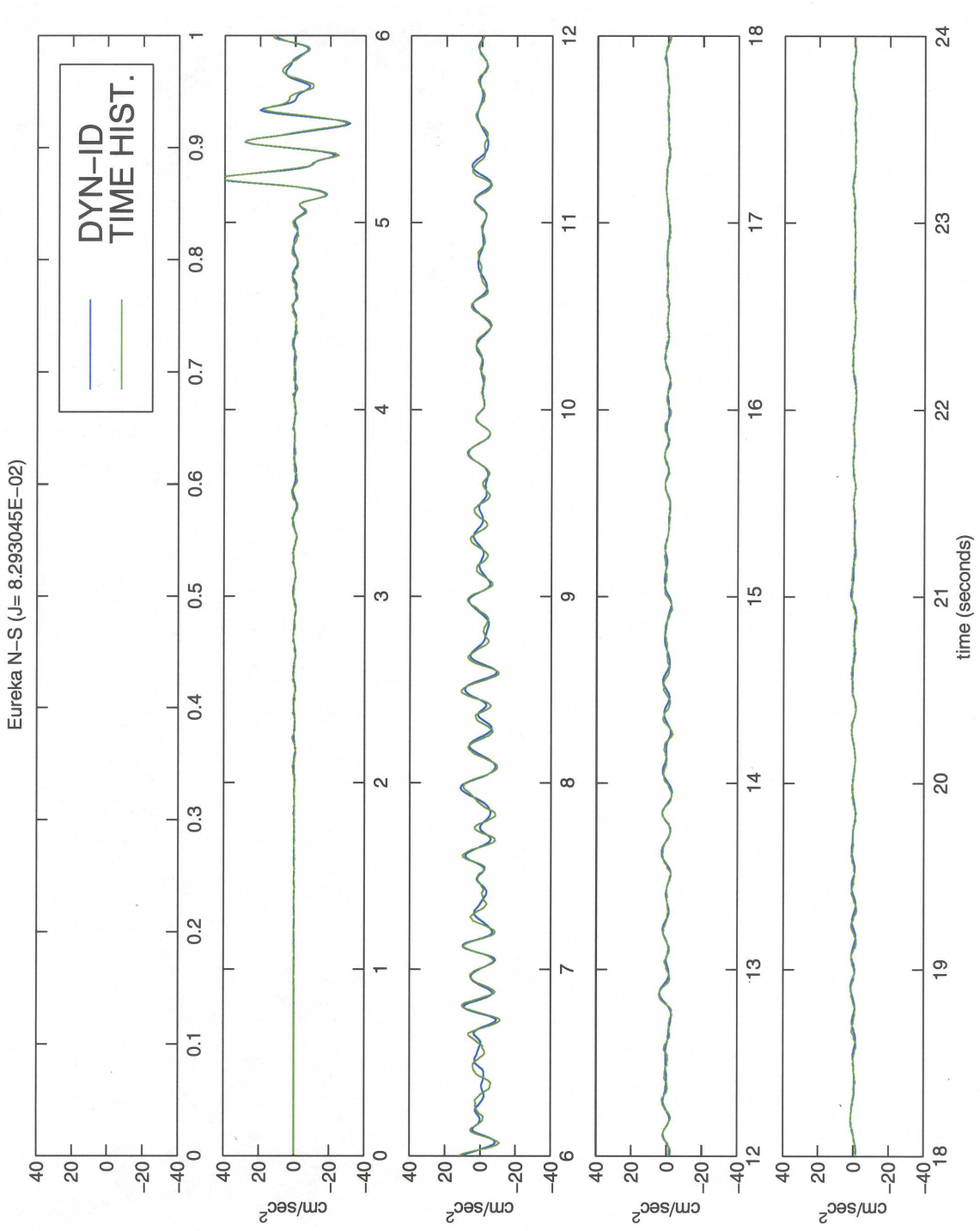

Figure B.11: Predicted Response Using MODE-ID Time-Invariant Results
Eureka 2-Story Office Building
(NS channel 7, 2nd floor at interior wall)

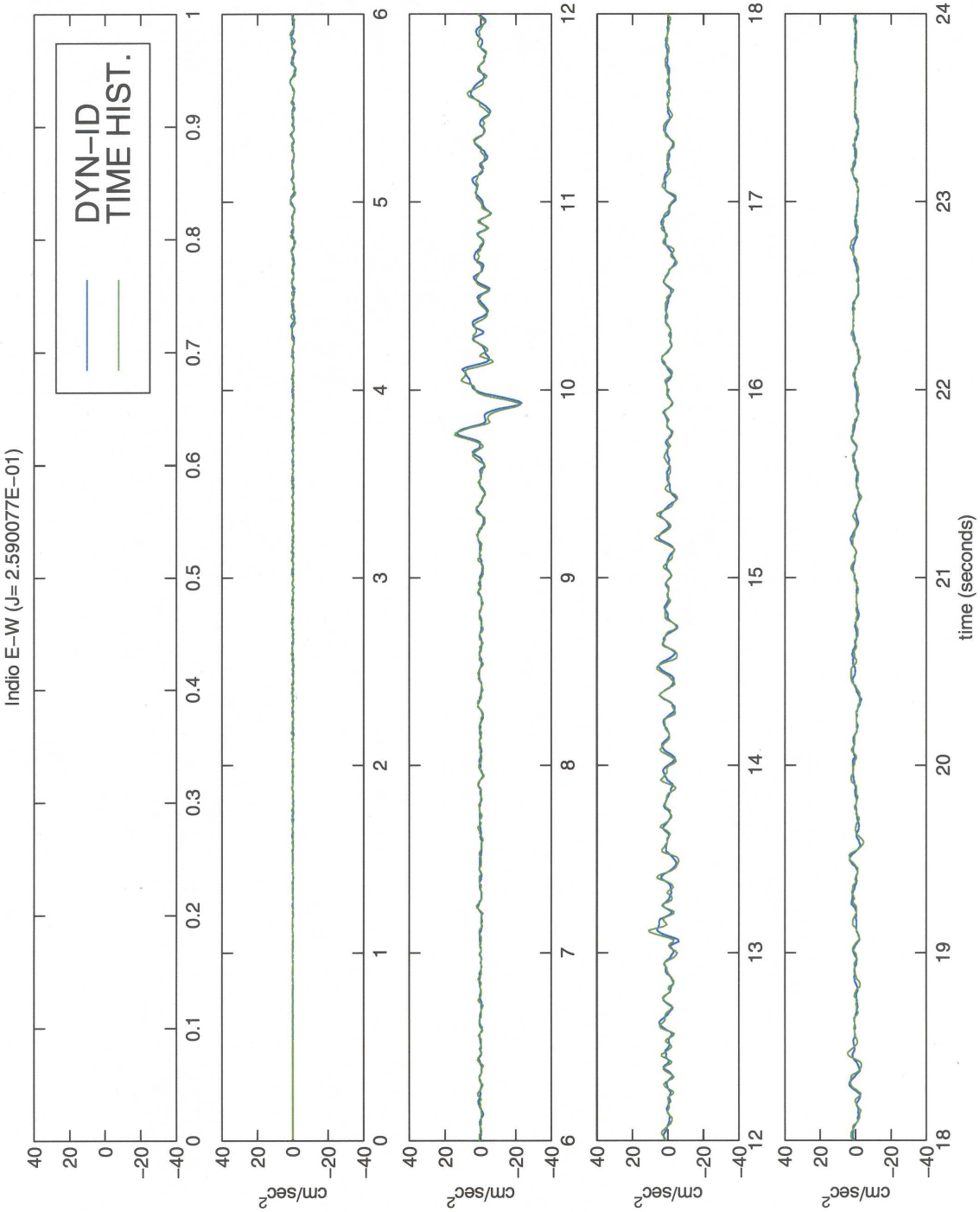

Figure B.12: Predicted Response Using MODE-ID Time-Invariant Results
Indio 1-Story Hospital
(EW channel 3, roof at south wall of south wing)

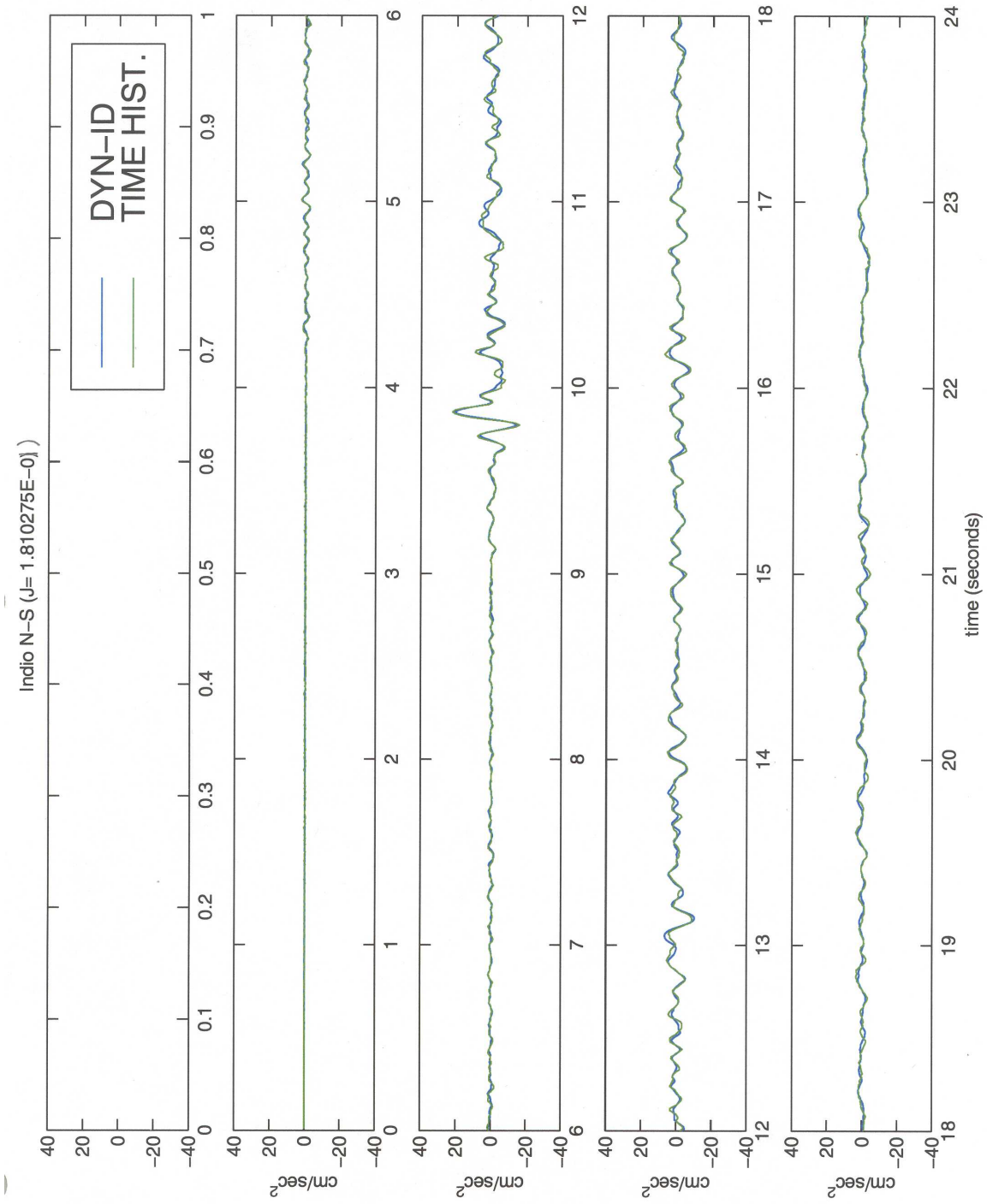

Figure B.13: Predicted Response Using MODE-ID Time-Invariant Results
Indio 1-Story Hospital
(NS channel 5, roof at west wall of south wing)

Appendix C

Forced Vibration Test Raw Data

C.1 2-Story House on S. Catalina Ave., Pasadena

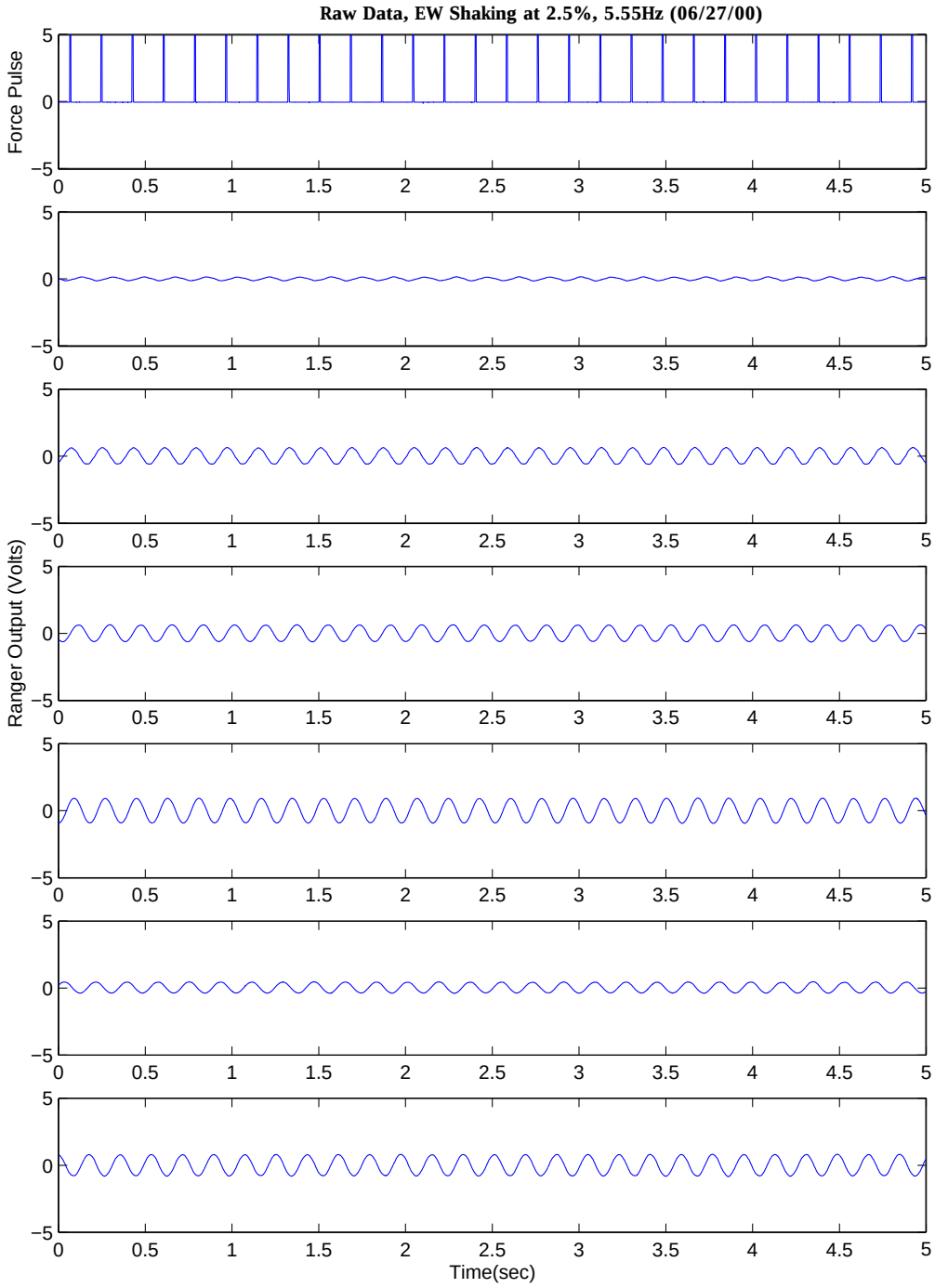

Figure C.1: 2-Story House FVT Raw Data (EW at 2.5%, 5.55Hz)

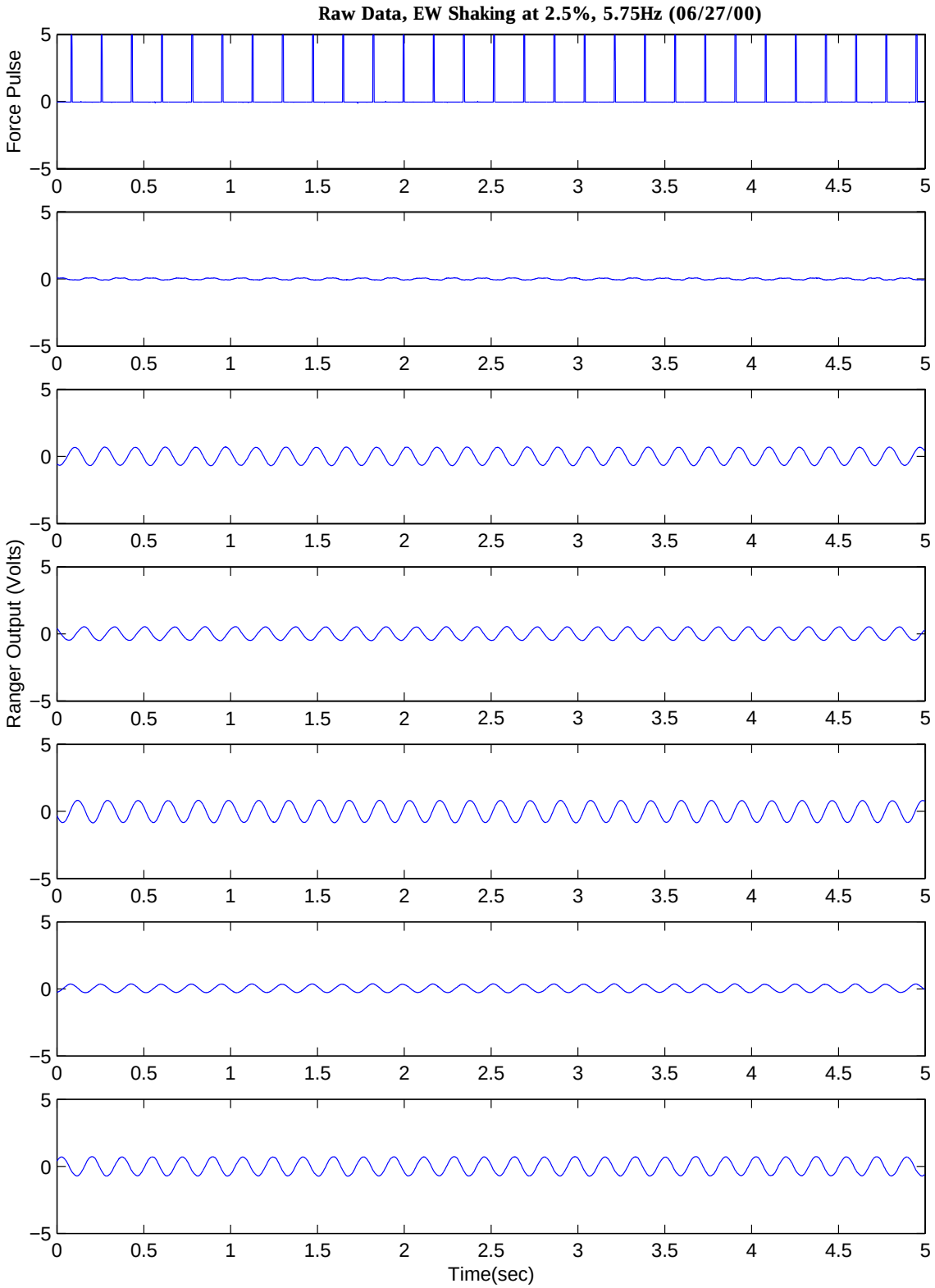

Figure C.2: 2-Story House FVT Raw Data (EW at 2.5%, 5.75Hz)

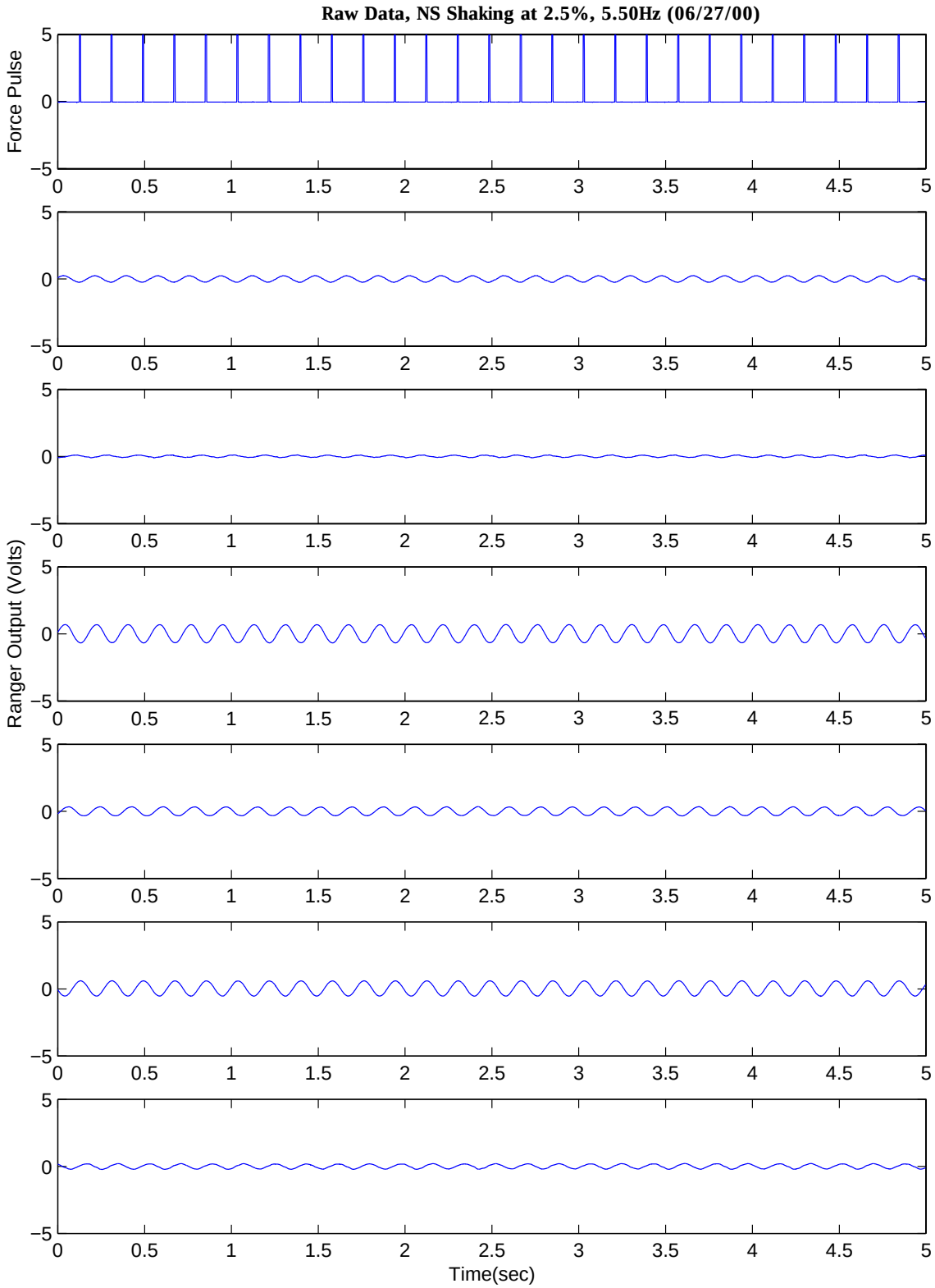

Figure C.3: 2-Story House FVT Raw Data (NS at 2.5%, 5.50Hz)

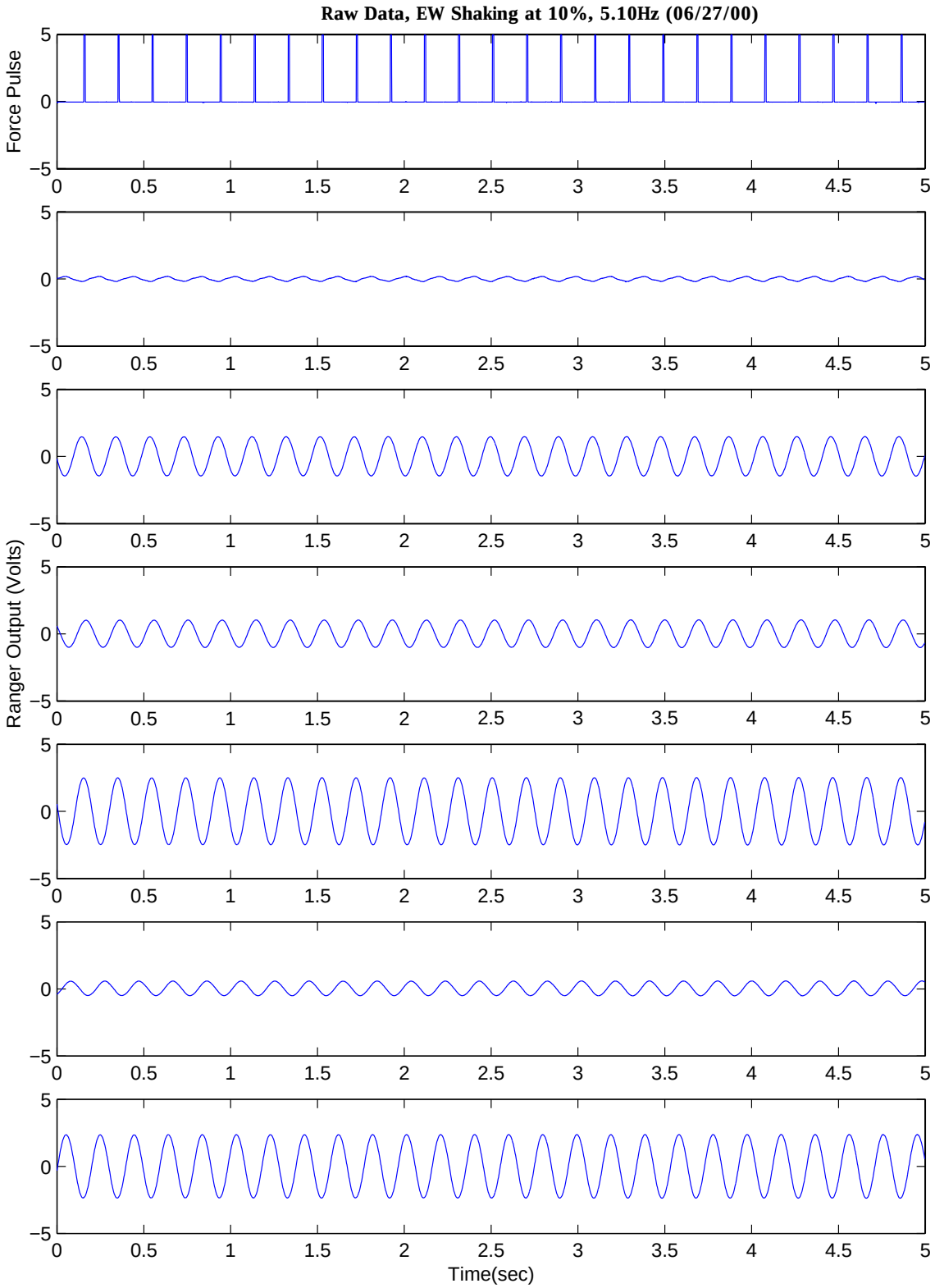

Figure C.4: 2-Story House FVT Raw Data (EW at 10%, 5.10Hz)

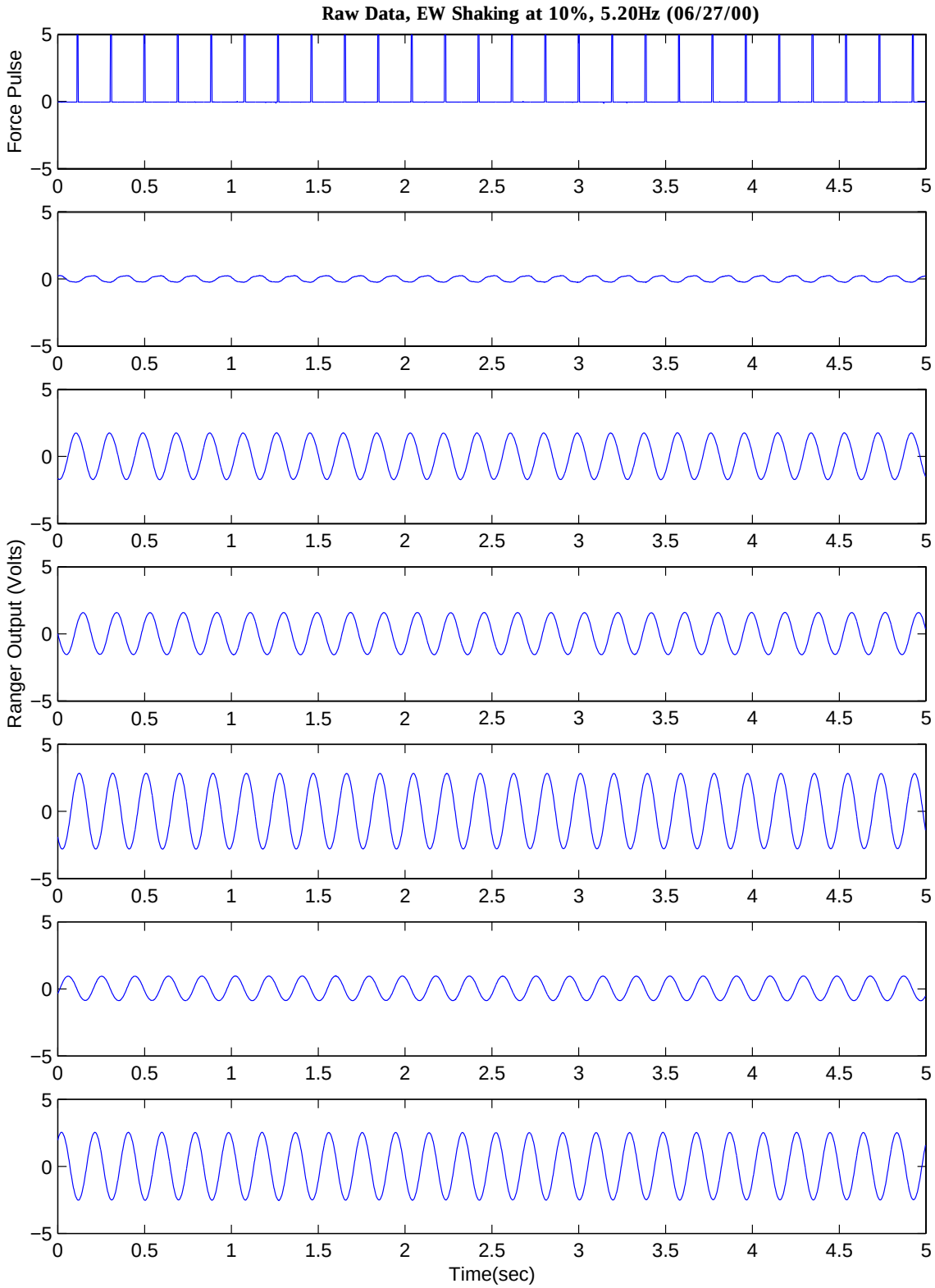

Figure C.5: 2-Story House FVT Raw Data (EW at 10%, 5.20Hz)

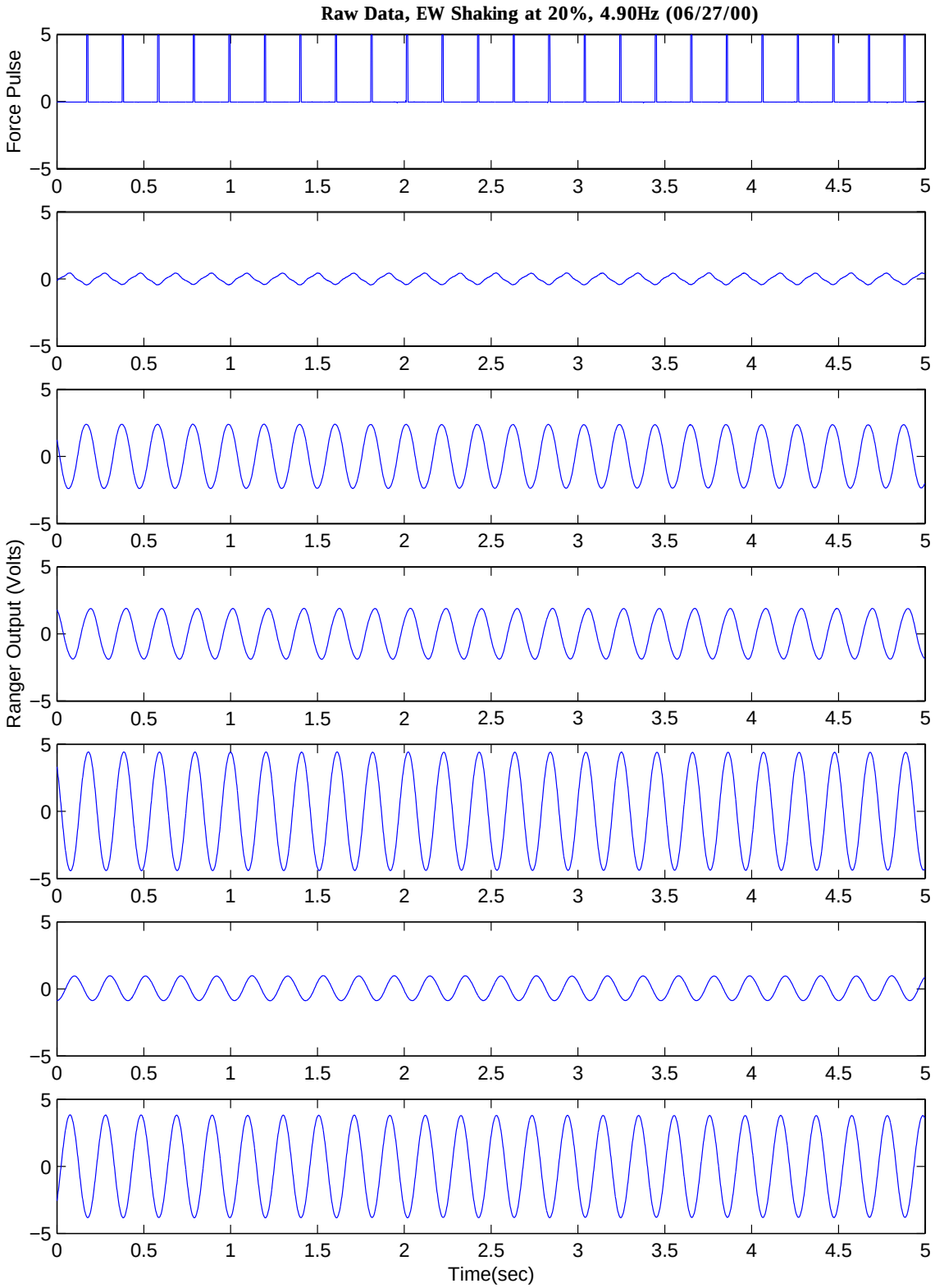

Figure C.6: 2-Story House FVT Raw Data (EW at 20%, 4.90Hz)

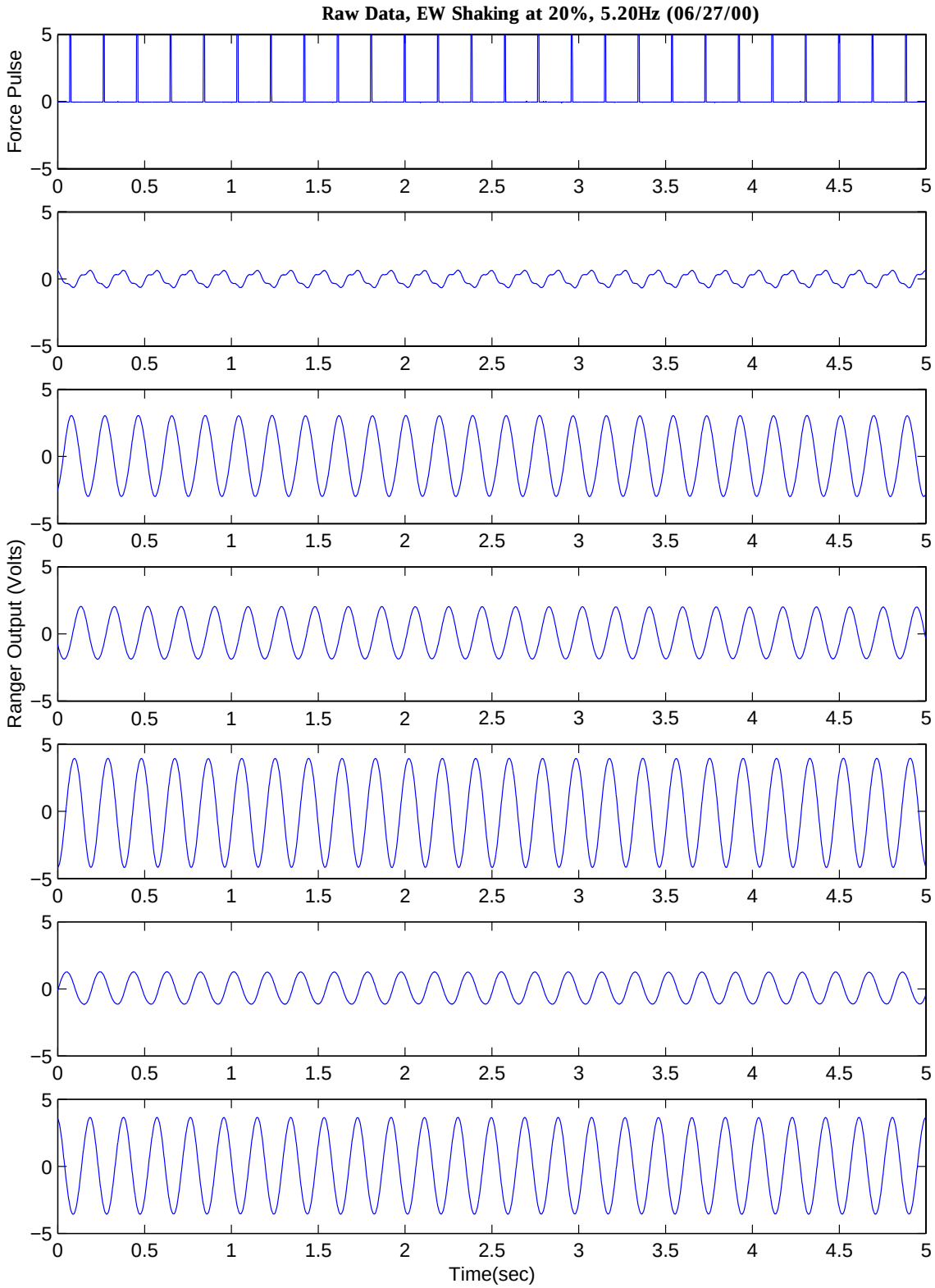

Figure C.7: 2-Story House FVT Raw Data (EW at 20%, 5.20Hz)

C.2 3-Story Building on S. Del Mar Ave., Pasadena

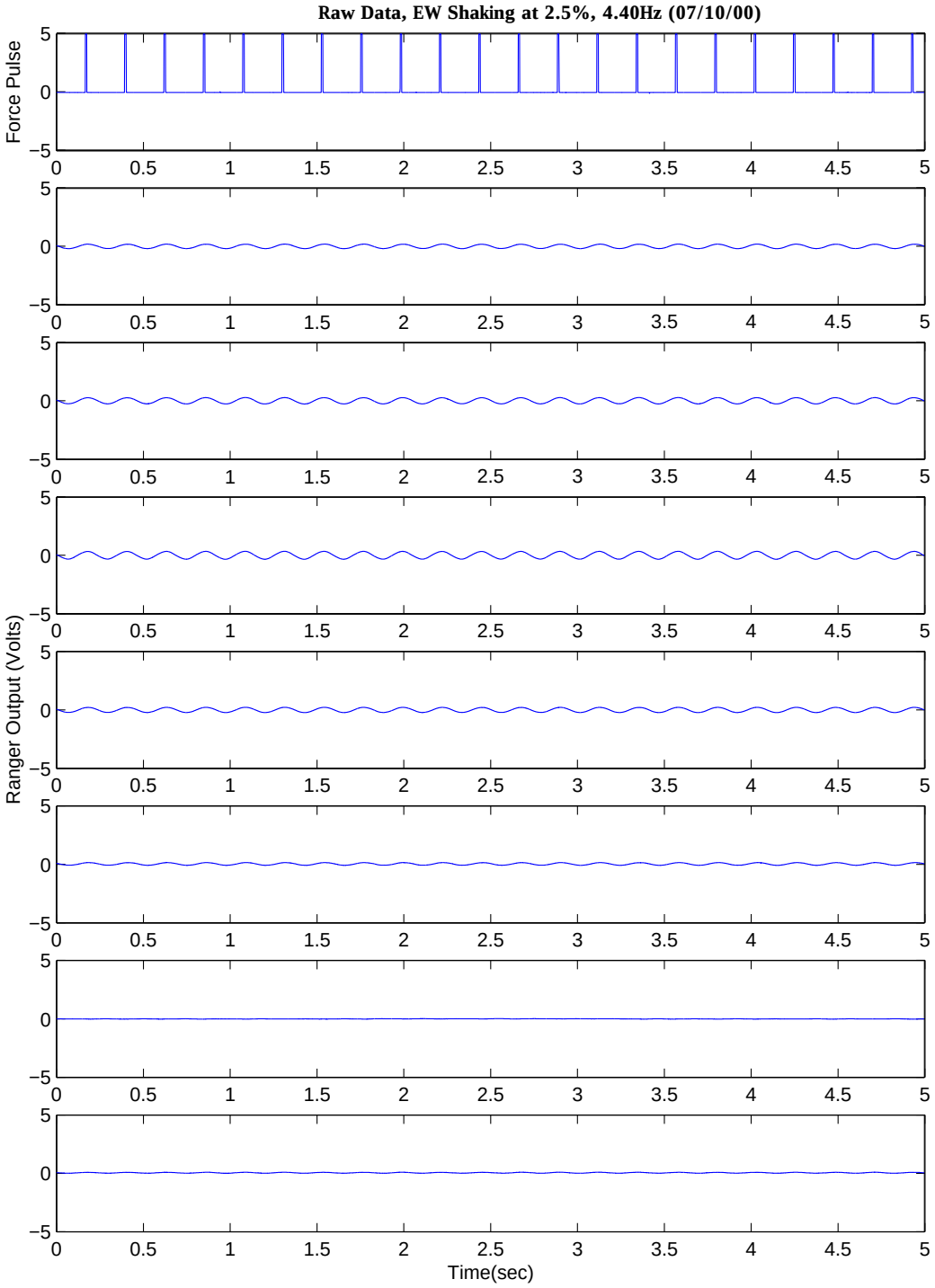

Figure C.8: 3-Story Building FVT Raw Data (EW at 2.5%, 4.40Hz)

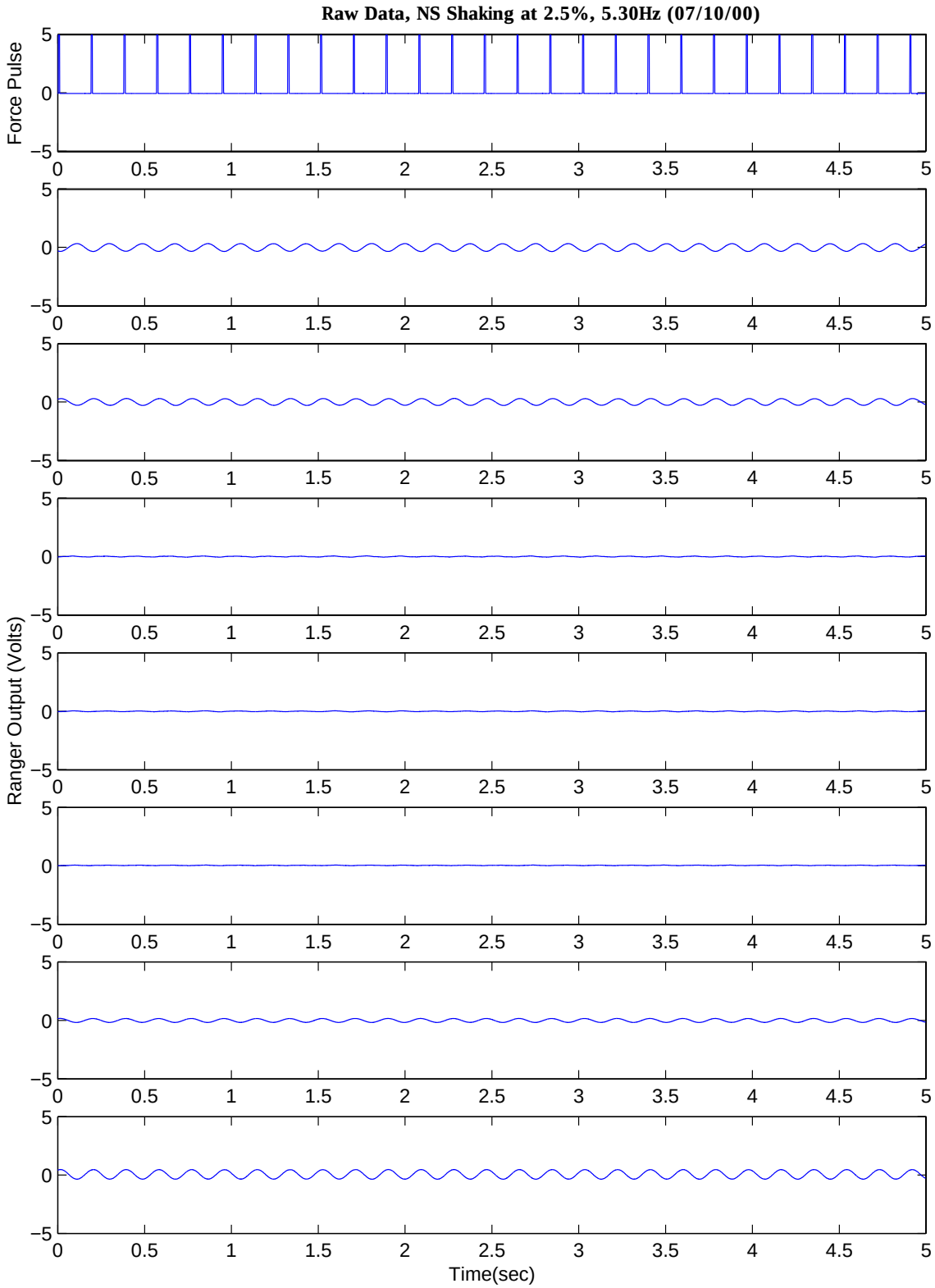

Figure C.9: 3-Story Building FVT Raw Data (NS at 2.5%, 5.30Hz)

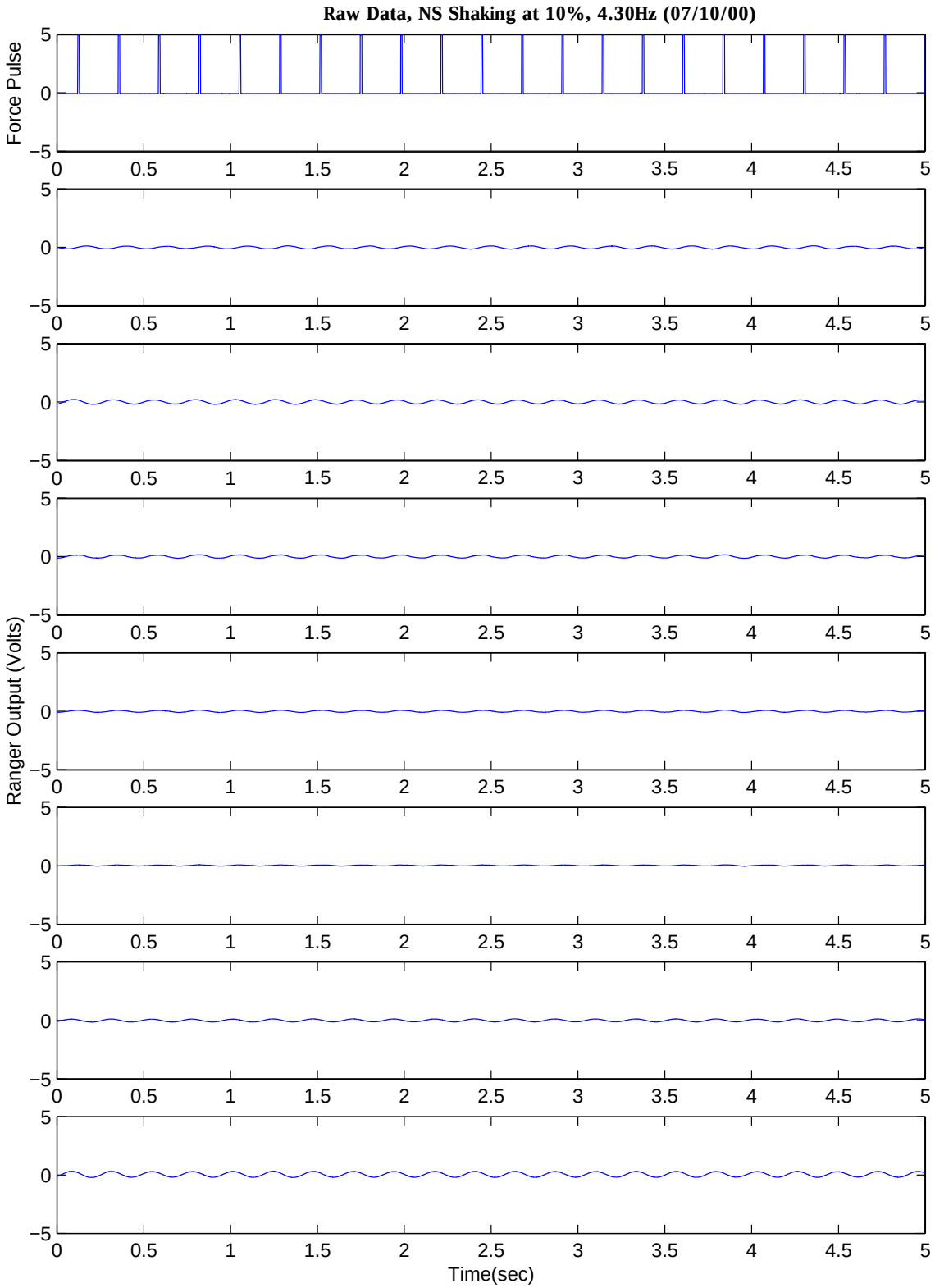

Figure C.10: 3-Story Building FVT Raw Data (NS at 10%, 4.30Hz)

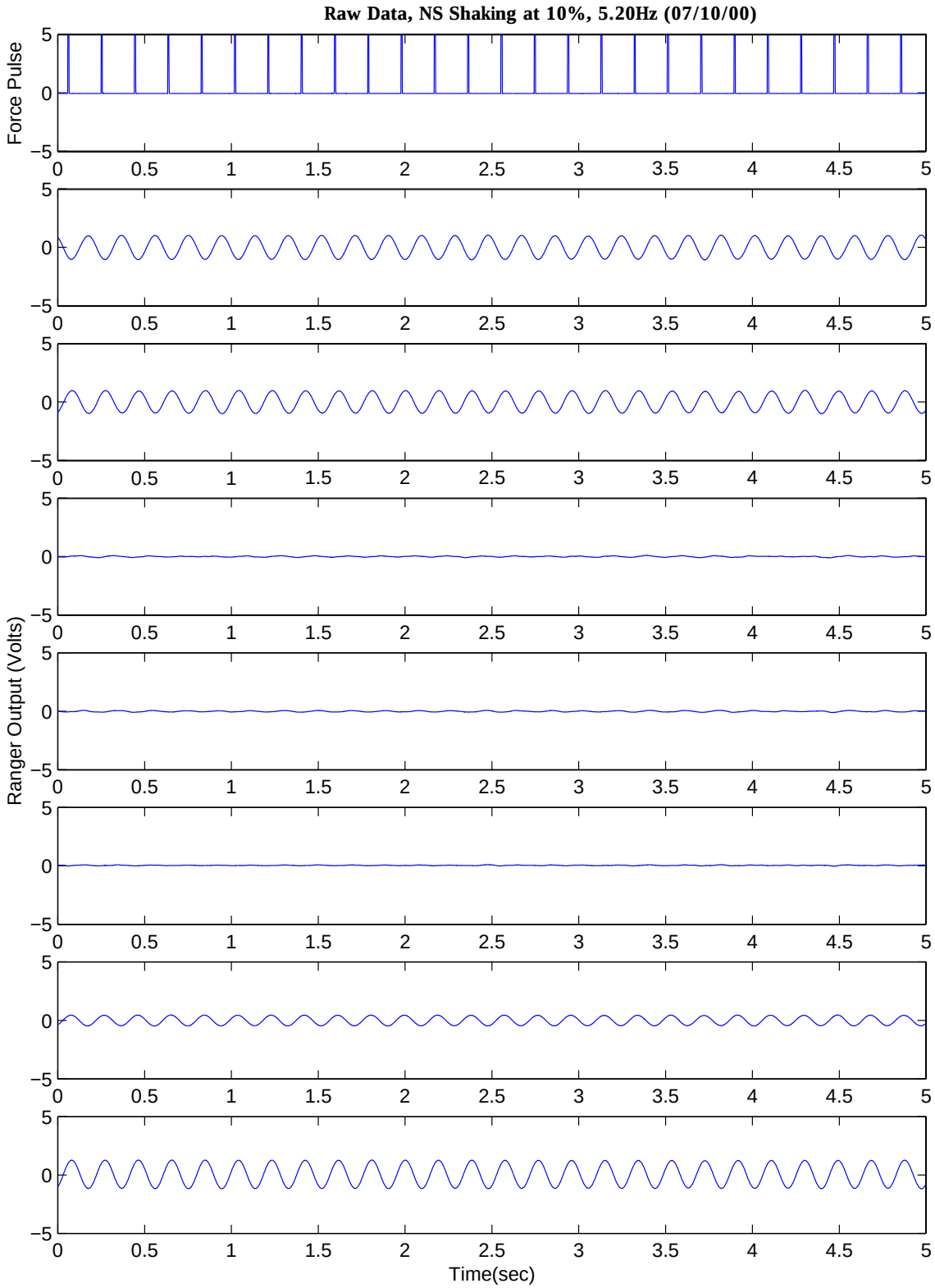

Figure C.11: 3-Story Building FVT Raw Data (NS at 10%, 5.20Hz)

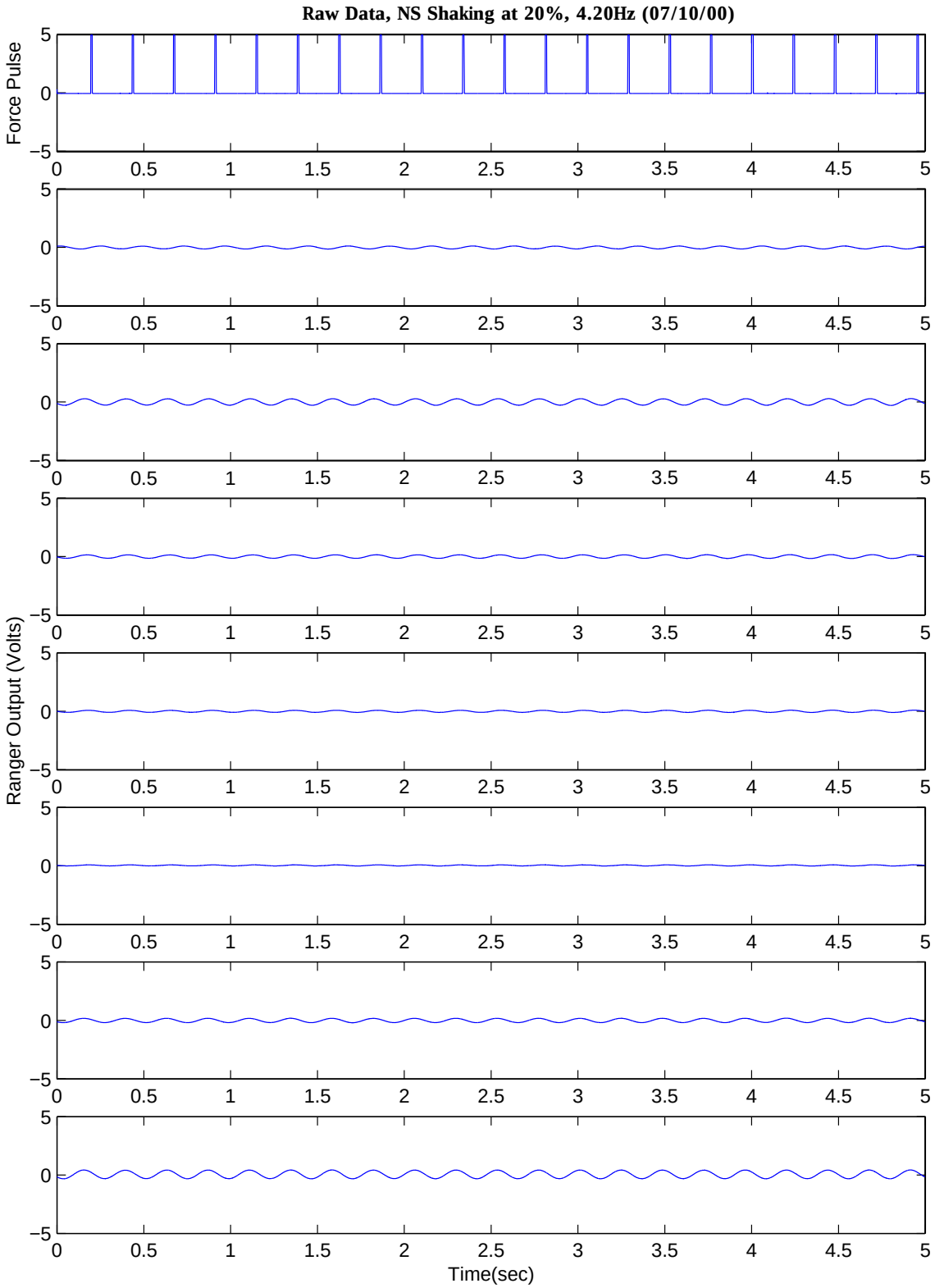

Figure C.12: 3-Story Building FVT Raw Data (NS at 20%, 4.20Hz)

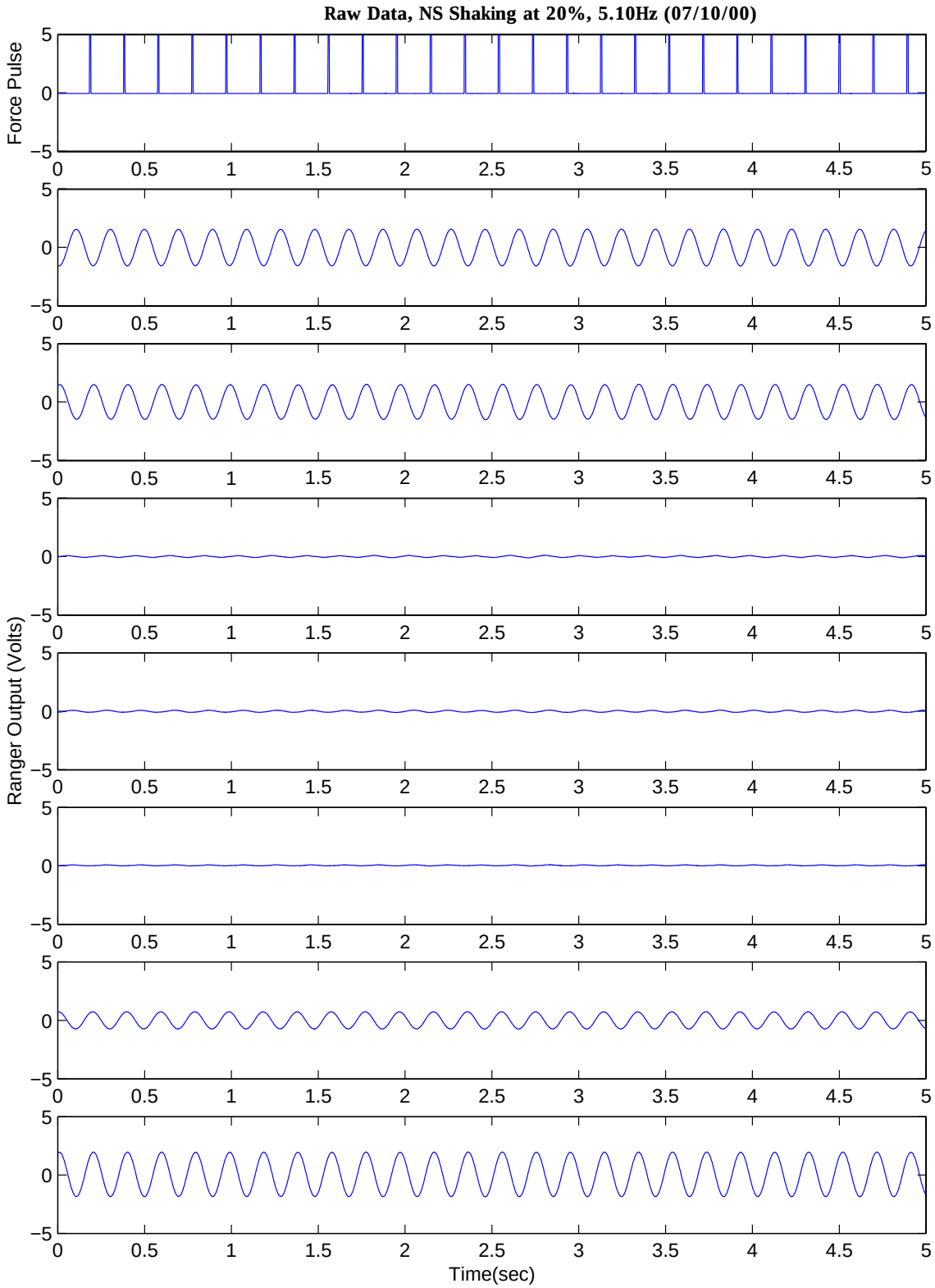

Figure C.13: 3-Story Building FVT Raw Data (NS at 20%, 5.10Hz)

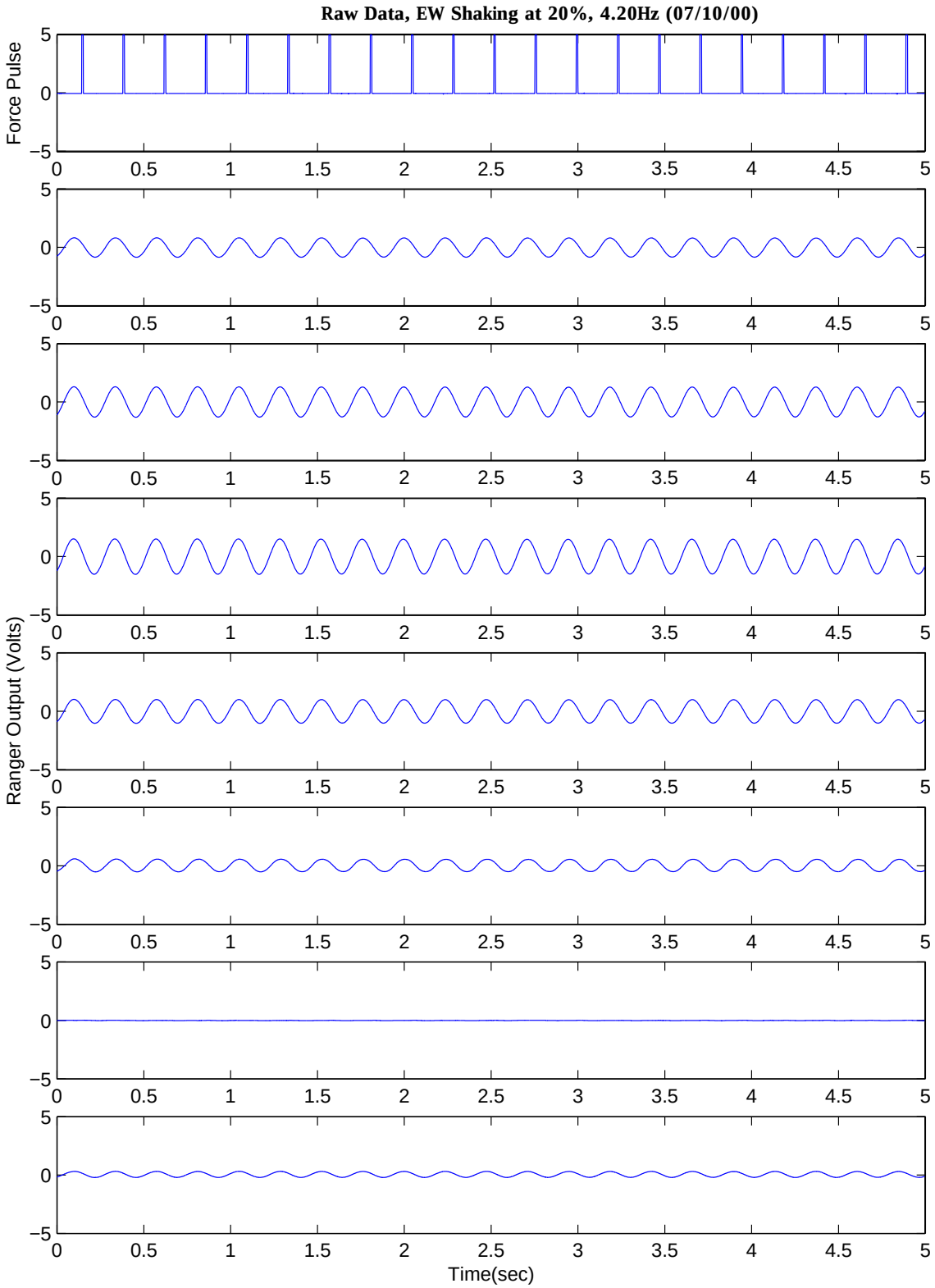

Figure C.14: 3-Story Building FVT Raw Data (EW at 20%, 4.20Hz)

C.3 2-Story Office on S. Chester Ave., Pasadena

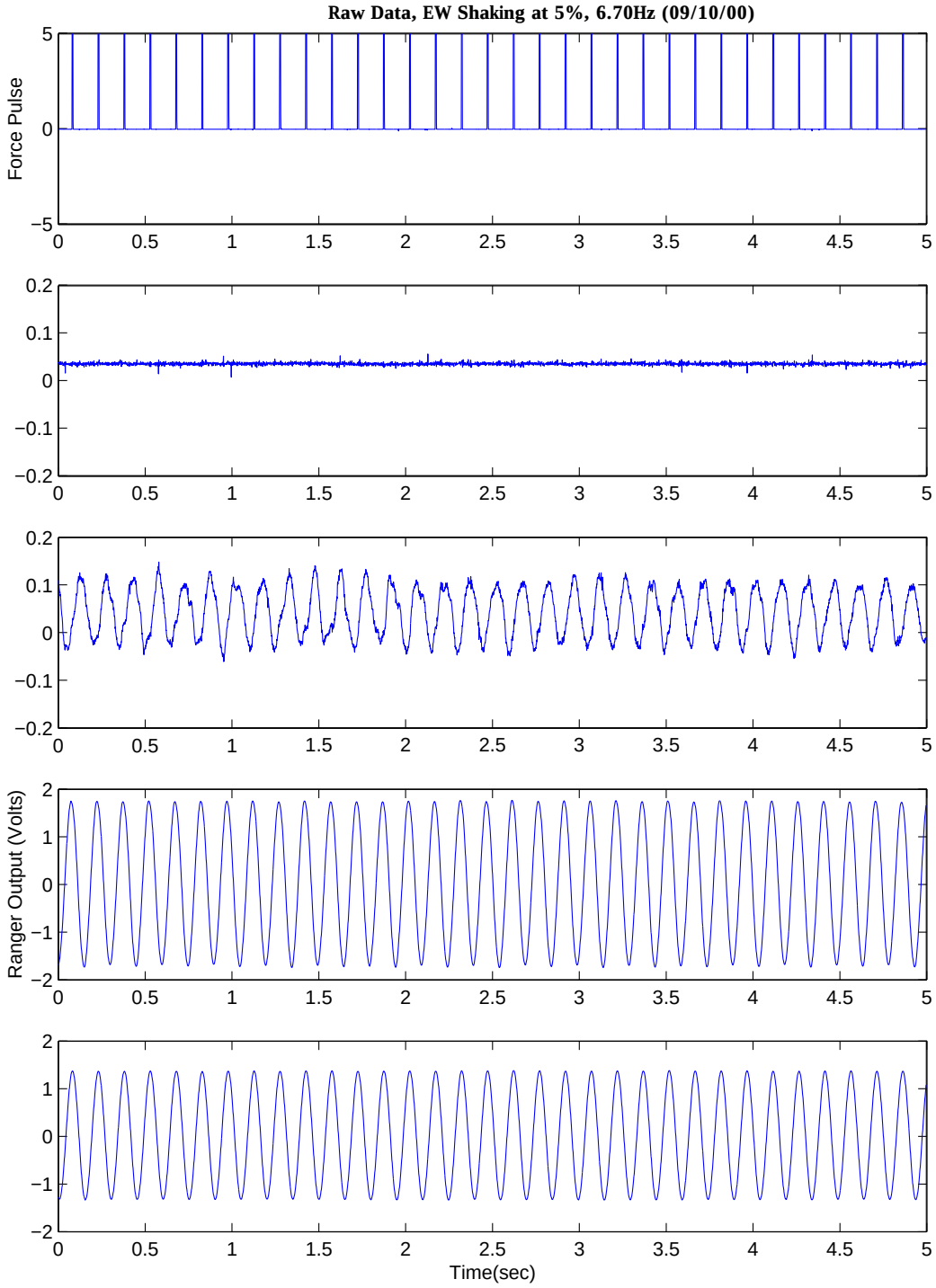

Figure C.15: 2-Story Office FVT Raw Data (EW at 5%, 6.70Hz)

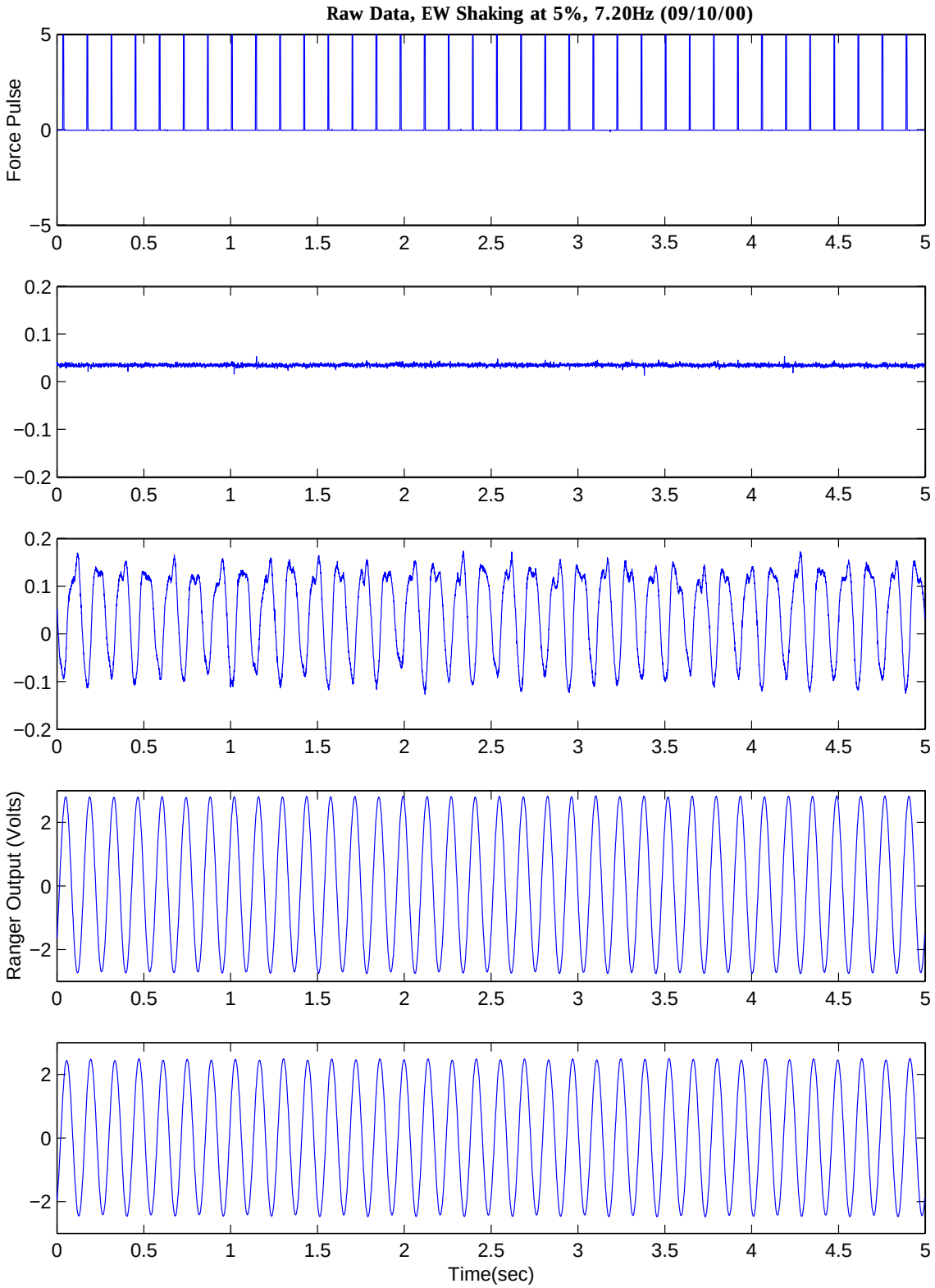

Figure C.16: 2-Story Office FVT Raw Data (EW at 5%, 7.20Hz)

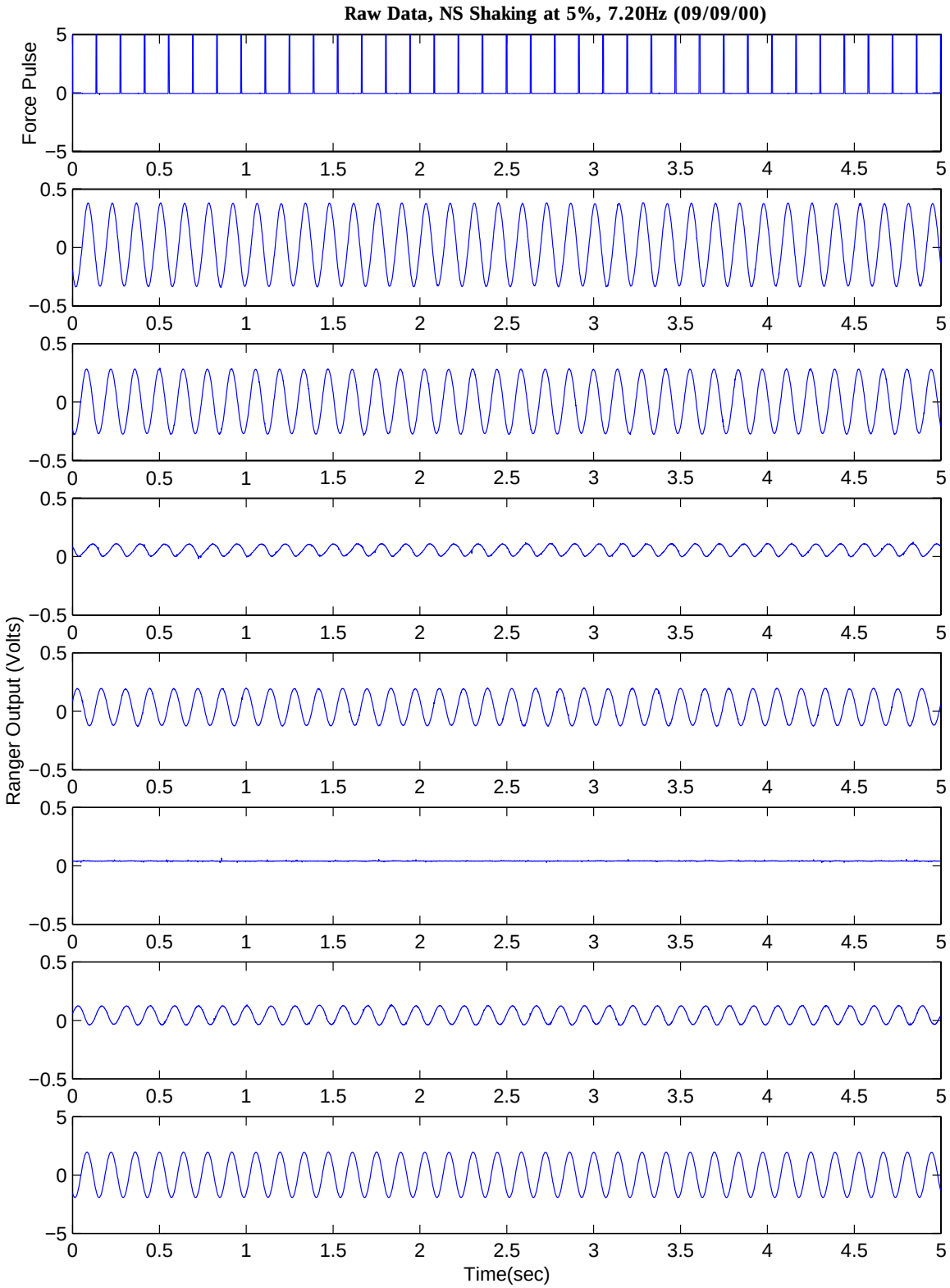

Figure C.17: 2-Story Office FVT Raw Data (NS at 5%, 7.20Hz)

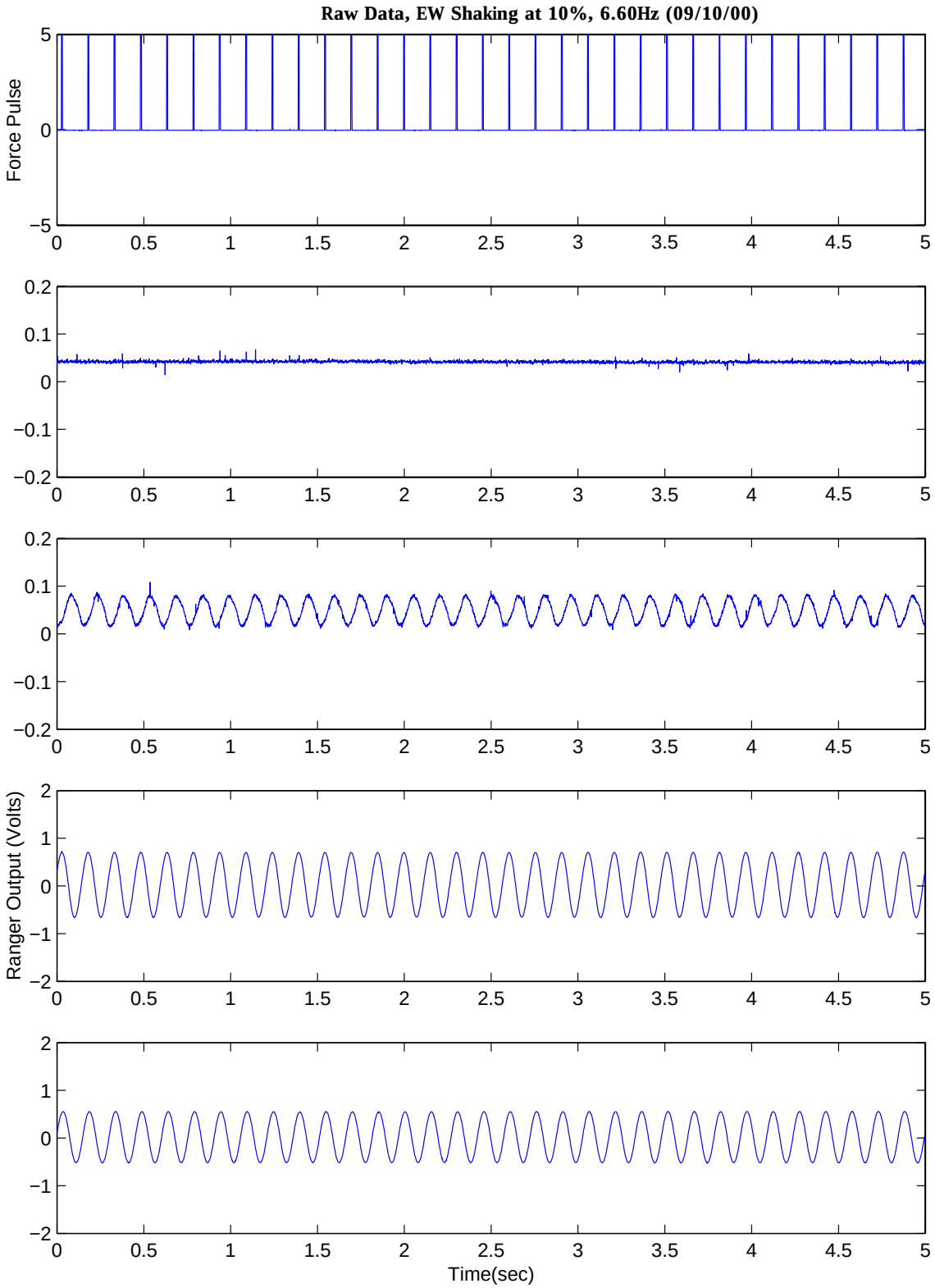

Figure C.18: 2-Story Office FVT Raw Data (EW at 10%, 6.60Hz)

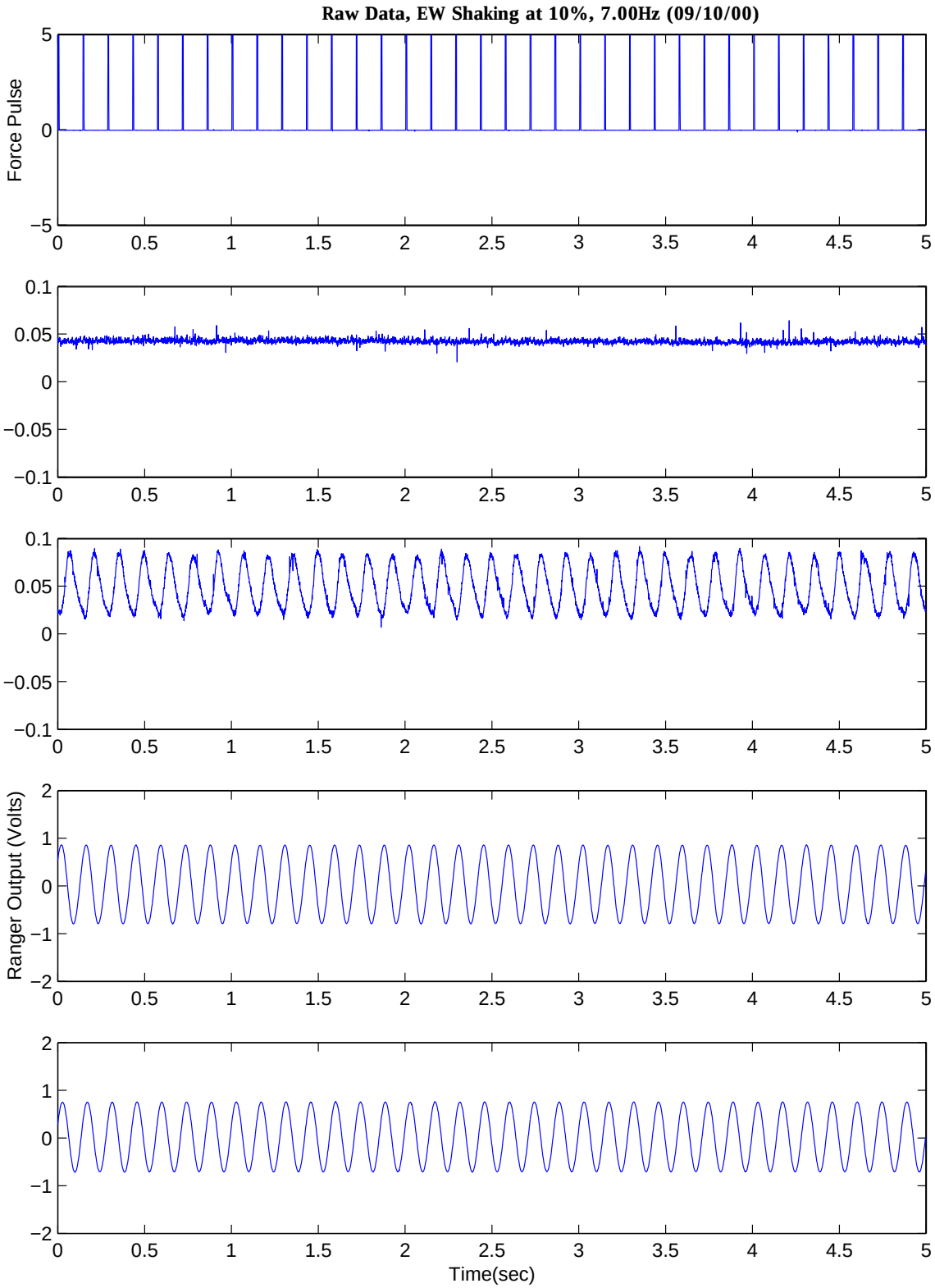

Figure C.19: 2-Story Office FVT Raw Data (EW at 10%, 7.00Hz)

C.4 2-Story Garage on S. Hill Ave., Pasadena

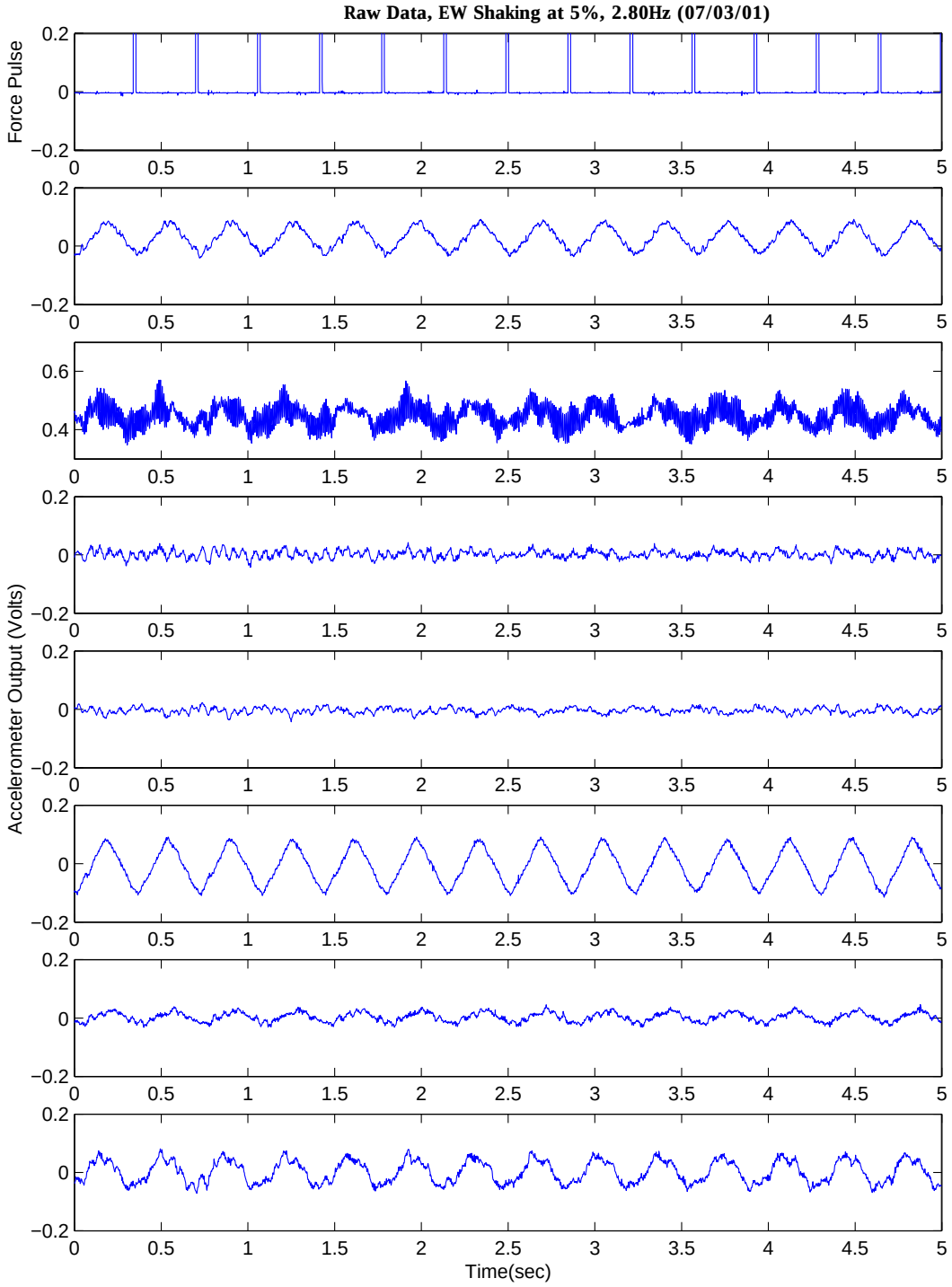

Figure C.20: 2-Story Garage FVT Raw Data (EW at 5%, 2.80Hz)

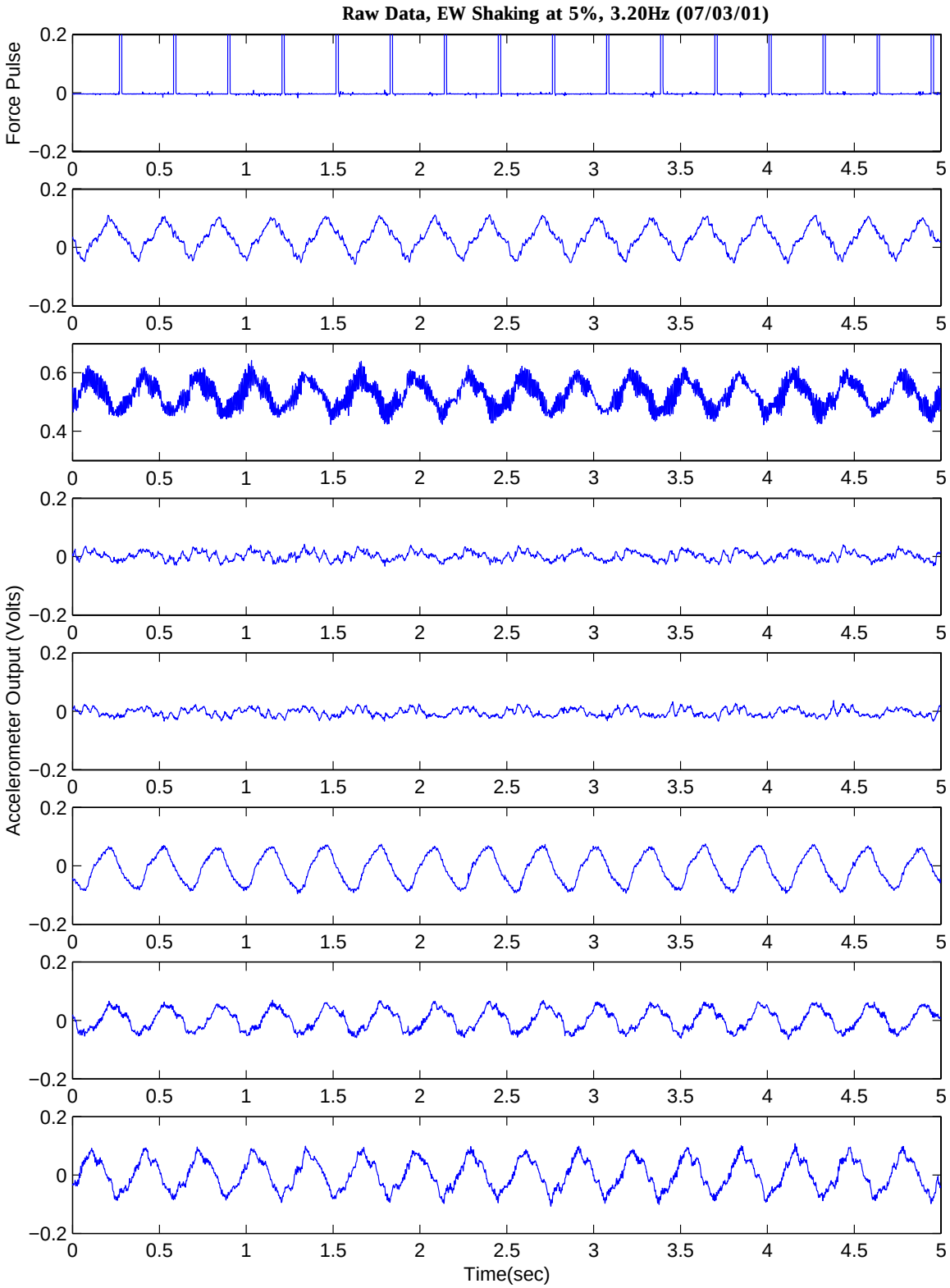

Figure C.21: 2-Story Garage FVT Raw Data (EW at 5%, 3.20Hz)

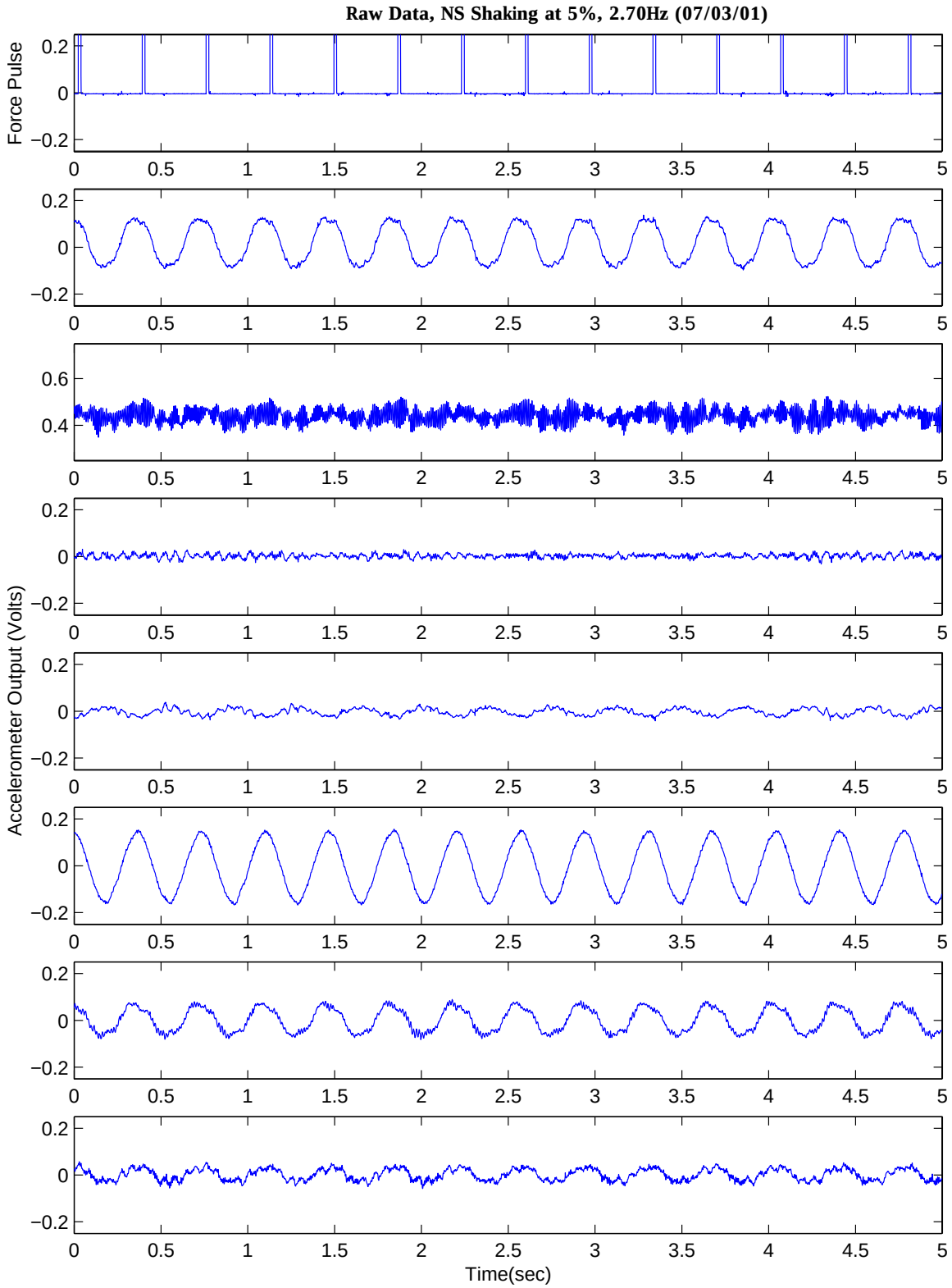

Figure C.22: 2-Story Garage FVT Raw Data (NS at 5%, 2.70Hz)

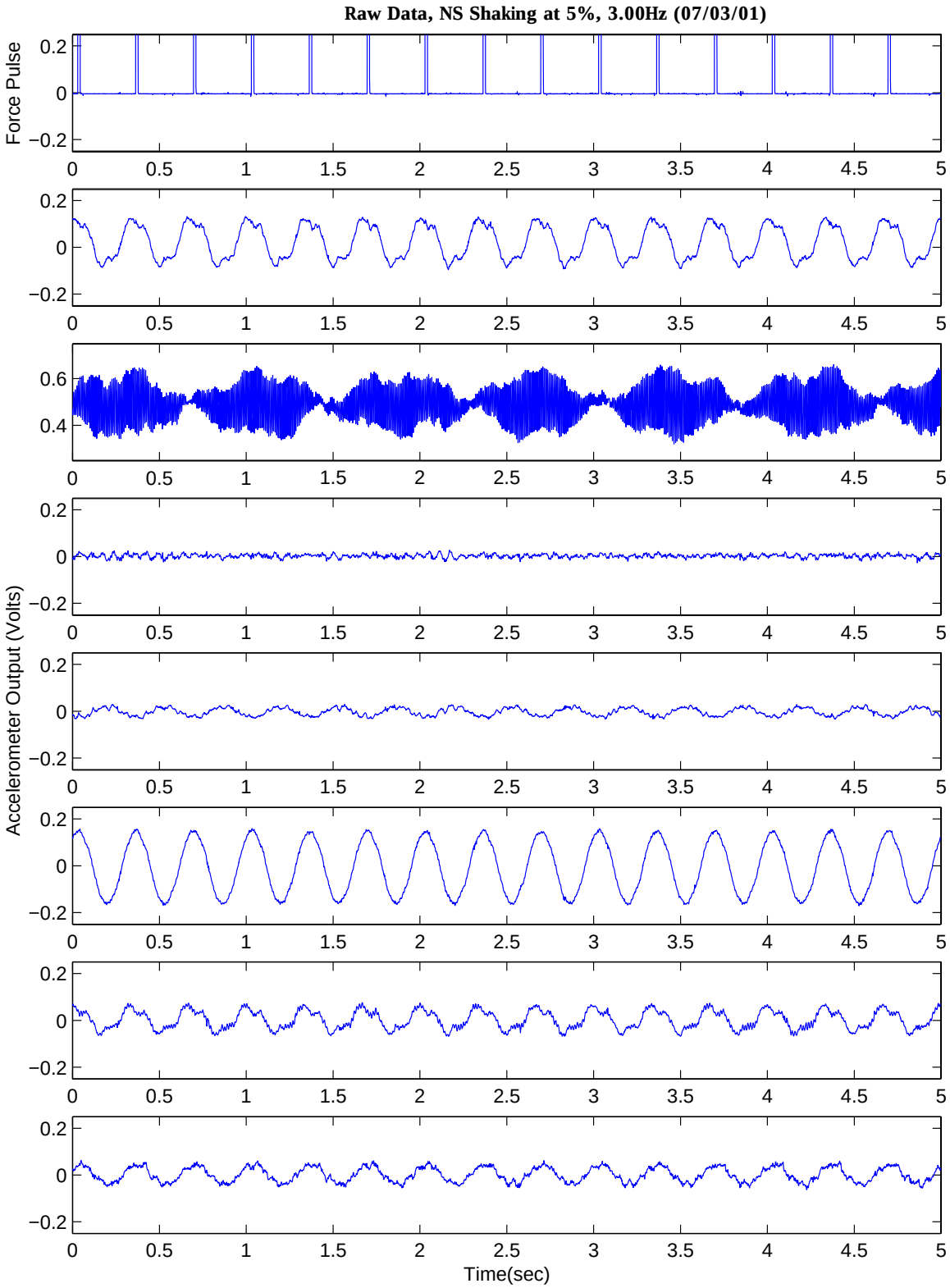

Figure C.23: 2-Story Garage FVT Raw Data (NS at 5%, 3.00Hz)

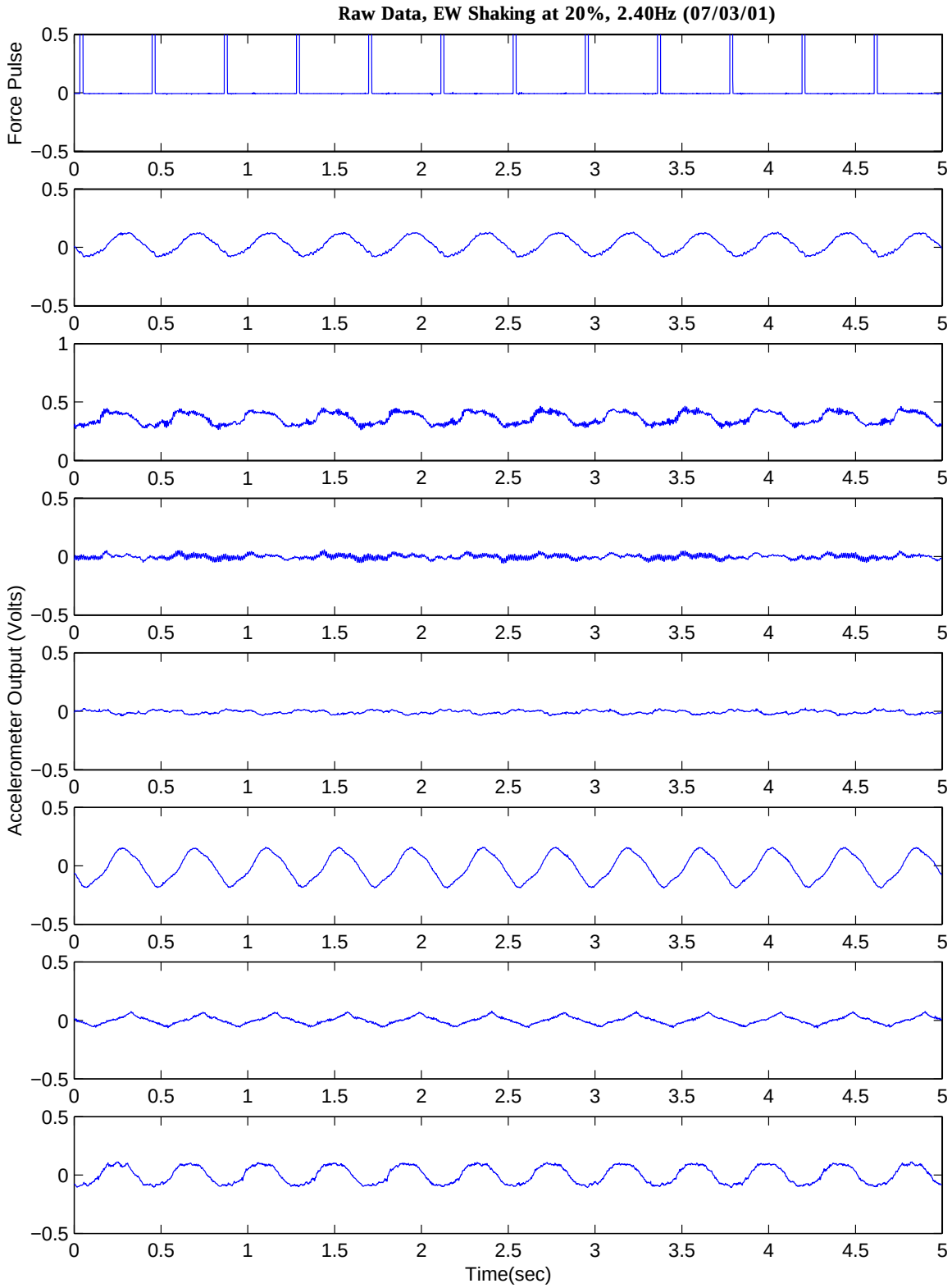

Figure C.24: 2-Story Garage FVT Raw Data (EW at 20%, 2.40Hz)

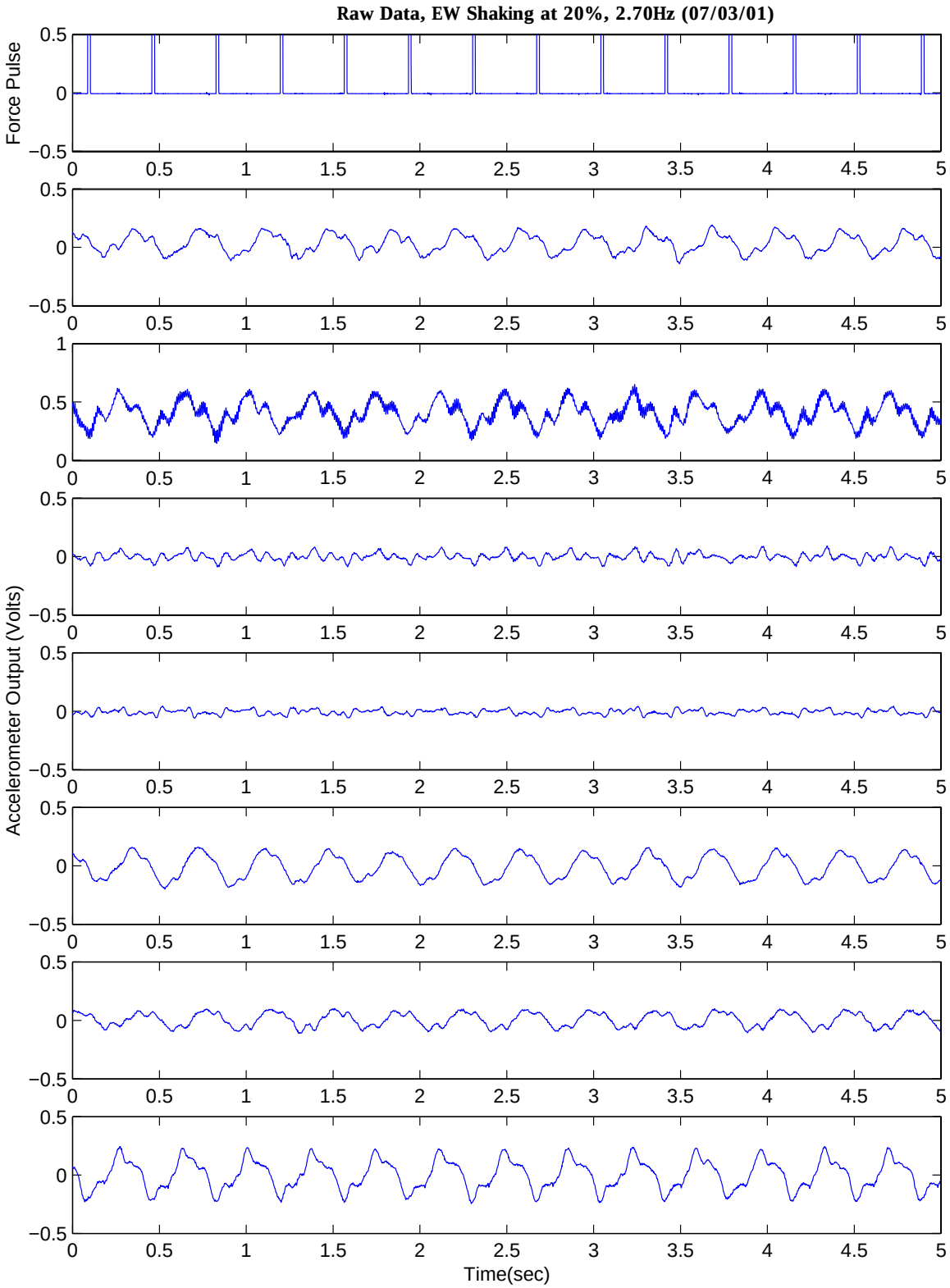

Figure C.25: 2-Story Garage FVT Raw Data (EW at 20%, 2.70Hz)

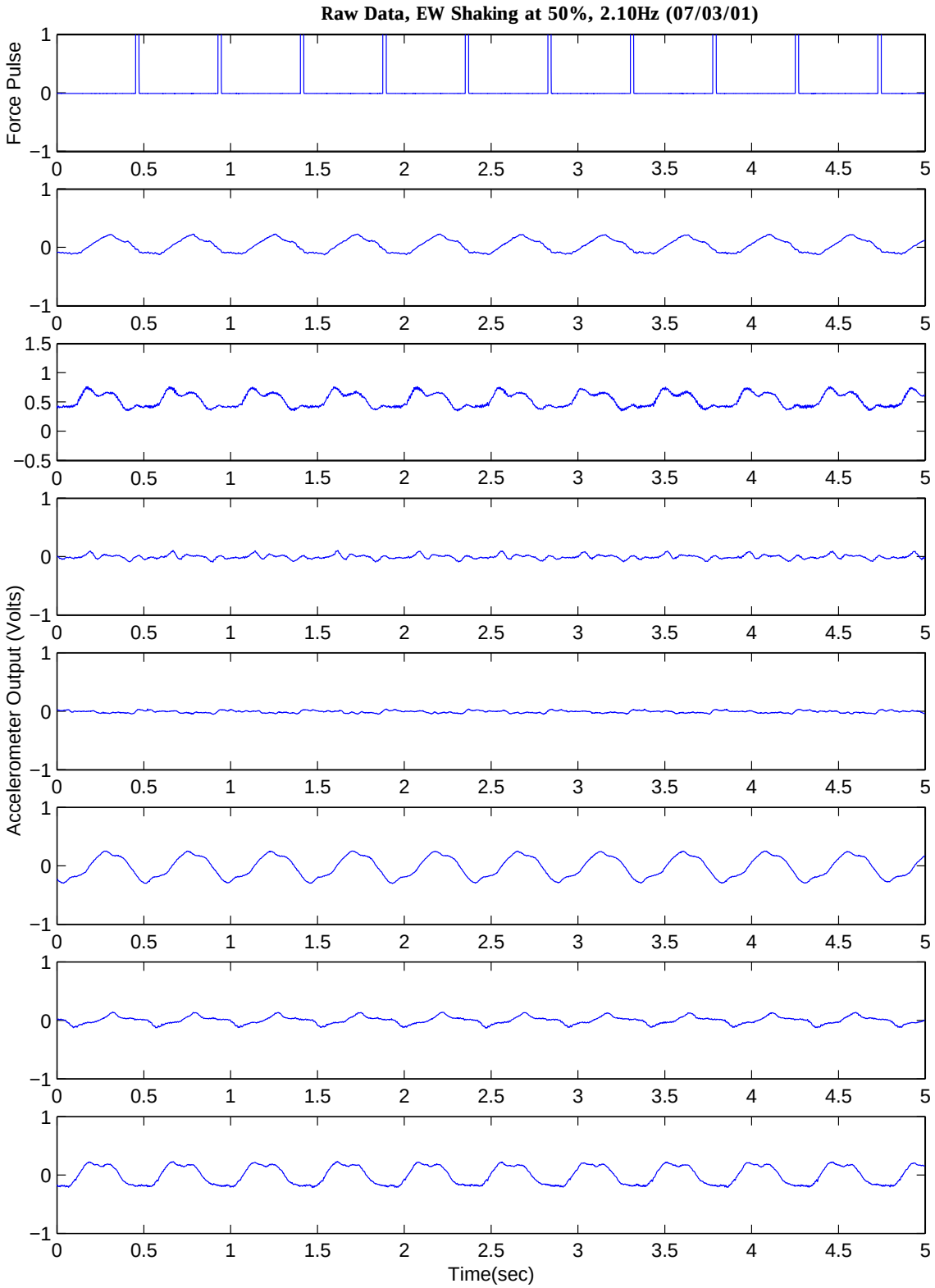

Figure C.26: 2-Story Garage FVT Raw Data (EW at 50%, 2.10Hz)

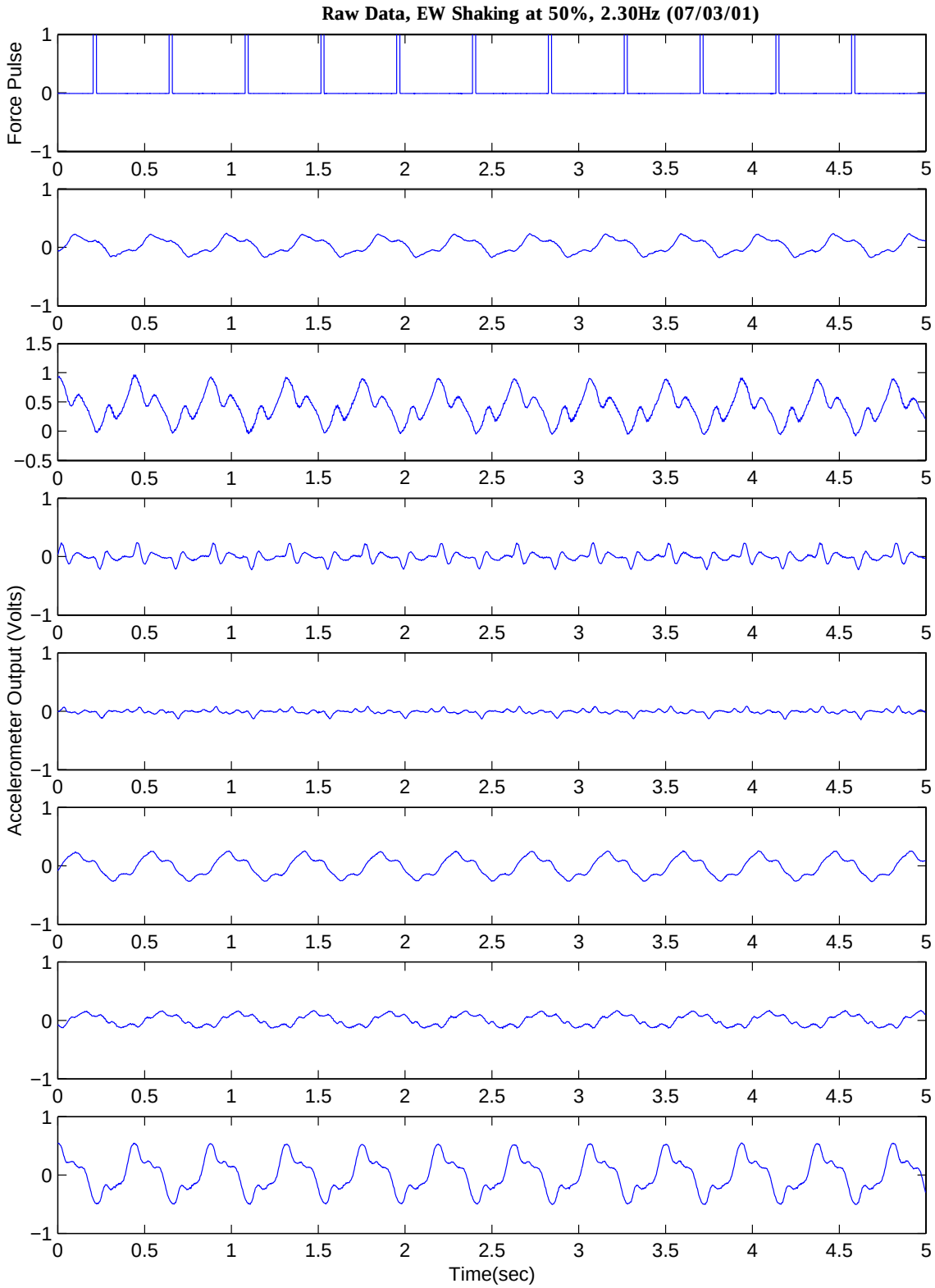

Figure C.27: 2-Story Garage FVT Raw Data (EW at 50%, 2.30Hz)

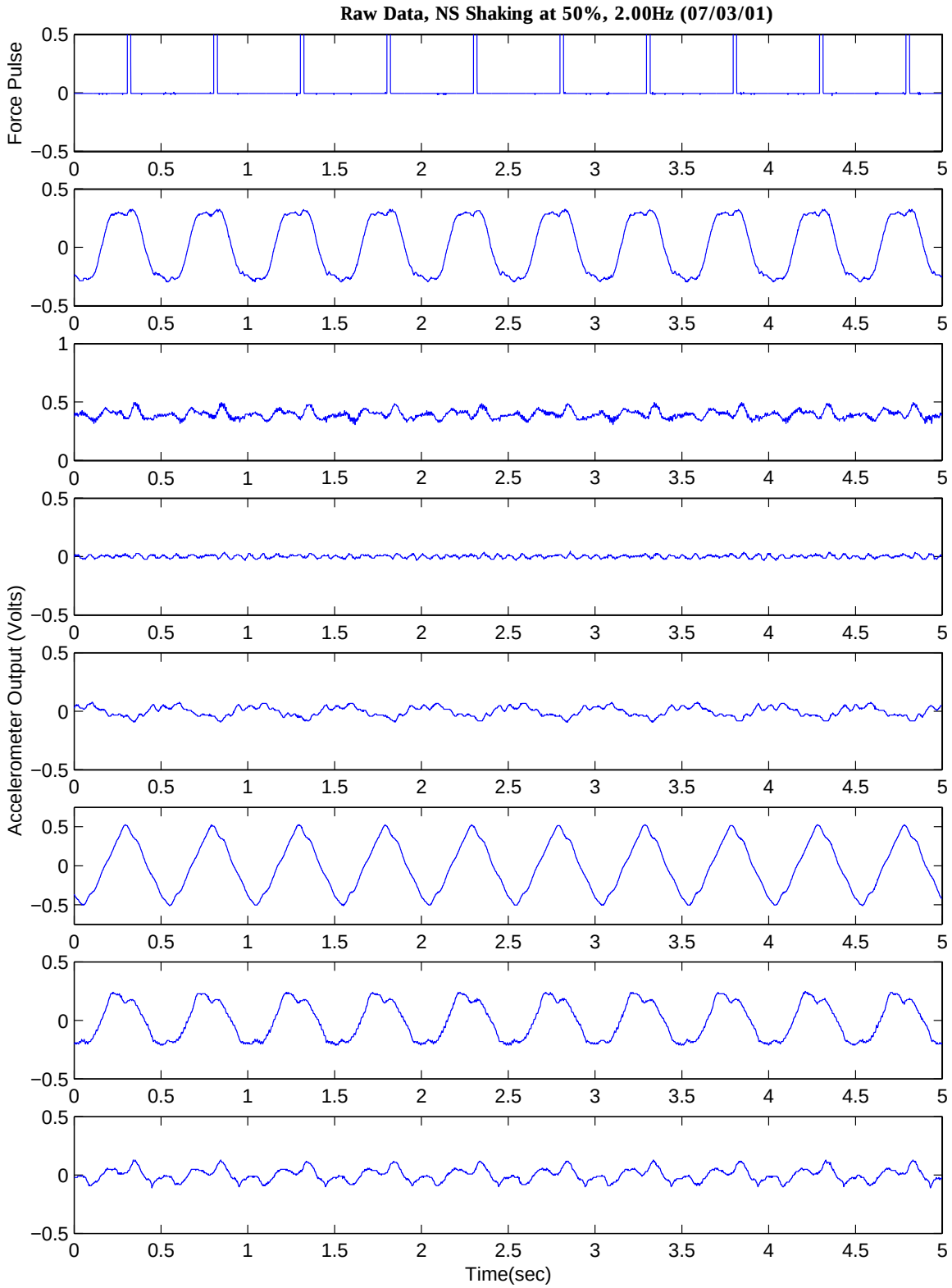

Figure C.28: 2-Story Garage FVT Raw Data (NS at 50%, 2.00Hz)

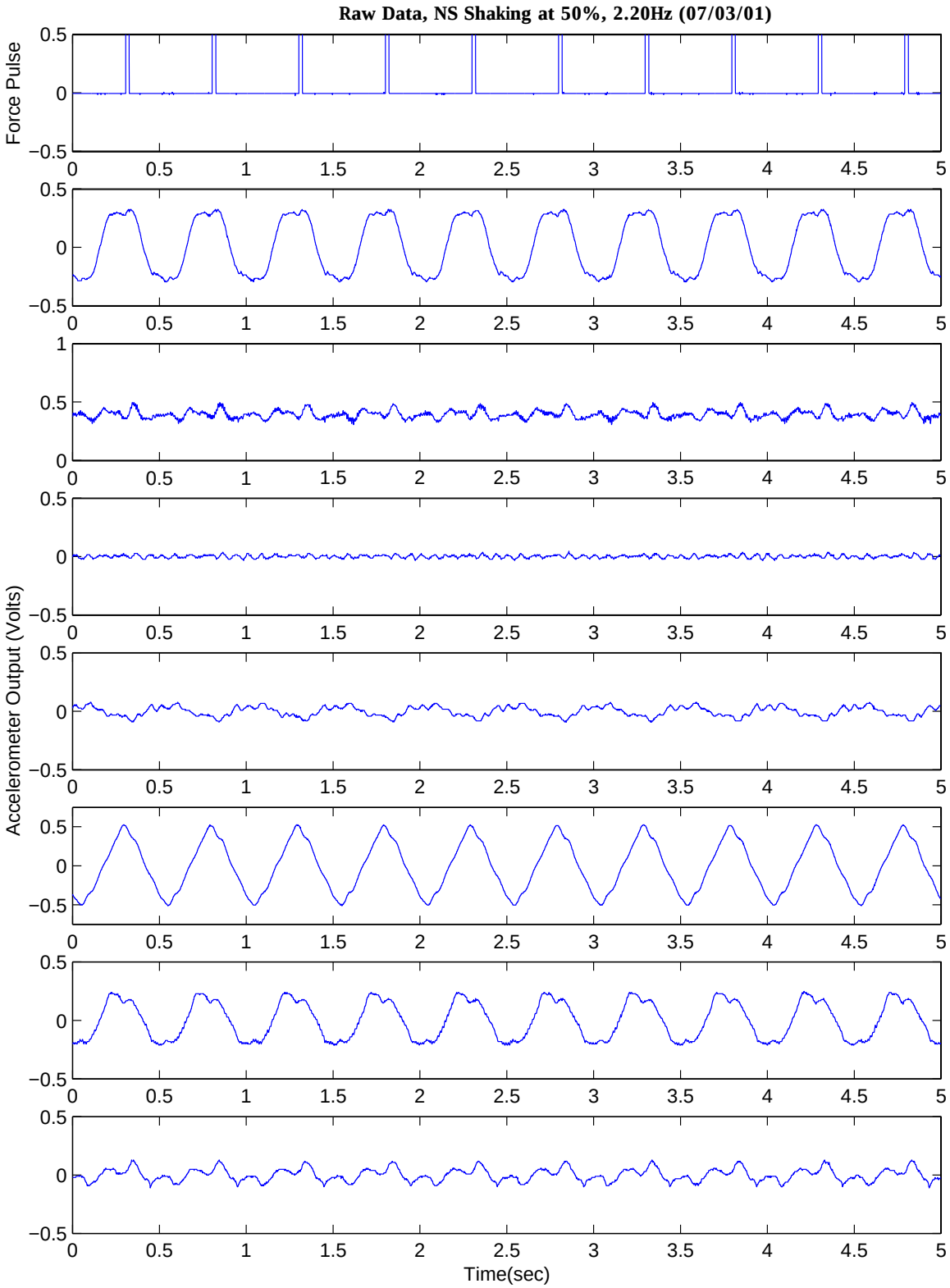

Figure C.29: 2-Story Garage FVT Raw Data (NS at 50%, 2.20Hz)

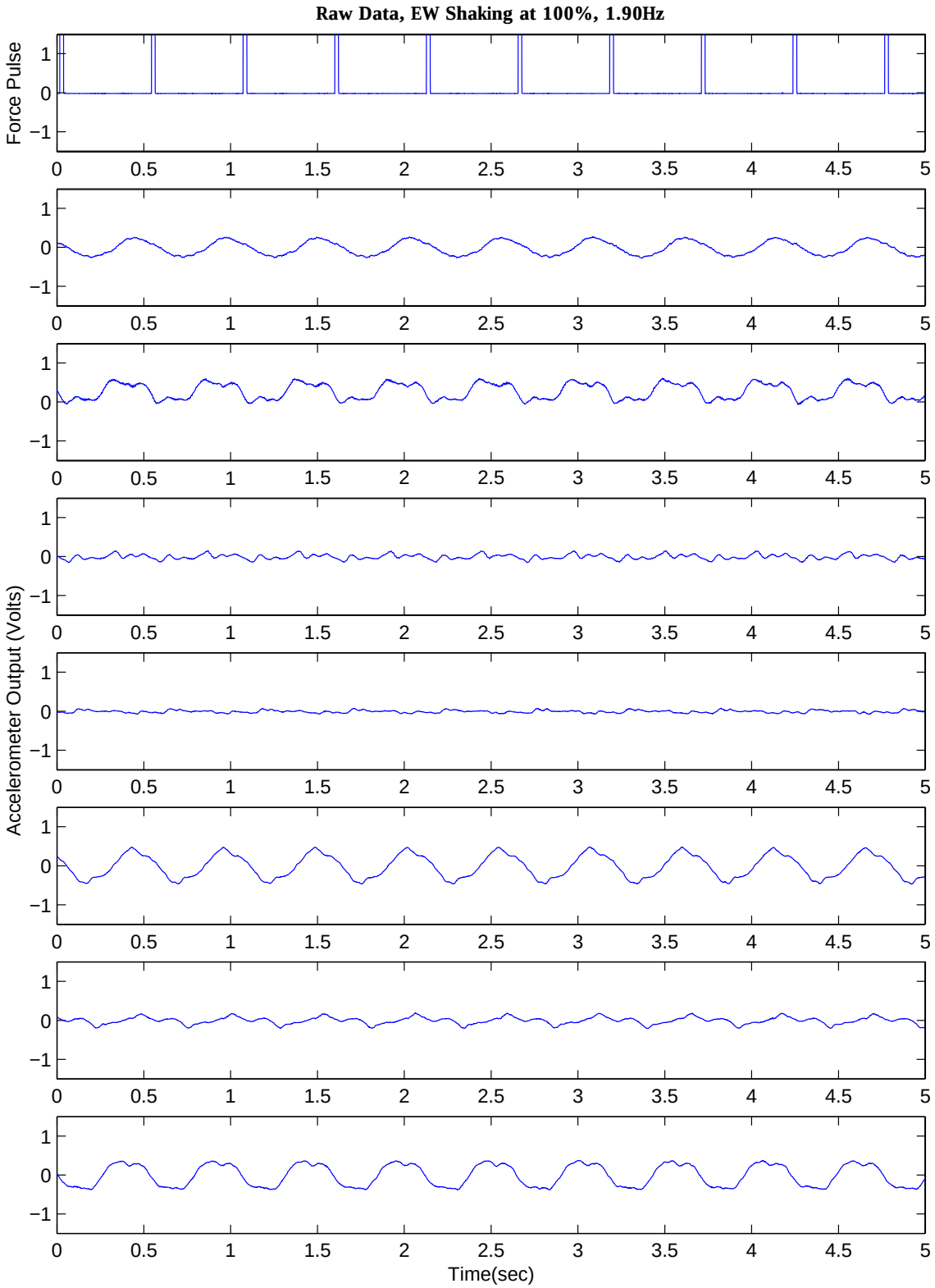

Figure C.30: 2-Story Garage FVT Raw Data (EW at 100%, 1.90Hz)

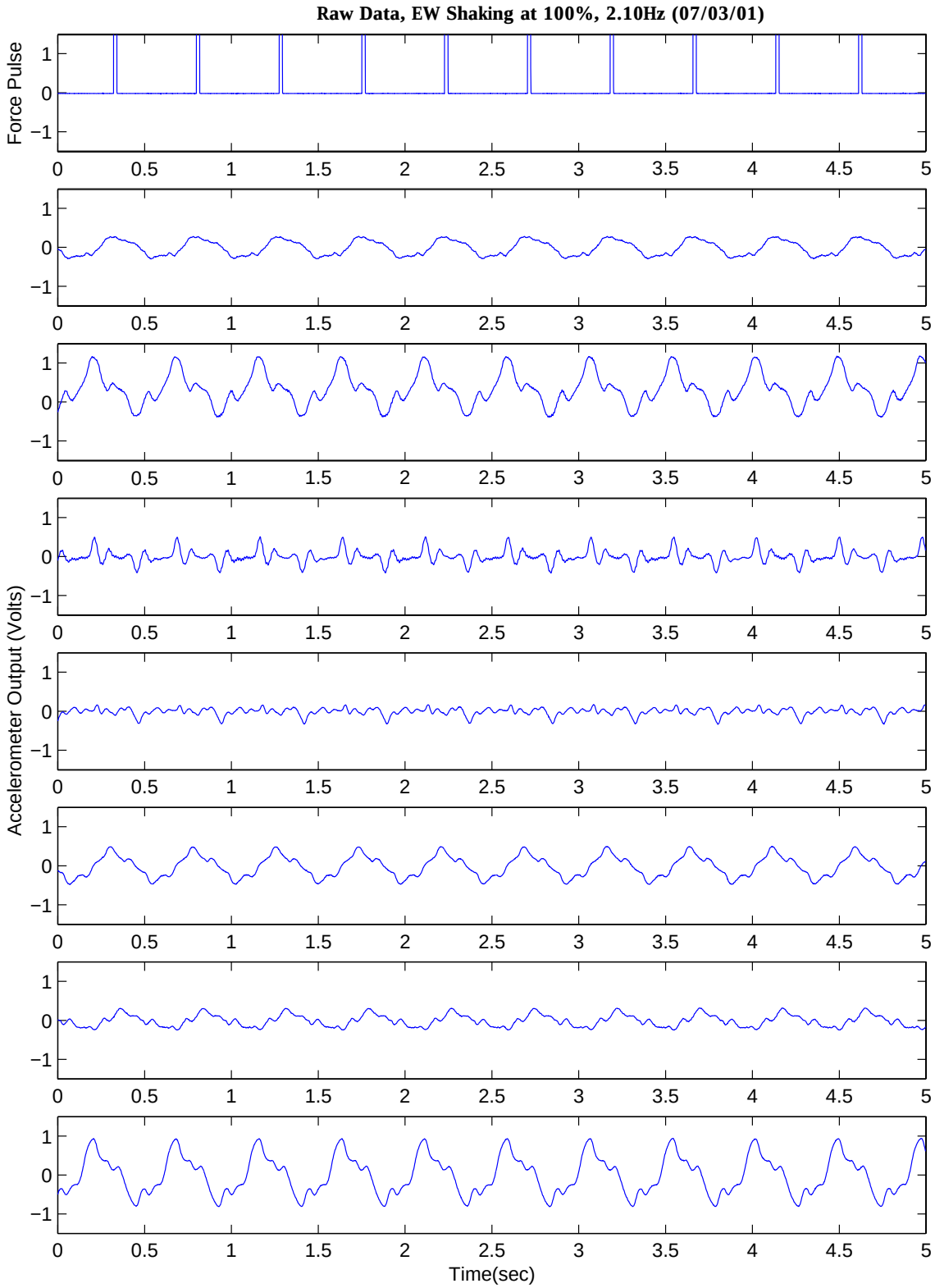

Figure C.31: 2-Story Garage FVT Raw Data (EW at 100%, 2.10Hz)

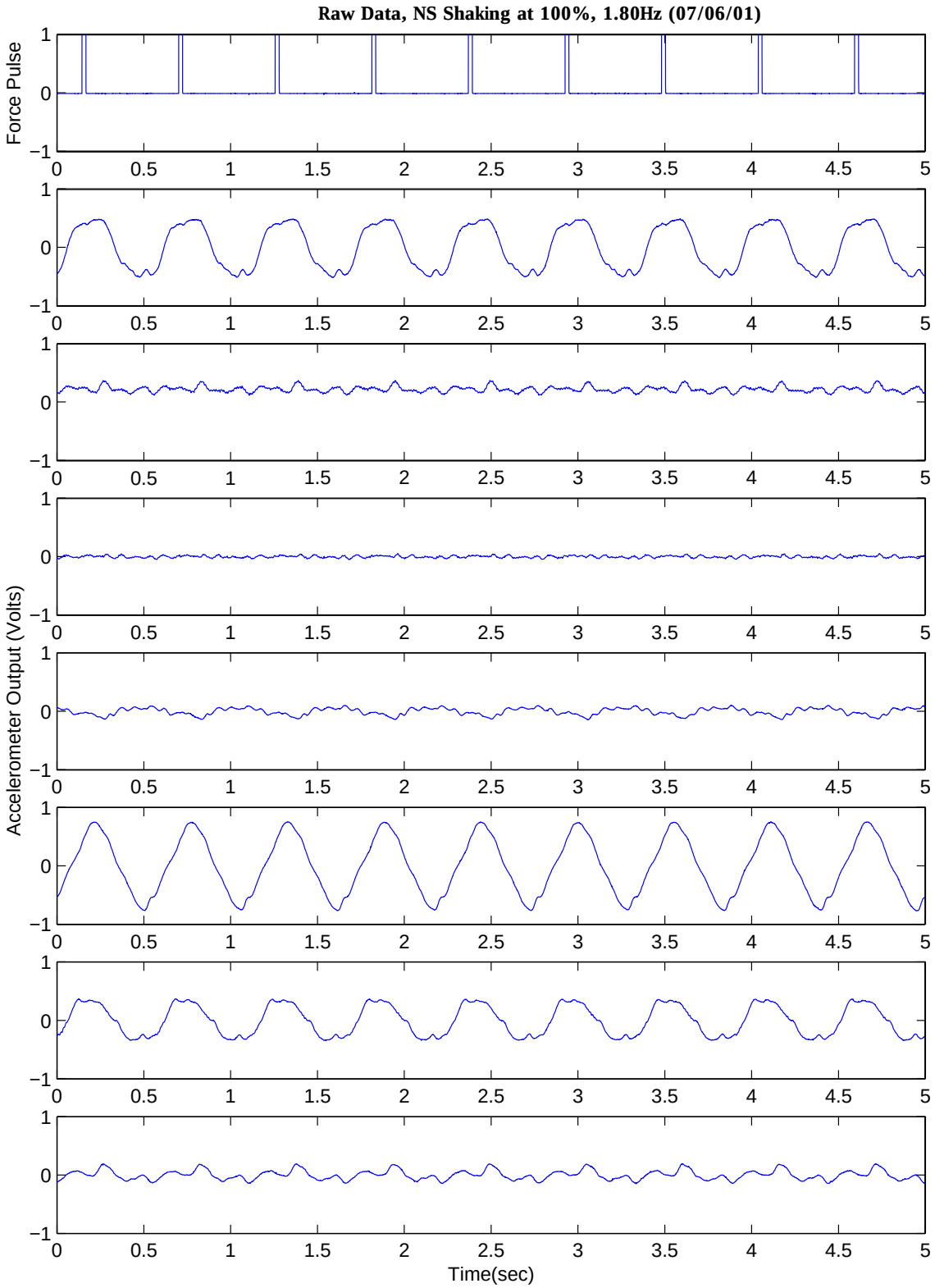

Figure C.32: 2-Story Garage FVT Raw Data (NS at 100%, 1.80Hz)

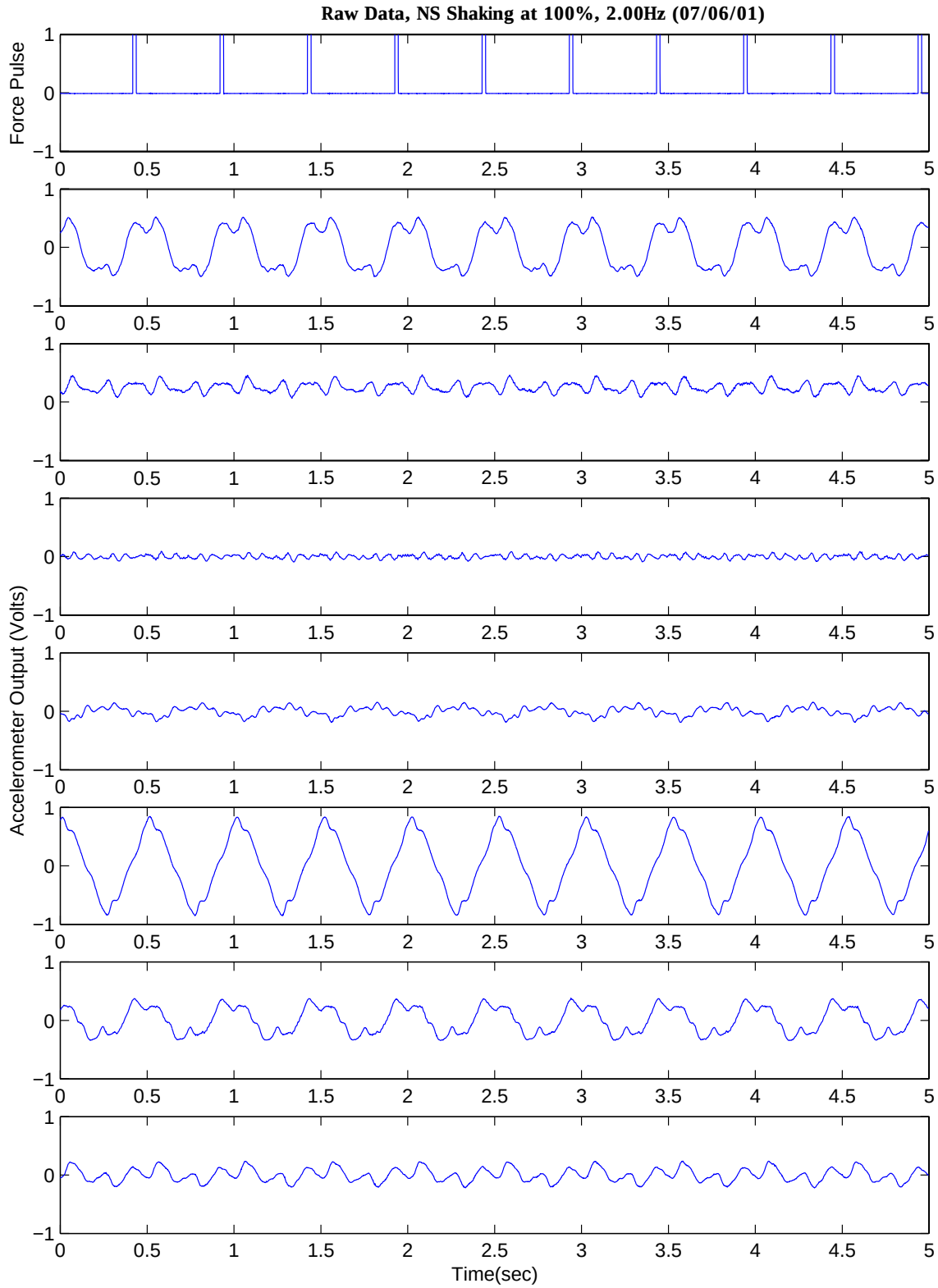

Figure C.33: 2-Story Garage FVT Raw Data (NS at 100%, 2.00Hz)

C.5 2-Story House on S. Hill Ave., Pasadena

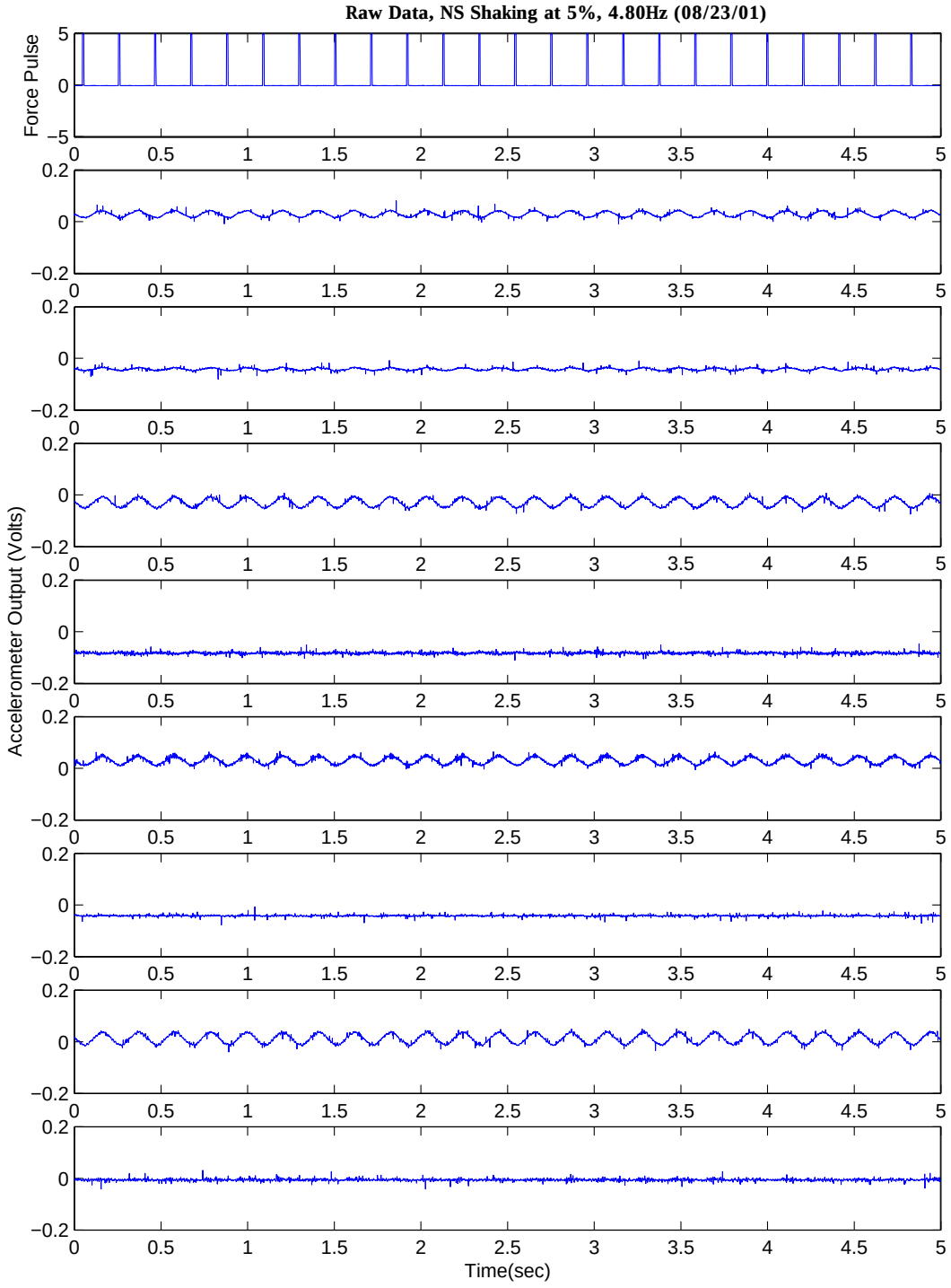

Figure C.34: 2-Story House FVT Accel. Data (NS at 5%, 4.80Hz)

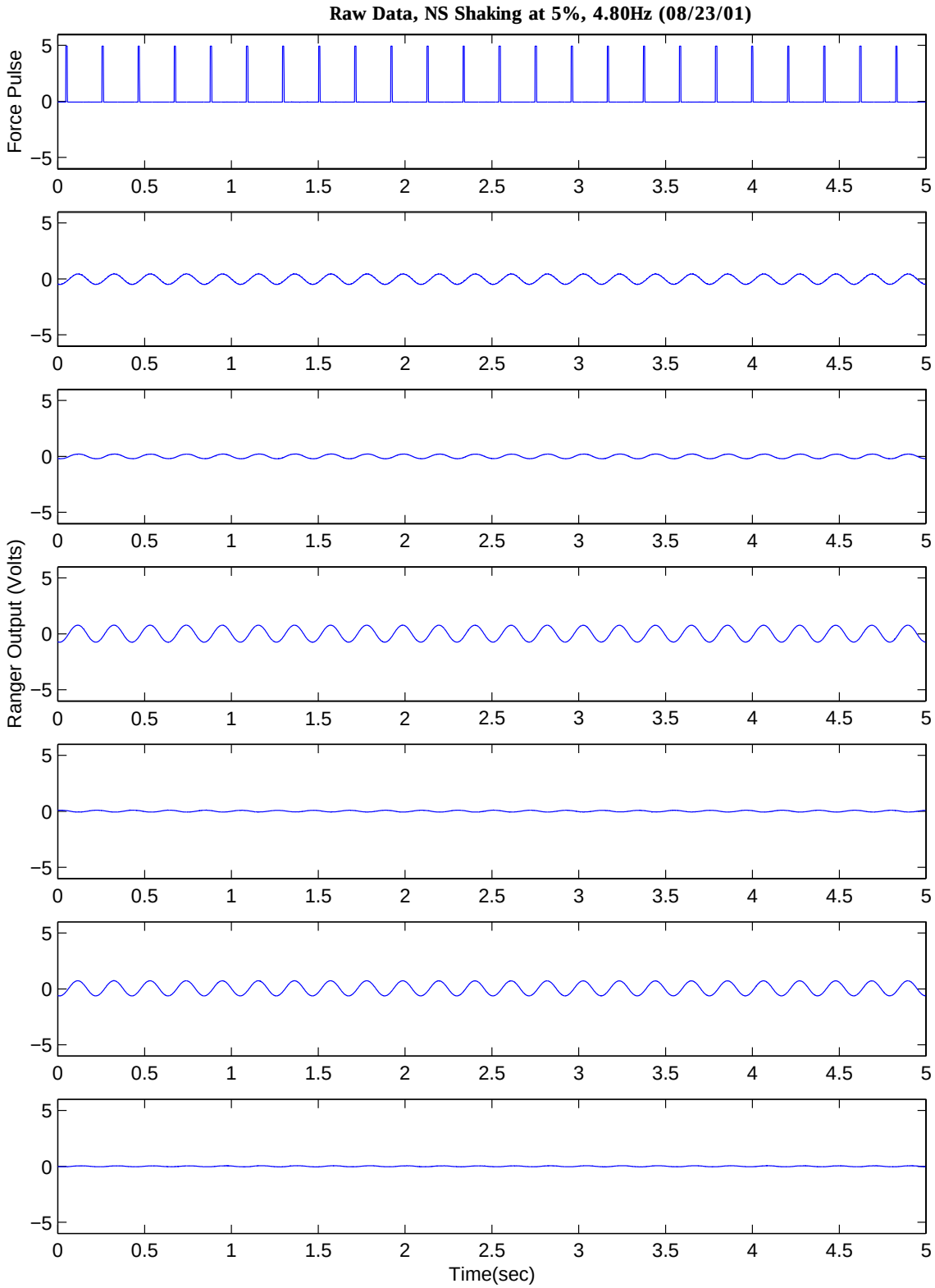

Figure C.35: 2-Story House FVT Seism. Data (NS at 5%, 4.80Hz)

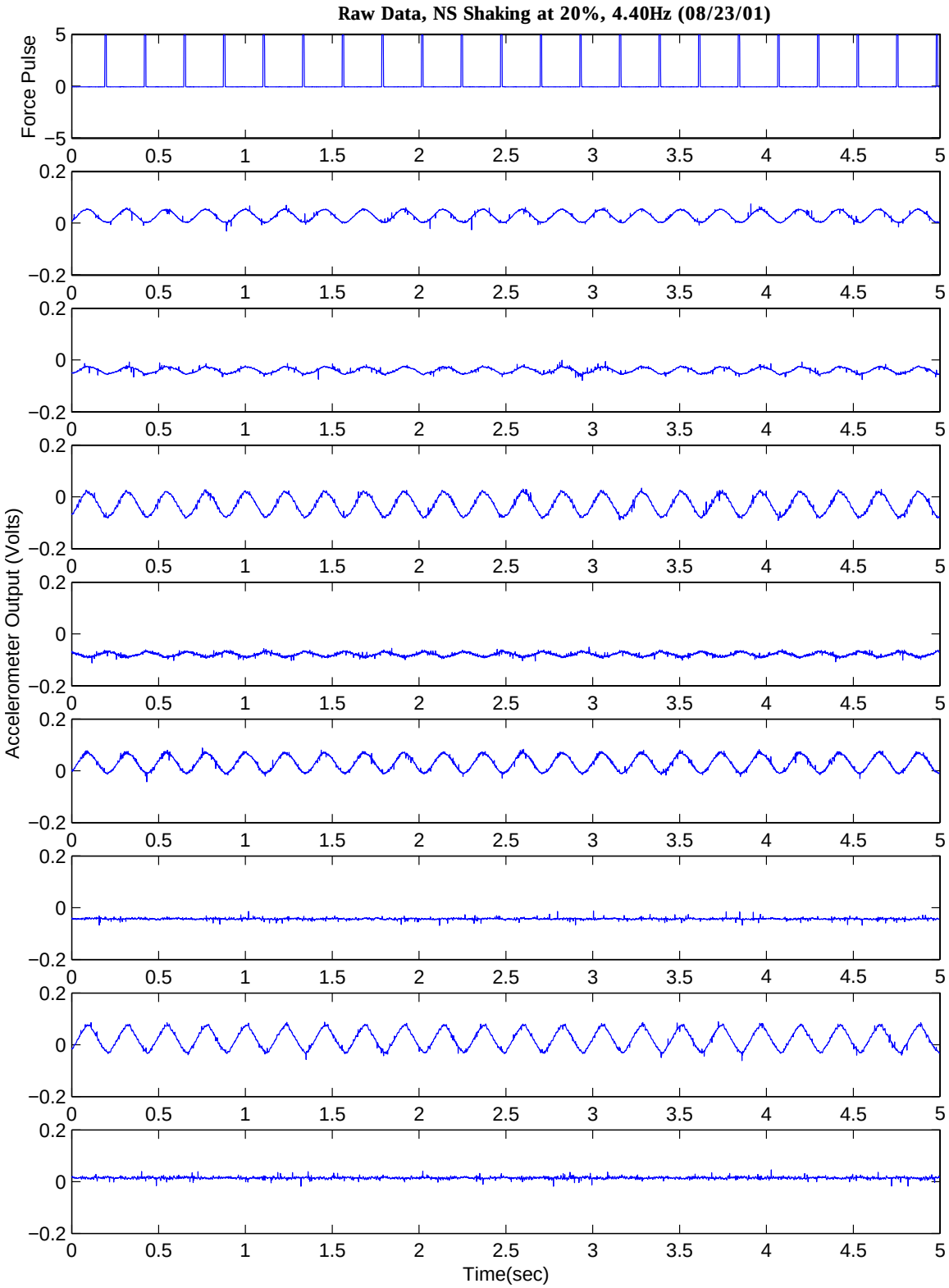

Figure C.36: 2-Story House FVT Accel. Data (NS at 20%, 4.40Hz)

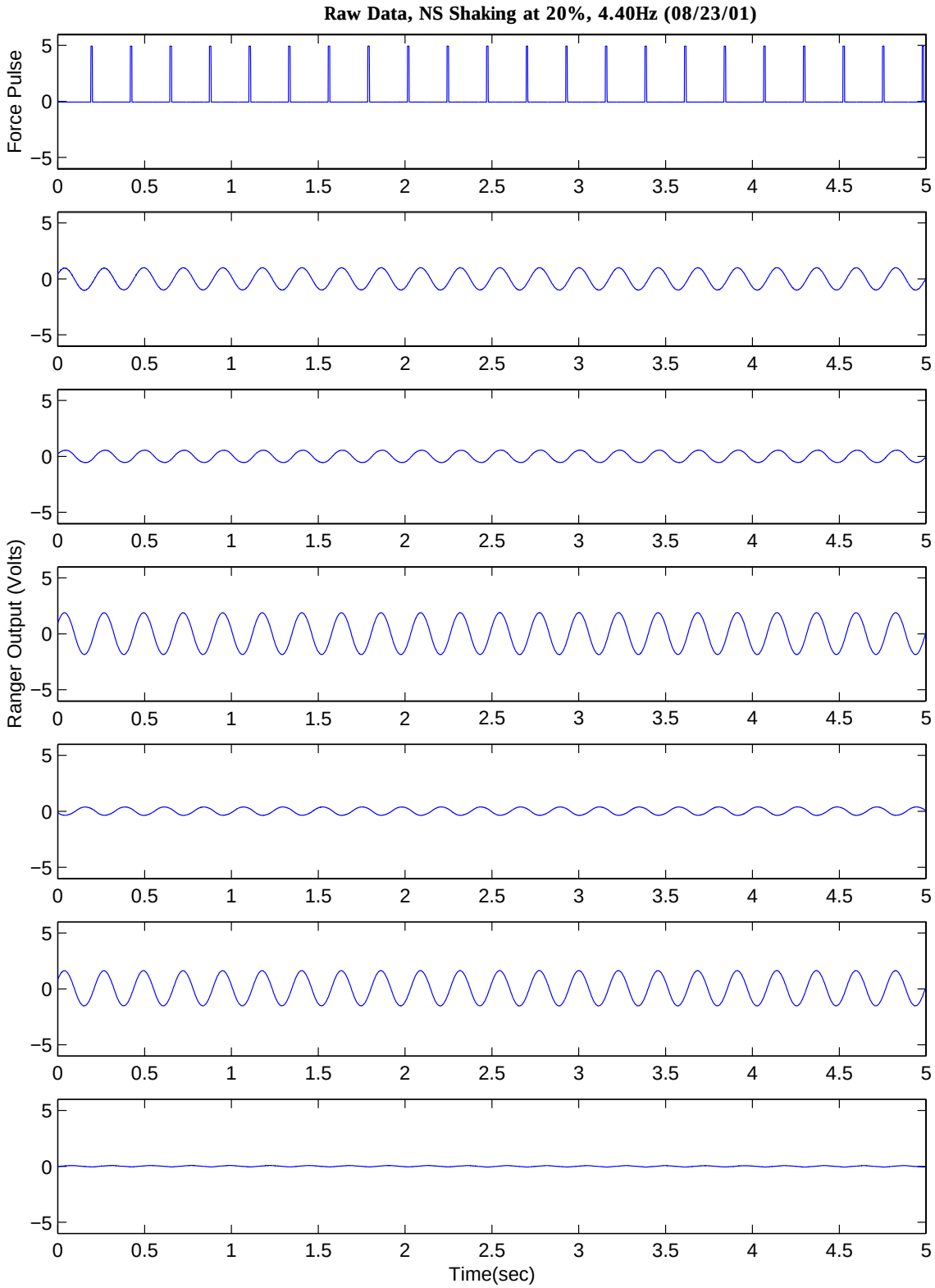

Figure C.37: 2-Story House FVT Seism. Data (NS at 20%, 4.40Hz)

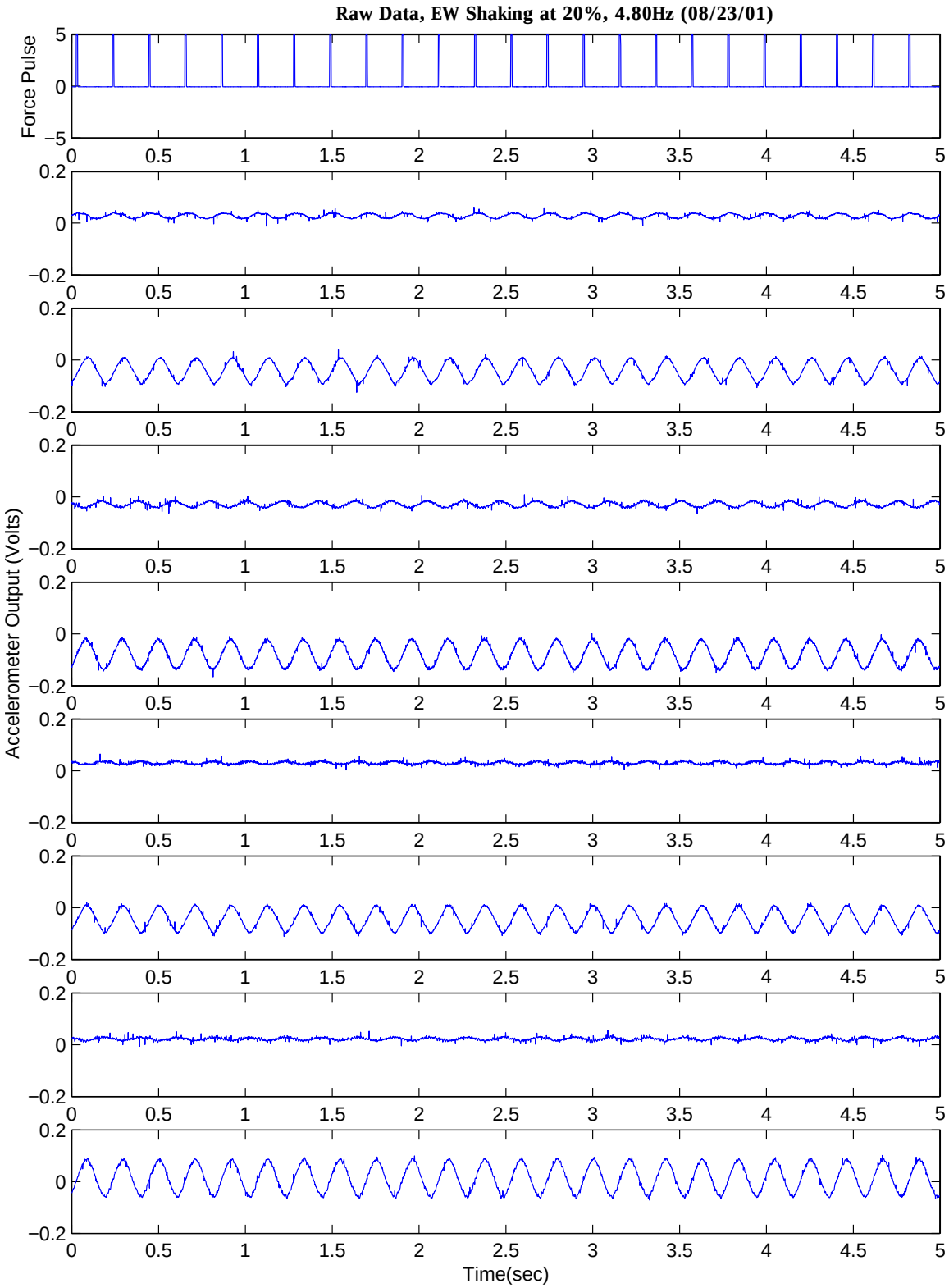

Figure C.38: 2-Story House FVT Accel. Data (EW at 20%, 4.80Hz)

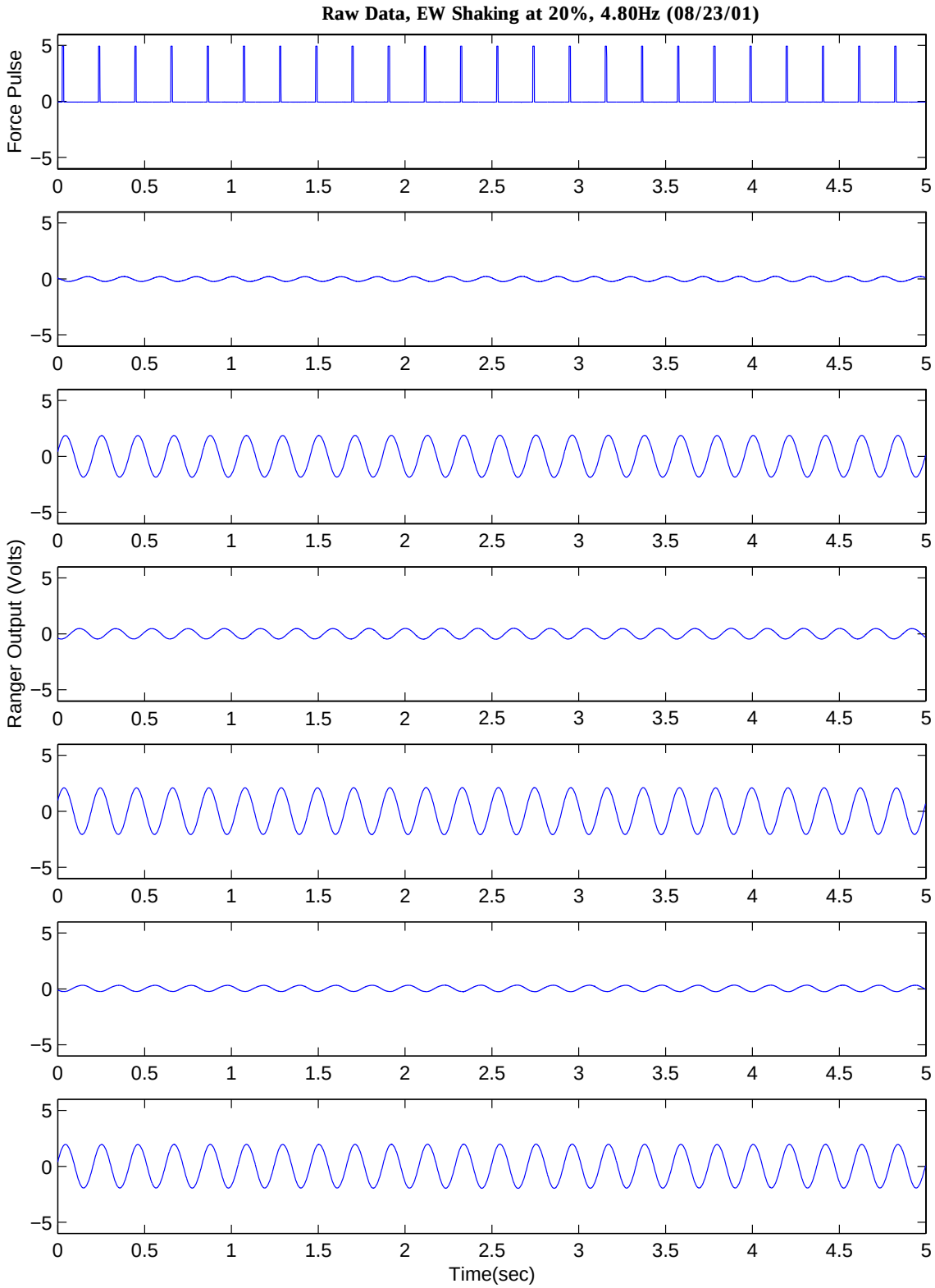

Figure C.39: 2-Story House FVT Seism. Data (EW at 20%, 4.80Hz)

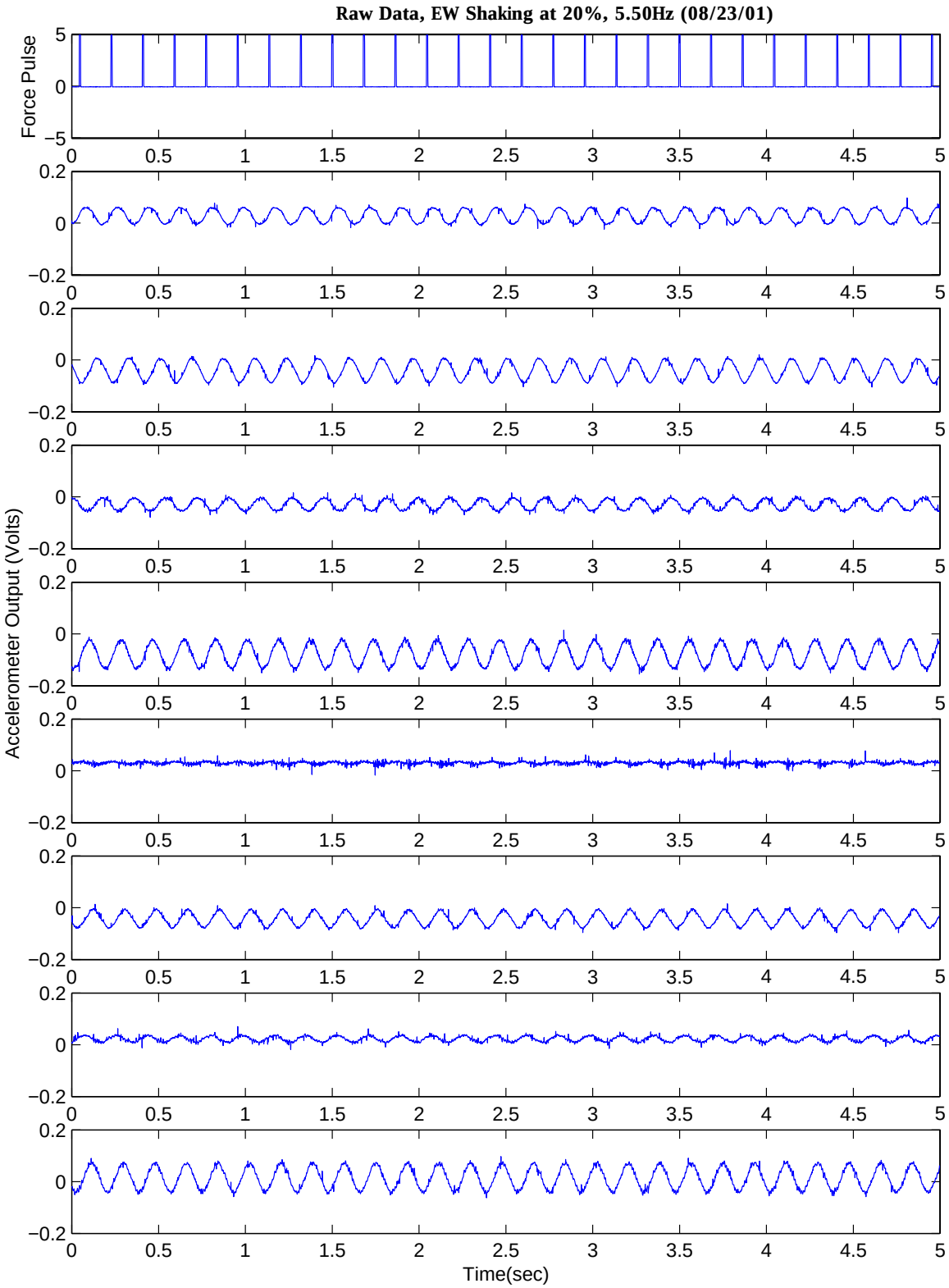

Figure C.40: 2-Story House FVT Accel. Data (EW at 20%, 5.50Hz)

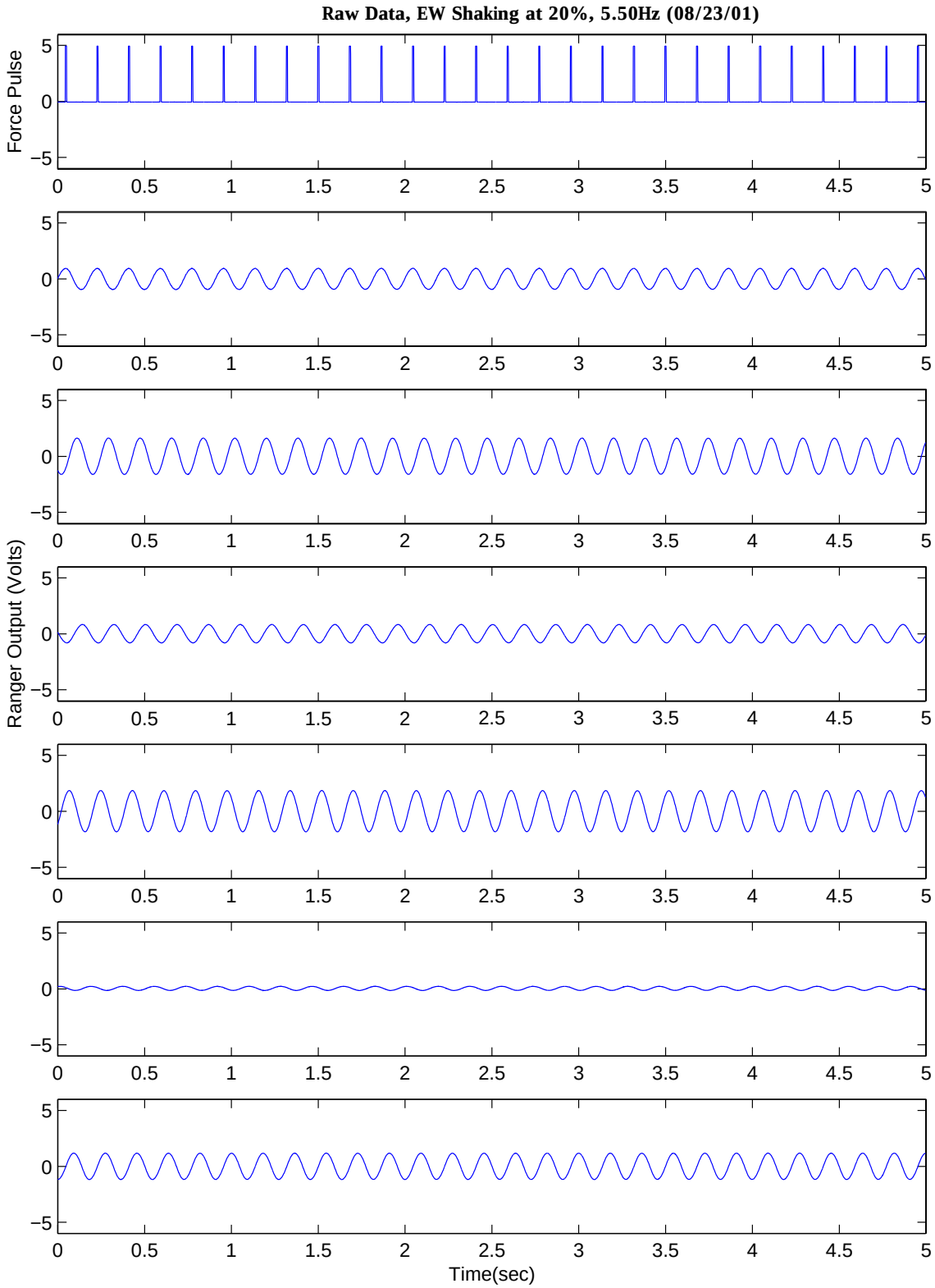

Figure C.41: 2-Story House FVT Seism. Data (EW at 20%, 5.50Hz)

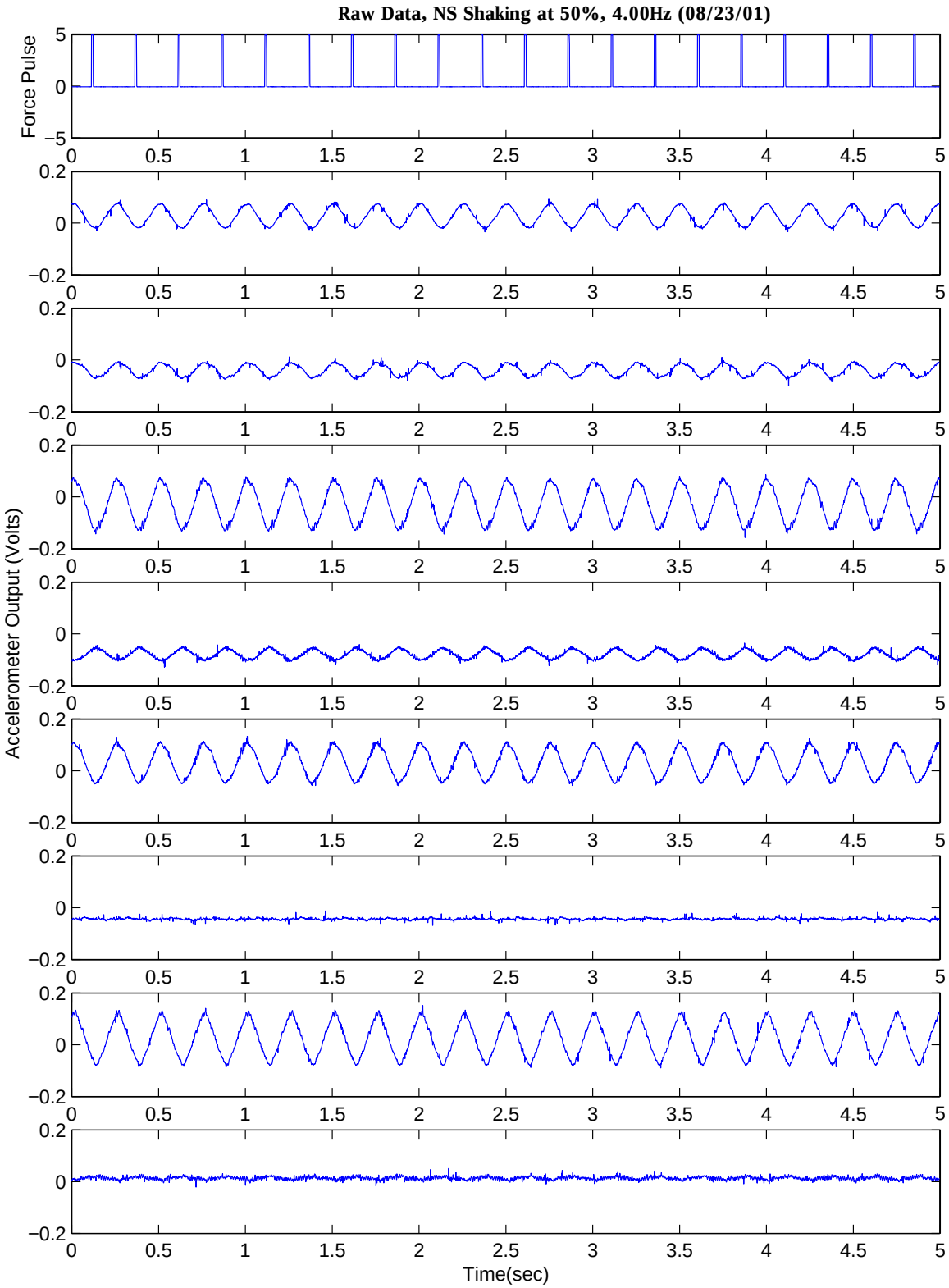

Figure C.42: 2-Story House FVT Accel. Data (NS at 50%, 4.00Hz)

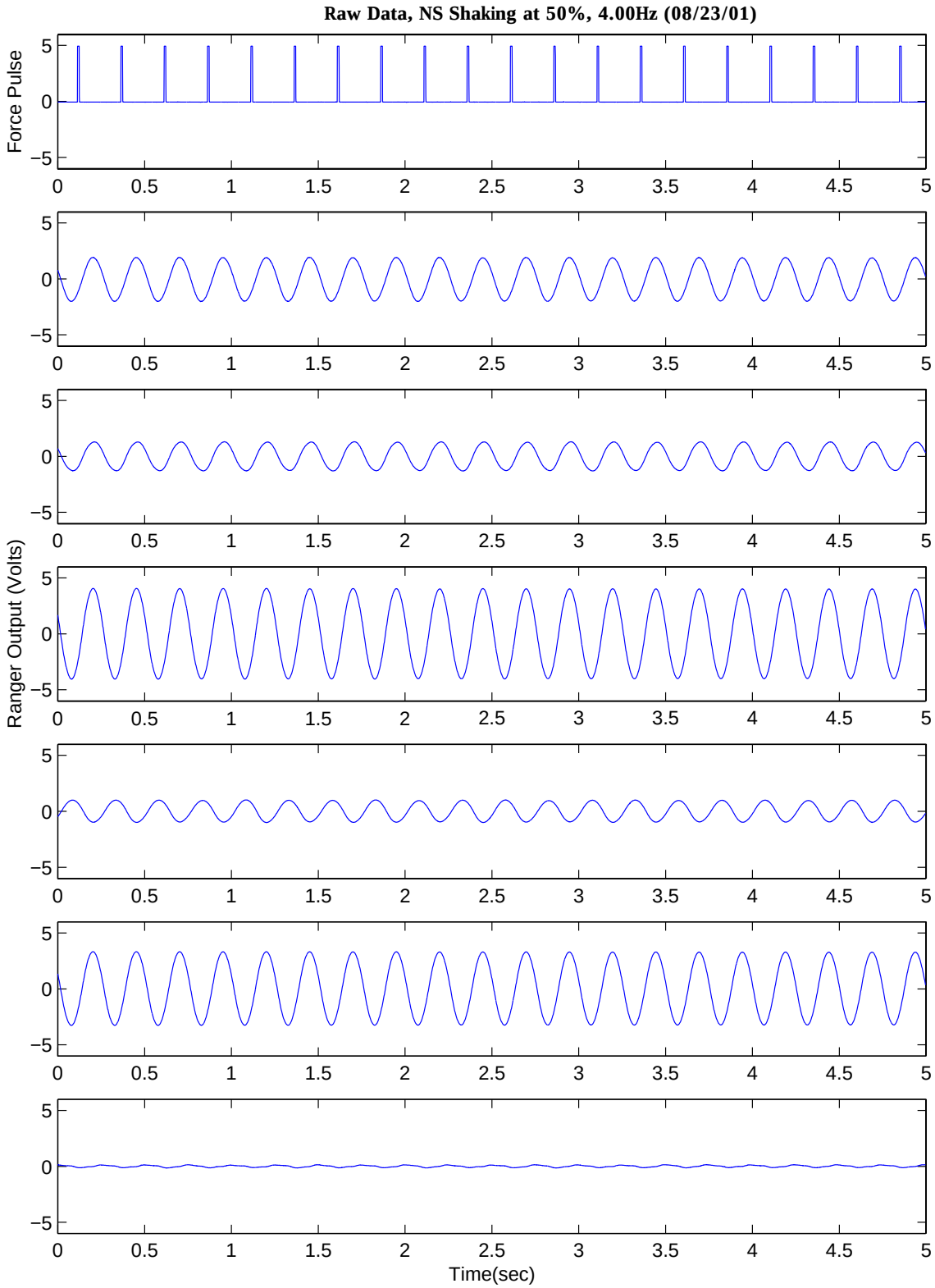

Figure C.43: 2-Story House FVT Seism. Data (NS at 50%, 4.00Hz)

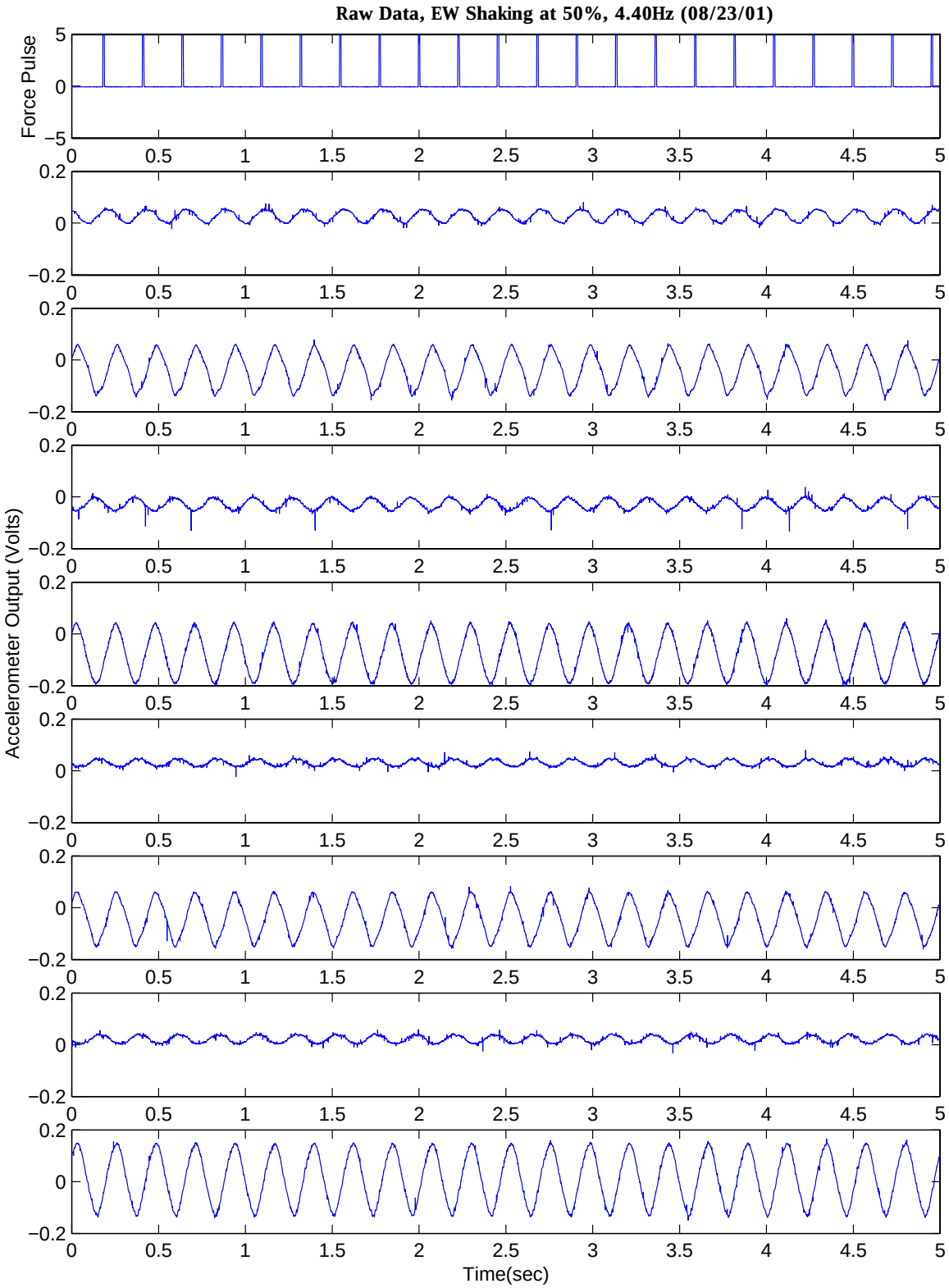

Figure C.44: 2-Story House FVT Accel. Data (EW at 50%, 4.40Hz)

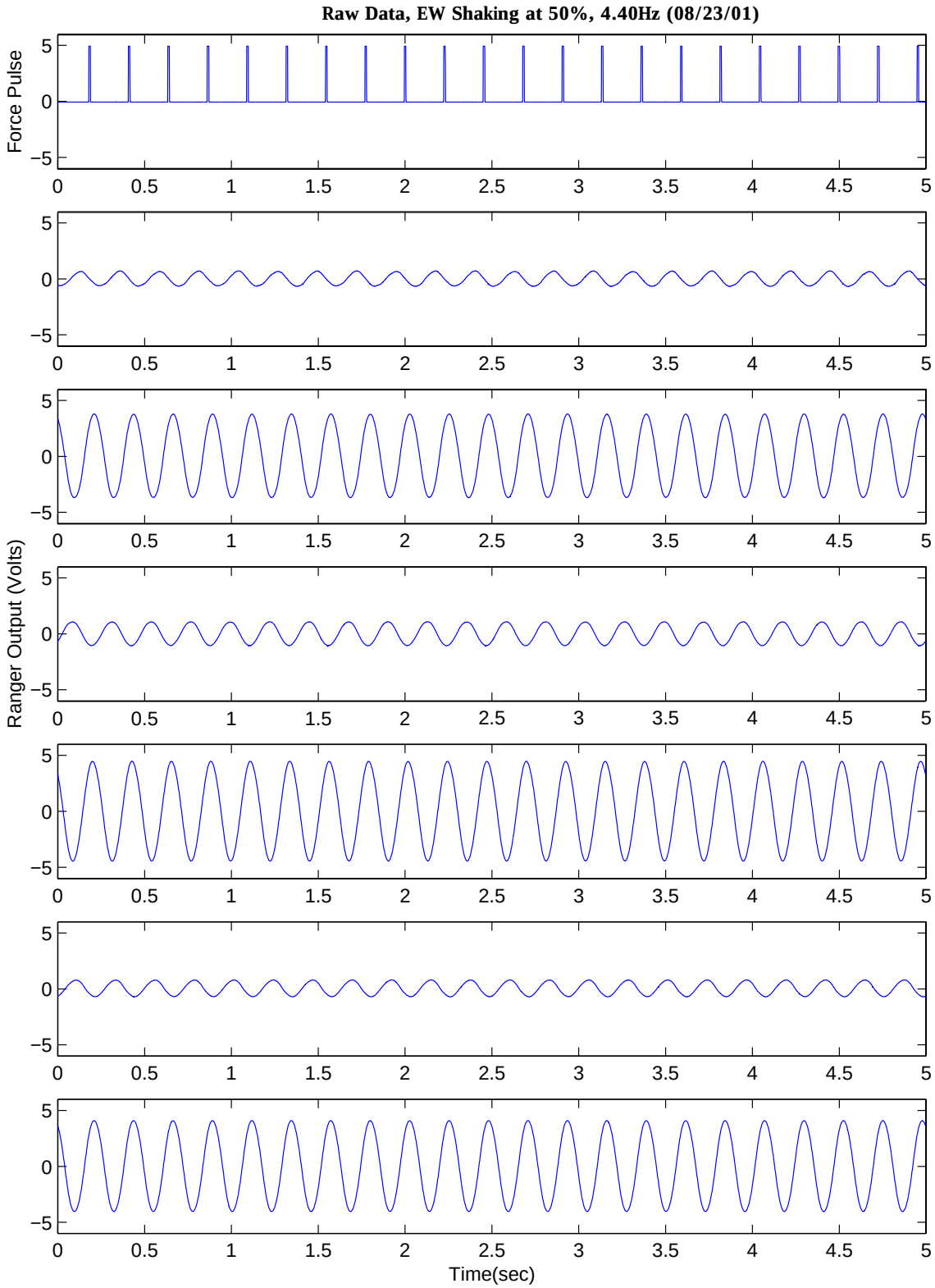

Figure C.45: 2-Story House FVT Seism. Data (EW at 50%, 4.40Hz)

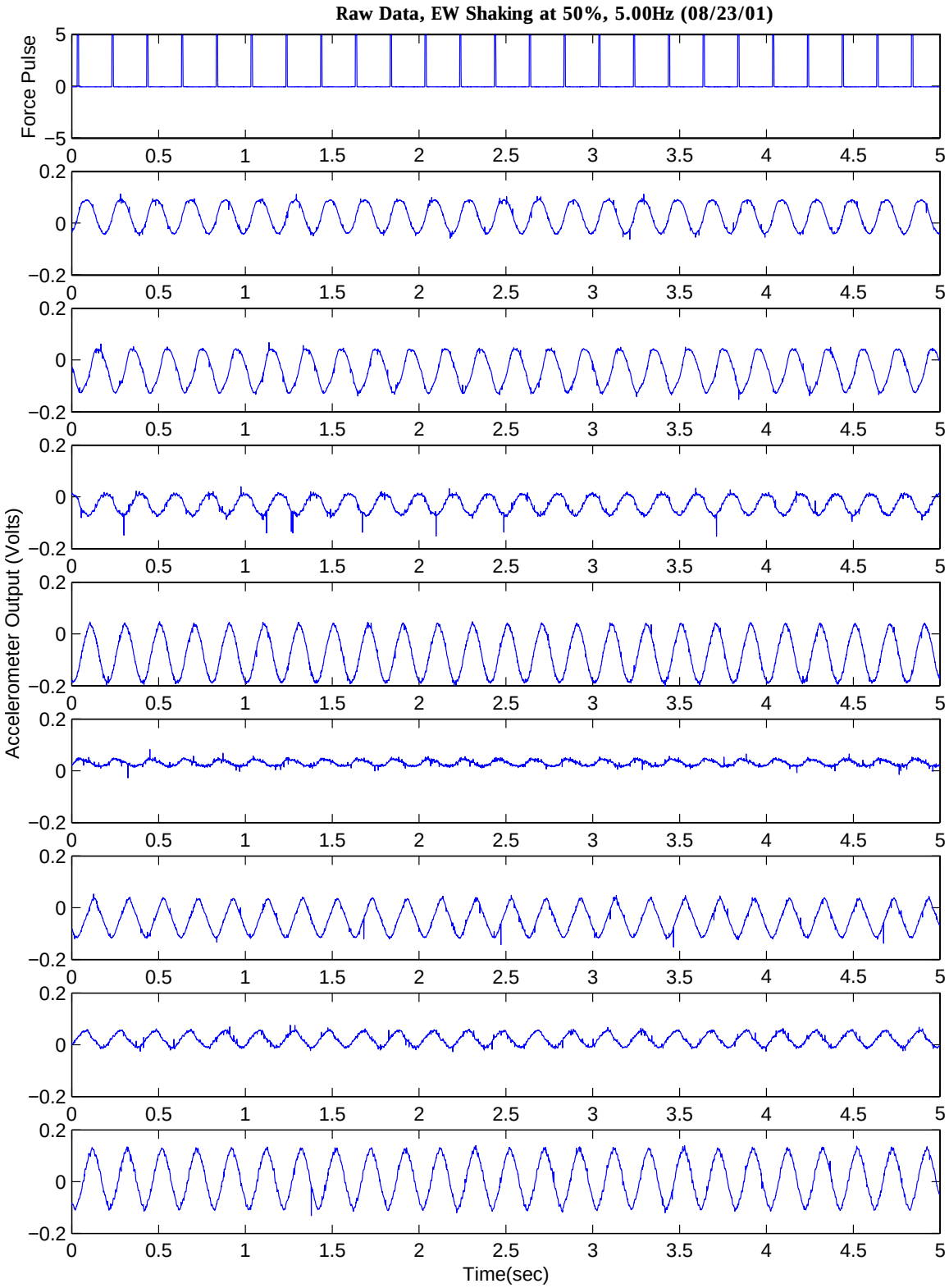

Figure C.46: 2-Story House FVT Accel. Data (EW at 50%, 5.00Hz)

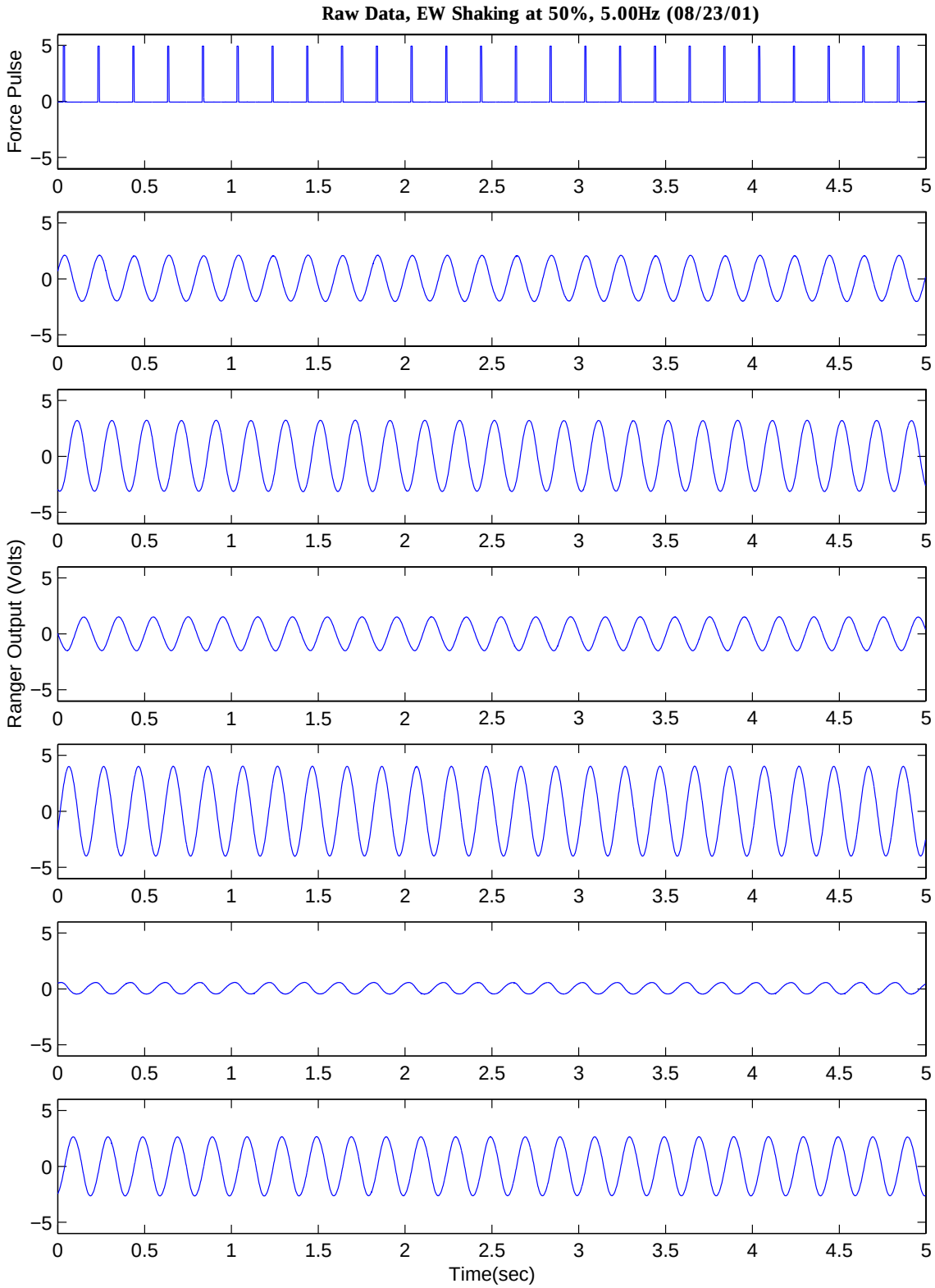

Figure C.47: 2-Story House FVT Seism. Data (EW at 50%, 5.00Hz)

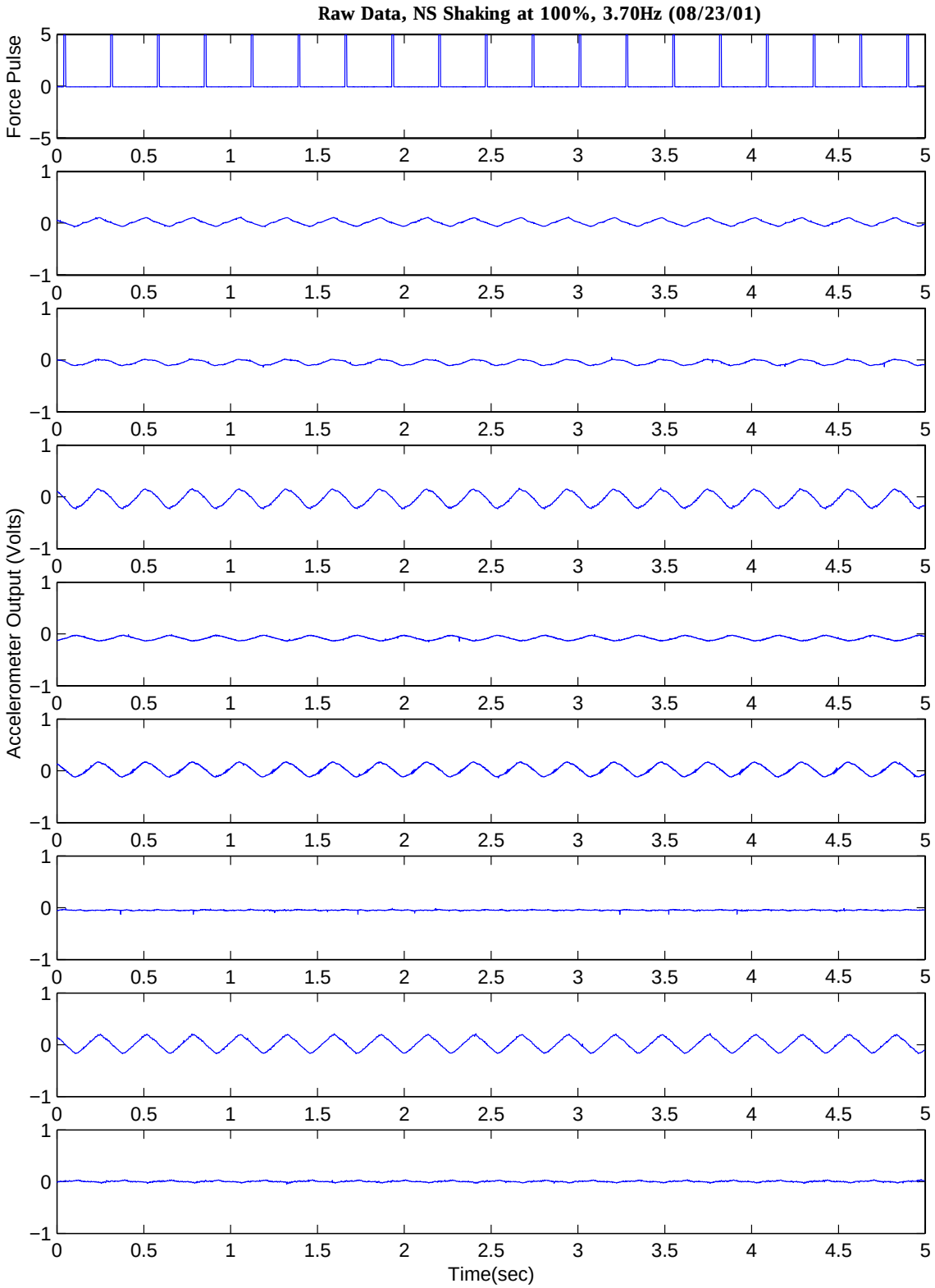

Figure C.48: 2-Story House FVT Accel. Data (NS at 100%, 3.70Hz)

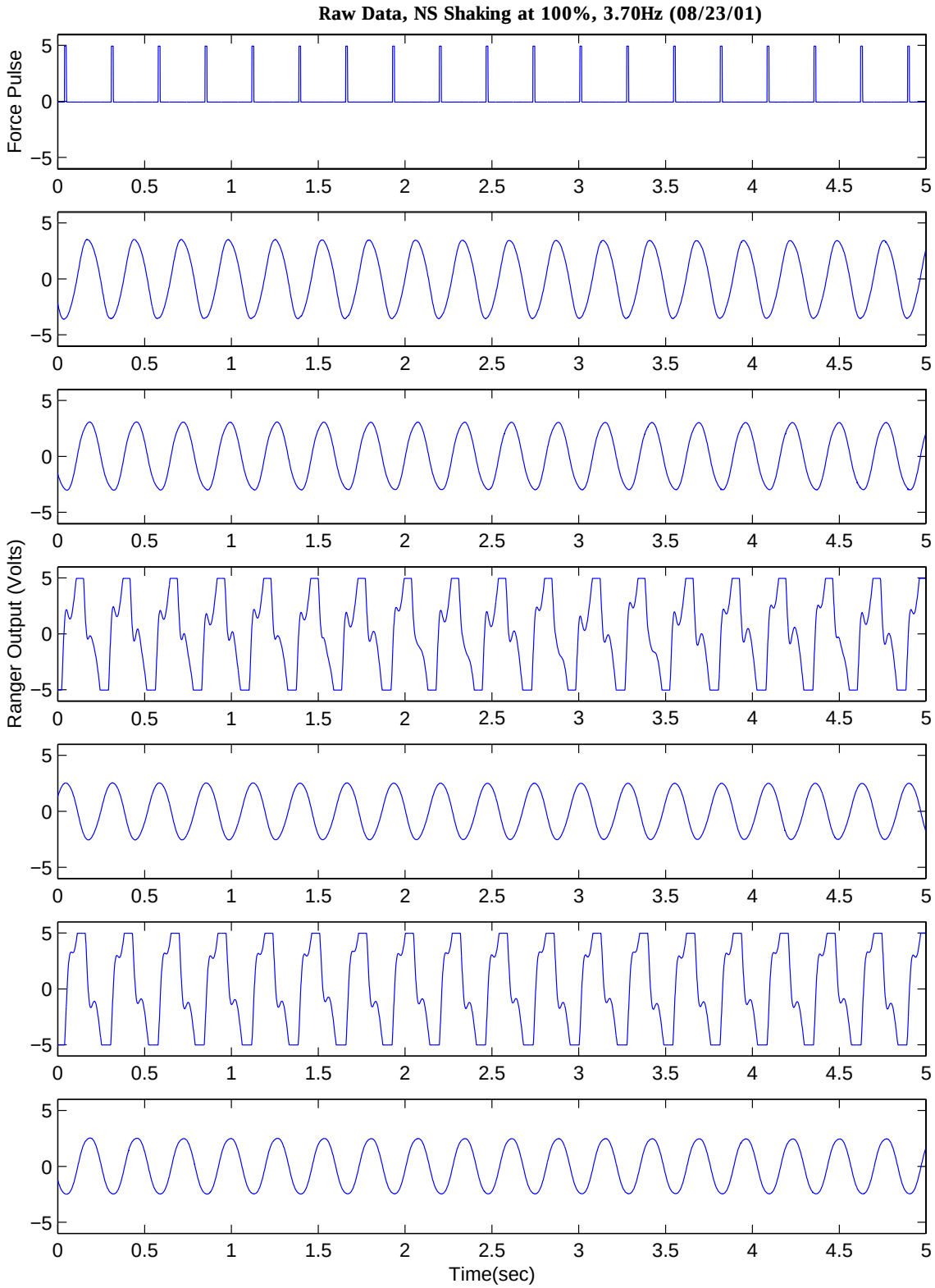

Figure C.49: 2-Story House FVT Seism. Data (NS at 100%, 3.70Hz)

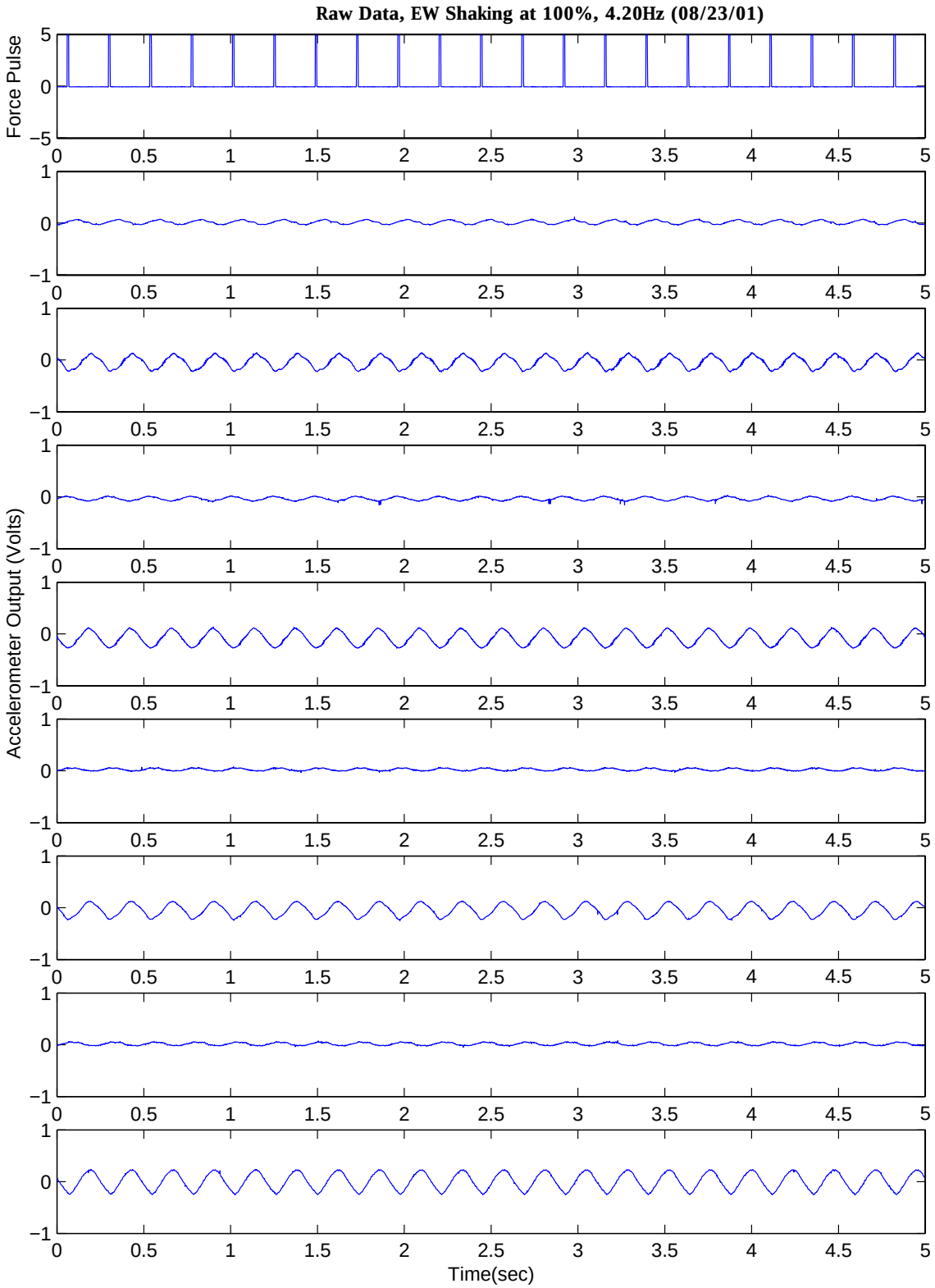

Figure C.50: 2-Story House FVT Accel. Data (EW at 100%, 4.20Hz)

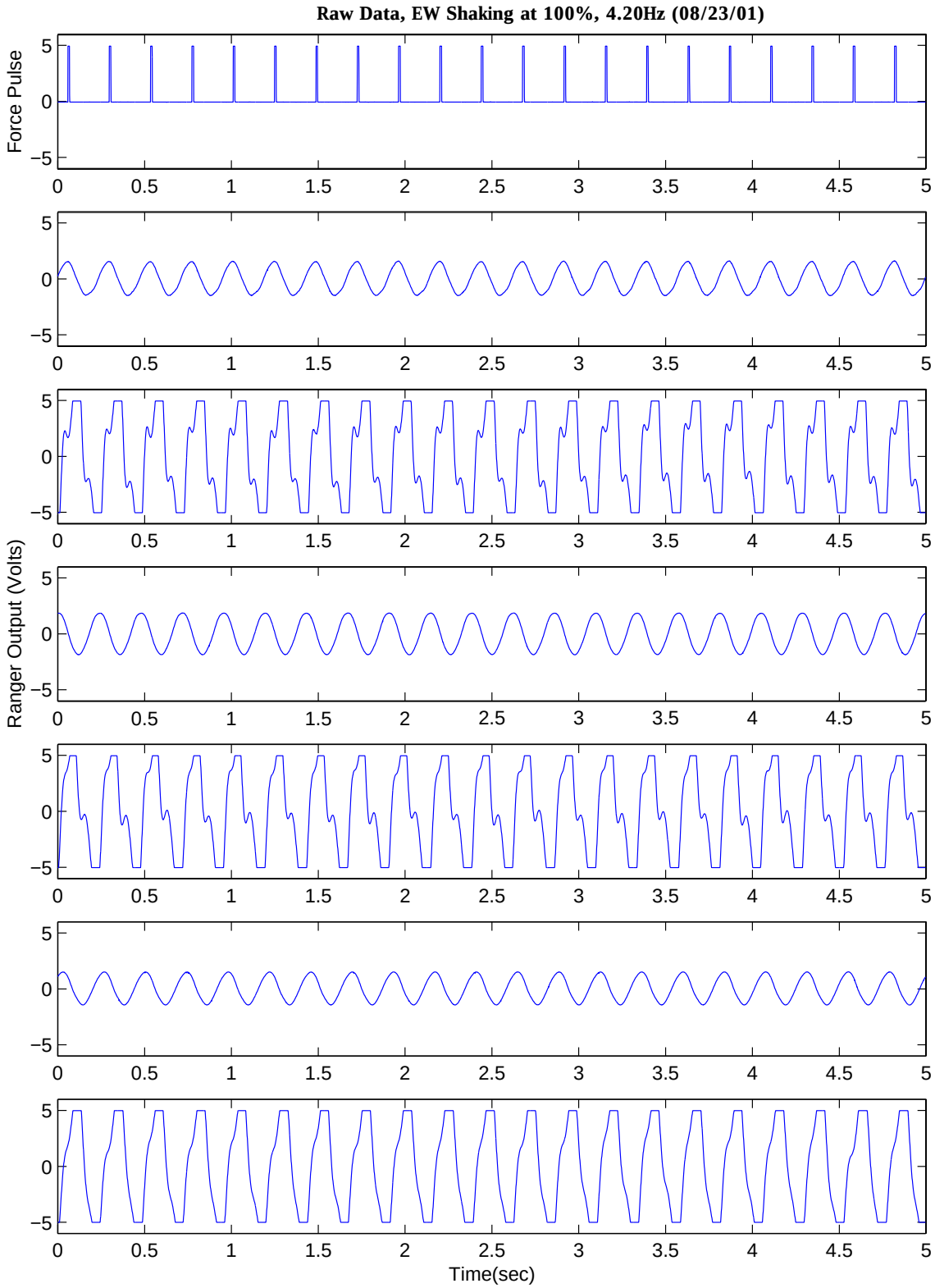

Figure C.51: 2-Story House FVT Seism. Data (EW at 100%, 4.20Hz)

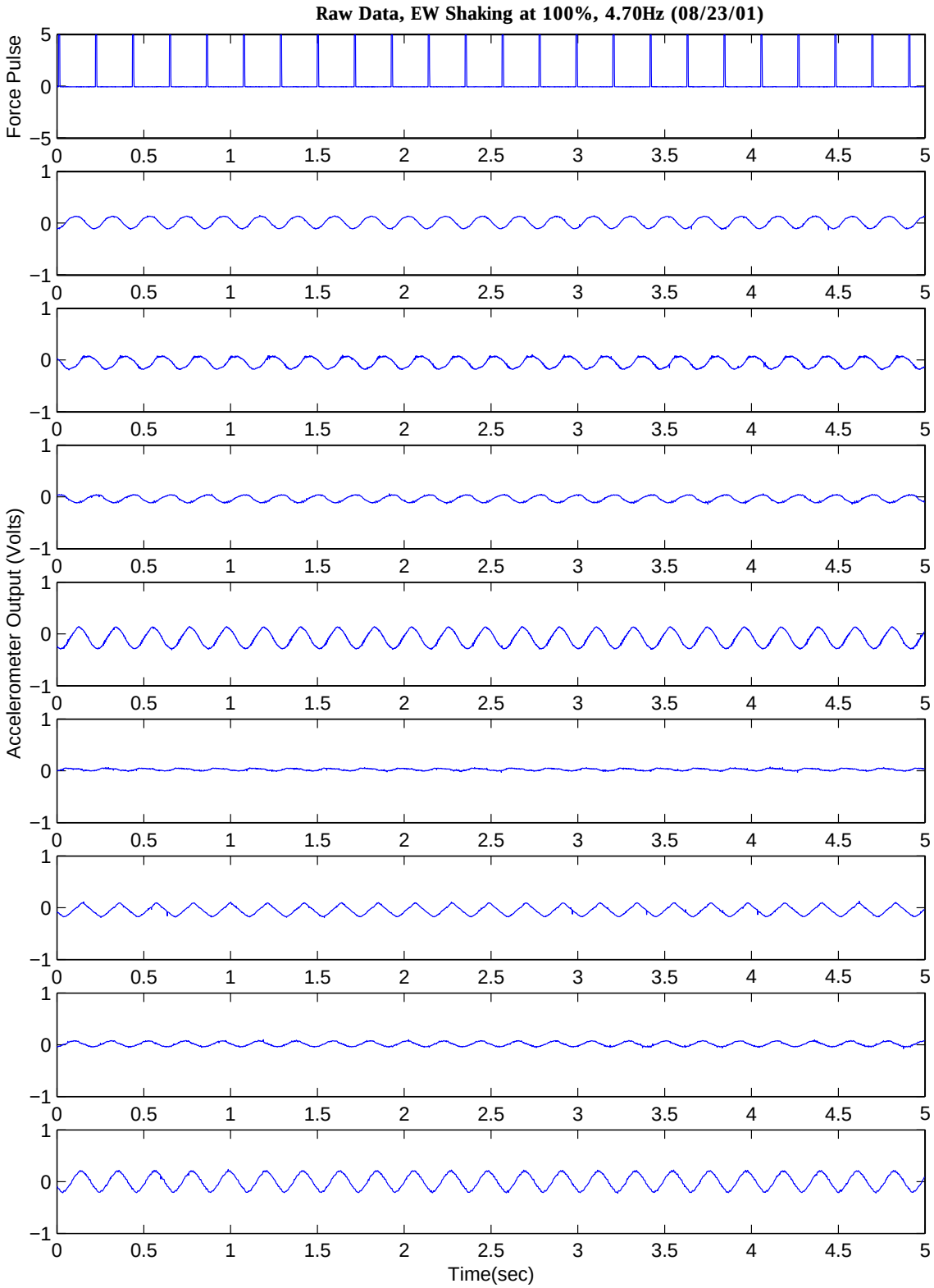

Figure C.52: 2-Story House FVT Accel. Data (EW at 100%, 4.70Hz)

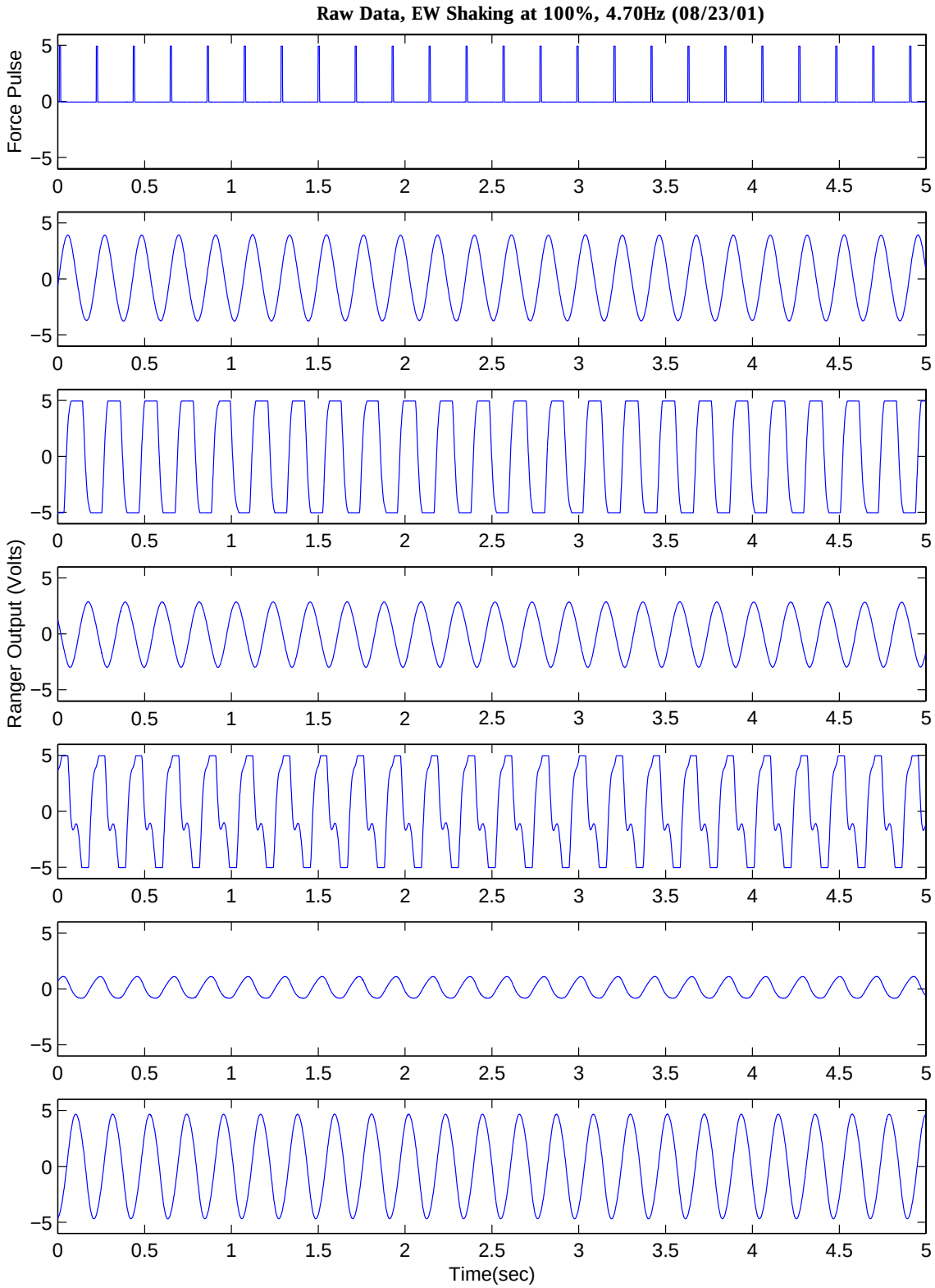

Figure C.53: 2-Story House FVT Seism. Data (EW at 100%, 4.70Hz)

Appendix D

Shake-Table Accelerations, UCSD 2-Story House

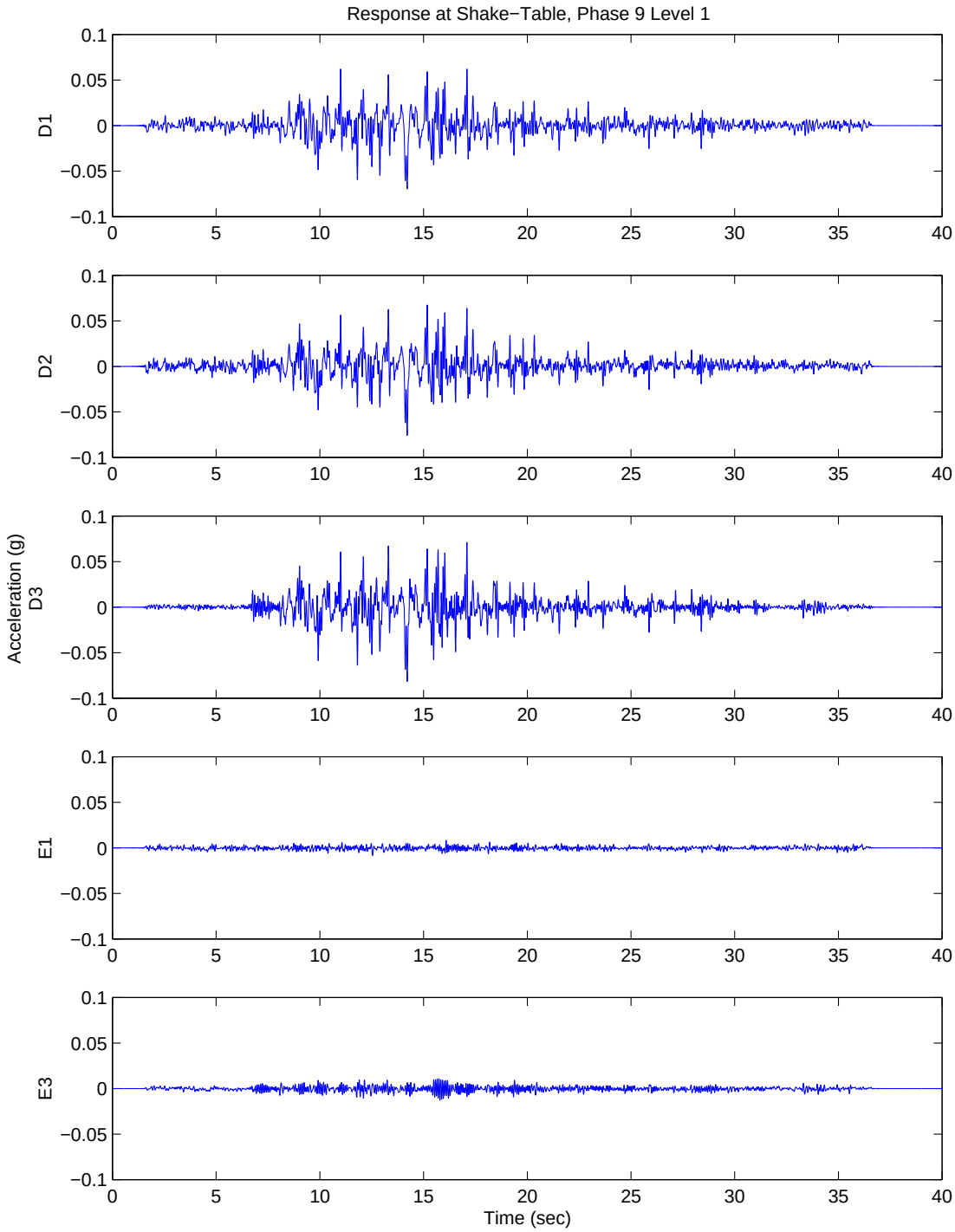

Figure D.1: Recorded Acceleration at Shake-Table, Phase 9 Level 1

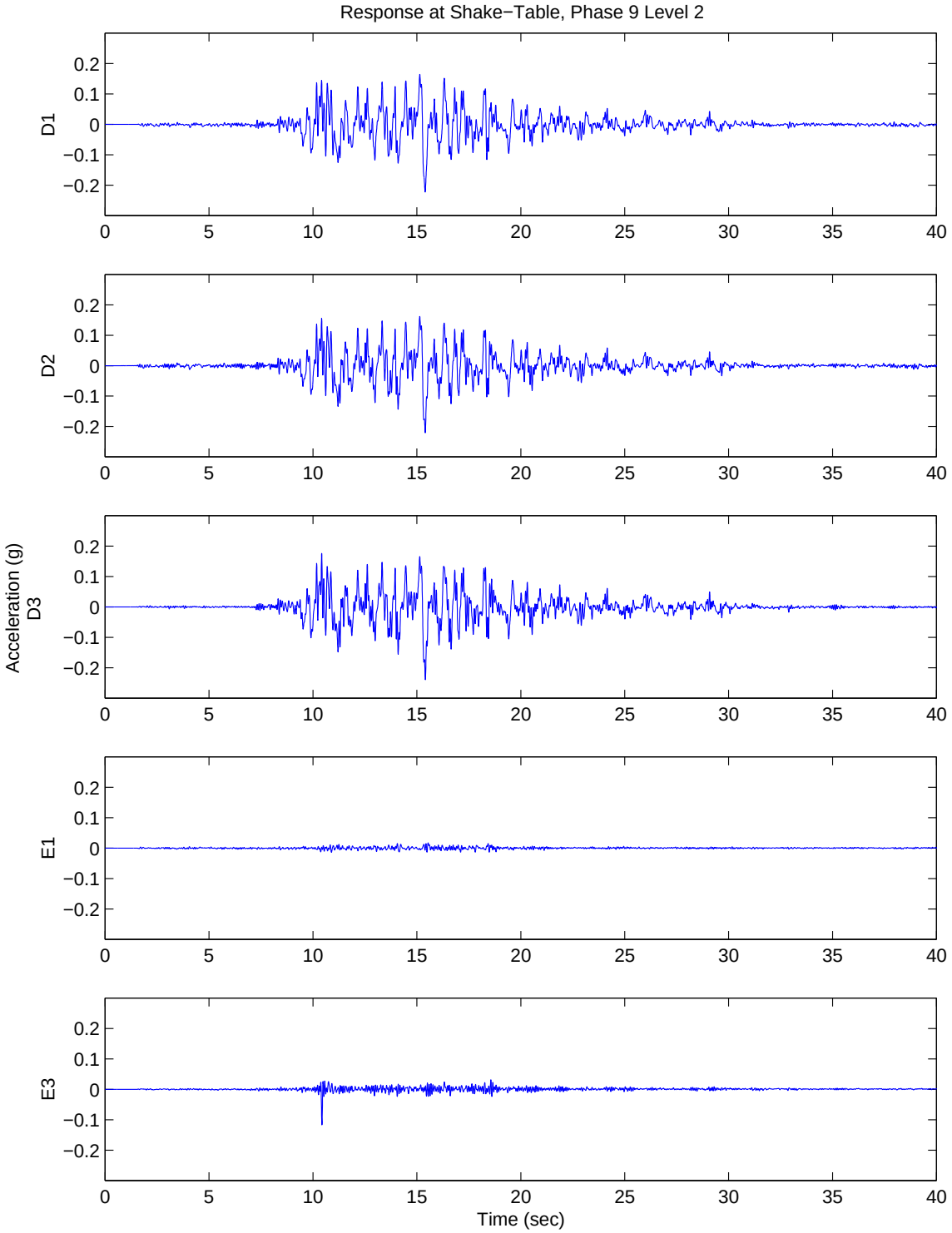

Figure D.2: Recorded Acceleration at Shake-Table, Phase 9 Level 2

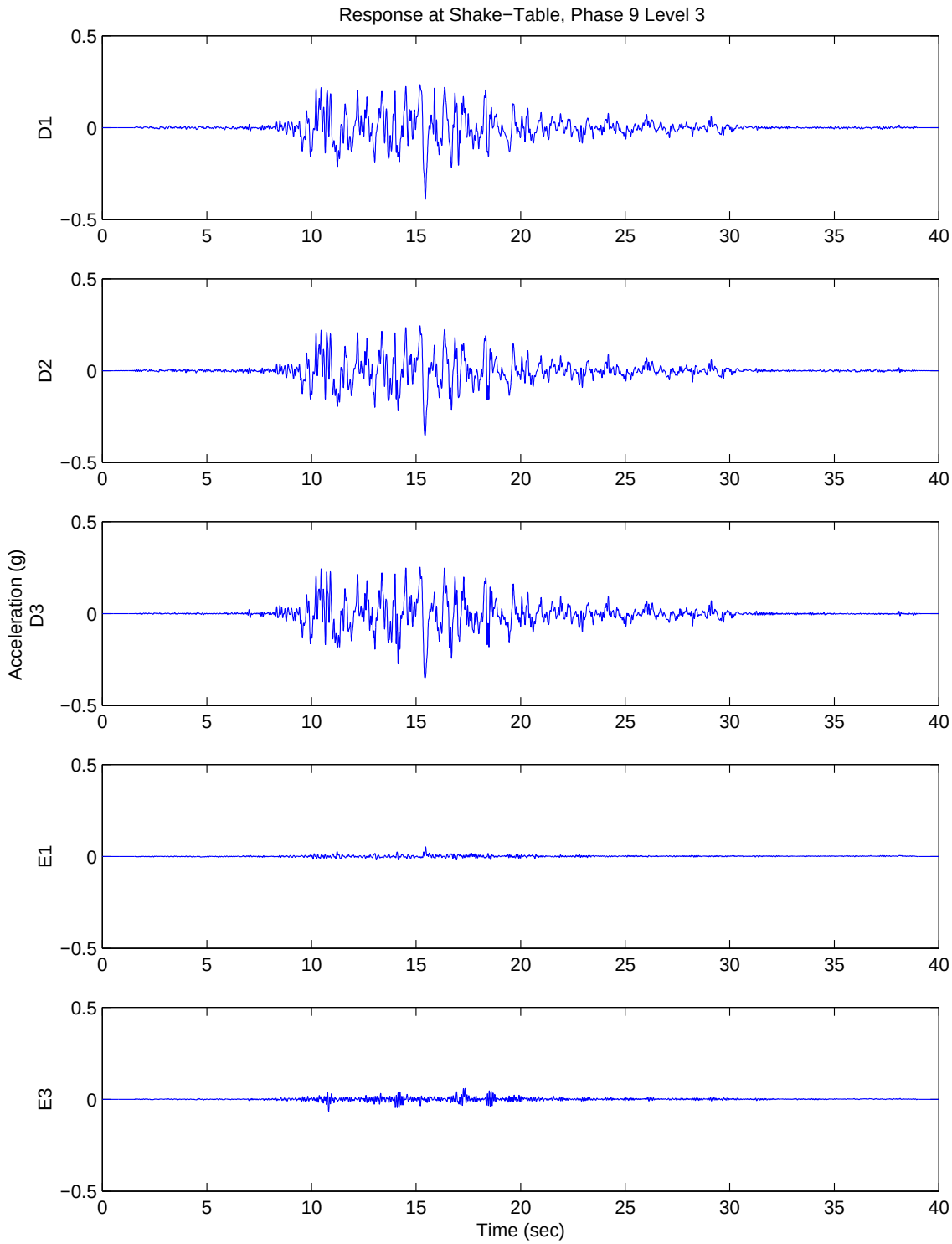

Figure D.3: Recorded Acceleration at Shake-Table, Phase 9 Level 3

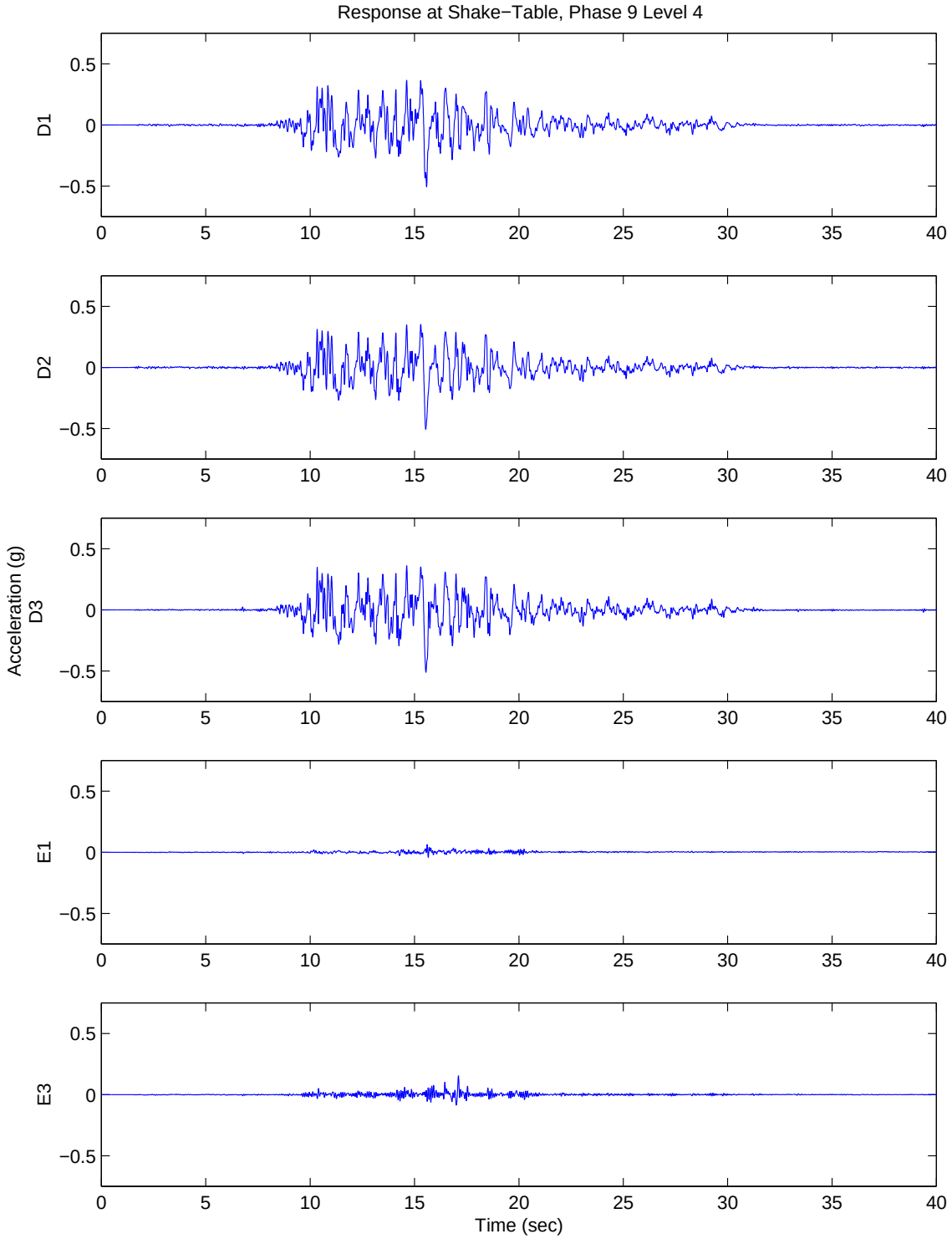

Figure D.4: Recorded Acceleration at Shake-Table, Phase 9 Level 4

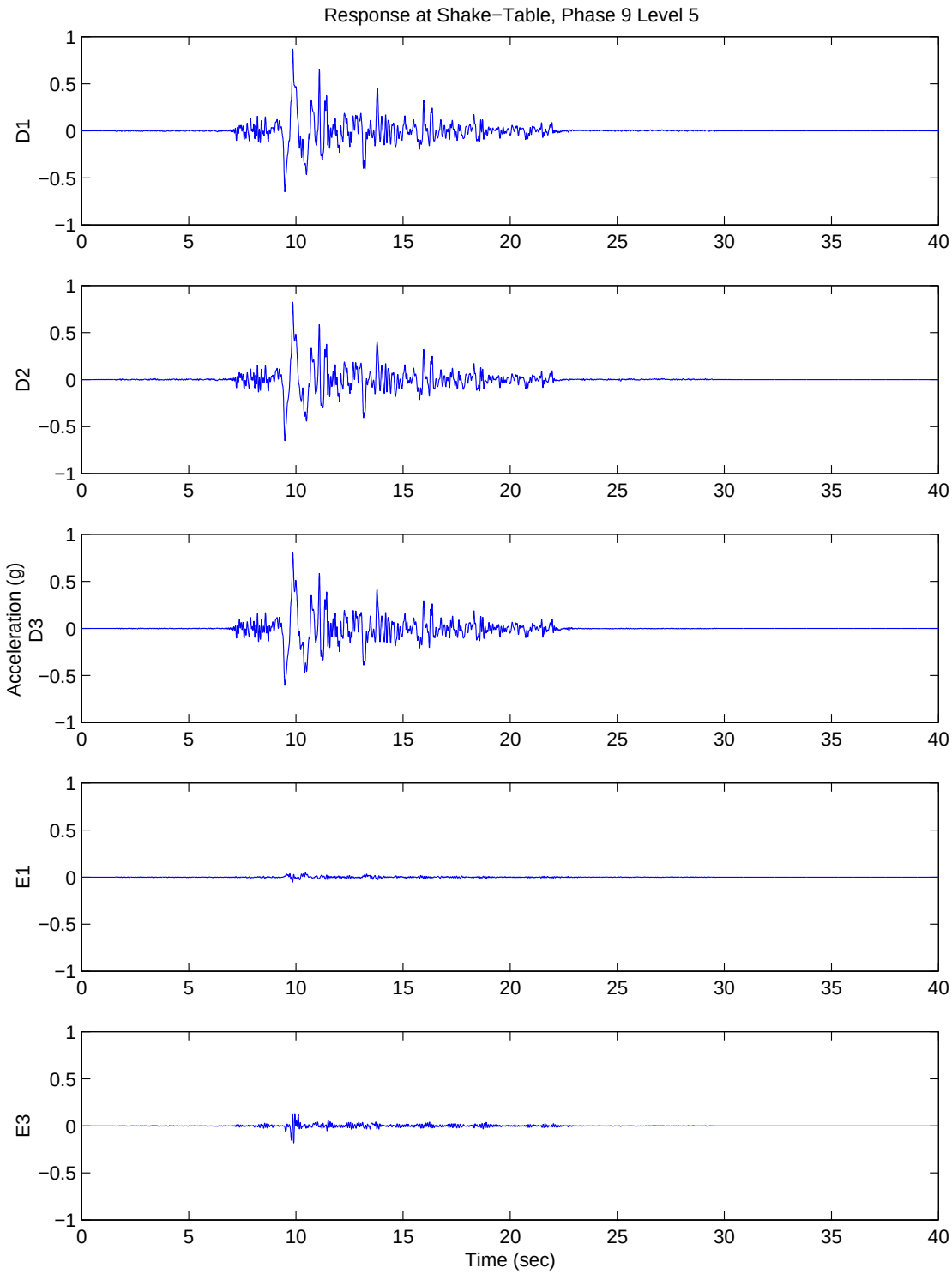

Figure D.5: Recorded Acceleration at Shake-Table, Phase 9 Level 5

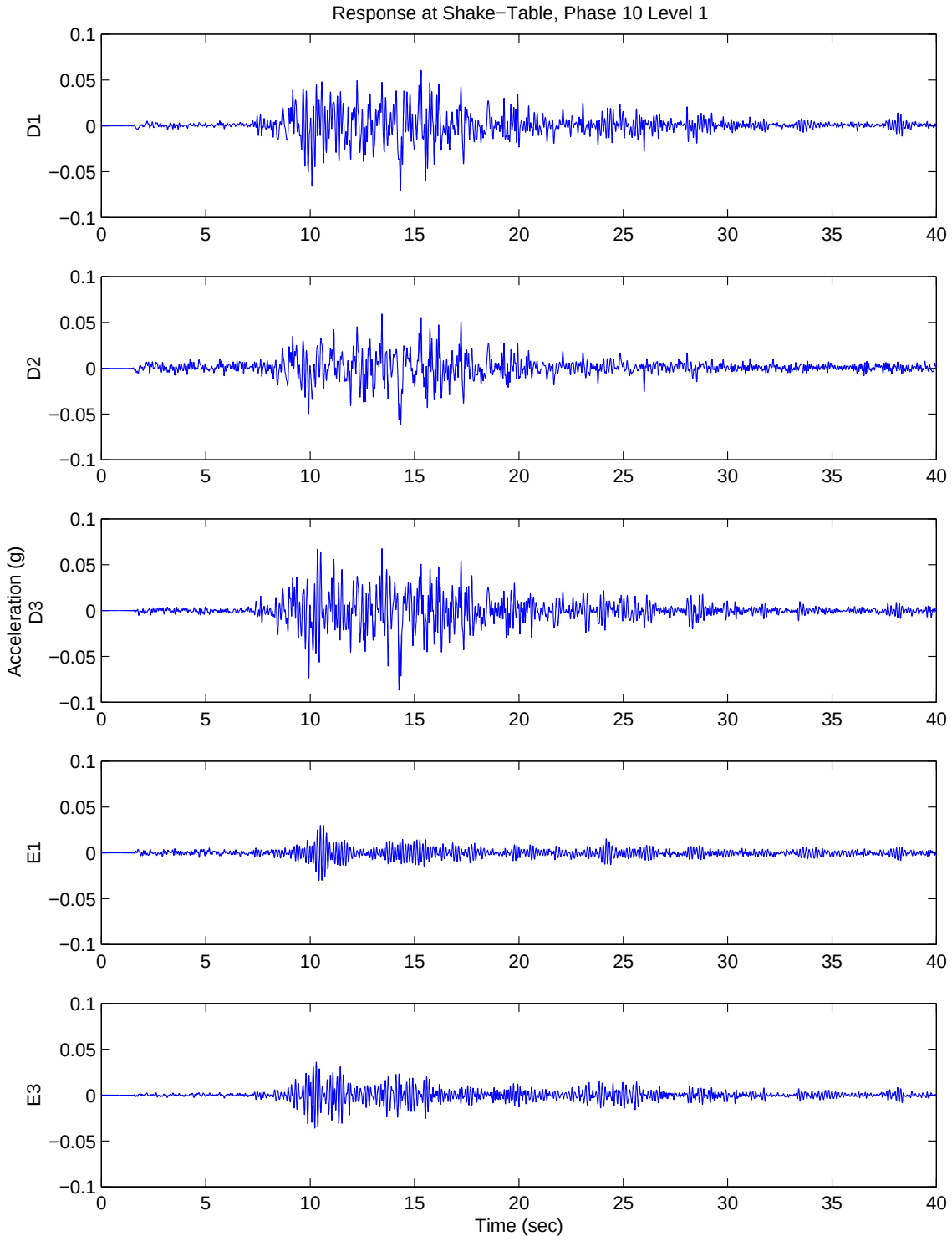

Figure D.6: Recorded Acceleration at Shake-Table, Phase 10 Level 1

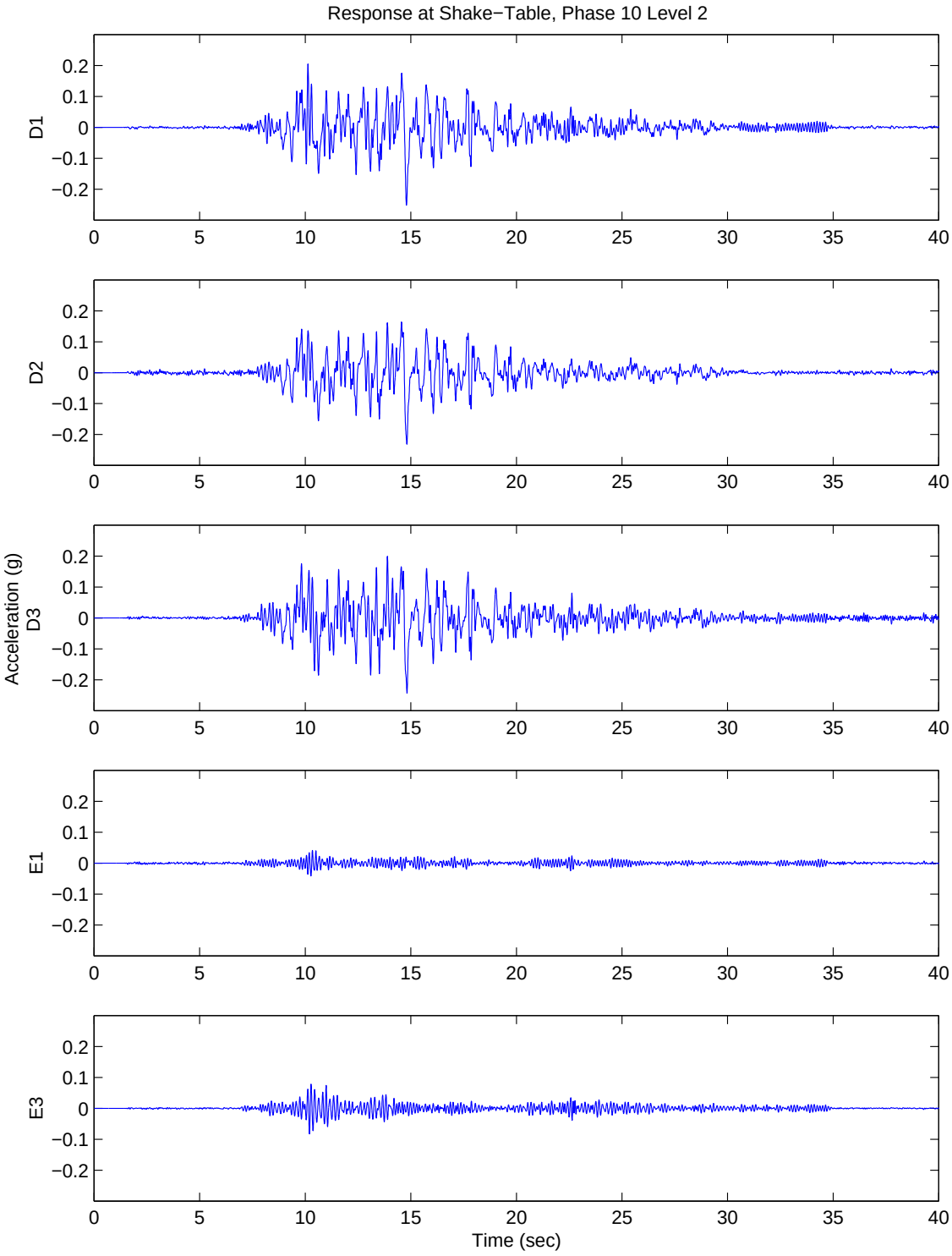

Figure D.7: Recorded Acceleration at Shake-Table, Phase 10 Level 2

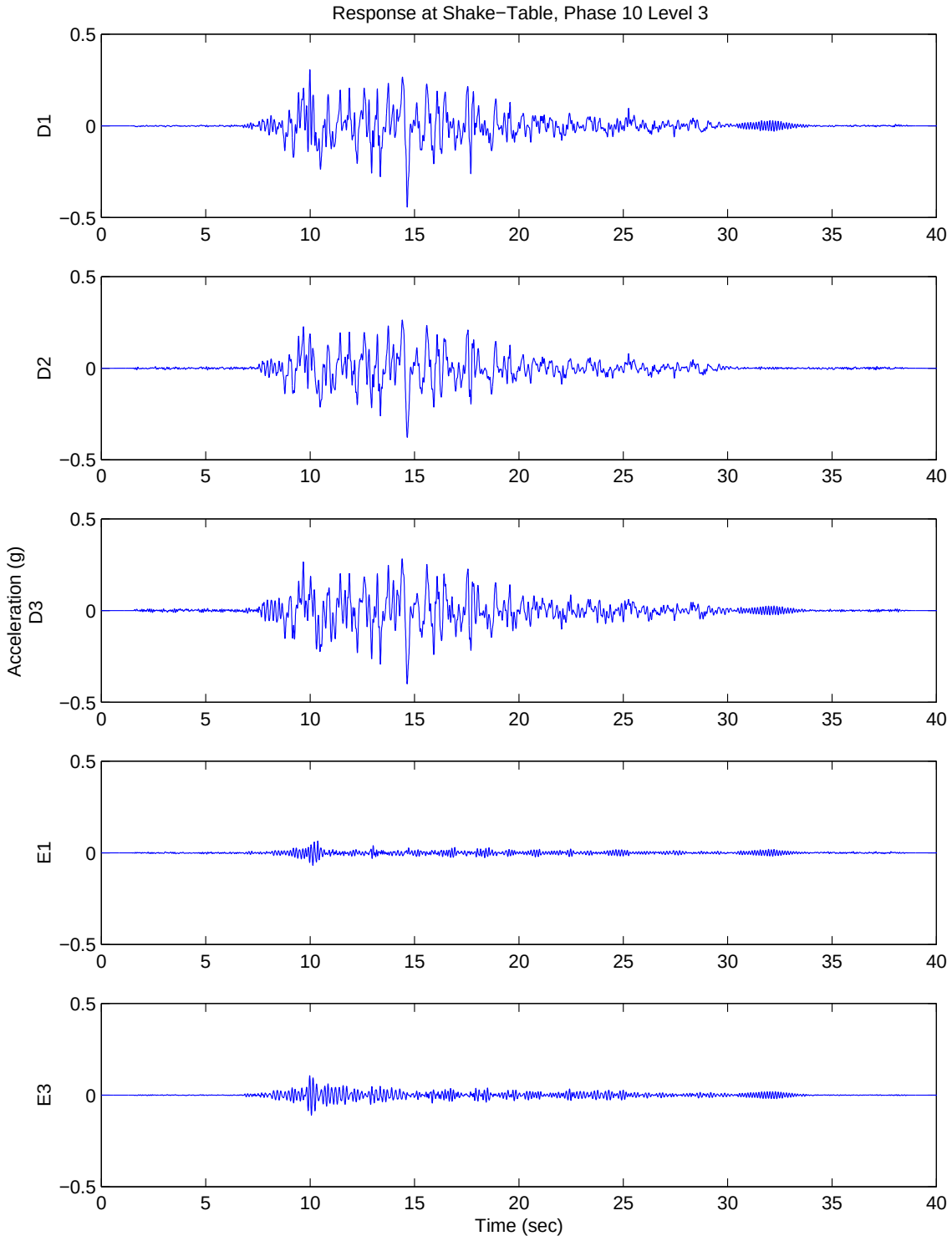

Figure D.8: Recorded Acceleration at Shake-Table, Phase 10 Level 3

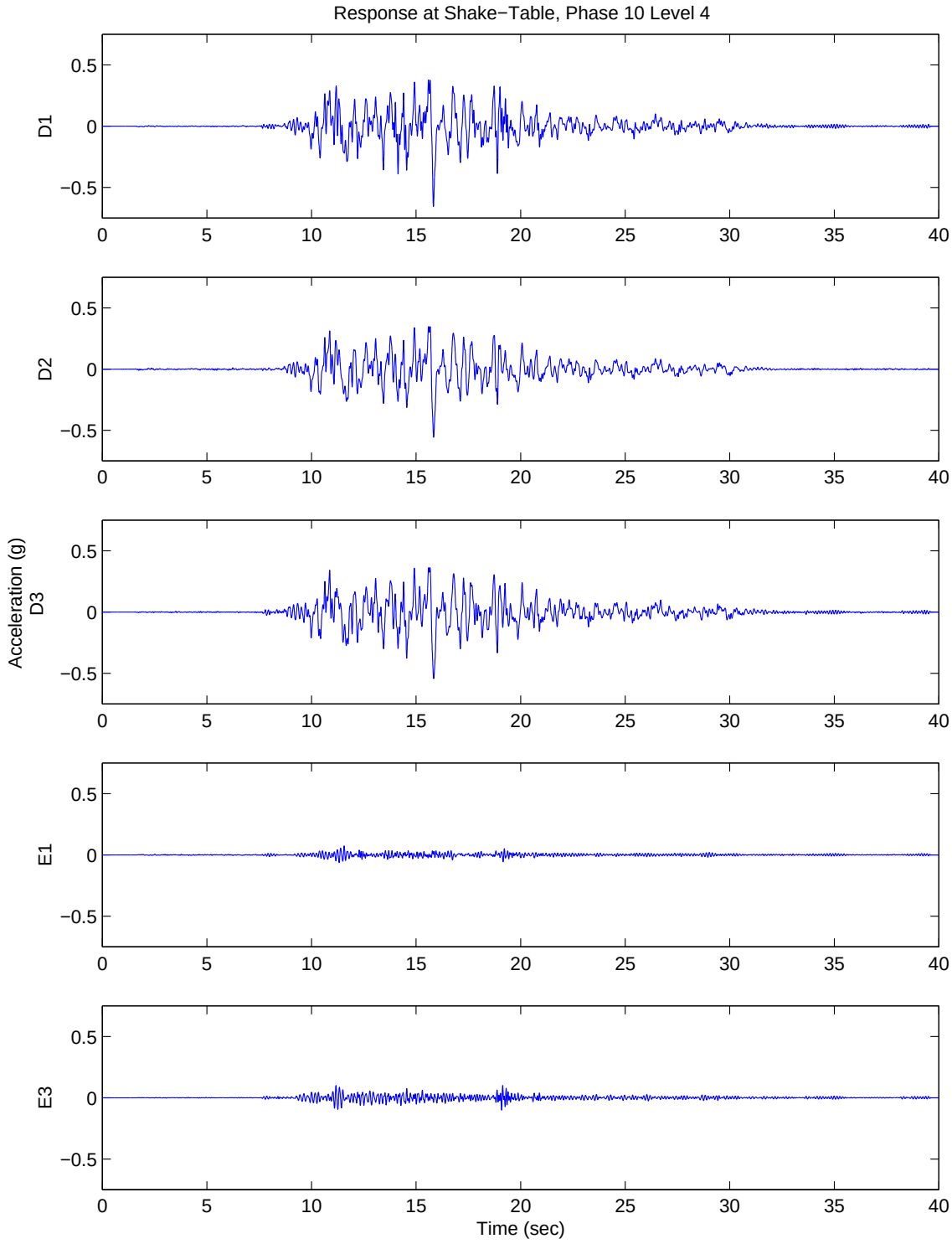

Figure D.9: Recorded Acceleration at Shake-Table, Phase 10 Level 4

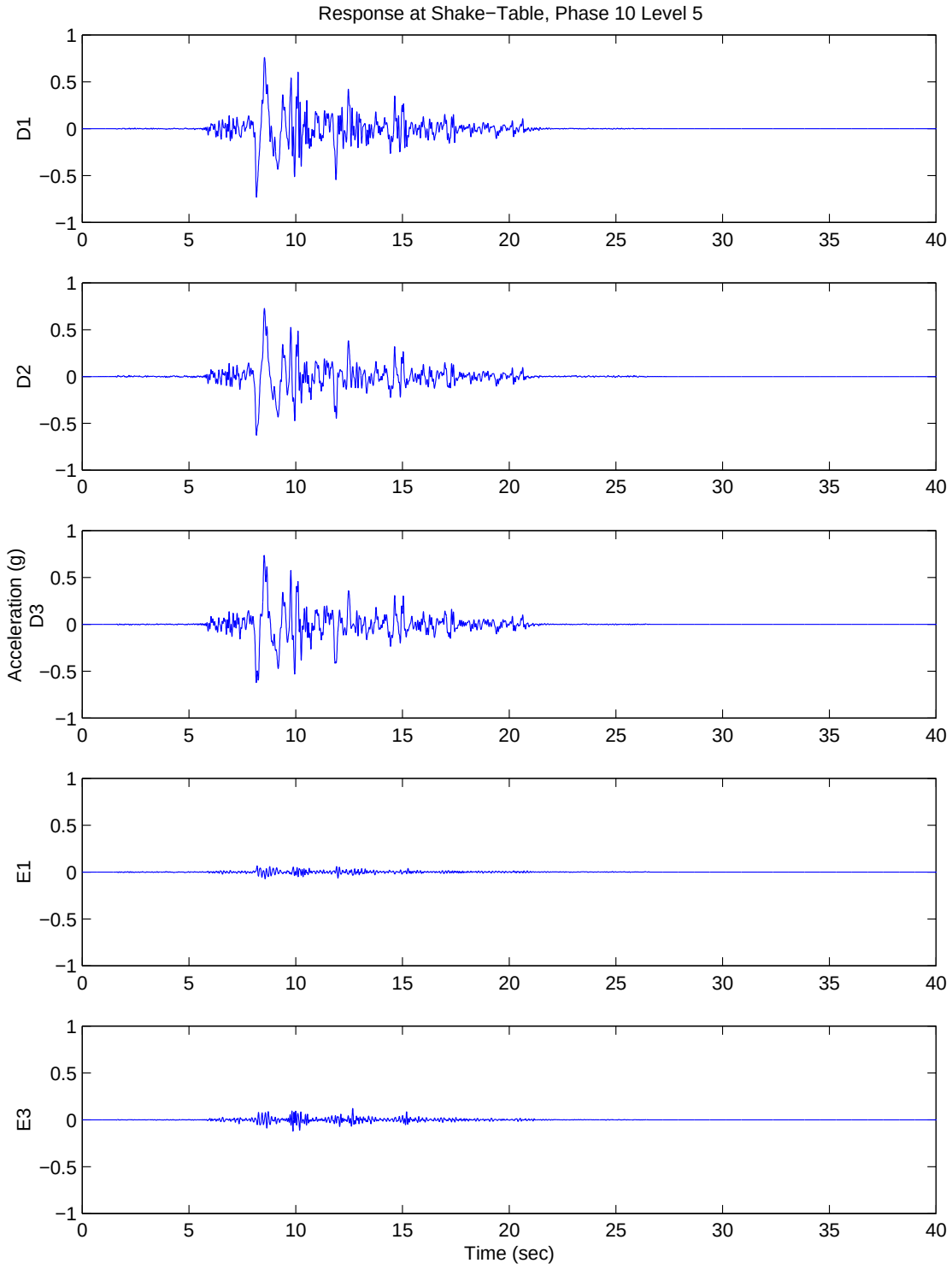

Figure D.10: Recorded Acceleration at Shake-Table, Phase 10 Level 5

Appendix E

Diaphragm Stiffness and Mass Distribution

The effects of diaphragm stiffness and mass distribution were studied using a symmetric 3-story test model with no garage opening and fixed spring stiffnesses along the entire height of the walls (see Tables E.1 and E.2). It was observed that the diaphragm behaves as nearly rigid as long as its stiffness is of similar or greater order of magnitude as those of the spring stiffnesses. As the diaphragm shear stiffness is reduced, the motion at the degrees of freedom perpendicular to the direction of shaking is reduced and approaches zero when the diaphragm is fully flexible (see Figures E.1 through E.4). Also, when the diaphragm stiffness approached zero, the model response had an antisymmetric mode in each direction instead of a torsional mode involving all degrees of freedom. The translational fundamental frequencies remained the same regardless of the diaphragm stiffness.

Regarding the effects of the mass distribution, it was observed that a diagonal mass matrix produces dramatically different results from those obtained using a non-diagonal mass matrix (see Figures E.1 through E.4). The diagonal mass matrix would result from lumping of the masses at each degree of freedom, while a non-diagonal mass matrix would result from assuming finite-element consistent mass distribution. The diagonal mass matrix results in torsional fundamental frequencies that are considerably lower (by a factor of $\sqrt{3}$) than the torsional frequencies produced by assuming the non-diagonal matrix (see Tables E.3 and E.4). This can be easily understood by

comparing the solutions to the eigenvalue problem of a two degree-of-freedom system (with springs of stiffness k at each degree of freedom and stiffness G coupling them) using a lumped mass matrix and a compatible mass matrix. The resulting symmetric and antisymmetric mode frequencies are $\sqrt{2k/m}$ and $\sqrt{2(k+2G)/m}$ in the case of the lumped mass matrix, but not in the case of the compatible mass matrix ($\sqrt{2k/m}$ and $\sqrt{6(k+2G)/m}$). The amplitude of the response at the torsional mode is also lower when the mass matrix is diagonal. The translational fundamental frequencies (i.e., symmetric modes) remained the same regardless of the mass distribution.

Table E.1: Test Model with Very Flexible Diaphragm

Spring Stiffness for Transverse Walls (NS)	1.0E+06 lbs/in
Spring Stiffness for Longitudinal Walls (EW)	1.5E+06 lbs/in
Diaphragm Stiffness (2nd and 3rd Floors)	2.0E+03 lbs/in
Diaphragm Stiffness (Roof)	1.5E+03 lbs/in
Weight at 2nd Floor	26,580 lbs
Weight at 3rd Floor	26,950 lbs
Weight at Roof	17,400 lbs
Damping Ratios	5%
Scaling Constant	1.0

Table E.2: Test Model with Rigid Diaphragm

Spring Stiffness for Transverse Walls (NS)	1.0E+06 lbs/in
Spring Stiffness for Longitudinal Walls (EW)	1.5E+06 lbs/in
Diaphragm Stiffness (2nd and 3rd Floors)	2.0E+06 lbs/in
Diaphragm Stiffness (Roof)	1.5E+06 lbs/in
Weight at 2nd Floor	26,580 lbs
Weight at 3rd Floor	26,950 lbs
Weight at Roof	17,400 lbs
Damping Ratios	5%
Scaling Constant	1.0

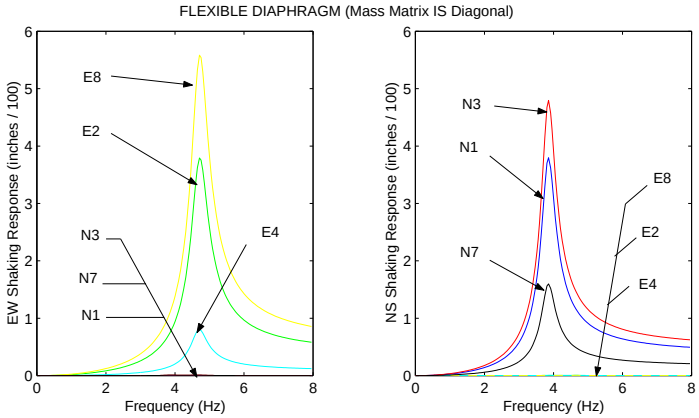

Figure E.1: Test Model with Very Flexible Diaphragm (mass matrix IS diagonal)

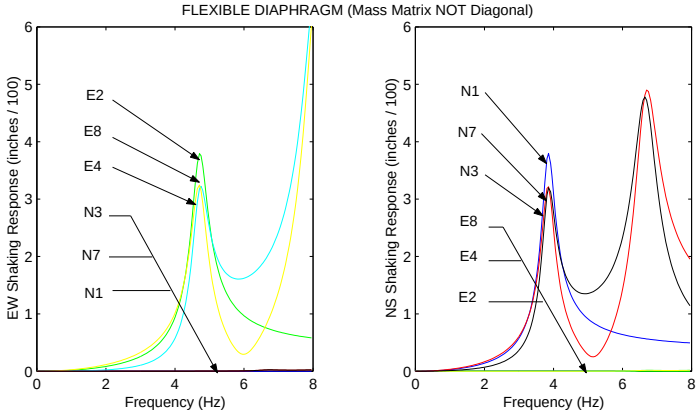

Figure E.2: Test Model with Very Flexible Diaphragm (mass matrix NOT diagonal)

Table E.3: Natural Frequencies (flexible diaphragm)

Lumped Mass (matrix IS diag.)			
ω_1	ω_2	ω_3	ω_4
3.85 Hz	3.85 Hz	4.71 Hz	4.71 Hz
NS	Tors	EW	Tors

Consistent Mass (matrix NOT diag.)			
ω_1	ω_2	ω_3	ω_4
3.85 Hz	4.71 Hz	6.66 Hz	8.17 Hz
NS	EW	Tors	Tors

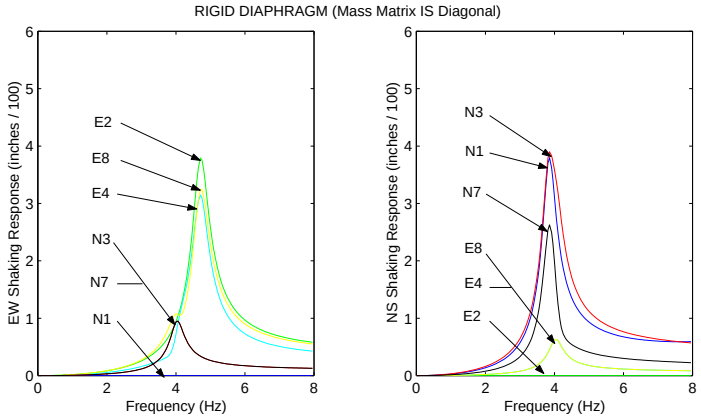

Figure E.3: Test Model with Rigid Diaphragm (mass matrix IS diagonal)

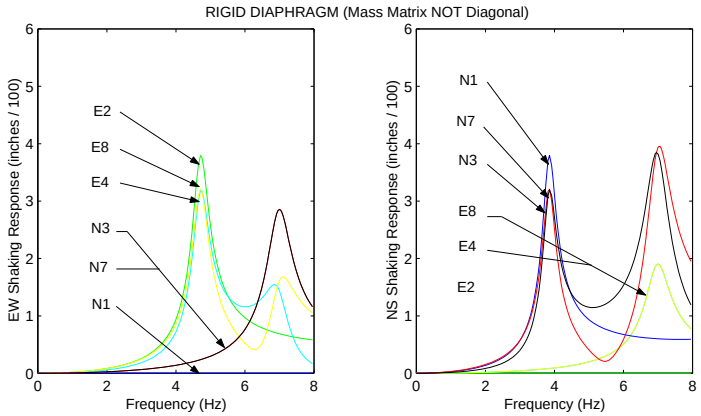

Figure E.4: Test Model with Rigid Diaphragm (mass matrix NOT diagonal)

Table E.4: Natural Frequencies (rigid diaphragm)

Lumped Mass (matrix IS diag.)			
ω_1	ω_2	ω_3	ω_4
3.85 Hz	4.03 Hz	4.71 Hz	10.6 Hz
NS	Tors	EW	NS
Consistent Mass (matrix NOT diag.			
ω_1	ω_2	ω_3	ω_4
3.85 Hz	4.71 Hz	6.98 Hz	10.6 Hz
NS	EW	Tors	NS

Appendix F

Weights Used in 3-Story Building Model

Table F.1: Phase I Floor Weights (continuous loads)

2ND FLOOR	Unit Weight	Trib. Area	Weight
Plywood (5/8")	1.9 PSF	512 ft$\hat{2}$	960 lbs
Beams (2x12 @ 16")	3.2 PSF	512 ft$\hat{2}$	1638 lbs
Misc. Blocking (2x4 @ 24")	0.7 PSF	512 ft$\hat{2}$	358 lbs
Partition Studs Above (2x4 @ 16")	1.0 PSF	144 ft$\hat{2}$	144 lbs
ADDED WEIGHTS			9400 lbs
TOTAL WEIGHT AT 2ND FLOOR			**12501 lbs**
3RD FLOOR	Unit Weight	Trib. Area	Weight
Plywood (5/8")	1.9 PSF	512 ft$\hat{2}$	960 lbs
Beams (2x12 @ 16")	3.2 PSF	512 ft$\hat{2}$	1638 lbs
Misc. Blocking (2x4 @ 24")	0.7 PSF	512 ft$\hat{2}$	358 lbs
Partition Studs Above (2x4 @ 16")	1.0 PSF	144 ft$\hat{2}$	144 lbs
ADDED WEIGHTS			11000 lbs
TOTAL WEIGHT AT 3RD FLOOR			**14101 lbs**
ROOF	Unit Weight	Trib. Area	Weight
Plywood (3/8")	1.1 PSF	512 ft$\hat{2}$	576 lbs
Beams (2x10 @ 16")	2.6 PSF	512 ft$\hat{2}$	1331 lbs
Misc. Blocking (2x4 @ 24")	0.7 PSF	512 ft$\hat{2}$	358 lbs
ADDED WEIGHTS			7600 lbs
TOTAL WEIGHT AT ROOF			**9866 lbs**

Table F.2: Phase I Wall Weights (nodal loads)

NODE 1 (2nd Floor, S Wall)	Unit Weight	Trib. Area	Weight
Plywood (3/8")	1.1 PSF	288 ft$\hat{2}$	324 lbs
1st Floor Studs (2x6 @ 16")	1.6 PSF	144 ft$\hat{2}$	230 lbs
2nd Floor Studs (2x4 @ 16")	1.0 PSF	144 ft$\hat{2}$	144 lbs
Misc. Blocking (2x4 @ 24")	0.7 PSF	288 ft$\hat{2}$	202 lbs
W1 =			**900 lbs**

NODE 2 (2nd Floor, N Wall)	Unit Weight	Trib. Area	Weight
Plywood (3/8")	1.1 PSF	144 ft$\hat{2}$	162 lbs
2nd Floor Studs (2x4 @ 16")	1.0 PSF	144 ft$\hat{2}$	144 lbs
Misc. Blocking (2x4 @ 24")	0.7 PSF	144 ft$\hat{2}$	101 lbs
Glulam Beam (6 3/4"x12")	16.9 PLF	32 ft	540 lbs
2 Steel Columns (3" STD)	14.9 PLF	9 ft	134 lbs
W2 =			**1081 lbs**

NODES 3,4 (2nd Floor, E and W Walls)	Unit Weight	Trib. Area	Weight
Plywood (3/8")	1.1 PSF	144 ft$\hat{2}$	162 lbs
1st Floor Studs (2x6 @ 16")	1.6 PSF	72 ft$\hat{2}$	115 lbs
2nd Floor Studs (2x4 @ 16")	1.0 PSF	72 ft$\hat{2}$	72 lbs
Misc. Blocking (2x4 @ 24")	0.7 PSF	144 ft$\hat{2}$	101 lbs
W3 = W4 =			**450 lbs**

NODES 5,6 (3rd Floor, S and N Walls)	Unit Weight	Trib. Area	Weight
Plywood (3/8")	1.1 PSF	288 ft$\hat{2}$	324 lbs
2nd and 3rd Floor Studs (2x4 @ 16")	1.0 PSF	288 ft$\hat{2}$	288 lbs
Misc. Blocking (2x4 @ 24")	0.7 PSF	288 ft$\hat{2}$	202 lbs
W5 = W6 =			**814 lbs**

NODES 7,8 (3rd Floor, E and W Walls)	Unit Weight	Trib. Area	Weight
Plywood (3/8")	1.1 PSF	144 ft$\hat{2}$	162 lbs
2nd and 3rd Floor Studs (2x4 @ 16")	1.0 PSF	144 ft$\hat{2}$	144 lbs
Misc. Blocking (2x4 @ 24")	0.7 PSF	144 ft$\hat{2}$	101 lbs
W7 = W8 =			**407 lbs**

NODES 9,10 (Roof, S and N Walls)	Unit Weight	Trib. Area	Weight
Plywood (3/8")	1.1 PSF	144 ft$\hat{2}$	162 lbs
2nd and 3rd Floor Studs (2x4 @ 16")	1.0 PSF	144 ft$\hat{2}$	144 lbs
Misc. Blocking (2x4 @ 24")	0.7 PSF	144 ft$\hat{2}$	101 lbs
W9 = W10 =			**407 lbs**

NODES 11,12 (Roof, E and W Walls)	Unit Weight	Trib. Area	Weight
Plywood (3/8")	1.1 PSF	72 ft$\hat{2}$	81 lbs
2nd and 3rd Floor Studs (2x4 @ 16")	1.0 PSF	72 ft$\hat{2}$	72 lbs
Misc. Blocking (2x4 @ 24")	0.7 PSF	72 ft$\hat{2}$	50 lbs
W11 = W12 =			**203 lbs**

Table F.3: Phase III Floor Weights (continuous loads)

2ND/3RD FLOOR	Unit Weight	Trib. Area	Weight
Plywood (5/8")	1.9 PSF	512 ft$\hat{2}$	960 lbs
Beams (2x12 @ 16")	3.2 PSF	512 ft$\hat{2}$	1638 lbs
Misc. Blocking (2x4 @ 24")	0.7 PSF	512 ft$\hat{2}$	358 lbs
Ceiling Drywall (5/8")	3.1 PSF	512 ft$\hat{2}$	1600 lbs
Partition Studs Above (2x4 @ 16")	1.0 PSF	144 ft$\hat{2}$	144 lbs
Partition Drywall (2-sides, 5/8")	3.1 PSF	288 ft$\hat{2}$	900 lbs
ADDED WEIGHTS			2000 lbs
TOTAL WEIGHT AT 2ND/3RD FLOOR			**7601 lbs**
ROOF	Unit Weight	Trib. Area	Weight
Plywood (3/8")	1.1 PSF	512 ft$\hat{2}$	576 lbs
Beams (2x10 @ 16")	2.6 PSF	512 ft$\hat{2}$	1331 lbs
Misc. Blocking (2x4 @ 24")	0.7 PSF	512 ft$\hat{2}$	358 lbs
Ceiling Drywall (5/8")	3.1 PSF	512 ft$\hat{2}$	1600 lbs
ADDED WEIGHTS			2600 lbs
TOTAL WEIGHT AT ROOF			**6466 lbs**

Table F.4: Phase III Wall Weights (nodal loads)

NODE 1 (2nd Floor, S Wall)	Unit Weight	Trib. Area	Weight
Plywood (3/8")	1.1 PSF	288 ft$\hat{2}$	324 lbs
1st Floor Studs (2x6 @ 16")	1.6 PSF	144 ft$\hat{2}$	230 lbs
2nd Floor Studs (2x4 @ 16")	1.0 PSF	144 ft$\hat{2}$	144 lbs
Misc. Blocking (2x4 @ 24")	0.7 PSF	288 ft$\hat{2}$	202 lbs
Drywall (1-side, 5/8")	3.1 PSF	288 ft$\hat{2}$	900 lbs
Stucco (5/8")	10.0 PSF	288 ft$\hat{2}$	2880 lbs
W1 =			**4680 lbs**

NODE 2 (2nd Floor, N Wall)	Unit Weight	Trib. Area	Weight
Plywood (3/8")	1.1 PSF	144 ft$\hat{2}$	162 lbs
2nd Floor Studs (2x4 @ 16")	1.0 PSF	144 ft$\hat{2}$	144 lbs
Misc. Blocking (2x4 @ 24")	0.7 PSF	144 ft$\hat{2}$	101 lbs
Glulam Beam (6 3/4"x12")	16.9 PLF	32 ft	540 lbs
2 Steel Columns (3" STD)	14.9 PLF	9 ft	134 lbs
Drywall (1-side, 5/8")	3.1 PSF	144 ft$\hat{2}$	450 lbs
Stucco (5/8")	10.0 PSF	144 ft$\hat{2}$	1440 lbs
W2 =			**2971 lbs**

NODES 3,4 (2nd Floor, E and W Walls)	Unit Weight	Trib. Area	Weight
Plywood (3/8")	1.1 PSF	144 ft$\hat{2}$	162 lbs
1st Floor Studs (2x6 @ 16")	1.6 PSF	72 ft$\hat{2}$	115 lbs
2nd Floor Studs (2x4 @ 16")	1.0 PSF	72 ft$\hat{2}$	72 lbs
Misc. Blocking (2x4 @ 24")	0.7 PSF	144 ft$\hat{2}$	101 lbs
Drywall (1-side, 5/8")	3.1 PSF	144 ft$\hat{2}$	450 lbs
Stucco (5/8")	10.0 PSF	144 ft$\hat{2}$	1440 lbs
W3 = W4 =			**2340 lbs**

Table F.5: Phase III Wall Weights (nodal loads)

NODES 5,6 (3rd Floor, S and N Walls)	Unit Weight	Trib. Area	Weight
Plywood (3/8")	1.1 PSF	288 ft$\hat{2}$	324 lbs
2nd and 3rd Floor Studs (2x4 @ 16")	1.0 PSF	288 ft$\hat{2}$	288 lbs
Misc. Blocking (2x4 @ 24")	0.7 PSF	288 ft$\hat{2}$	202 lbs
Drywall (1-side, 5/8")	3.1 PSF	288 ft$\hat{2}$	900 lbs
Stucco (5/8")	10.0 PSF	288 ft$\hat{2}$	2880 lbs
W5 = W6 =			**4594 lbs**
NODES 7,8 (3rd Floor, E and W Walls)	Unit Weight	Trib. Area	Weight
Plywood (3/8")	1.1 PSF	144 ft$\hat{2}$	162 lbs
2nd and 3rd Floor Studs (2x4 @ 16")	1.0 PSF	144 ft$\hat{2}$	144 lbs
Misc. Blocking (2x4 @ 24")	0.7 PSF	144 ft$\hat{2}$	101 lbs
Drywall (1-side, 5/8")	3.1 PSF	144 ft$\hat{2}$	450 lbs
Stucco (5/8")	10.0 PSF	144 ft$\hat{2}$	1440 lbs
W7 = W8 =			**2297 lbs**
NODES 9,10 (Roof, S and N Walls)	Unit Weight	Trib. Area	Weight
Plywood (3/8")	1.1 PSF	144 ft$\hat{2}$	162 lbs
2nd and 3rd Floor Studs (2x4 @ 16")	1.0 PSF	144 ft$\hat{2}$	144 lbs
Misc. Blocking (2x4 @ 24")	0.7 PSF	144 ft$\hat{2}$	101 lbs
Drywall (1-side, 5/8")	3.1 PSF	144 ft$\hat{2}$	450 lbs
Stucco (5/8")	10.0 PSF	144 ft$\hat{2}$	1440 lbs
W9 = W10 =			**2297 lbs**
NODES 11,12 (Roof, E and W Walls)	Unit Weight	Trib. Area	Weight
Plywood (3/8")	1.1 PSF	72 ft$\hat{2}$	81 lbs
2nd and 3rd Floor Studs (2x4 @ 16")	1.0 PSF	72 ft$\hat{2}$	72 lbs
Misc. Blocking (2x4 @ 24")	0.7 PSF	72 ft$\hat{2}$	50 lbs
Drywall (1-side, 5/8")	3.1 PSF	72 ft$\hat{2}$	225 lbs
Stucco (5/8")	10.0 PSF	72 ft$\hat{2}$	720 lbs
W11 = W12 =			**1148 lbs**

Appendix G

Stiffness Matrix Used in 3-Story Building Model

$$\begin{bmatrix} K_{1,1} & K_{1,2} & K_{1,3} & \dots & K_{1,12} \\ K_{2,1} & K_{2,2} & K_{2,3} & \dots & K_{2,12} \\ K_{3,1} & K_{3,2} & K_{3,3} & \dots & K_{3,12} \\ \vdots & \vdots & \vdots & \ddots & \vdots \\ K_{12,1} & K_{12,2} & K_{12,3} & \dots & K_{12,12} \end{bmatrix}$$

where

$K_{1,1} = k1 + k5 + GP2 * L/D$

$K_{1,2} = -GP2 * L/D$

$K_{1,3} = GP2$

$K_{1,4} = -GP2$

$K_{1,5} = -k5$

$K_{2,2} = k2 + k6 + GP2 * L/D$

$K_{2,3} = -GP2$

$K_{2,4} = GP2$

$K_{2,6} = -k6$

$K_{3,3} = k3 + k7 + GP2 * D/L$

$K_{3,4} = -GP2 * D/L$

$K_{3,7} = -k7$

$K_{4,4} = k4 + k8 + GP2 * D/L$

$K_{4,8} = -k8$

$K_{5,5} = k5 + k9 + GP3 * L/D$

$K_{5,6} = -GP3 * L/D$

$K_{5,7} = GP3$

$K_{5,8} = -GP3$

$K_{5,9} = -k9$

$K_{6,6} = k6 + k10 + GP3 * L/D$

$K_{6,7} = -GP3$

$K_{6,8} = GP3$

$K_{6,10} = -k10$

$K_{7,7} = k7 + k11 + GP3 * D/L$

$K_{7,8} = -GP3 * D/L$

$K_{7,11} = -k11$

$K_{8,8} = k8 + k12 + GP3 * D/L$

$K_{8,12} = -k12$

$K_{9,9} = k9 + GPR * L/D$

$K_{9,10} = -GPR * L/D$

$K_{9,11} = GPR$

$K_{9,12} = -GPR$

$K_{10,10} = k10 + GPR * L/D$

$K_{10,11} = -GPR$

$K_{10,12} = GPR$

$K_{11,11} = k11 + GPR * D/L$

$K_{11,12} = -GPR * D/L$

$K_{12,12} = k12 + GPR * D/L$

and

$k1, k2, k3, \ldots, k12$ = spring stiffness at each wall

$GP2, GP3, GPR$ = diaphragm stiffness at 2nd, 3rd and roof levels

L, D = building length, width in longitudinal, transverse directions

Bibliography

[1] Applied Technology Council, Washington, D.C. *NEHERP Guidelines for the Seismic Rehabilitation of Buildings (FEMA-273)*, 1997.

[2] T. Arima and et al. Dynamic behavior and stiffness of full-scale houses during progressive stages of construction. In *Proceedings of the 1990 International Timber Engineering Conference*, volume 3, pages 778–785, Tokyo, Japan, 1990.

[3] J. L. Beck. *Determining Models of Structures from Earthquake Records.* EERL Report No. 78-01. California Institute of Technology, Pasadena, Calif., 1978.

[4] J. L. Beck. System identification methods applied to measured seismic response. In *Proceedings from 11th World Conference on Earthquake Engineering*, Acapulco, Mexico, 1996.

[5] J. L. Beck and M. Dowling. Quick algorithms for computing either displacement, velocity or acceleration of an oscillator. *Earthquake Engineering and Structural Dynamics*, 16:245–253, 1988.

[6] J. L. Beck and et al. *Ambient Vibration Surveys of Three Steel-Frame Buildings Strongly Shaken by the 1994 Northridge Earthquake.* EERL Report No. 95-06. California Institute of Technology, Pasadena, Calif., 1995.

[7] J. L. Beck and P.C. Jennings. Structural identification using linear models and earthquake records. *Earthquake Engineering and Structural Dynamics*, 8:145–160, 1980.

[8] H. J. Blass and et al. Timber structures in seismic regions - rilem state-of-the-art report. *Materials and Structures*, 27(167):157–184, 1994.

[9] J. G. Bouwkamp, R. O. Hamburger, and J. D. Gillengerten. *Degradation of Plywood Roof Diaphragms under Multiple Earthquake Loading*. Data Utilization Report CSMIP/94-02. California Department of Conservation, Division of Mines and Geology, Office of Strong Motion Studies, Sacramento, Calif., 1994.

[10] D. E. Breyer. *Design of Wood Structures*. McGraw-Hill, Inc., 1993.

[11] D. J. Dowrick. *Earthquake Resistant Design: For Engineers and Architects*. John Wiley and Sons, Inc., New York, NY, 1987.

[12] R. Falk. *Damage and Collapse Behavior of Low-Rise Woodframed Buildings*. PhD thesis, Washington State University, Pullman, Wash., 1986.

[13] D. Fischer and et al. *Shake Table Tests of a Two-Story Woodframe House*. CUREE-Caltech Woodframe Project Task 1.1.1 Report. Consortium of Universities for Research in Earchquake Engineering (CUREE), Richmond, Calif., 2001.

[14] G. C. Foliente. Analysis, design and testing of timber structures under seismic loads. In *Proceedings from 11th World Conference on Earthquake Engineering*, 1994.

[15] G. C. Foliente, P. J. Paevere, and F. Ma. Parameter identification and seismic response analysis of timber buildings. In *Proceedings of the World Conference on Timber Engineering*, Lausanne, Switzerland, 1998.

[16] G. C. Foliente and E. Zacher. *Performance Tests of Structural Systems under Seismic Loads*. 1994.

[17] International Association for Earthquake Engineering. *Regulations For Seismic Design: A World List*. 1992.

[18] P. Gavrilovic and K. Gramatikov. Experimental and theoretical investigations of wooden truss-frame structures under quasi-static and dynamic loads. In *Proceedings of the Workshop on Full-Scale Behavior of Woodframed Buildings in*

Earthquakes and High Winds, volume XXVI-1-37, Watford, United Kingdom, 1991.

[19] R. K. Goel and A. K. Chopra. Period formulas for moment resisting frame buildings. *Journal of Structural Engineering*, ASCE 123(11):454–461, 1997.

[20] R. K. Goel and A. K. Chopra. Period formulas for concrete shear wall buildings. *Journal of Structural Engineering*, ASCE 124(4):426–433, 1998.

[21] Y. Hirashima. Analysis of observed earthquake response of post-and-beam wood structure. In *Proceedings from the International Conference on Timber Engineering*, Seattle, Washington, 1988.

[22] ICBO, International Conference of Building Officials, Whittier, Calif. *Uniform Building Code*, 1997.

[23] R. Itani and C. Cheung. Nonlinear analysis of sheathed wood diaphragms. *Journal of Structural Engineering*, ASCE 110(9):2137–2147, 1983.

[24] N. Kawai. Seismic performance testing on woodframed shear walls. In *Proceedings of the 31st Meeting of CIB W18*, pages paper 31–15–1, 1998.

[25] C. A. Kircher and et al. Estimation of earthquake losses to buildings. *EERI Spectra*, 13(4):703–720, November 1997.

[26] Malik. *Estimating Building Stocks for Earthquake Mitigation and Recovery Planning*. Cornell Institute for Social and Economic Research, 1995.

[27] K. Mosalam and et al. *Seismic Evaluation of an Asymmetric Three-Story Woodframe Building*. CUREE-Caltech Woodframe Project Task 1.1.2 Report. Consortium of Universities for Research in Earchquake Engineering (CUREE), Richmond, Calif., 2002.

[28] S. Nakajima, T. Arima, and N. Nakamura. Vibrating properties of middle-storied wooden structures: Vibrating analysis of full-scale 3-storied conventional house. *Journal of Japan Wood Research Society*, 39(8):910–916, 1993.

[29] T. Phillips, R. Itani, and D. McLean. Lateral load sharing by diaphragms in woodframed buildings. *Journal of Structural Engineering*, ASCE 119(5):1556–1571, 1993.

[30] A. Polensek and K. M. Bastendorff. Damping in nailed joints of light-frame wood buildings. *Wood and Fiber Science*, 19(2):110–125, 1987.

[31] A. Polensek and B. D. Schimel. Dynamic properties of light-frame wood subsystems. *Journal of Structural Engineering*, ASCE 117(4):1079–1095, 1991.

[32] I. Sakamoto, Y. Ohashi, and Y. Fujii. Seismic behavior of base isolated two-storied wooden building - static loading tests and earthquake observation. In *Proceedings of the 1990 International Timber Engineering Conference*, volume 3, pages 938–945, Tokyo, Japan, 1990.

[33] F. Seible, A. Filiatrault, and C. M. Uang, editors. *Proceedings of the Invitational Workshop on Seismic Testing, Analysis and Design of Woodframe Construction.* CUREE-Caltech Woodframe Project. Consortium of Universities for Research in Earchquake Engineering (CUREE), Richmond, Calif., 1999.

[34] J. M. Seo, I. K. Choi, and J. R. Lee. Static and cyclic behavior of wooden frames with tenon joints under lateral load. *Journal of Structural Engineering*, ASCE 125(3):344–349, 1999.

[35] L. A. Soltis, D. S. Gromala, and R. L. Tuomi. Seismic performance of low-rise wood buildings. *Seismic Performance of Low-Rise Buildings- State of the Art and Research Needs*, pages 78–91, 1981.

[36] H. Sugiyama. Japanese experience and research on timber buildings in earthquakes. In *Proceedings of Pacific Timber Engineering Conference*, volume 2, pages 431–438, Auckland, New Zealand, 1984.

[37] H. Sugiyama, S. Kikuchi, and H. Noguchi. Full scale test on a two-story platform-framing house subjected to lateral load. *Transaction of The Architectural Institute of Japan*, 247:11–23, 1976.

[38] A. M. Tarabia and R. Y. Itani. Seismic response of light-frame wood buildings. *Journal of Structural Engineering*, ASCE 123(11):1470–1477, 1997.

[39] P. G. Touleatos, E. P. Tsakanika, and P. G. Carydis. On the greek experience concerning the structural behavior of timber construction in seismic zones. In *Proceedings of the Workshop on Full-Scale Behavior of Woodframed Buildings in Earthquakes and High Winds*, volume XIV-1-86, Watford, United Kingdom, 1991.

[40] S. D. Werner, J. L. Beck, and M. B. Levine. Seismic response evaluation of meloland road overpass using 1979 imperial valley earthquake records. *Earthquake Engineering and Structural Dynamics*, 15:249–274, 1987.

[41] C. W. Yancey and et al. *A Summary of the Structural Performance of Single-Family, Woodframe Housing (NISTIR 6224).* Building and Fire Research Laboratory, National Institute of Standards and Technology, Gaithersburg, Maryland, 1998.

[42] M. Yasumura and et al. Experiments on a three-storied wooden frame building subjected to horizontal load. In *Proceedings of the 1988 International Conference on Timber Engineering*, volume 2, pages 262–275, Seattle, Wash., 1988.

[43] F. Y. Yokel, G. Hsi, and N. F. Somes. *Full Scale Test on a Two-Story House Subjected to Lateral Load.* National Bureau of Standards, Washington, D.C., 1973.